UNIVERSIDADE FEDERAL DO RIO GRANDE DO SUL

CENTRO ESTADUAL DE PESQUISAS EM SENSORIAMENTO REMOTO E METEOROLOGIA

PROGRAMA DE PÓS-GRADUAÇÃO EM SENSORIAMENTO REMOTO

ADRIANA COROMOTO BECERRA RONDÓN

RADIAÇÃO ATMOSFÉRICA NO ULTRAVIOLETA NO RIO GRANDE DO SUL: FATORES DETERMINANTES E SUA DISTRIBUIÇÃO A PARTIR DE DADOS ORBITAIS

PORTO ALEGRE

2022

ADRIANA COROMOTO BECERRA RONDÓN

RADIAÇÃO ATMOSFÉRICA NO ULTRAVIOLETA NO RIO GRANDE DO SUL: FATORES DETERMINANTES E SUA DISTRIBUIÇÃO A PARTIR DE DADOS ORBITAIS

Tese apresentada ao Programa de Pós-Graduação em Sensoriamento Remoto da Universidade Federal do Rio Grande do Sul, como requisito para obtenção do título de Doutora em Sensoriamento Remoto e Geoprocessamento.

Orientador: Prof. Dr. Jorge Ricardo Ducati

Coorientador: Prof. Dr. Rafael Haag

PORTO ALEGRE

2022

CIP - Catalogação na Publicação

ADRIANA COROMOTO BECERRA RONDÓN

RADIAÇÃO ATMOSFÉRICA NO ULTRAVIOLETA NO RIO GRANDE DO SUL: FATORES DETERMINANTES E SUA DISTRIBUIÇÃO A PARTIR DE DADOS ORBITAIS

Tese apresentada ao Programa de Pós-Graduação em Sensoriamento Remoto da Universidade Federal do Rio Grande do Sul, como requisito para obtenção do título de Doutora em Sensoriamento Remoto e Geoprocessamento.

Aprovada em 24/02/2022

Pela Banca Examinadora:

_____
Prof. Dr. Jorge Ricardo Ducati
Orientador
(PPGSR/UFRGS)

_____
Prof. Dr. Rafael Haag
Coorientador
(UERGS)

_____
Prof. Dr. Marcelo de Paula Corrêa
(UNIFEI)

_____
Profa. Dra. Tatiana Mora Kuplich
(INPE e PPGSR)

_____
Profa. Dra. Rita de Cássia Marques Alves
(PPGSR/UFRGS)

PORTO ALEGRE

2022

Dedicado ao meu marido Fernando Rojas, por incentivar a esta jovem barinesa a acreditar nela. Te amo.

AGRADECIMENTOS

À Universidade Federal do Rio Grande do Sul e CAPES pela estrutura e bolsa de estudos disponibilizada para a minha formação acadêmica e para o desenvolvimento desta tese.

Ao Prof. Dr. Jorge Ricardo Ducati pelo acolhimento, orientação, e pela forma sábia e calma como transmitiu os seus conhecimentos, bem como ter acreditado em mim e no meu trabalho. Foi uma honra conhecê-lo. Gratidão eterno.

Ao Prof. Dr. Rafael Haag pela orientação, por me apresentar um mundo novo de tecnologia e principalmente pela contribuição nos últimos anos. Obrigada.

À minha família por absolutamente tudo. Em especial, aos amores da minha vida, meus avós Coromoto e Martín, pelo amor e apoio incansável. À minha rainha Lennys, por estares aí sempre com teus braços abertos para dar-me amor de mãe. Aos meus irmãos Rolando e Simón, por estarem ao meu lado ainda na distância. Ao meu sobrinho primogênito amado Juan Pablo, que este mérito seja a desculpa da minha ausência física e que no futuro possas sentir orgulho de mim. À minha sogra Giselle pelo carinho e apoio. Amo muito vocês.

Aos irmãos da vida/amigos/colegas, Arennis Zabala, Kellen Labrador, Betzabeth Macias, Olga Herrera, Andrés Jaramillo, Gabriel Pittingliani, Pámela Pithan, Diniz Arruda e Adriane Thum. A todos aqueles que de alguma forma contribuíram para a realização deste trabalho e me incentivaram sempre ir à busca de conhecimento.

Como sempre, deixamos a cereja do bolo para o final. Gostaria de agradecer ao meu marido Fernando, que durante todo o meu percurso acadêmico desde a graduação até o doutorado, tornou-se meu maior companheiro e mentor, com ensinamento, paciência, compreensão e amor, principalmente nos tempos de estresse. À Miga, Lilo e Mili, pelos olhares profundos de amor e companhia.

A todos vocês, o meu agradecimento.

RESUMO

A radiação ultravioleta (RUV) desempenha um papel fundamental na fotoquímica da atmosfera, através de processos de absorção ou dispersão por seus constituintes. Quantificar a RUV espaço-temporalmente e conhecer sua relação com variáveis moduladoras é importante para o estado do Rio Grande do Sul, região com um dos maiores índices de neoplasias de pele do Brasil e onde, hoje em dia, são poucas as cidades que monitoram a RUV *in situ* e raras as que fazem o monitoramento contínuo. Deste modo, o objetivo desta tese foi gerar conhecimento sobre o comportamento local da RUV no intuito de contribuir na tomada de decisões para mitigar os efeitos causados pela exposição a esta radiação. Para isto, abordamos três tópicos: i) avaliamos as variações de poluentes atmosféricos e seu impacto na RUV, num cenário de redução de atividades antrópicas; ii) medimos o potencial do método Random Forest para reconstrução espaço-temporal a longo prazo, combinando dados superficiais e orbitais; iii) estimamos a distribuição espaço-temporal da RUV e suas relações com fatores moduladores. Nossos resultados mostram que em um cenário de redução de atividades antrópicas, as emissões de dióxido de nitrogênio diminuíram, enquanto os níveis de ozônio total e ultravioleta aumentaram; o aumento simultâneo de ozônio e ultravioleta sugerem que o ozônio não é o único fator que influencia a radiação ultravioleta na superfície. Tendo em vista que as estações de monitoramento ambiental existentes no Rio Grande do Sul são esparsas e distribuídas de forma desigual, foram usadas tecnologias como o método Random Forest, em combinação com uma extensa coleta de dados de múltiplos parâmetros de satélite e estações terrestres como uma ferramenta válida para prever variáveis ao nível do solo, bem como reconstruções espaço-temporais a longo prazo. Através de dados de sensoriamento remoto pudemos analisar as características espaço-temporais, determinando-se que no Rio Grande do Sul locais em latitudes mais baixas e altitudes mais elevadas apresentam maiores incidências de radiação ultravioleta; há um padrão temporal bem definido, com maior valor no verão e menor valor no inverno. Mostrou-se ainda que ocasiões de incidência da radiação mais intensa são correlacionadas de forma negativa com ozônio total, e de forma variável com dióxido de nitrogênio total.

Palavras-chave: radiação ultravioleta, constituintes atmosféricos, Rio Grande do Sul.

ABSTRACT

Ultraviolet radiation (UVR) plays a fundamental role in the photochemistry of the atmosphere, through processes of absorption or dispersion by its constituents. Quantifying UVR spatio-temporally and knowing its relationship with modulating variables is important for the state of Rio Grande do Sul, a region with one of the highest rates of skin neoplasms in Brazil and where, nowadays, few cities have *in situ* UVR monitoring and even fewer have continuous monitoring. Thus, the objective of this thesis was to generate knowledge about the local behavior of UVR aiming to contribute to decision-making to mitigate the effects caused by exposure to this radiation. This was approached in three ways: i) we evaluated the variations of atmospheric pollutants and their impact on UVR, in a scenario of reduction of anthropic activities; ii) we measured the potential of the Random Forest method for long-term space-time reconstruction, combining surface and orbital data; iii) we estimated the space-time distribution of UVR and its relationship with modulating factors. Our results show that in a scenario of reduced human activities, nitrogen dioxide emissions decreased, while total and ultraviolet ozone levels increased; the simultaneous increase of ozone and ultraviolet suggests that ozone is not the only factor influencing ultraviolet radiation at the surface. Considering that the existing environmental monitoring stations in Rio Grande do Sul are sparse and unevenly distributed, technologies such as the Random Forest method were used in combination with extensive data collected from multiple satellite parameters and ground stations as a tool for predicting ground-level variables as well as long-term spatio-temporal reconstructions across the study area. Through remote sensing data, we were able to analyze the spatio-temporal characteristics, determining that, in Rio Grande do Sul, locations at lower latitudes and higher altitudes have higher incidences of ultraviolet radiation; there is a well-defined temporal pattern, with a higher value in the summer and a lower value in the winter. It was also shown that occasions of more intense radiation incidence are negatively correlated with total ozone, and in variably forms with total nitrogen dioxide.

Keywords: ultraviolet radiation, atmospheric constituents, Rio Grande do Sul.

SUMÁRIO

LISTA DE FIGURAS

Figuras do Artigo 3

LISTA DE TABELAS

ESTRUTURA DA TESE

Esta tese "Radiação atmosférica no ultravioleta no Rio Grande do Sul: fatores determinantes e sua distribuição a partir de dados orbitais" foi estruturada na forma de artigos científicos, estando organizada conforme normas do PPGSR.

São apresentados quatro capítulos contendo os seguintes temas: No primeiro e segundo capítulo são abordados assuntos como relevância e introdução, objetivos, fundamentação teórica e metodologia. Os resultados e discussões são apresentados em forma de artigos no capítulo III, cujos títulos são:

Artigo 1 aceito na Revista Atmósfera com o título: *Partial COVID-19 lockdown effect in atmospheric pollutants and indirect impact in UV radiation in Rio Grande do Sul, Brazil*. onde avaliamos os efeitos da desaceleração das atividades humanas durante a pandemia COVID-19 nos parâmetros atmosféricos, sendo mostrado que o bloqueio parcial ocorrido no sul do Brasil teve efeitos mensuráveis na atmosfera local.

Artigo 2 encaminhado para Revista Atmósfera com o título: *Satellite-based estimation of NO_2 concentrations using a machine-learning model: a case study on Rio Grande do Sul, Brazil*, onde reconstruímos as concentrações de NO_2 espaço-temporais de longo prazo ao nível do solo usando um modelo de aprendizado de máquina., sendo mostrado que este algoritmo constitui uma ferramenta válida para prever NO_2 ao nível do solo.

Artigo 3 encaminhado para Revista Atmósfera com o título: *Spatiotemporal distributions of ultraviolet radiation from OMI orbital data and relationships with Total O_3 and Total NO_2*, onde quantificamos a incidência de radiação ultravioleta, e mostramos como as mudanças espaço-temporais de componentes na atmosfera local tiveram efeitos mensuráveis nas ocorrências de altos valores de Dose Eritemal Diária.

No capítulo IV, "Considerações Finais", são apresentadas as principais conclusões referentes ao monitoramento de radiação ultravioleta e suas interações no Rio Grande do Sul a partir do sensoriamento remoto com base nos resultados obtidos nos artigos apresentados nos capítulos anteriores. Finalmente no Apêndice A, encontra-se na íntegra o trabalho apresentado no Congresso de Energia Solar de 2020, reportando uma análise anual das componentes direta, difusa e global da radiação solar em Porto Alegre, RS.

1 INTRODUÇÃO

A energia proveniente do Sol e que atinge a Terra é composta essencialmente das radiações infravermelha, visível e ultravioleta; ao atravessar a camada atmosférica estas radiações passam por processos físicos (reflexão, difusão e absorção), chegando à superfície de forma direta (que provém diretamente do Sol), difusa (energia dispersada) e global (soma da energia direta e difusa) (IQBAL, 1983).

A Radiação Ultravioleta (RUV,100–400 nm) representa aproximadamente 8% da radiação eletromagnética total emitida pelo Sol (ROBINSON, 1966; ANDRADE; TIBA, 2016) e, a quantidade que chega até a superfície da Terra tem proporção menor (aprox. 4%), devido aos processos físicos da atmosfera e à influência de parâmetros geográficos, temporais, atmosféricos e astronômicos que aumentam ou diminuem a sua intensidade (SILVA et al., 2008). Esta radiação é dividida em três bandas denominadas A, B e C (SLINEY, 2007), sendo composta por 96% de RUV−A (315 a 400 nm, que chega até a superfície terrestre, sendo pouco absorvida pelos componentes atmosféricos) e 4% de RUV−B (280 a 315 nm; incide na superfície em níveis muito tênues, porém suficientes para desencadear processos fotoquímicos e fotobiológicos relevantes), enquanto a RUV−C (100–280 nm) é absorvida na estratosfera no processo de formação da camada de ozônio (KOLLER, 1965; INIRC, 1985).

O conhecimento sobre intensidade desta radiação na superfície da Terra é importante, já que a evolução e crescimento da maioria das formas de vida terrestres e aquáticas são influenciados por variáveis ambientais, incluindo a intensidade da RUV (KERR; FIOLETOV, 2008). Alguns dos efeitos na biosfera pela exposição excessiva a esta energia geram prejuízos na produtividade primária e nos organismos aquáticos (CARDOSO, 2011), na produtividade das culturas agrícolas e florestais (CALDWELL et al., 2003), na morte de anfíbios indicadores de qualidade ambiental (TIEGTE et al., 2001), na degradação de materiais e na fotoquímica da poluição troposférica urbana (DAVIS; SIMS, 1983) e na pele, olhos e sistema imunológico do ser humano (COARITI, 2017).

1.1 Problematização

As mudanças na atmosfera terrestre são um assunto de grande interesse público e político (WMO, 1999). Três tópicos tem sido de grande preocupação: (1) aumento na transmissão atmosférica da radiação ultravioleta (RUV), em função da redução na concentração do ozônio estratosférico (FARMAN *et al.*, 1985), (2) a poluição da troposfera por gases traços que levam a mudanças na capacidade oxidante da atmosfera e são prejudiciais à saúde humana (SEINFELD; PANDIS, 1998), e (3) o aumento significativo dos chamados gases de "estufa" que absorvem pouca RUV, onde esta tem seu máximo, mas fortemente na região do infravermelho onde a emissão da Terra é mais forte, diminuindo assim o ciclo de resfriamento do sistema terrestre (RAMANATHAN; FENG, 2009).

Os fatores que afetam a radiação ultravioleta são bem conhecidos (KERR; FIOLETOV, 2008; KERR, 2005), e a importância de cada um deles varia com a latitude, o clima e a quantidade de poluição atmosférica em cada local, dando origem a interações não lineares que envolvem processos complexos de absorção e espalhamento (KERR, 2002; MCKENZIE *et al.*, 2007). Contudo, o principal fator modulador da absorção ultravioleta é o ozônio estratosférico (correspondente ao 90% do O_3 total), que apresenta padrão sazonal devido aos processos naturais de formação, transporte e destruição, sendo suas concentrações mais baixas no outono e mais altas na primavera (WAKAMATSU *et al.*, 1989; ANDRÉ *et al.*, 2003). Porém, essa variabilidade é influenciada por fenômenos naturais e atividades antrópicas (FAHEY; HEGGLIN, 2011; BAIS *et al.*, 2015), estas última ligadas à produção industrial de dióxido de nitrogênio (NO_2) formado a partir da oxidação do óxido nitroso (N_2O) proveniente da troposfera. O NO_2 pode atingir altas concentrações na estratosfera (90% de todo o NO_2), onde destrói O_3 através de processos catalíticos sequestrando radicais ativos (SEINFELD; PANDIS, 1998). Baseado nisto, em áreas urbanas, aerossóis e poluentes atmosféricos como ozônio e dióxido de nitrogênio podem atenuar a RUV (KORONAKIS *et al.*, 2002; CHUBAROVA, 2004). No entanto, aumentos na RUV também têm sido reportados e não podem ser explicados apenas por mudanças nas quantidades de ozônio e, portanto, é necessário incluir influências de outros fatores, como poluição nesses locais (ZEREFOS *et al.*, 2001; ZEREFOS, 2002; CHEYMOL; DE BACKER, 2003; ISAKSEN *et al.*, 2005).

1.2 Justificativa

A região sul da América do Sul, por estar próxima do buraco na camada de ozônio da Antártica, é de particular interesse para estudos de RUV (DIAZ, 2006). Altos índices são aferidos em grande parte desta região ao longo do ano (CORRÊA; PIRES, 2013; ZARATTI *et al.*, 2014; MORAES, 2015). No Brasil tem sido documentada uma variabilidade significativa na RUV entre diferentes estações do ano e entre regiões do país e, perante esta situação, em 1995 o Brasil, através do Instituto Nacional de Pesquisas Espaciais (INPE) aderiu a outros países pioneiros (Canada, Alemanha, Estados Unidos, entre outros) para monitorar e informar sobre a concentração de ozônio e a intensidade da radiação ultravioleta. O plano inicial foi medir RUV em superfície em três macrorregiões do país, mas hoje em dia são poucas as cidades que monitoram a RUV *in situ* e raras as que fazem o monitoramento contínuo há mais de 10 anos (KIRCHHOFF *et al.*, 2000; SERAFINI, 2008; TERAMOTO *et al.*, 2014; CORRÊA, 2015).

O conhecimento detalhado da magnitude e distribuição da RUV no sul do Brasil, e especialmente no Rio Grande do Sul, é interessante por razões demográficas: o estado apresenta as maiores taxas de câncer de pele (melanoma e não melanoma) do país, fato atribuído a uma maior porcentagem de pessoas de origem caucasiana ou europeia, que expostas à RUV apresentam maior predisposição para desenvolver essa patologia (LEE-TAYLOR *et al.*, 2010; CORRÊA, 2015; INCA, 2020).

Atualmente, várias pesquisas vêm sendo desenvolvidas para compreender os resultados das atividades humanas sobre o clima futuro e seus possíveis impactos (SICILIANO et al., 2020; GONZÁLEZ-RODRÍGUEZ *et al.*,2021; KUMAR *et al.*, 2022; WANG *et al.*, 2022; WASTI *et al.*, 2022). Entender e prever os efeitos nas mudanças de uma variável importante como a RUV é essencial para planejar medidas afim de mitigar os possíveis impactos sobre a saúde e os ecossistemas. Neste contexto e diante do exposto, monitorar a longo prazo a RUV, através de sensoriamento remoto, além de fornecer informações relevantes sobre sua cobertura espacial e temporal, permitirá estimar tendências, relações e mudanças espaço−temporais, focados em regiões específicas (ORPHAL, 2002; IALONGO *et al.*, 2008; HERMAN, 2010).

1.3 Hipótese

Dado que o principal absorvedor da RUV na atmosfera é o ozônio estratosférico, havendo ainda outros agentes que induzem mudanças na composição atmosférica que dificultam a estimativa da magnitude desta radiação na superfície terrestre, é possível levar em conta o conjunto de agentes absorvedores numa estimava da intensidade da RUV a níveis espaciais e temporais, através de sensoriamento remoto, podendo-se descrever a sua variabilidade em função destes agentes.

1.4 Objetivos

1.4.1 Geral

Estimar a quantidade espaço-temporal da radiação ultravioleta que incide no Rio Grande do Sul.

1.4.2 Objetivos específicos

- Avaliar as variações de poluentes atmosféricos e seu impacto na RUV, num cenário de redução de atividades antrópicas.

- Avaliar o potencial do método Random Forest na estimativa espaço-temporal de NO_2 a longo prazo, no Rio Grande do Sul.

- Avaliar a distribuição espaço-temporal da RUV e suas relações com dois dos principais fatores moduladores, o O_3 e o NO_2.

1.5 Referencial teórico

As principais fontes naturais de energia eletromagnética utilizadas no sensoriamento remoto da superfície terrestre são o Sol e a Terra (CHUVIECO, 1996; JENSEN, 2009). Esta energia pode ser ordenada de forma contínua em função de seu comprimento de onda ou da sua frequência, sendo esta disposição denominada de espectro eletromagnético, o qual apresenta subdivisões de acordo com o tipo de processo físico que dá origem a esta, e da interação que ocorre entre a radiação-atmosfera-superfície (CHUVIECO, 1996). A radiação eletromagnética em comprimentos de onda menores que a região do visível e maiores que a região dos raios X é chamada de radiação ultravioleta (RUV) (Figura 2).

Figura 1 – Representação do Espectro Eletromagnético.
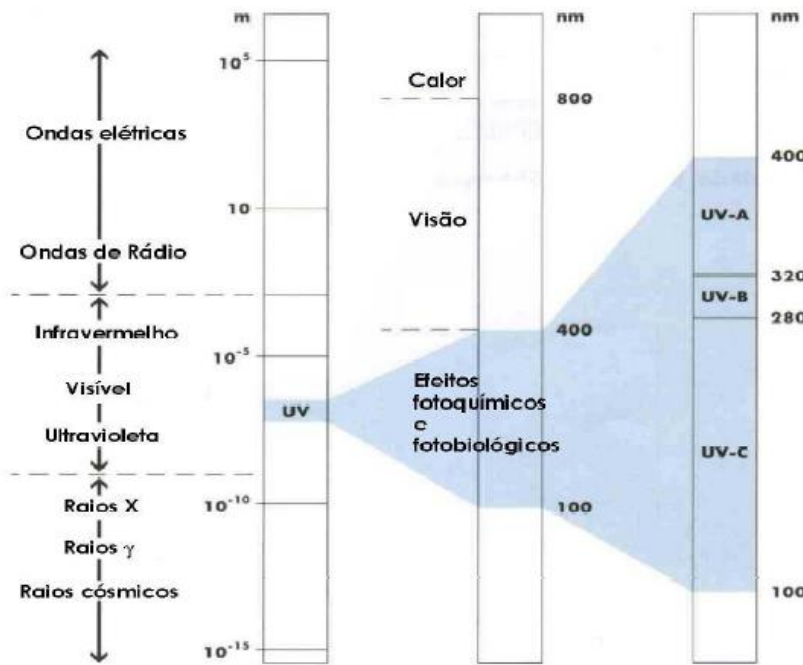
Fonte: CORRÊA, 2003.

As interações da RUV são numerosas, constituindo um fator fundamental para o clima da Terra e exercendo influência significativa no ambiente. A distribuição não uniforme dos fatores predominantes que interagem com a RUV torna a sua estimativa uma tarefa relevante. O impacto desses fatores nem sempre podem ser tratados de forma independente, pois na maioria dos casos eles agem sinergicamente (KERR *et al.*, 2003; KERR, 2005). Na sequência é explicitado como cada um deles modifica a intensidade desta irradiância:

1.5.1 O espectro solar

O conhecimento do espectro solar é importante para o estudo da RUV na superfície, uma vez que a intensidade desta em um determinado comprimento de onda (Figura 2) é proporcional à emissão radiativa do Sol no mesmo comprimento (BAIS et al., 2007; KERR; FIOLETOV, 2008). Portanto, como a atividade solar está ligada à quantidade de RUV que chega até a superfície da Terra tanto direta como indiretamente através de mudanças na produção de ozônio estratosférico. Quando a atividade solar é alta, geralmente há mais RUV emitida pelo Sol, havendo um leve aumento desta na superfície, e em consequência um aumento da produção de ozônio estratosférico (KERR, 1991; CHIPPERFIELD *et al.*, 2003).

Figura 2 – Distribuição do espectro solar na superfície terrestre.
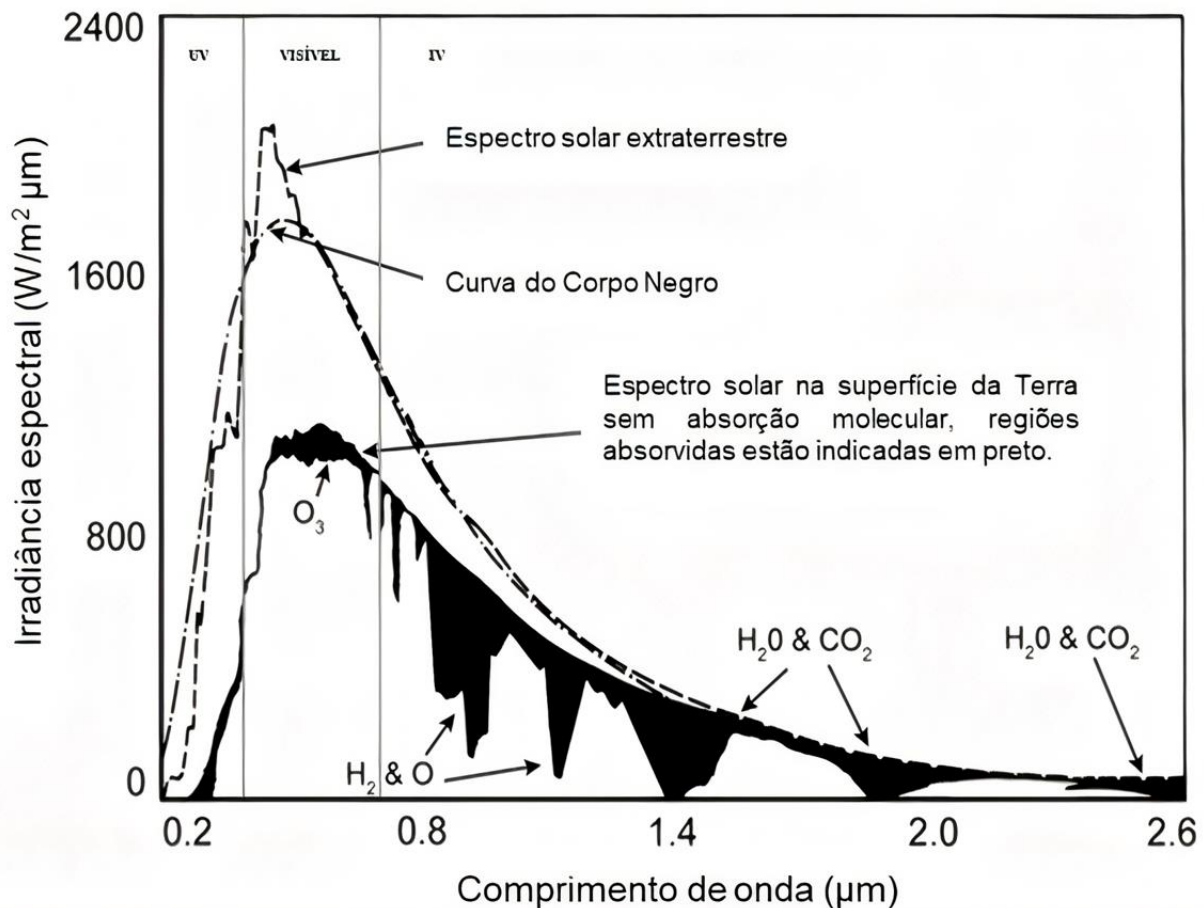
Fonte: ITACA, 2022.

1.5.2 *Distância Terra-Sol*

A intensidade da radiação solar fora da atmosfera da Terra em todos os comprimentos de onda é proporcional ao inverso do quadrado da distância entre a Terra e o Sol. Durante sua órbita elíptica anual ao redor do Sol, a Terra está mais próxima do Sol no início de janeiro e mais distante no início de julho, fazendo com que a diferença na intensidade da radiação solar entre o máximo de janeiro e o mínimo de julho seja de quase 7% em todos os comprimentos de onda, sob condições de atmosfera limpa (Figura 3). Essa assimetria tem consequências para a distribuição geográfica da RUV, uma vez que o máximo ocorre durante o verão no hemisfério sul, enquanto o mínimo ocorre durante o inverno no hemisfério sul. Além disso, a RUV no hemisfério sul é aumentada pelo menor ozônio total da coluna (KERR; FIOLETOV, 2008).

Figura 3 – Distância Terra-Sol.
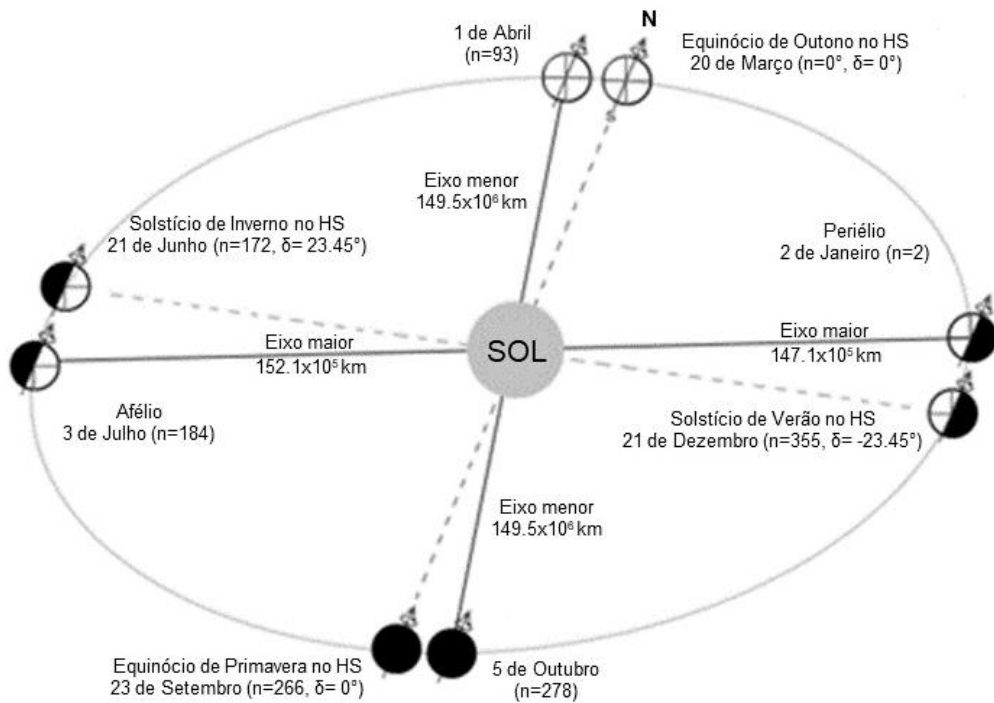
1.5.3 Ângulo Zenital Solar

Para um determinado local na superfície da Terra, o Ângulo Zenital Solar (SZA) pode ser calculado e depende da latitude, hora do dia e estação do ano. A RUV da superfície incidindo em uma superfície horizontal diminui com o aumento do SZA (Figura 4). Essa diminuição tem duas causas: Primeiro, a radiação que cai em uma superfície horizontal na superfície da Terra é proporcional ao cosseno de SZA. Em segundo lugar, o comprimento relativo do caminho da irradiância direta que passa pela atmosfera aumenta com o aumento de SZA, de modo que qualquer absorção e espalhamento por gases atmosféricos ou aerossóis é aumentada pelo aumento do comprimento do caminho através da atmosfera (KERR, 2005; KERR; FIOLETOV, 2008). Portanto, a atenuação do feixe solar direto por processos de dispersão e absorção na atmosfera aumenta com o aumento da SZA.

Figura 4 – Distância percorrida através da atmosfera pelos raios do Sol.
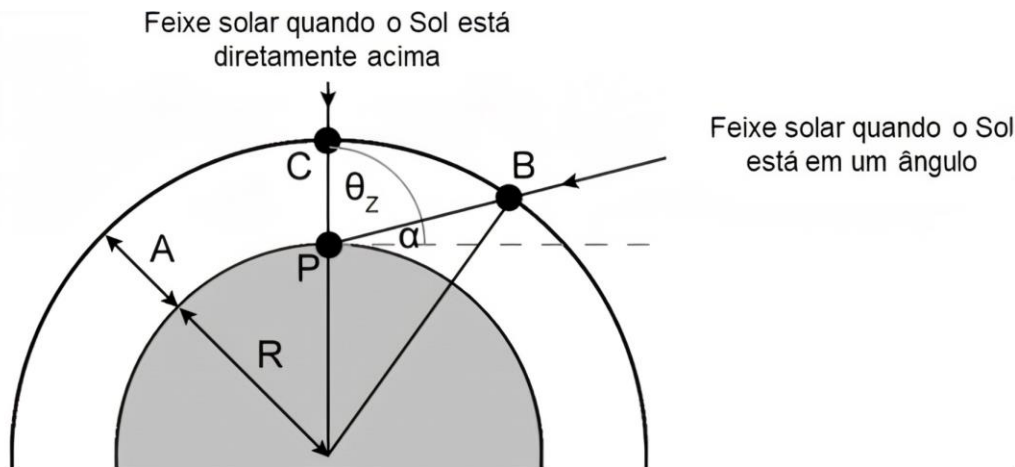
Fonte: ITACA, 2022.

1.5.4 Dispersão Molecular

A radiação solar é espalhada por moléculas de ar à medida que passa pela atmosfera. O espalhamento Rayleigh por moléculas de ar é inversamente proporcional à quarta potência do comprimento de onda (λ) (BATES, 1984), havendo consideravelmente mais espalhamento Rayleigh em comprimentos de onda UV do que em comprimentos de onda visíveis, uma vez que o comprimento de onda da RUV é menor que o da radiação visível. Portanto, a proporção de irradiação difusa para direta é maior em comprimentos de onda UV, uma vez que o céu é mais claro devido à maior dispersão e a intensidade solar reduzida devido à uma maior atenuação (KERR, 2005; KERR; FIOLETOV, 2008).

1.5.5 Absorção por Ozônio e Outros Gases Atmosféricos

Vários gases atmosféricos absorvem a radiação solar em comprimentos de onda do ultravioleta. O absorvedor mais significativo é o ozônio estratosférico, que faz com que aproximadamente 4% da RUV chegue até a troposfera inferior e a superfície da Terra. A correlação negativa entre a quantidade de ozônio na coluna e RUV foi bem documentada sob todas as condições meteorológicas (KERR; MCELROY, 1993) e quando todas as outras variáveis (cobertura de nuvens, neve) permanecem constantes (MCKENZIE *et al.*, 1999; FIOLETOV *et al.*, 1997; BODHAINE *et al.*, 1997), particularmente nas condições que causam o buraco na camada de ozônio da Antártida (DIAZ *et al.*, 2001). Em um estudo para a região de Toronto, Canadá, foi

reportado que uma diminuição de 1% no ozônio normalmente leva a um aumento na RUV entre 1% e 1,3% na maioria das condições locais (KERR *et al.*, 1994). Outros absorvedores naturais da RUV incluem dióxido de enxofre (SO_2) e dióxido de nitrogênio (NO_2). Grandes erupções de vulcões podem emitir SO_2 suficiente para causar absorção significativa, de até 50%, da RUV (KRUEGER *et al.*, 1995). O NO_2 também ocorre naturalmente na estratosfera (BREWER *et al.*, 1973), mas a absorção da RUV pelo NO_2 estratosférico é insignificante (<1%).

Vários gases resultantes da atividade antrópica estão presentes na troposfera e absorvem a RUV. Esses gases incluem ozônio, NO_2, SO_2, vários gases orgânicos e alguns compostos de cloro e bromo. Em geral, a quantidade na coluna atmosférica da maioria desses gases residuais não é alta o suficiente para gerar um efeito apreciável na RUV da superfície em áreas amplas. No entanto, perto de fontes de emissão, a quantidade na coluna de alguns gases da poluição pode levar a alterações de até 5 UD (Unidades Dobson) com base em medições terrestres (KERR, 1998; CEDE *et al.*, 2006; CEDE; HERMAN, 2005) e medições aéreas (WANG *et al.*, 2005a, WANG *et al.*, 2005b). Em casos extremos, os gases da poluição podem reduzir a RUV em até 10−15% em áreas urbanas (KORONAKIS *et al.*, 2002; CHUBAROVA, 2004), particularmente com absorção combinada de mais de um gás.

1.5.6 Dispersão por nuvens

As nuvens causam mais variabilidade na RUV da superfície do que todas as outras variáveis geofísicas. Para a maioria dos locais, a variabilidade das nuvens limita a capacidade de detectar mudanças de longo prazo devido a outras causas, como o ozônio (GLANDORF *et al.*, 2005). Quanto aos diferentes tipos de nuvens, estes têm efeitos significativamente diferentes na intensidade e distribuição angular da RUV na superfície. Uma fina camada de nuvens reduz a componente direta da radiação superficial e geralmente aumenta a componente difusa, levando a uma distribuição angular diferente. Uma camada de nuvens mais espessa bloqueia o componente direto, deixando apenas o componente difuso (KERR; FIOLETOV, 2008). Além disso, nuvens também podem aumentar a absorção por qualquer absorvedor atmosférico dentro da nuvem, tendo como resultado um aumento significativo no comprimento do caminho da radiação através da nuvem e do absorvedor, devido ao espalhamento múltiplo (WARDLE *et al.*, 1997).

1.5.7 Dispersão e Absorção por Aerossóis

Os aerossóis atmosféricos são partículas suspensas na atmosfera. Eles desempenham um papel importante na transferência radiativa da atmosfera, bem como na definição da intensidade, distribuição angular, dependência do comprimento de onda e variação de longo prazo da RUV na superfície (KERR; FIOLETOV, 2008). Existem muitas fontes de aerossóis atmosféricos, tanto naturais quanto antropogênicos, e uma grande variedade de tipos de aerossóis. As fontes naturais incluem vulcões, incêndios florestais (FIOLETOV *et al.*, 2001) e desertos (DI SARRA *et al.*, 2002); as fontes antropogênicas incluem emissões de usinas de energia, fábricas, queima de biomassa (KIRCHOFF *et al.*, 2001), automóveis e aeronaves. Seus processos de espalhamento e absorção dependem das propriedades químicas e físicas das partículas.

1.5.8 Albedo da Superfície

A RUV na superfície aumenta com o albedo da superfície, que espalha a radiação para cima para a atmosfera. A principal causa da variabilidade do albedo da superfície no ultravioleta é a cobertura de neve, e superfícies de areia podem ter albedo alto (PARISI *et al.*, 2003). Em geral, as diferenças espaciais no uso do solo (por exemplo, urbano, agrícola, florestal, etc.) têm pouco efeito óptico na RUV (KERR *et al.*, 2003).

1.5.9 Altitude

Com o aumento da altitude, a componente direta da RUV na superfície aumenta enquanto a componente difusa diminui, uma vez que há menos moléculas espalhadoras acima de uma superfície elevada. No geral, a RUV aumenta com a altitude e locais em altitudes maiores recebem mais radiação do que aqueles próximos ao nível do mar. Os gases que absorvem a RUV estão frequentemente presentes na troposfera, particularmente na camada limite planetária próxima às regiões urbanas, e reduzem esta radiação na superfície. Além disso, pode haver aerossóis absorventes ou não absorventes que reduzem a RUV (KERR, 2005; KERR; FIOLETOV, 2008)

1.5.10 Dependência Angular da Radiação UV

A distribuição angular da RUV depende de muitos fatores, incluindo a claridade do céu, o SZA, comprimento de onda, albedo da superfície, a quantidade de ozônio na coluna e outros absorvedores gasosos e suas distribuições verticais. Em condições de céu limpo, a radiação vem diretamente do Sol, bem como difusamente do céu. Com nuvens horizontalmente uniformes, o componente difuso aumenta em relação ao componente direto. Com nuvens espalhadas ou quebradas, a dependência angular é exclusiva para um padrão de nuvem específico (KERR, 2005; KERR; FIOLETOV, 2008).

1.5.11 Efeitos combinados

A presença de mais de uma variável pode levar a interações não lineares envolvendo processos complexos de absorção e espalhamento. A presença de ozônio ou outro gás absorvente dentro de uma nuvem ou camada de aerossol geralmente resulta em mais atenuação do que a soma das atenuações individuais. Isso ocorre porque o comprimento do caminho da radiação que passa pelo absorvedor dentro da nuvem é aumentado pela dispersão múltipla dentro da nuvem. É mais proeminente sob nuvens cumulonimbus espessas, onde o ozônio total pode parecer aumentar para cerca de 1.000 DU (WARDLE *et al.*, 1997). No entanto, nuvens convectivas moderadas no verão podem levar a variações aparentes do ozônio total em cerca de 10% (KERR; DAVIS, 2007). Outra situação comum em que processos combinados podem resultar em um efeito complexo, é a presença de nuvens ou neblina sobre uma superfície de neve ou gelo de alto albedo (KROTKOV *et al.*, 2001). Em geral, esses efeitos combinados dependem de muitos parâmetros, como altura e distribuição vertical de nuvens, aerossóis e ozônio.

1.6 Trabalhos realizados no Brasil

O Brasil é uma das regiões de América do Sul com índices elevados de RUV e poucas localidades de monitoramento. Alguns trabalhos têm sido feitos para suprir esta demanda e caracterizar o comportamento desta radiação nas diferentes regiões do país.

Kirchhoff (2000) fez medições com biômetros para as estações de Blumenau (SC), Cachoeira Paulista (SP), Campo Grande (MS), Natal (RN), Porto Alegre (RS) e

Ribeirão Preto (SP) no Brasil, La Paz na Bolívia e Punta Arenas no Chile, no ano de 1999. Concluiu que uma marcada variação sazonal da RUV-B não é devida ao ozônio e sim ao ângulo solar zenital. Tal efeito implica em radiação mais intensa em menores latitudes; por exemplo, maior na região de Campo Grande e de Natal do que nas regiões de Cachoeira Paulista e de Porto Alegre.

Corrêa (2003) concluiu que as variações exercidas pelos aerossóis na radiação ultravioleta são menores do que aquelas relativas às variações do conteúdo de ozônio e da posição do disco solar, e que na cidade de São Paulo em dias de céu claro, durante o verão e partes do outono e primavera, a RUV atinge níveis considerados extremos. Além disso, foi notado que o alto número de casos de câncer de pele parece estar associado à distribuição étnica, com maior incidência nas regiões Sul e Sudeste onde se concentra a maior parte da população branca. Esse tipo de análise reforça a necessidade de uma maior atenção das autoridades quanto às deficiências nos serviços de informação e alertas à sociedade.

Andrade (2007) estimou a radiação solar ultravioleta horária no semiárido pernambucano a partir de códigos computacionais no SMARTS2. Os resultados das simulações mostraram um erro máximo de 6,4% para o meio dia solar, e um erro máximo entre 10 e 12% para 09 h e 15 h, respectivamente, quando comparados com os valores medidos com o piranômetro TUVR.

Coariti (2011) analisou os efeitos da radiação solar ultravioleta (RUV) em populações habitantes a diferentes altitudes e concluiu que a altitude é uma característica relevante, independentemente dos outros fatores ambientais, na observação de radiação ultravioleta extrema.

Silva *et al*. (2012) analisaram a radiação UV através de um modelo empírico que relaciona a RUV com a componente solar global sob diferentes condições do céu, notando que a maior contribuição para a variação anual dos totais diários de R-UV pode ser atribuída à nebulosidade e não à sazonalidade.

Lopo *et al*. (2013) realizaram um estudo na cidade de Natal sobre a variabilidade da RUV em relação ao ozônio total, aerossóis, radiação solar global e nebulosidade. Destacam que a intensidade da RUV no primeiro semestre do ano é mais intensa que no segundo, sendo neste último a maior concentração anual de ozônio total, e que a maior quantidade de aerossóis contribui em menor escala para este evento. Também indicaram que o ozônio total e aerossóis possuem uma forte correlação negativa com a RUV nos referidos meses.

Coariti (2017) determinou as características da Radiação Ultravioleta Solar e seus efeitos na saúde humana nas cidades de La Paz – Bolívia e Natal – Brasil, e recomenda realizar mais pesquisas que avaliem as interações entre o clima e a RUV, para estabelecer os fatores agravantes e atenuadores.

Teramoto *et al.* (2020) compararam quatro modelos empíricos considerados clássicos para a estimativa da radiação solar UV horária em Botucatu (SP) e concluíram que os métodos Redes Neurais Artificiais (RNA) e Máquina de Vetores de Suporte (MVS) geraram os melhores resultados utilizando um número menor de variáveis de entrada. Este último, considerado a melhor alternativa devido ao pequeno número de variáveis de entrada utilizadas e pela relativa acurácia.

2   MATERIAIS E MÉTODOS

Neste capítulo se abordam de forma breve a fonte de dados e principais métodos. Maiores detalhes sobre os procedimentos metodológicos adotados são descritos nos artigos apresentados no capítulo III.

2.1   Área de estudo

O Rio Grande do Sul é o estado mais meridional do Brasil, com fronteiras internacionais com a Argentina ao oeste e com o Uruguai ao sul. Sua superfície é de 281.707 km² e, com mais de 11,5 milhões de habitantes, é o quinto estado mais populoso do país. A região possui um clima subtropical úmido com grande variação sazonal com verões quentes e invernos frios e bem definidos. As temperaturas médias variam de 15 °C a 18 °C, com mínimas de até -10 °C (junho e julho) e máximas de até 40 °C (dezembro a março) (LIVI, 2002). A elevação da superfície varia do nível do mar até 1.200 m com os pontos mais altos no nordeste do estado.

Figura 5 – Mapa com a localização do Estado do Rio Grande do Sul, Brasil (contorno vermelho) e sua representação topográfica (direita).
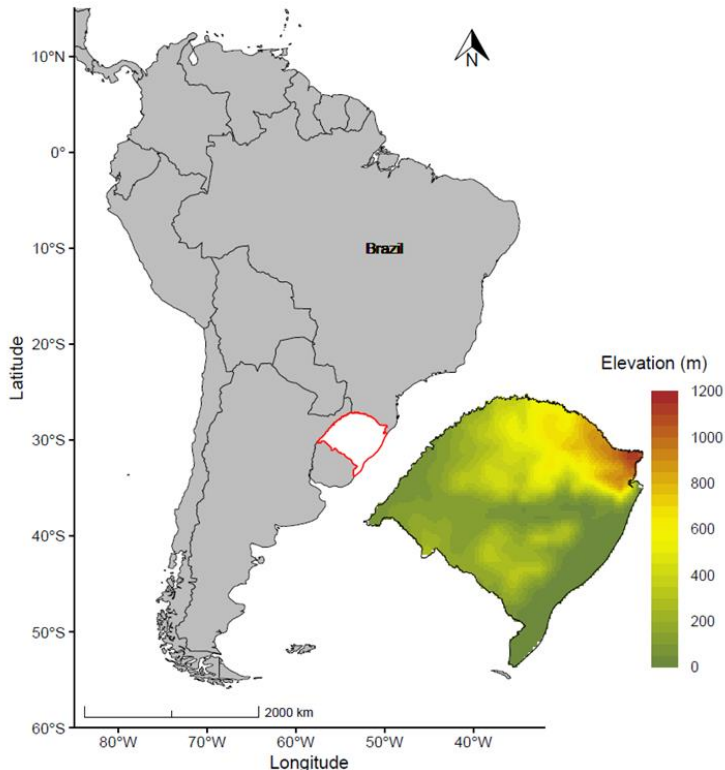
Fonte: Elaborado pelo autor.

2.2   Aquisição de dados

O monitoramento atmosférico tem sido tradicionalmente realizado *in situ,* obtendo-se assim uma visão parcial do papel que os seus diferentes constituintes desempenham na sua dinâmica. No entanto, ao ser complementados com sensoriamento remoto, pode-se compreender a dinâmica da atmosfera e seu impacto no clima, bem como a qualidade do ar local. Isto deve-se à versatilidade, quantidade e qualidade das informações obtidas através desta. Dados de sensoriamento remoto, ainda, oferecem informação sobre a estrutura atmosférica, sua composição e dinâmica, através da determinação das propriedades físicas e radiativas dos vários elementos que a constituem (LAHOZ *et al.*, 2012; DUNCAN *et al.*, 2014; NISPERUZA *et al.*, 2020). Para os artigos produzidos no marco desta tese, utilizamos dados de fontes tanto superficiais quanto do orbitais, descritos a seguir:

2.2.1   Dados superficiais

A Fundação Estadual de Proteção Ambiental (FEPAM), órgão do governo do estado do Rio Grande do Sul, é a instituição encarregada pelo monitoramento da qualidade do ar no estado, através de uma rede de estações automáticas. Estas análises são realizadas, automaticamente, por equipamentos que utilizam princípios físicos e químicos, no instante em que o ar é amostrado a cada hora. Os dados de concentração gerados (MP10, SO_2, NO_x, CO e O_3 e parâmetros meteorológicos), periodicamente são enviados a uma central, o que permite acompanhamento virtual da qualidade do ar e das condições meteorológicas, nos locais onde estão instaladas as estações de monitoramento. Possui estações fixas que se constituem de um container, dotado de equipamentos de análise, necessários e inerentes à sua área de abrangência, e mais estação móvel (trailer rebocável) para deslocamento aos locais de interesse não previstos pelas fixas (FEPAM, 2022). Para o desenvolvimento desta tese foram utilizados dados de NO_2 ao nível do solo, adquiridos por nove locais de monitoramento (Tabela 1).

Tabela 1 – Monitoramento diário (dias julianos) de NO_2 ao nível do solo em cada estação, durante o período de estudo.

	Canoas	Charqueadas	Esteio	Gravataí	Guaíba	Porto Alegre (Bombeiros)	Porto Alegre (Rodoviária)	Triunfo (DEPREC)	Triunfo (Petroquímico/ Móvel)
2006	337	0	340	0	0	0	89	0	0
2007	333	0	305	0	0	0	0	0	0
2008	324	0	0	0	0	0	0	0	0
2009	308	0	0	0	0	175	76	0	0
2010	53	0	0	0	0	0	0	0	0
2011	0	24	0	0	0	0	0	20	0
2012	0	0	0	0	0	0	0	0	0
2013	258	241	207	0	0	0	0	233	0
2014	0	295	328	0	166	0	0	285	0
2015	0	260	85	0	306	0	0	223	0
2016	281	284	220	191	342	0	0	239	64
2017	221	230	289	156	253	0	0	228	177
2018	304	216	286	243	339	0	0	133	129
2019	244	0	33	262	331	0	0	0	140

Fonte: Elaborado pelo autor.

2.2.2 Dados orbitais

O OMI (Ozone Monitoring Instrument) é um espectrômetro a bordo do satélite Aura que começou a coleta de dados em 2004, sendo uma contribuição do Programa Aeroespacial da Netherlands's Agency (NIVR) em colaboração com o Finnish Meteorological Institute (FMI) para a Missão Aura EOS, dando continuidade às medidas do Total Ozone Mapping Spectrometer (TOMS), do Global Ozone Monitoring Experiment (GOME) e Solar Backscatter Ultraviolet (SBUV), quando estes cessaram suas operações. Este instrumento faz a medição da quantidade de radiação solar que é dispersa pela atmosfera da Terra e pela sua superfície na faixa de faixas 264–504 nm, a partir de uma técnica chamada Backscatter Ultraviolet (BUV), que através de duas imagens faz mapeamento da luz ultravioleta emitida pelo Sol e retroespalhada pela atmosfera terrestre em direção ao satélite. O sensor observa vários comprimentos de onda para medir a capacidade de absorção das espécies atmosféricas O_3, NO_2, SO_2, BrO, HCHO e Aerossol. Além disso, como faz medições quase que em tempo real, disponibiliza medidas da pressão e da cobertura de nuvens, e pode mapear a distribuição global de radiação ultravioleta e suas tendências (OMI, 2022).

MERRA-2 (Modern-Era Retrospective analysis for Research and Applications): é uma reanálise atmosférica projetada para fornecer um conjunto de dados intermediário e uma ponte entre a primeira reanálise do MERRA (com dados desde 1980) e, seu objetivo de longo prazo é produzir: a) assimilação de observações de

aerossóis que podem interagir com processos radiativos atmosféricos; b) modificação no modelo atmosférico para conservar a massa atmosférica de ar seco mesmo com a análise de vapor d'água, permitindo um equilíbrio global entre evaporação e precipitação; c) uso de esfera cúbica para reduzir o efeito das singularidades do gridpoint no polo, permitindo melhor circulação polar; d) um modelo de transferência radiativa atualizado para permitir a assimilação de dados de muito mais instrumentos do que poderia ter sido incluído no MERRA; e) inclusão de novo forçamento observacional para o modelo de terra para fornecer processos de feedback de terra mais estáveis (GELARO *et al.*, 2017)

SRTM (Shuttle Radar Topography Mission): é um radar de abertura sintética, que no ano 2000 através da Administração Nacional de Aeronáutica e Espaço (NASA) e a Agência Nacional de Inteligência Geoespacial (NGA) criou o primeiro conjunto quase global de elevações de terra, necessários na elaboração de um Modelo Digital de Elevação (MDE) das terras continentais. Esta missão usou interferometria de passagem única, que adquiriu dois sinais ao mesmo tempo usando duas antenas de radar diferentes. Uma antena localizada a bordo do ônibus espacial coletou um conjunto de dados e o outro conjunto de dados foi coletado por uma antena localizada na extremidade de um mastro de 60 metros que se estendia do ônibus espacial. As diferenças entre os dois sinais permitiram o cálculo da elevação da superfície (USGS, 2022).

2.3 Métodos

Nesta tese, informações diárias de quinze anos (2006-2020) foram usadas para avaliar RUV, O_3 e NO_2, bem como variáveis meteorológicas conforme os objetivos traçados acima da área de estudo. Estas foram adquiridas através dos provedores de dados GES-DISC (https://urs.earthdata.nasa.gov), POWER (https://power.larc.nasa.gov/), Fundação Estadual de Proteção Ambiental (FEPAM); e reamostradas para 0,25º para ter uniformidade entre elas.

Para analisar a variação espaço-temporal, tendências e predições ao longo prazo na área de estudo, realizamos os seguintes cálculos:

- As médias foram calculadas usando os valores diários, como segue:

$$Var_{i=} \frac{\sum_{t}^{\substack{data\ inicial \\ data\ final}} Var_{i,t}}{n}$$ (Equação 1)

onde $\text{Var}i$ é a média da variável em cada pixel para o respectivo período; data de início e data de término correspondem à primeira e última data de cada período; n é o número de dias no período.

- As mudanças percentuais espaço-temporais foram calculados usando diferenças entre suas médias, como segue:

$$P = \frac{(C_2 - C_1)}{C_1} \times 100\%$$ (Equação 2)

onde P é a variação percentual entre diferentes períodos, $C1$ é a concentração média do período anterior, $C2$ é a média do último período.

- Coeficiente de variação (CV), que é uma medida estatística da dispersão de pontos de dados em uma série de dados em torno da média, expresso como:

$$CV = \frac{\sigma}{\mu} * 100$$ (Equação 3)

- A tendência espaço-temporal foi determinada usando o teste de Mann-Kendall (indica tendência) e o Theil-Sen (indica a magnitude) (MANN, 1945; KENDALL, 1975), da seguinte forma:

$$Q = \frac{EDD_i - EDD_j}{T_i - T_j}$$ (Equação 4)

onde EDDi e EDDj indicam os valores de dados sequenciais da série temporal no ano Ti e Tj, respectivamente, com j > i. O Q calculado é a magnitude estimada da inclinação da tendência na série temporal dos dados, onde valores negativos indicam uma tendência de queda e valores positivos indicam uma tendência de alta.

- As predições espaço-temporais foram baseadas no modelo de aprendizado de máquina Random Forest (BREIMAN, 2001) que combinam dados de várias plataformas. Este é um modelo não linear simples, que requer menos recursos computacionais e possui capacidades de interpretação mais fortes; além disso, é menos propenso a sobrestimar e menos sensível a outliers (PAN *et al.*, 2021).

- Finalmente, percentis, coeficientes de correlação e correlação parcial com nível de significância estatística α≤ 0,05 foram derivados para estimar a relação entre as variáveis.

3 RESULTADOS E DISCUSSÕES

3.1 Artigo 1: Partial COVID-19 lockdown effect in atmospheric pollutants and indirect impact in UV radiation in Rio Grande do Sul, Brazil.

Artigo aceito na Revista Atmósfera— Universidad Nacional Autónoma de México

Partial COVID-19 lockdown effect in atmospheric pollutants and indirect impact in UV radiation in Rio Grande do Sul, Brazil

Adriana Becerra-Rondón [1]*, Jorge Ducati [1] and Rafael Haag [2]

[1] *Centro Estadual de Pesquisas em Sensoriamento Remoto e Meteorologia, Universidade Federal do Rio Grande do Sul, Av. Bento Gonçalves, 9500, Porto Alegre, RS, Brazil.*

[2] *Universidade Estadual do Rio Grande do Sul, Av. Bento Gonçalves, 8855, Porto Alegre, RS, Brazil.*

* Corresponding author: abecerrarondon@gmail.com

Partial COVID-19 lockdown effect in atmospheric pollutants and UV

HIGHLIGHTS

- Up to 33.9% decrease of NO_2 was observed for 2020 in relation to 2019.
- Up to 3.5% increase of total O_3 was observed for 2020 in relation to 2019.
- Up to 4.8% increase of UV index was observed for 2020 in relation to 2019.

GRAPHICAL ABSTRACT
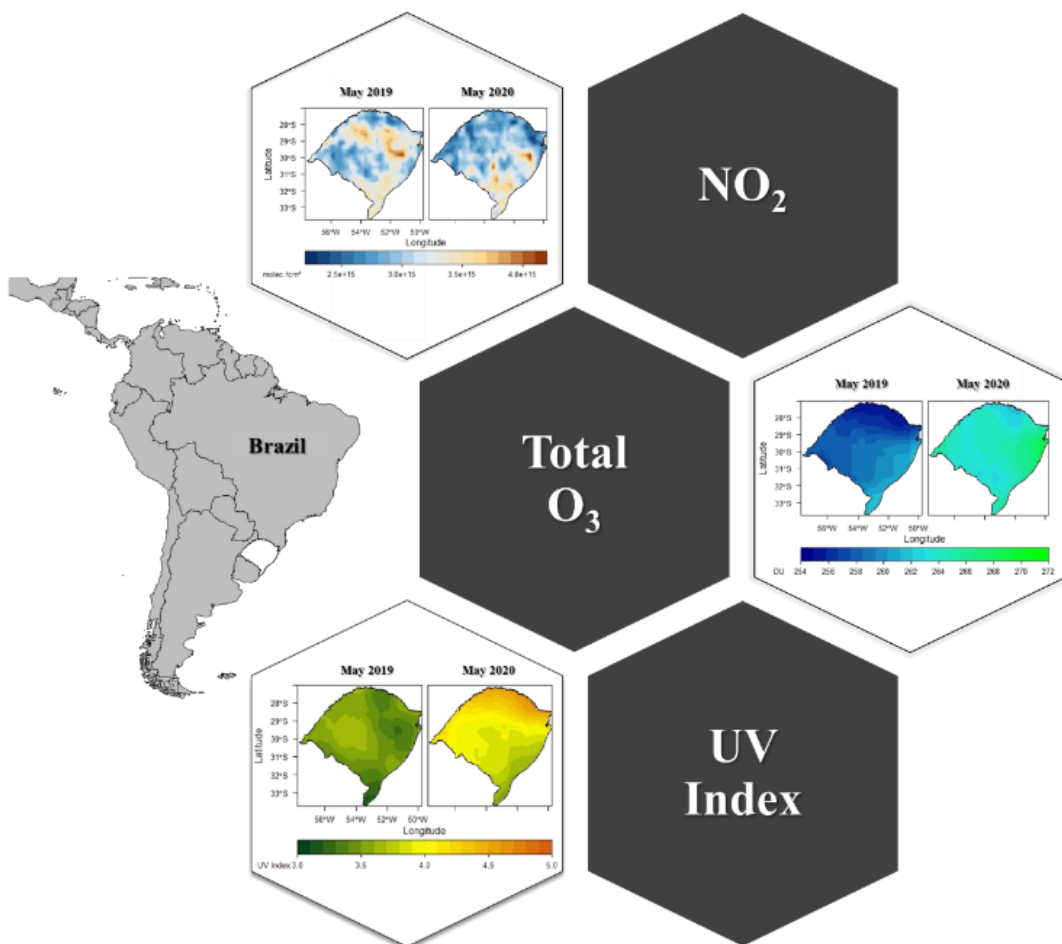
RESUMEN

La pandemia de COVID-19 redujo notablemente las actividades industriales y otras intervenciones antrópicas sobre el ambiente, lo cual disminuyó la emisión de gases contaminantes y aerosoles. El monitoreo de la calidad del aire comúnmente es desempeñado por estaciones automatizadas, las cuales proporcionan información precisa casi en tiempo real; no obstante, estas están sujetas a problemas de mantenimiento y no permiten alcanzar una cobertura total de grandes áreas geográficas. Alternativamente, los sensores orbitales proporcionan información detallada para grandes áreas a bajo costo. En consecuencia, este estudio tuvo por objeto analizar el efecto del cese parcial de actividades por la COVID-19 sobre los contaminantes atmosféricos y su impacto indirecto sobre la radicación UV en Rio Grande do Sul, Brasil. Analizamos la concentración de dióxido de nitrógeno (NO_2), ozono total (O_3) e índice ultravioleta (UVI) adquiridos por el sensor OMI (a bordo del satélite Aura), durante mayo, para los períodos de 2010 a 2018, 2019 y 2020. Calculamos las diferencias durante estas tres series temporales. Los resultados mostraron reducciones de hasta 33,9% del NO_2 en la mayor parte del área de estudio, acompañadas de incrementos de hasta 3,5% en el ozono total y hasta 4,8% en el UVI. Aunque el NO_2 desempeña un rol fundamental en la química estratosférica, nuestros resultados sugieren que su disminución en 2020 no tuvo incidencia directa en el incremento de O_3; sin embargo, el NO_2 fue en parte responsable del incremento en el UVI, que a su vez provocó calentamiento en la estratósfera y aumento del O_3.

ABSTRACT

The COVID-19 pandemic introduced a significant decrease in industrial activities and other anthropic interventions on the environment, followed by a reduction of the emission of pollutant gases and aerosols. Monitoring of air quality is commonly performed through automatic stations, which can provide nearly real-time, accurate information. However, stations located in urban areas are subject to maintenance problems and extensive coverage for large areas is not feasible. As an alternative approach, data from orbital sensors can provide useful information for large areas at a low cost. Consequently, this study aimed to analyze the partial COVID-19 lockdown effect in atmospheric pollutants and indirect impact in UV radiation in Rio Grande do Sul, Brazil. Data on concentrations of nitrogen dioxide (NO_2), total ozone (O_3), and ultraviolet index (UVI) acquired by the OMI sensor aboard the Aura satellite were

accessed for May, for the entire period 2010 to 2018, 2019, and 2020. Differences between these time series were calculated. Results showed significant reductions in nitrogen dioxide in most of the study area by as much as 33.9%, followed by increases in total ozone of up to 3.5% and the ultraviolet index by up to 4.8%. Although NO_2 plays a fundamental role in stratospheric chemistry, our results suggest that its decrease in 2020 was not directly responsible for the increase in total O_3; however, NO_2 was partially the cause for the increase in UVI, which in turn led to the heating of the stratosphere, generating an increase in ozone.

Keywords: OMI sensor, ultraviolet index, total ozone, nitrogen dioxide, southern Brazil.

1. Introduction

Ultraviolet (UV) radiation from 100 to 400 nm constitutes about 8% of the electromagnetic radiation emitted by the Sun (Robinson, 1966; Andrade and Tiba, 2016), whereas the proportion which reaches the ground at Earth is reduced to 4% due to physical processes in the atmosphere and to additional—geographical, temporal, astronomical and others—factors (Iqbal, 1983; Huffman, 1992; Guarnieri et al., 2004; Silva et al., 2008; Fountoulakis et al., 2020). Its intensity is frequently expressed on a time basis by the Ultraviolet Index (UVI) through a dimensionless numerical scale (WHO, 2002; WMO, 2011). Despite this sharp reduction, the UV radiation reaching the ground still has the potential to induce significant damages to the primary productivity and aquatic organisms (Cardoso, 2011), in the yield of forest and crops (Caldwell et al., 2003), on the survival of amphibians as environmental indicators (Tiegte et al., 2007), while increasing the degradation of some materials and inducing alterations in photochemical reactions linked to tropospheric urban pollution (Davis and Sims, 1983). UV radiation is also known to have negative impacts on human skin, eyes, and immune system (Rodriguez, 2017). Therefore, the knowledge of UV spatio-temporal variability has received considerable attention from research projects (Bais et al., 2007; Kerr and Fioletov, 2008).

The main parameter modulating ultraviolet absorption is stratospheric ozone (90% of total O_3), which presents a seasonal pattern due to natural processes of formation, transport, and destruction; ozone concentrations are at their lowest levels in Fall and highest in Spring (Wakamatsu et al., 1989; André et al., 2003). However, this variability is influenced by natural phenomena and anthropogenic activities (Fahey and Hegglin,

2011; Bais et al., 2015), the latter being linked to the industrial production of nitrogen dioxide (NO_2) formed from the oxidation of nitrous oxide (N_2O) coming from the troposphere. NO_2 can attain high concentrations in the stratosphere (90% of all NO_2), where it destroys O_3 through catalytic processes by sequestering active radicals (Seinfeld and Pandis, 1998).

Changes in natural processes and phenomena, amplified or caused by human actions, can generate potential hazards both to human communities and to the environment (Cheval et al., 2020). A notable change started in the end of 2019 with the unexpected outbreak of coronavirus disease (COVID-19), later declared a "global pandemic" by the World Health Organization (WHO) in the first semester of 2020. This disease has been reported in almost all geographic areas and climatic conditions, with a great impact on both economies and environments. Zambrano-Monserrate et al., (2020) mention that the indirect impact of the pandemic on the environment has been little analyzed, and estimate that negative indirect effects would be greater than positive. Thus, studies that evaluate these impacts and how they are linked to infection and death rates are increasingly urgent and necessary to inform decision-makers at all levels (Liu et al., 2021; Paital and Agrawal, 2021; Travaglio et al., 2021; Vasquez-Apestegui et al., 2021).

Against the COVID-19 crisis, global drastic actions were taken by the majority of nations aiming to slow disease propagation. These actions had as collateral effects a significant global reduction of consumption of fossil fuels and decrease of levels of NO_2 and other atmospheric pollutants by 20 to 50%, facts that improved air quality (Tobias et al., 2020; Sharma et al., 2020; Zheng et al., 2020). South America is one of the regions most affected by COVID-19 (Zhu et al., 2020), and in Brazil restrictions on most activities started in March; as a result, drastic reductions in NO (up to 77.3%), NO_2 (up to 54.3%) and CO (up to 64.8%) were reported in São Paulo State, for the five-year monthly mean and the four-week period prior to the restrictions. On the other hand, ozone concentrations increased by 30%, possibly related to the decrease in nitrogen monoxide (Nakada and Urban, 2020; Siciliano et al., 2020).

In the state of Rio Grande do Sul a partial lockdown was declared (starting March 16 and extending for several months), with public and private recreational areas and educational centers, besides commerce in general (except food and medicine) being closed. Land transport had a 40% reduction, air transport 90%, and use of private vehicles was significantly reduced; however, industrial activities, health, and basic

services were not suspended (Ubiratan, 2020; Google, 2021). This scenario offers an opportunity to evaluate variations and trends of atmospheric physical processes over an area exposed to high levels of ultraviolet radiation for being close to the Antarctic ozone hole (Kirchhoff et al., 2000; Guarnieri et al., 2004).

Remote sensing provides a cost-effective method to estimate many variables from regional to global scales. A large set of data on the atmosphere is continuously acquired and generated by a combination of satellite radiance measurements and radiative transfer models, providing spatial and temporal information under widely different atmospheric conditions. The accuracy of the models is limited mostly by uncertainties in input parameters representing the atmosphere and the Earth's surface, a limitation that is mitigated by the combined use of ground-based monitoring and information of satellite sensors. With the increasing use of satellite images, improvements in algorithms have been implemented to offer expeditious, accurate information over changes in air quality and their human impacts (Bais et al., 2007; Liu et al., 2016; Mostafa et al., 2021).

Catalytic agents like NO_2 have an important role in atmospheric chemistry related to ozone formation and destruction, ozone being the main vector to absorption of UV reaching the planet's surface. In the recent context of reduction of activities due to the pandemics, emissions of greenhouse gases had fallen to levels not reported since World War II (Global Carbon Project, 2020). Monitoring these changes by conventional ground-level stations provide near-surface information, which however has spatial resolution limited by the surface density of stations; this limitation presently can be mitigated by data acquired by satellite remote sensing, which provides data with large spatial cover and capability to detect spatio-temporal changes of several atmospheric pollutants and UV processes (Liu et al., 2016). Given that, presently, a series of sensors in Earth orbit display capabilities to detect several atmospheric pollutants and UV processes, the objective of this paper was to analyze the partial COVID-19 lockdown effect on atmospheric pollutants and its indirect impact on UV radiation in Rio Grande do Sul. To this end, our analysis will be based on widely available data on the atmosphere, acquired from orbital sensors.

2. Material and methods

2.1 Study area

Rio Grande do Sul is the Brazilian southernmost state, having international borders with Argentina to the West and with Uruguay to the South. Its area is 281,707 km², and with more than 11 million inhabitants it is the fifth most populated state in the country. The capital is Porto Alegre; its metropolitan area concentrates an important fraction of the State's population and economic activities. Regarding the consumption of fossil fuels, the State has about 7.1 million vehicles (IBGE, 2019). The region has a humid subtropical climate with a large seasonal variation with hot summers and well-defined, cold winters. Mean temperatures vary from 15 to 18°C, with lows of as much as -10°C (June and July) and highs going up to 40°C (December to March) (Livi, 2002).

2.2. Satellite observations

This research was performed from data acquired by the sensor OMI (Ozone Monitoring Instrument) aboard satellite Aura. This instrument is equipped with a spectrometer pointed to the nadir which measures the ultraviolet light (264–504 nm) coming from the Sun and back-scattered by the atmosphere. The algorithms Differential Optical Absorption Spectroscopy (DOAS) and Total Ozone Mapping Spectrometer (TOMS) were developed to derive several products (Levelt et al., 2006), of which we used nitrogen dioxide (OMNO2d), total ozone (OMTO3d), and ultraviolet index (OMUVBd) (Krotkov et al., 2006; Tanskanen et al., 2006).

For product OMNO2d (total column density) the data is provided in molecules/cm^2, a spatial resolution of 0.25º × 0.25º (Lat/Lon), and with a daily frequency; also daily, but with 1.0º x 1.0º (Lat/Lon) spatial resolution and Dobson Units (where 1 DU = 2.7 x 10^{18} molecules O_3/cm^3) for product OMTO3d (total column density), and in a non-dimensional scale for product OMUVBd (intensity at local solar noon).

Since restrictions to social mobility started in March and considering that after two months environmental changes would be well-established, we selected May as our period of assessment. A time series of eleven years (2010–2020) with 1003 images with daily measurements (97% of the series) was acquired from the data provider GES-DISC (NASA, 2020). Processing was performed using free software RStudio, and the spatial resolution of products OMUVBd and OMTO3d was resampled to 0.25º to have uniformity with product OMNO2d. For this 0.25º resolution, the study area is covered by 420 cells.

2.3. Data analysis

To evaluate the behavior of these variables in this unique scenario, we selected three different periods: 2010 to 2018 (long-term trend), 2019 (period prior to the partial lockdown scenario), and 2020 (partial lockdown scenario). For each product, we calculated the average per cell for all 420 cells of the study area, for May, in these three periods. The averages were calculated using the daily values for each of these periods, as follows:

$$Var_{i=} \frac{\sum_t {}_{end\ date}^{start\ date} Var_{i,t}}{n} \tag{1}$$

where *Var$_i$* is the average of the variable in each cell for the respective period; start date and end date correspond to the first and last date of each period; *n* is the number of days in the period.

To assess spatio-temporal percentage changes of variables in May 2020 in relation to previous periods, we calculated differences between their means. From these differences, we calculated the percentages of variation by dividing them by the mean of each period prior to the pandemics:

$$P = \frac{(C_2 - C_1)}{C_1} \times 100\% \tag{2}$$

where *P* is percentage change between different periods, C_1 is the mean concentration of the previous period, C_2 is the average of the latter period.

Finally, Pearson correlation coefficients were derived to estimate the relation of nitrogen dioxide with total ozone and the ultraviolet index, taking as values to be compared the measured concentrations or index in the 420 cells covering the State.

3. Results

Table I. Results for May for the Ultraviolet Index, nitrogen dioxide and total ozone for Rio Grande do Sul State, Brazil, with respect to the historical mean for 2010 to 2018, mean for 2019, and mean for 2020.

	UV Index	NO$_2$ (10^{15} molec./cm^2)	Total O$_3$ (DU)
Mean 2010 to 2018	3.64	3.06	267
Mean 2019	3.49	3.18	258
Mean 2020	4.02	3.02	264

Table I presents the averages for May in the years 2010 to 2018, 2019, and 2020. Taking 2020 as reference, and for NO$_2$, a drop of 1.30% was observed with respect to the historical mean derived for the 2010 to 2018 period; compared with 2019, 2020

displays a decrease of 5.03% in NO_2. Now considering total O_3, in 2020 a drop of 1.12% was observed with respect to the historical mean for 2010 to 2018, but if compared only with 2019, 2020 shows an increase of 2.32% in total O_3. For the ultraviolet index (UVI), an increase of 10.43% was observed in 2020 compared to the 2010–2018 time series, and of 15.18% compared with 2019.
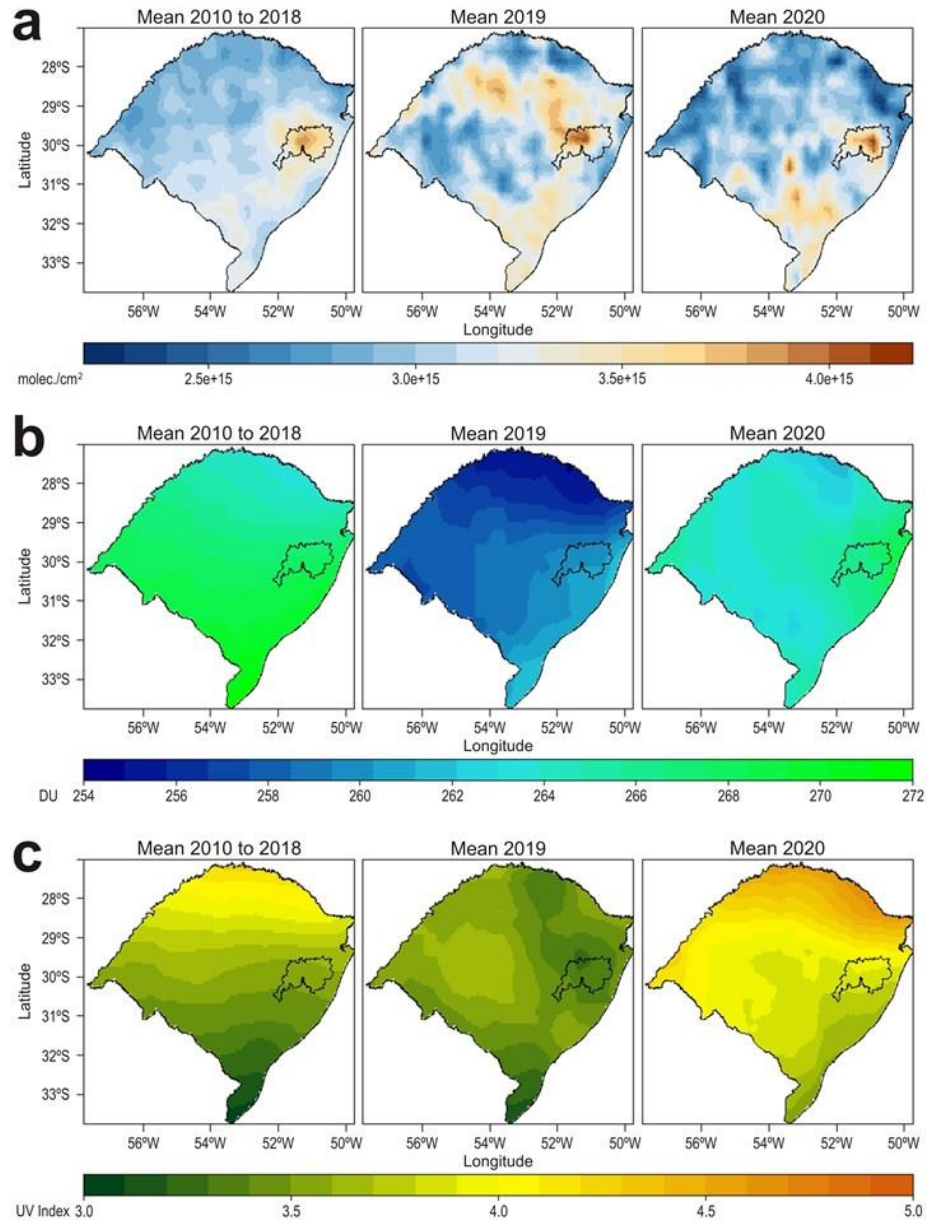
Fig. 1. Spatio-temporal variability of the studied variables for Rio Grande do Sul State, Brazil. a) NO_2; b) total O_3; c) Ultraviolet Index. The metropolitan area of the State capital is highlighted.

Figure 1b presents results for total O_3, where it is possible to observe a gradient in latitude, with this variable decreasing southward. Maximum and minimum averages were 271 and 263 DU for 2010-2018; 262 and 255 (2019); and 269 and 262 (2020). In

Figure 1c we present results for the ultraviolet index; again, there is a gradient in latitude, but inversely if compared with O_3, since now UVI decreases northwards. Values for UVI are 4.25 and 3.06 (2010–2018); 3.69 and 3.15 (2019); and 4.64 and 3.55 (2020).
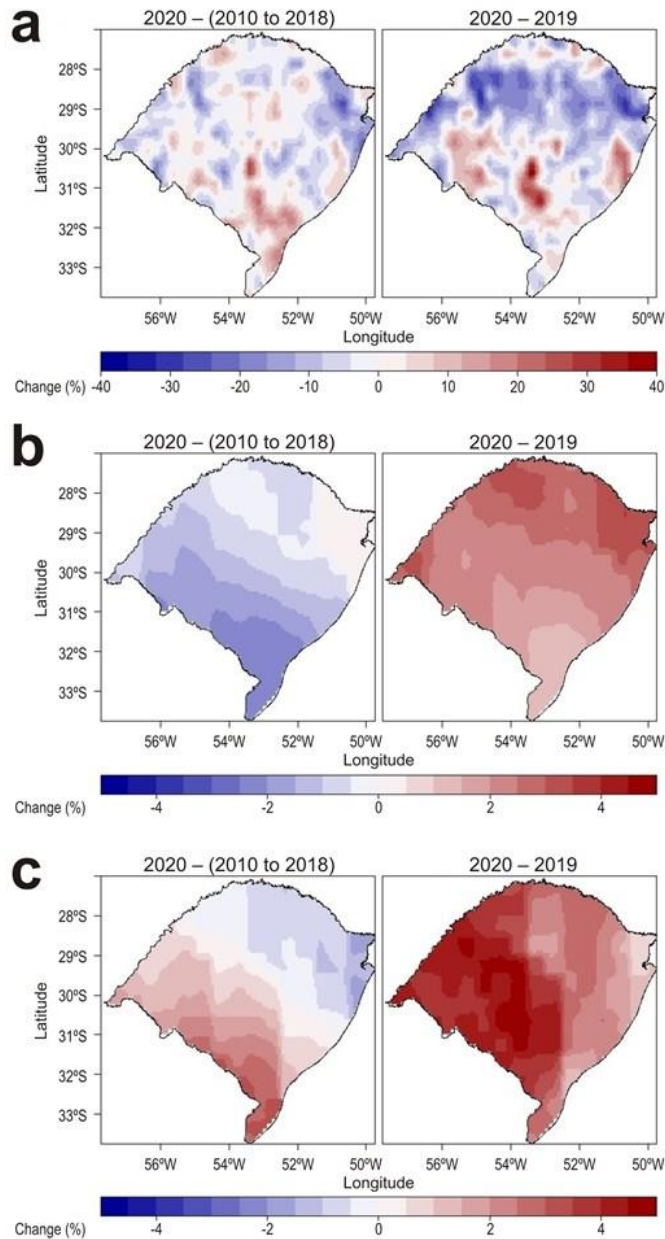
Fig. 2. Spatio-temporal variability of the studied variables for Rio Grande do Sul State, Brazil, in the sense 2020 *minus* the indicated period. a) NO_2; b) total O_3; c) Ultraviolet Index.

Figure 2 presents the variation of the studied variables, taking 2020 as reference. Figure 2a is for NO_2. Compared with the time series 2010–2018, we can see that in 55.5% of the studied area values of NO_2 dropped, being lower in amounts up to 28.7%. In the remaining area, the increase of NO_2 was up to 30.9%. However, compared with

2019, 2020 showed decreasing NO_2 in 66.4% of the State area, by amounts up to 33.9%, while in the remaining area increases up to 45.4% in NO_2 were observed.

Figure 2b presents results for total O_3. Compared with the time series 2010–2018, in 2020 total O_3 dropped as much as 0.5% in 89.6% of the studied area; in the remaining 10.4% of the State, total O_3 increased as much as 2.5%. However, when compared with 2019, it was observed that in 2020 total O_3 increased in all studied cells by values up to 3.5%.

Figure 2c presents results for the ultraviolet index. Compared with the time series 2010–2018, in 2020 UVI increased in 60.5% of the area, by values up to 3.3%, while in the remaining cells UVI was up to 1.7% smaller. Compared with 2019, in 2020 100% of the cells had increased UVI in values up to 4.8%.

Figures 3 present correlations of NO_2 with ultraviolet index and total ozone for the studied periods taking the whole set of 420 cells covering the State.
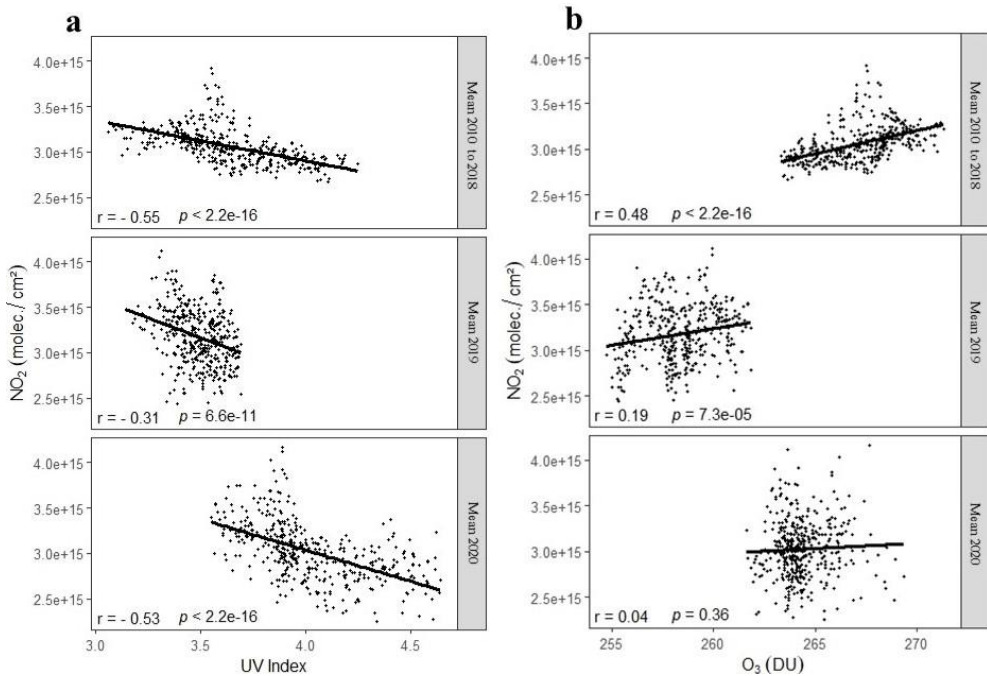
Fig. 3. Correlations of averages of NO_2 to: a) Ultraviolet Index; b) Ozone, for Rio Grande do Sul State, Brazil. In each box, the coefficient of correlation *r* and the *p*-value are provided.

4. Discussion

Air pollution represents a significant risk to both health and the environment, with nitrogen dioxide (NO_2) being one of the key pollutants, reacting with other chemicals to generate acid rain, which is harmful to the ecosystem. Its concentration level is

influenced by complex variables such as wind, temperature, burning material, besides policies and other anthropogenic factors of each city (Wang and Su, 2020; Liu et al., 2021). According to the World Health Organization (WHO), current levels of NO_2 should be 40 µg/m^3 for the annual mean and 200 µg/m^3 for the one-hour mean (WHO, 2005). In Brazil, regulated levels are higher, with 60 µg/m^3 for the annual average and 260 µg/m^3 for the one-hour average (CONAMA, 2018). However, for the state of Rio Grande do Sul, the recommended levels are equal to those stipulated by the WHO (FEPAM, 2019).

During the pandemic, this pollutant received wide attention from the international community, since partial lockdown measures promoted the decrease of the main sources of NO_2. According to the State Environmental Protection Foundation of Rio Grande do Sul, the concentration of NO_2 in the surface during the first months (January to May) of this extreme event was within the recommended limits and did not show a significant reduction or alteration of the levels concerning the previous years; this was due to the location of the stations (in just five cities) outside the urban center and the possible influence of emissions of industrial facilities that could have remained in operation in the places where the monitoring was being carried out (FEPAM, 2020).

Our results from satellite data suggest significant changes in NO_2 emissions by May 2020; these were reduced in more than half of the State area by 28.7 to 33.9% depending on the considered period, changes which point to a temporary improvement of air quality. Such decreases in NO_2 emissions are in agreement with recent reports of variations from 20 to 54.3% in several countries (Muhammad et al., 2020; Nakada and Urban, 2020; Siciliano et al., 2020; Sharma et al., 2020; Tobias et al., 2020; Wang and Su, 2020; Zheng et al., 2020). This temporary reduction of NO_2 emissions in a short period is important even when the largest emitter of pollution (diesel transport) has continued to contribute on a smaller scale. However, Wang and Su (2020) mention that in the long run, a rebound in air pollutants is inevitable.

Discrepancies between ground measurements and satellite data do exist, mainly because ground stations, which are few and not evenly distributed, monitor the daily maximum concentrations from one-hour averages near the surface, while the satellite data recover the daily density of the NO_2 column measured for the whole area. Therefore, units from these two sources are different and orbital data is not comparable with the recommended national and international levels (Liu et al., 2021). In this context our work, being carried out from satellite data, only allows us to detect changes over

time, to understand the impact of the partial lockdown on air pollution and various related factors in areas that have not yet been quantitatively considered.

Regarding total O_3, which increased from 2.5 to 3.5%, and UVI, which increased from 3.3 to 4.8%, it is to be noted that these increases in May 2020 are in contrast with expected drops in total O_3 in epochs corresponding to May due to secondary effects in the Antarctic ozone hole, and a similar decrease in UVI due to a lower zenith solar angle, larger cloudiness and temperature drops between April and August in South America (Kirchhoff et al., 1996; Guarnieri et al., 2004; Kerr and Fioletov, 2008; Salgado et al., 2010; Schmalfuss et al., 2014; Nunes, 2017). These two variables used to have a well-defined pattern in May, but in May 2020, compared to May 2019, increases were observed in 100% of the State area. We note that, although both NO_2 and total O_3 changed in 2020, these alterations were not spatially correlated: as it can be seen in Figure 3b for the year 2020, from a cell-to-cell basis there is no significant correlation between these two variables. Only for a longer time series (2010 to 2018), some significant correlation is suggested.

In contrast with the weak or non-existent correlation between NO_2 and total O_3, Figure 3a shows significant, inverse correlations between NO_2 and the ultraviolet Index, especially for the 2010 to 2018 time series and for 2020.

Atmospheric processes involving ultraviolet radiation act in a complex form. In the stratosphere, UV radiation participates in the Chapman Cycle, being significantly absorbed at 310 nm and with decreasing intensity up to 345 nm (Kirchhoff et al., 2000; Koronakis et al., 2002). Simultaneously, nitrogen dioxide NO_2, generated by oxidation of nitrous oxide N_2O transported from the troposphere, acts in a catalytic form destroying O_3 and suppressing its loss through other catalytic mechanisms sequestering free radicals (Seinfeld and Pandis, 1998). However, in the troposphere, the UV radiation acts in photochemical reactions of several pollutants, the rates of these reactions being dependent on the concentrations of stratospheric ozone, natural and anthropogenic aerosol particles, and cloudiness (Chubarova, 2006). Even at low concentrations, tropospheric gases and particles have an effect on UV similar to their stratospheric counterparts; this is due to higher absorption in the UV interval at lower altitudes (Chubarova, 2006; Barnard and Wenny, 2010). Particulate material like black carbon is generated in most combustion processes, and its action in light extinction leads to a decrease in transmission of ultraviolet (Barnard and Wenny, 2010). Therefore, in polluted-atmosphere conditions, the UV intensity can decrease by up to

15% in areas of anthropic activity (Koronakis et al., 2002; Chubarova, 2004; Barnard and Wenny, 2010); low pollutant concentrations lead to higher UVI, which in turn leads to stratospheric warming and an influx from the lower atmosphere of ozone-enriched air (WMO, 2020).

Even though NO_2 has a crucial role in atmospheric chemistry, its decrease in 2020 was not correlated with the total O_3 increase (r = -0.04 in Fig. 3b). However, NO_2 correlated negatively with UVI (r = -0.53 in Fig. 3a). This suggests that, in opposition to the well-known adverse effects of atmospheric pollutants, in certain aspects, they have an apparently beneficial effect in reducing the ultraviolet flux on the surface.

5. Conclusions

Air pollutant concentrations are influenced by variables as wind, temperature, burning materials, and other anthropic factors. In this paper, we looked for the effects of the slowing of human activities (e.g., vehicular traffic, industrial complex, and mining activities) on atmospheric parameters. This was done by the sole use of remote sensing data, a resource that is widely available and covers large areas. It was shown that the slowing of activities in 2020 leads to a reduction in nitrogen dioxide emissions (up to 33.9 %), and increased levels of total ozone (up to 3.5 %), and the ultraviolet index (up to 4.8 %). This simultaneous increase in ozone and ultraviolet suggests that ozone is not the only factor influencing the ultraviolet radiation at the surface, and future monitoring actions may have to look for other factors. We would cite these findings, which add to the mounting evidence linking NO_2 to total O_3 and UVI, as the main contribution of this research.

This work generated some perceptions: First of all, about the magnitude of the impact of human activity on the environment, where this impact is extended well beyond urban areas. This impact is not sustainable, but a discussion on its nature, be it positive or negative, was not part of the aims of this work. Second, initiatives taken by the authorities, eventually supported by the population, can be effective to change the environmental profile in large areas, being therefore potentially and equally effective in the effort against the disease spread. Finally, we hope that in the medium-long term this assessment can be helpful to decision-makers, in their actions to improve policies that promote a balance between economic growth, air pollution, and health.

References

André IRN, Ferreira NJ, Conforte JC. 2003. Análise do comportamento do ozônio estratosférico na América do Sul e vizinhanças utilizando-se imagens do satélite NIMBUS7/TOMS. In: Anais do XI Simpósio Brasileiro de Sensoriamento Remoto. Belo Horizonte. 1117–1124.

Andrade RC, Tiba C. 2016. Extreme global solar irradiance due to cloud enhancement in northeastern Brazil. Renewable Energy 86: 1433–1441. https://doi.org/10.1016/j.renene.2015.09.012

Bais AF, Lubin D, Arola A, Bernhard G, Blumthaler M, Chubarova N, Erlick C, Gies HP, Krotkov NA, Lantz K, Mayer B, Mckenzie RL, Piacentini RD, Seckmeyer G, Slusser JR, Zerefos CS. 2007. Surface ultraviolet radiation: past, present, and future. In: Scientific assessment of ozone depletion: 2006. Geneva: World Meteorological Organization, 21.

Bais AF, Mckenzie RL, Bernhard G, Aucamp PJ, Ilyas M, Madronich S, Tourpali K. 2015. Ozone depletion and climate change: impacts on UV radiation. Photochemical & Photobiological Sciences 14: 19–52. https://doi.org/10.1039/C4PP90032D

Barnard WF, Wenny BN. 2010. Ultraviolet radiation and its interaction with air pollution. In: Gao W, Slusser JR, Schmoldt DL, eds. UV Radiation in Global Climate Change. Berlin: Springer, 291–330. https://doi.org/10.1007/978-3-642-03313-1_11

Caldwell MM, Ballaré CL, Bornman JF, Flint SD, Björn LO, Teramura AH, Kulandaivelu G, Tevini M. 2003. Terrestrial ecosystems, increased solar ultraviolet radiation and interactions with other climatic change factors. Photochemical & Photobiological Sciences 2: 29–38. https://doi.org/10.1039/B211159B

Cardoso VM. 2011. Efeitos da radiação ultravioleta-A e ultravioleta-B sobre os embriões do camarão de água-doce Macrobrachium olfersii (Crustacea, Decapoda) e o papel da radiação ultravioleta-A na fotorreativação. Master's thesis, Federal University of Santa Catarina.

Cheval S, Mihai-Adamescu C, Georgiadis T, Herrnegger M, Piticar A, Legates DR. 2020. Observed and potential impacts of the COVID-19 pandemic on the environment. International Journal of Environmental Research and Public Health 17: 4140. https://doi.org/10.3390/ijerph17114140

Chubarova NE. 2004. Influence of aerosol and atmospheric gases on ultraviolet radiation in different optical conditions including smoky mist of 2002. Doklady Earth Sciences 394: 62–67.

Chubarova NE. 2006. Role of tropospheric gases in the absorption of UV radiation. Doklady Earth Sciences 407: 294–297. https://doi.org/10.1134/S1028334X06020322

Coariti JR. 2017. Características da Radiação Ultravioleta Solar e seus efeitos na saúde humana nas cidades de La Paz – Bolívia e Natal – Brasil. Doctoral thesis, Federal University of Rio Grande do Norte.

CONAMA (Conselho Nacional do Meio Ambiente). 2018. Padrões de Qualidade do Ar (Resolução nº 491/2018). Diário Oficial da União 223: 155–156.

Davis A, Sims D. 1983. Weathering of Polymers. London: Applied Science Publishers.

Fahey DW, Hegglin MI. 2011. Twenty questions and answers about the ozone layer: 2010 update. In: Scientific Assessment of Ozone Depletion, 2010. Global Ozone Research and Monitoring Project—Report. Geneva: World Meteorological Organization, 52.

FEPAM (Fundação Estadual de Proteção Ambiental Henrique Luis Roessler). 2019. Rede estadual de monitoramento automático da qualidade do ar. Available at http://www.fepam.rs.gov.br/qualidade/relatorios.asp (accessed 2021 March 19).

FEPAM (Fundação Estadual de Proteção Ambiental Henrique Luis Roessler). 2020. Efeito do isolamento Covid−19 na qualidade do ar. Available at http://www.fepam.rs.gov.br/qualidade/relatorios.asp (accessed 2021 March 19).

Fountoulakis I, Diémoz H, Siani A-M, Laschewski G, Filippa G, Arola A, Bais AF, De Backer H, Lakkala K, Webb AR, De Bock V, Karppinen T, Garane K, Kapsomenakis J, Koukouli M-E, Zerefos CS. 2020. Solar UV Irradiance in a changing climate:

trends in Europe and the significance of spectral monitoring in Italy. Environments 7, 1. https://doi.org/10.3390/environments7010001

Global Carbon Project. 2020. Available at https://www.globalcarbonproject.org/carbonbudget/index.htm (accessed 2020 April 4).

Google. 2020. COVID-19 Community Mobility Report. Available at https://www.google.com/covid19/mobility?hl=en (accessed 21 March 2021).

Guarnieri RA, Guarnieri FL, Contreira DB, Padilha LF, Echer E, Pinheiro DK, Schuch AMP, Makita K, Schuch NJ. 2004. Ozone and UV-B radiation anticorrelations at fixed solar zenith angles in southern Brazil. Geofísica Internacional 43: 17–22. https://doi.org/10.22201/igeof.00167169p.2004.43.1.209

Huffman RE. 1992. Atmospheric ultraviolet remote sensing. California: Academic Press.

IBGE (Instituto Brasileiro de Geografia e Estatística). 2019. Cidades. Rio Grande do Sul. Available at http://www.cidades.ibge.gov.br (accessed 2020 August 10).

Iqbal M, 1983. An introduction to solar radiation. Toronto, New York, London: Academic Press.

Kerr JB, Fioletov VE. 2008. Surface ultraviolet radiation. Atmosphere-Ocean 46: 159–184. https://doi.org/10.3137/ao.460108

Kirchhoff VWJH, Schuch NJ, Pinheiro DK, Harris JM. 1996. Evidence for an ozone hole perturbation at 30° South. Atmospheric Environment 30: 1481–1488. https://doi.org/10.1016/1352-2310(95)00362-2

Kirchhoff VWJH, Echer E, Leme NP, Silva AA. 2000. A variação sazonal da radiação ultravioleta solar biologicamente ativa. Revista Brasileira de Geofísica 18: 63– 74. https://doi.org/10.1590/S0102-261X2000000100006

Koronakis PS, Sfantos GK, Paliatsos AG, Kaldellis JK, Garofalakis JE, Koronaki IP. 2002. Interrelations of UV-global/global/diffuse solar irradiance components and UV-global attenuation on air pollution episode days in Athens, Greece. Atmospheric Environment 36: 3173–3181. https://doi.org/10.1016/S1352-2310(02)00233-9

Krotkov NA, Carn SA, Krueger AJ, Bhartia PK, Yang K. 2006. Band residual difference algorithm for retrieval of SO2 from the Aura Ozone Monitoring Instrument (OMI). IEEE Transactions on Geoscience and Remote Sensing 44: 1259–1266. https://doi.org/10.1109/TGRS.2005.861932

Levelt PF, van den Oord GHJ, Dobber MR, Mälkki A, Visser H, de Vries J, Stammes P, Lundell JOV, Saari H. 2006. The Ozone Monitoring Instrument. IEEE Transactions on Geoscience and Remote Sensing 44: 1093–1101. https://doi.org/10.1109/TGRS.2006.872333

Liu F, Zhang Q, van der A RJ, Zheng B, Tong D, Yan L, Zheng Y, He K. 2016. Recent reduction in NOx emissions over China: synthesis of satellite observations and emission inventories. Environmental Research Letters 11: 114002. https://doi.org/10.1088/1748-9326/11/11/114002

Livi FP. 2002. O clima em Porto Alegre no século XX: uma análise de séries temporais. Master's thesis. Federal University of Rio Grande do Sul.

Mostafa MK, Gamal G, Wafiq A. 2021. The impact of COVID 19 on air pollution levels and other environmental indicators - A case study of Egypt. Journal of Environmental Management 277: 111496. https://doi.org/10.1016/j.jenvman.2020.111496

Nakada LYK, Urban RC. 2020. COVID-19 pandemic: Impacts on the air quality during the partial lockdown in São Paulo state, Brazil. Science of the Total Environment 730: 139087. https://doi.org/10.1016/j.scitotenv.2020.139087

NASA. 2020. National Aeronautics and Space Administration. Earth Observatory. Available at https://urs.earthdata.nasa.gov (accessed 2020 August 10).

Nunes M. 2017. Influência da coluna total de ozônio na variabilidade da radiação ultravioleta sobre o sul da América do Sul. Master's thesis, Federal University of Pelotas.

Paital, B, Agrawal PK. 2021. Air pollution by NO2 and PM2.5 explains COVID-19 infection severity by overexpression of angiotensin-converting enzyme 2 in respiratory cells: a review. Environmental Chemistry Letters 19: 25–42. https://doi.org/10.1007/s10311-020-01091-w

Robinson N. 1966. Solar Radiation. New York: Elsevier.

Salgado CAC, Paes Leme NM, Zamorano F, Quel EJ, Viana R. 2010. Influence of the ozone hole on the American South Cone 1992-2009. In: Proceedings of the 2010 Meeting of the Americas. Foz do Iguaçu.

Schmalfuss LSM, Mariano GL, Pinheiro DK, Peres LV. 2014. Análise dos dois principais fatores de decaimento da coluna total de Ozônio sobre o sul da América do Sul. Ciência e Natura 36: 415–422. https://doi.org/10.5902/2179460X12812

Seinfeld JH, Pandis SN. 1998. Atmospheric Chemistry and Physics: from air pollution to climate change. New York: Wiley Interscience.

Sharma S, Zhang M, Anshika, Gao J, Zhang H, Kota SH. 2020. Effect of restricted emissions during COVID-19 on air quality in India. Science of the Total Environment 728: 138878. https://doi.org/10.1016/j.scitotenv.2020.138878

Siciliano B, Dantas G, da Silva CM, Arbilla G. 2020. Increased ozone levels during the COVID19 lockdown: Analysis for the city of Rio de Janeiro, Brazil. Science of the Total Environment 737: 139765. https://doi.org/10.1016/j.scitotenv.2020.139765

Silva F, Oliveira HSM, Marinho GS. 2008. Variação do índice de radiação solar ultravioleta em Natal-RN entre 2001 e 2007. In: II Congresso Brasileiro de Energia Solar e III Conferência Regional Latino-Americana da ISES. Florianópolis.

Tanskanen A, Krotkov NA, Herman JR, Arola A. 2006. Surface ultraviolet irradiance from OMI. IEEE Transactions on Geoscience and Remote Sensing 44: 1267–1271. https://doi.org/10.1109/TGRS.2005.862203

Tiegte JE, Diamond SA, Ankley GT, DeFoe DL, Holcombe GW, Jensen KM, Degitz SJ, Elonen GE, Hammer E. 2001. Ambient solar UV radiation causes mortality in larvae of three species of Rana under controlled exposure conditions. Photochemistry and Photobiology 74: 261–268. https://doi.org/10.1562/0031-8655(2001)0740261ASURCM2.0.CO2

Tobias A, Carnerero C, Reche C, Massagué J, Via M, Minguillón MC, Alastuey A, Querol X. 2020. Changes in air quality during the lockdown in Barcelona (Spain)

one month into the SARSCoV-2 epidemic. Science of the Total Environment 726: 138540. https://doi.org/10.1016/j.scitotenv.2020.138540

Travaglio M, Yu Y, Popovic R, Selley L, Santos-Leal N, Martins LM. 2021. Links between air pollution and COVID-19 in England. Environmental Pollution 268: 115859. https://doi.org/10.1016/j.envpol.2020.115859

Ubiratan E. 2020. No limite a aviação brasileira registra queda de 90%. Available at https://aeromagazine.uol.com.br/artigo/no-limite-aviacao-brasileira-registra-queda-de90_5420.html (accessed 21 March 2021).

Vasquez-Apestegui V, Parras-Garrido E, Tapia V, Paz-Aparicio VM, Rojas JP, Sánchez-Ccoyllo OR, Gonzales GF. 2020. Association between air pollution in Lima and the high incidence of COVID-19: Findings from a post hoc analysis. Research Square (preprint). https://doi.org/10.21203/rs.3.rs-39404/v1

Wakamatsu S, Uno I, Ueda H, Uehara K, Tateishi H. 1989. Observational study of stratospheric ozone intrusions into the lower troposphere. Atmospheric Environment 23: 1815–1826. https://doi.org/10.1016/0004-6981(89)90065-6

Wang Q, Su M. 2020. A preliminary assessment of the impact of COVID-19 on environment – A case study of China. Science of the Total Environment 728: 138915. https://doi.org/10.1016/j.scitotenv.2020.138915

WHO (World Health Organization). 2006. Air quality guidelines – Global update 2005. Particulate matter, ozone, nitrogen dioxide and sulfur dioxide. World Health Organization.

WHO, WMO, UNEP, ICNIRP (World Health Organization, World Meteorological Organization, United Nations Environment Programme, International Commission on Non-Ionizing Radiation Protection). 2002. Global solar UV index: a practical guide. Geneva: World Health Organization.

WMO (World Meteorological Organization). 2011. Scientific assessment of ozone depletion: Global Ozone Research and Monitoring Project–Report No. 52. Geneva: World Meteorological Organization.

WMO (World Meteorological Organization). 2020. Arctic ozone depletion reached record level. Available at https://public.wmo.int/en/media/news/arctic-ozone-depletion-reached-record-level (accessed 2020 August 10).

Zambrano-Monserrate MA, Ruano MA, Sanchez-Alcalde L. 2020. Indirect effects of COVID-19 on the environment. Science of the Total Environment 728: 138813. https://doi.org/10.1016/j.scitotenv.2020.138813

Zheng B, Geng G, Ciais P, Davis SJ, Martin RV, Meng J, Wu N, Chevallier F, Broquet G, Boersma F, van der AR, Lin J, Guan D, Lei Y, He K, Zhang Q. 2020. Satellite-based estimates of decline and rebound in China's CO2 emissions during COVID-19 pandemic. Science Advances 6: 1–10. https://doi.org/10.1126/sciadv.abd4998

Zhu L, Liu X, Huang H, Avellán-Llaguno RD, Llaguno Lazo MM, Gaggero A, Soto-Rifo R, Patiño L, Valencia-Avellan M, Diringer B, Huang Q, Zhu Y-G. 2020. Meteorological impact on the COVID-19 pandemic: A study across eight severely affected regions in South America. Science of the Total Environment: 744: 140881. https://doi.org/10.1016/j.scitotenv.2020.140881

3.2 Artigo 2: Satellite-based estimation of NO2 concentrations using a machine-learning model: a case study on Rio Grande do Sul, Brazil.

Artigo submetido na Revista Atmósfera—Universidad Nacional Autónoma de México

Satellite-based estimation of NO2 concentrations using a machine-learning model: a case study on Rio Grande do Sul, Brazil

Adriana BECERRA-RONDÓN[1][*], Jorge DUCATI[1] and Rafael HAAG[2]

[1] *Centro Estadual de Pesquisas em Sensoriamento Remoto e Meteorologia, Universidade Federal do Rio Grande do Sul, Av. Bento Gonçalves, 9500, Porto Alegre, RS, Brazil.*
[2] *Universidade Estadual do Rio Grande do Sul, Av. Bento Gonçalves, 8855, Porto Alegre, RS, Brazil.*

* Corresponding author: abecerrarondon@gmail.com

Satellite-based estimation of NO$_2$ concentrations using a machine-learning model

HIGHLIGHTS

- A machine learning method was applied to derive NO$_2$ ground-level concentrations.
- Modeled mean NO$_2$ concentrations in the study area are 18.73 µg/m^3 for the 2006 to 2019 period.
- The highest concentrations were recorded in winter and the lowest in summer.
- A decreasing trend of 2.9 µg/m^3 yr−1 was observed over fourteen years.
- Combined meteorological/geographical/anthropogenic factors defined distributions.

GRAPHICAL ABSTRACT
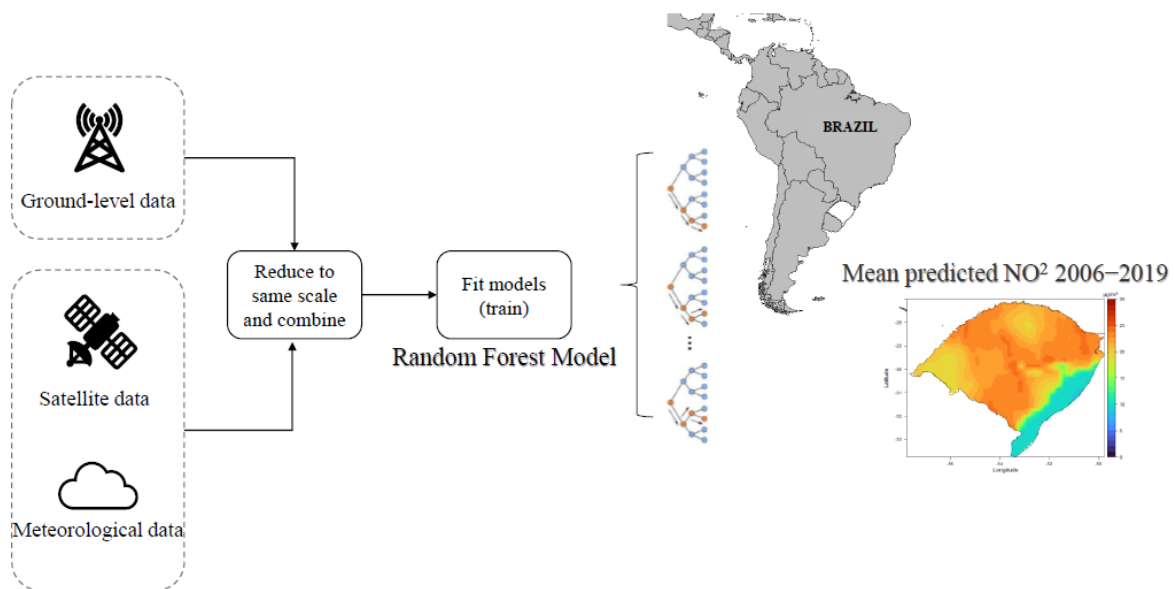
RESUMEN

El dióxido de nitrógeno (NO$_2$) es uno de los contaminantes atmosféricos más importantes que afecta la salud humana (mayor susceptibilidad a infecciones respiratorias) y el medio ambiente (acidificación del suelo y agua). A nivel del suelo, las fuentes más significativas de NO$_2$ son la quema de combustibles fósiles y biomasa. En muchas regiones de Brasil las mediciones de NO$_2$ en tierra, encuentran dificultades debido a que la red de estaciones de monitoreo es escasa y desigualmente espaciada. Esta falta de datos puede mitigarse mediante el uso de mediciones satelitales de NO$_2$, a partir de las cuales se infieren las concentraciones en la superficie, complementando los datos de las estaciones terrestres existentes y proporcionando cobertura donde los datos no están disponibles. Las observaciones satelitales combinadas con métodos estadísticos basados en modelos de aprendizaje automático pueden producir predicciones espacio-temporales sobre las concentraciones de NO$_2$. Este artículo es el resultado de una investigación sobre la capacidad de un enfoque de aprendizaje automático (un algoritmo estadístico no lineal de bosques aleatorios, en adelante RF) para ejecutar una reconstrucción espacio-temporal de las concentraciones de NO$_2$ a nivel del suelo, de 2006 a 2019, utilizando como parámetros de entrada datos de NO$_2$ recuperados del sensor del Instrumento de Monitoreo de Ozono (OMI) a bordo del satélite AURA, además de covariables meteorológicas y mediciones localizadas de NO$_2$ a nivel del suelo. Los resultados muestran que el modelo de RF desarrollado actualmente predice las concentraciones de NO$_2$ con una precisión expresada por una correlación $R^2 = 0{,}68$ basada en una validación cruzada de 10 veces. El modelo también predijo una concentración media de NO$_2$ de 18,73 µg/m^3 (± 3,86 µg/m^3) para el lapso estudiado. La concentración total de NO$_2$ en toda la región analizada mostró una tendencia decreciente ($2{,}9\ \mu g/m^3\ yr^{-1}$) entre 2006 y 2017. En general, este estudio demuestra que las estadísticas no lineales empleadas por el algoritmo de RF pueden ser herramientas complementarias a las observaciones in situ y por satélite para predecir las concentraciones de NO$_2$.

ABSTRACT

Nitrogen dioxide (NO$_2$) is one of the most important atmospheric pollutants, affecting human health (increasing susceptibility to respiratory infections) and the environment (soil and water acidification). At ground level, the most significant sources of NO$_2$ are fossil fuel combustion and biomass burning, and in many regions, NO$_2$ measurements

through monitoring stations meet difficulties due to a sparse and unevenly spaced network like, as an example, in many regions in Brazil. Such lack of data can be mitigated by using NO_2 satellite measurements, from which surface concentrations are inferred. Satellite observations combined with statistical methods based on machine learning models may produce spatiotemporal predictions on NO_2 concentrations, supplementing existing ground-based stations and providing coverage where ground-based data are unavailable. This paper report results from an investigation on the ability of a machine learning approach (a non-linear statistical Random Forests algorithm, hereafter RF) to reconstruct the long-term spatiotemporal ground-level NO_2 concentrations from 2006 to 2019 using as input parameters NO_2 data retrieved from the Ozone Monitoring Instrument (OMI) sensor aboard AURA satellite, besides meteorological covariates and localized ground-level NO_2 measurements. Results show that the RF model presently developed predicts NO_2 concentrations with an accuracy expressed by an $R^2=0.68$ correlation based on a 10-fold cross-validation. The model also predicted ground-level NO_2 concentrations for the period 2006−2019 with a mean of 18.73 µg∕m^3 (± 3.86 µg∕m^3). The total NO_2 concentration over the entire region analyzed showed a decreasing trend (2.9 µg/$m^3\ yr^{-1}$), being the year 2006 with the higher concentrations and 2017 with the lowest. Overall, this study demonstrates that non-linear statistical using by RF algorithm reconstructions can be complementary tools to *in situ* and satellite observations to predict NO_2 concentrations.

Keywords: Nitrogen dioxide (NO_2), Random Forest algorithm, OMI sensor, southern Brazil.

1. Introduction

The industrial revolution changed dramatically the planet's atmospheric composition bringing air pollution, making it one of the biggest ongoing threats facing global public health. It is estimated that ~ 90% of the world's population lives in areas where levels of air pollution are above limits deemed safe for human health (WHO, 2018). These levels are, worldwide, influenced by pressures for economic development (combustion processes for energy generation using technologies not internationally recommended) and, regionally, by each area's topography and climate (Parra et al., 2009). This last factor, climate, acts from large to small scales, modulating emissions by increasing or decreasing them. The nature of emissions depends on their source and can be primary air pollutants (emitted directly into the air from a source) with direct impacts, or can be

precursors for secondary air pollutants, formed through reactions in the atmosphere (often in the presence of sunlight), such as oxides of nitrogen (Bimbaitė and Girgždienė, 2007; Schnitzhofer et al., 2008)

There are many chemical species of nitrogen oxides (NOx), but the air pollutant of most interest is nitrogen dioxide (NO_2), not only because of its effects on human health but also because (a) it absorbs visible solar radiation and contributes to impaired atmospheric visibility; (b) as an absorber of visible radiation it can have a potential direct role in global climate change if its concentrations become high enough; (c) it is, along with nitric oxide (NO) a chief regulator of the oxidizing capacity of the troposphere by controlling the build-up and fate of radical species, including hydroxyl radicals; and (d) it plays a key role in atmospheric chemistry related to ozone formation and destruction, this being the main vector to absorption of ultraviolet radiation reaching the planet's surface, whether in polluted or unpolluted atmospheres (WHO, 2000). As a significant contributor to air pollution NO_2 is released into the atmosphere from both natural and anthropogenic sources, being the major ones the fossil fuel combustion, biomass burning, lightning, and oxidation of ammonia. It is estimated that the lifetime of NO_2 in the atmosphere varies from six hours in summer to 18−24 h in winter (Seinfeld and Pandis, 1998; Bond et al., 2001; Beirle et al., 2003; Zhang et al., 2003). Its concentration level is influenced by complex variables such as wind, temperature, burning material, besides policies and other anthropogenic factors of each city (e.g., urban areas) (Wang and Su, 2020; Liu et al., 2016).

The growing trend in the emission of atmospheric nitrogen dioxide (NO_2) has been the major concern around the world, the developing countries being at larger risk owing to fewer resources and socio-economic vulnerability (Munzi et al., 2009). Traditionally, this trace gas is measured through a network of monitoring stations in the ground, but such an extensive network may not exist in all areas of interest and particularly in lower-income countries. An alternative approach to overcome these limitations is to use satellite data, which provide spatiotemporal data from regional to global scales under widely different atmospheric conditions and offer expeditious accurate information about changes in air quality and their human impacts (Bais et al., 2007; Liu et al., 2016; Mostafa et al., 2021).

In South America, studies on air pollution are limited to a few cities, because air quality monitoring stations tend to be expensive, and not all air pollutants are monitored (Réquia et al., 2015; Fajersztajn et al., 2017; Silva et al., 2020). An example of the lack

of an extensive network for environmental monitoring is Rio Grande do Sul State, located in south Brazil, with only nine stations within its borders. Compared to other regions of the country, the State is exposed to higher levels of ultraviolet radiation for being closer to the Antarctic ozone hole (Kirchhoff et al., 2000; Guarnieri et al., 2004), and is strongly influenced by transient meteorological systems (cold and hot fronts), isentropic transport (between the tropical stratosphere reservoir, polar vortex, middle-latitude) and exchange processes (between upper troposphere–lower stratosphere) (Reboita et al., 2010; Bittencourt et al., 2019).

Recently, spaceborne observations were combined with statistical methods to produce spatiotemporal predictions on NO_2 concentrations, supplementing existing ground-based stations and providing coverage where ground-based data are unavailable (Hoek et al., 2015; Larkin et al., 2017; Quin et al., 2020). These predictions are based on machine learning models ranging from linear regression models to non-linear, being the latter the ones that perform better since they consider that there is a non-linear relationship between predictor variables and dependent variables (Zhan et al., 2018). Predictive variables of models for air pollutants usually include satellite data, meteorology, population density, elevation, and land-use type variables (Zhan et al., 2018; Pan et al., 2021).

Random Forest is a non-linear model simple in structure, requires less computational resources, and has stronger interpretation capabilities; besides giving importance weights for each of the included variables to select the model predictors, it is also less prone to overfitting and less sensitive to outliers (Pan et al., 2021). Many of the studies on NO_2 based on this model have focused on short and long-term spatio-temporal changes (Hoek et al., 2015; Araki et al., 2018; Zhan et al., 2018; Kamińska, 2019; Zhu et al., 2019; Qin et al.,2020), showing good prediction performance, with cross-validation R^2 from 0.69 to 0.84. In addition, the models in these studies exhibit higher accuracies when the dataset is of integrated temporal and spatial information.

Given that the existing environmental monitoring stations in Rio Grande do Sul are sparse and unevenly distributed, the objective of this study is to reconstruct the long-term spatiotemporal environmental NO_2 concentrations from 2006 to 2019 in the State, through machine learning model Random Forest (RF) methods using as input parameters data retrieved from the Ozone Monitoring Instrument (OMI) sensor aboard AURA satellite, besides meteorological covariates and ancillary data.

2. Material and methods

2.1 Study area

Rio Grande do Sul is the Brazilian southernmost state, having international borders with Argentina to the West and with Uruguay to the South (Fig. 1). Its area is 281,707 km², and with more than 11.5 million inhabitants it is the fifth most populated state in the country; about 85% of its population lives in urban areas (Fig. 2). The metropolitan area of its capital, Porto Alegre, concentrates an important fraction of the State's population and economic activities. Regarding the consumption of fossil fuels, the State has about 7.5 million vehicles (IBGE, 2021). The region has a humid subtropical climate with a large seasonal variation with hot summers and well-defined, cold winters. Mean temperatures vary from 15 to 18 °C, with lows of as much as -10 °C (June and July) and highs going up to 40°C (December to March) (Livi, 2002). The surface elevation ranges from sea level up to 1400 m with the highest points northeast of the state (Fig. 2).
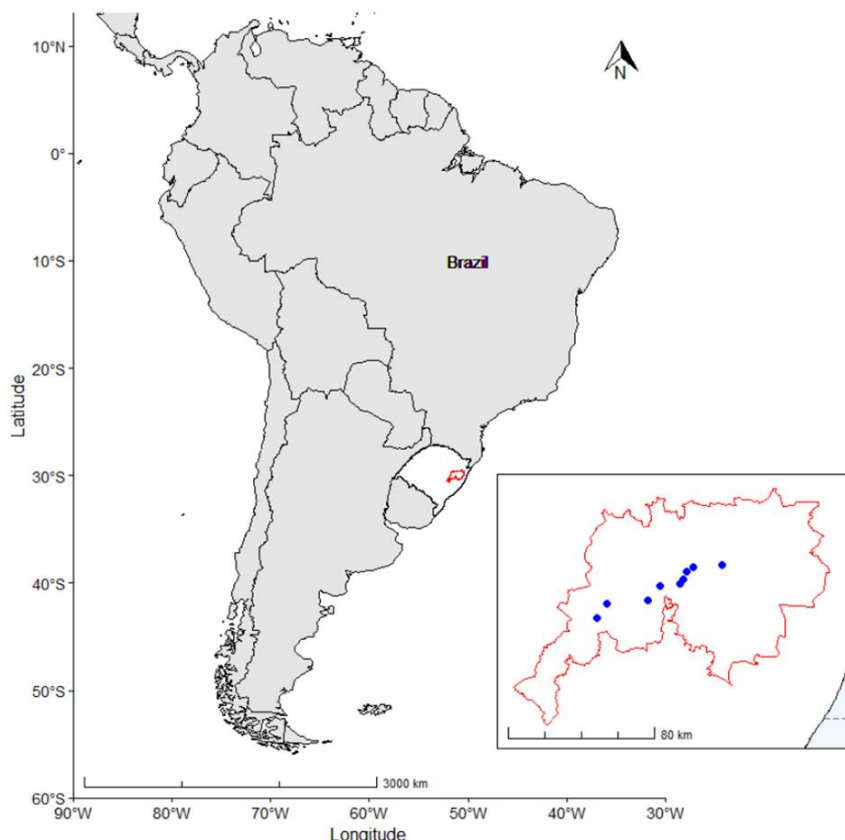
Fig. 1. Map with the State location (in white) and its metropolitan area (red contour), with the positions of NO_2 monitoring sites (blue points).
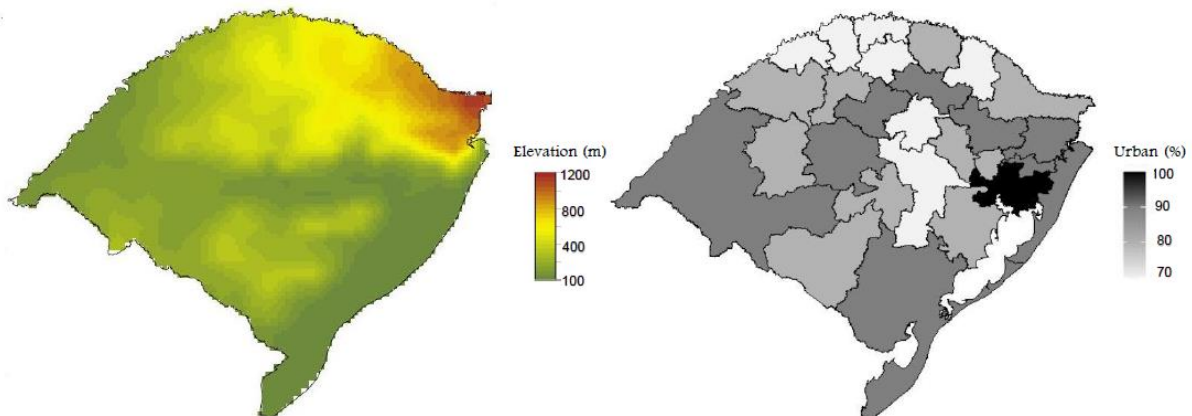
Fig. 2. Topographic and demographic representations of Rio Grande do Sul, Brazil. Elevation (left), Urbanization (right) (COREDEs, 2010).

2.2. Data set

Ground-level NO_2 data

The ground-level NO_2 data was acquired by nine monitoring sites (Fig. 1) managed by the Fundação Estadual de Proteção Ambiental (FEPAM – State's Environmental Protection Foundation), measured hourly by chemiluminescence method from 2006 to 2019, with the occurrence of some discontinuous periods (FEPAM, 2021). For this research, we integrated the hourly average concentrations to daily values for all stations, and then all data were interpolated to a 0.25°×0.25° grid. This spatial resolution was the standard in this study, and 420 such cells are necessary to cover the State. After this pre-processing, a total of 2229 daily measurements of ground-level NO_2 were used to develop to model. This number represents 43.5 % of the time series of fourteen years if data were acquired every day during the studied period.

Satellite NO_2 data

The orbital data used in this study come from sensor OMI (Ozone Monitoring Instrument) aboard satellite Aura. This instrument is equipped with a spectrometer pointed to the nadir which measures the ultraviolet light (264–504 nm) coming from the Sun and back-scattered by the atmosphere. The algorithm Differential Optical Absorption Spectroscopy (DOAS) was developed to derive nitrogen dioxide (product OMNO2d) (Krotkov et al., 2006). The data provided in this product are expressed in molecules/cm^2 units daily at 0.25° × 0.25° (Lat/Lon) spatial resolution, these column densities being adequate to track spatial patterns for ground-level NO_2. Therefore, it is unnecessary to convert vertical column density to ambient concentrations in the input

model (Bechle et al. 2015). This data is represented in a time series of fourteen years (2006–2019), with 5092 daily images (99 % of the series) which were acquired from the data provider GES-DISC (https://urs.earthdata.nasa.gov).

Meteorological data

The data of meteorological covariates were acquired from MERRA-2 (Modern-Era Retrospective analysis for Research and Applications), produced by the NASA Global Modeling and Assimilation Office (GMAO) which provides a global atmospheric reanalysis beginning in 1980. These data were initially produced on a 1/2-degree by 2/3-degree global grid and were re-gridded by the POWER project to the $0.5^{\circ} \times 0.5^{\circ}$ (Lat/Lon) bilinear interpolated spatial grid with daily resolution. The daily meteorological conditions used in the model include surface temperature, wind speed, humidity, surface pressure, all variables to 2 m (Rienecker et al., 2011). This data is represented in a time series of fourteen years (2006–2019) with 5113 images for each variable with daily measurements (100 % of the series), acquired from the data provider POWER (https://power.larc.nasa.gov/).

Ancillary data

To support our model data on elevation were included, on the form of 90 m vertical resolution measurements collected by STRM (Shuttle Radar Topography Mission) and made available at https://www.ufrgs.br/labgeo/, from which a mean elevation $0.25^{\circ} \times 0.25^{\circ}$ grid was compiled.

Information on the Erythemal Daily Dose and Ozone were also added, provided by satellite OMI through product OMUVBG (Erythemal Daily Dose) in joules/m^2 units with a daily spatial resolution of $0.25^{\circ} \times 0.25^{\circ}$ (Lat/Lon), and also daily, but with $1.0^{\circ} \times 1.0^{\circ}$ (Lat/Lon) spatial resolution the product OMTO3d (ozone total column density) in Dobson Units (where 1 DU = 2.7×1018 molecules O_3/cm^3) (Levelt et al., 2006; Tanskanen et al., 2006). These data are represented in a time series of fourteen years (2006–2019), with 5092 images daily (99 % of the series), acquired from the data provider GES-DISC (https://urs.earthdata.nasa.gov).

2.3 Statistical Model

Predicting NO_2 concentration with sufficient spatial and temporal resolution and accuracy is not a simple task. Although satellite measurements could contribute to this problem, they are usually limited to a single measurement per day which units, in

vertical column density, are difficult to compare with ground data (Liu et al., 2021). Nevertheless, there is a growing interest in combining ground-based data and satellite observations to produce information comparable with measurements at surface level (Lu et al., 2020).

The Random Forest (Breiman, 2001) is an alternative to complex atmospheric processes by using a simple regression model, providing a spatiotemporal estimate of air pollutants (Qin et al., 2020; Chan et al., 2021). The RF regression model consists of a collection of regression trees trained by bootstrap samples and that splits each node in the regression tree according to the best of a subset of randomly chosen predictors (Liaw and Wiener, 2002). Each tree is a regression function on its own, and the final output is the average of the individual tree outputs. In this study, from the collected dataset of ground-level NO_2 concentrations and various predictors such as satellite NO_2 retrievals and meteorological variables (temperature, wind speed, relative humidity, and atmospheric pressure), plus the ancillary data, the ground NO_2 concentrations were simulated with the following expression:

$NO_2Ground_{ij}$ ~ $NO_2Satellite_{ij}$ + $Wind_{ij}$ + $Temperature_{ij}$ + $Pressure_{ij}$ + $Humidity_{ij}$ + $Erythemal\ Dose_{ij}$ + $Ozone_{ij}$ + Elevation + Year + Julian day   (1)

where cell is j and day is i.

The application of this regression model was performed into three phases: First (training set), where we used 70 % of the database, with the ability to predict concentrations observed in monitoring sites based on a set of predictors; at the end of this phase the relative importance of the predictors is directly provided by the RF model. Second (performance) where, since our objective was to estimate ground-level NO_2 concentrations over places with no monitoring stations and from limited input data, we applied two validation methods: ten-fold cross-validation (over the training set), which is a re-sampling procedure used to evaluate if our model is under-fitting/over-fitting; and test set validation (with 30 % of the database), used to the evaluation of the final model fit on the training dataset, with an assessment of the discrepancies between predictions and observations of the monitoring sites. These comparisons were summarized in terms of R^2 (% of explained variance), root means square error (RMSE), as well as Mean Absolute Error (MAE). These two latest metrics explain the differences between the predicted and the true values; the smaller RMSE and MAE are, the smaller the error between these two. Finally, the third phase (generalize)

estimates the concentrations in the cells where no ground-level observations were available (Liaw and Wiener, 2002; Zhu et al., 2019; Gariazzo et al., 2020; Dou et al., 2021).

2.4. Analysis
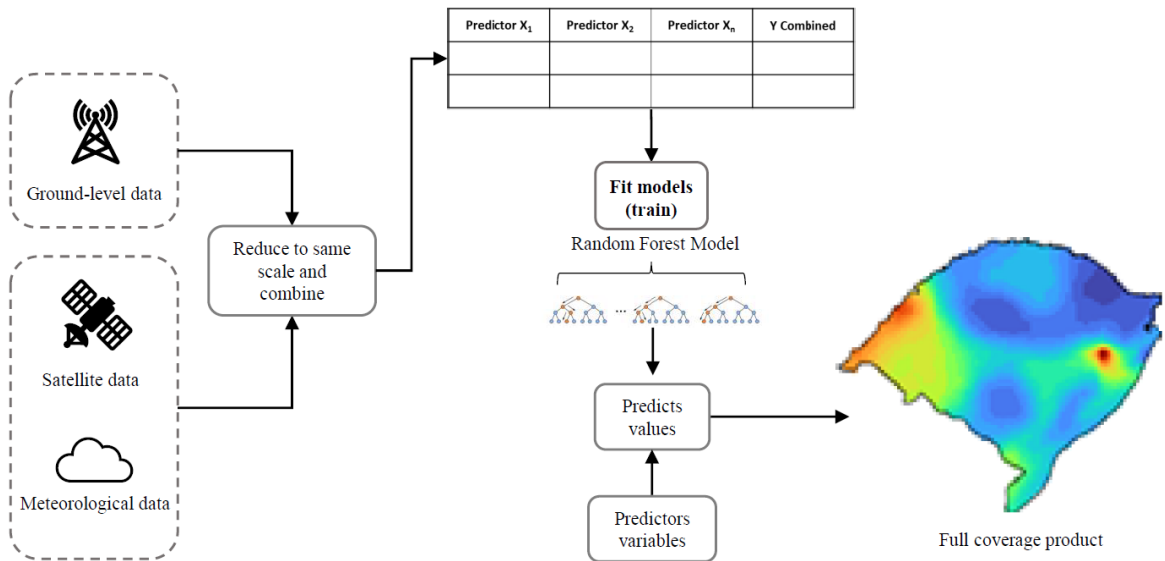
Fig. 3. Flow diagram of this study: daily ground-level NO$_2$ concentrations based on the Random Forest model.

The machine learning method used to estimate ground-level NO$_2$ concentrations in the study area is summarized in Figure 3, which shows collected and standardized multi-source data used to obtain the desired dataset with uniform spatial-temporal resolution (0.25⁰ × 0.25⁰ (Lat/Lon), daily resolution). The Pearson correlation coefficient was calculated for all predictors and ground observation data before running the model to evaluate the effect of these parameters. The predictions for all 420 cells were obtained using the "caret" and "ranger" R packages for RF model (Kuhn, 2008; Wright and Ziegler, 2017). All maps have been produced with the R statistical software, version 4.0.5 (http://R-project. org).

The evaluation of the long-term trend (2006 to 2019) of ground-level NO$_2$ concentrations was made using the predicted values, calculating the cell averages for all 420 cells of the study area, for the whole period (historical series), and as well for month and season. The averages were calculated using the daily values for each of these periods, as follows:

$$Var_i = \frac{\sum_t {}^{start\ date}_{end\ date} Var_{i,t}}{n} \qquad (2)$$

where Var_i is the average of the variable in each cell for the respective period; start date and end date correspond to the first and last date of each period; n is the number of days in the period.

The total average concentrations of ground-level NO_2 were evaluated by summarizing average concentrations across all cells that represent the State throughout each period.

3. Results and discussion

Model performance assessment

Relationships between ground-level NO_2 and each independent attribute are shown in Figure 4. The variables with the highest correlations were: 0.44 (Year), 0.24 (Satellite NO_2), -0.21 (Erythemal Daily Dose), -0.17 (Wind speed). It can be noted that the dependent variable is influenced by interannual variations, dispersion, and photochemistry; however, variables with lower correlations also play a role in the model construction, as shown in Figure 5, which give a perception on the contribution of the variables to the final model.
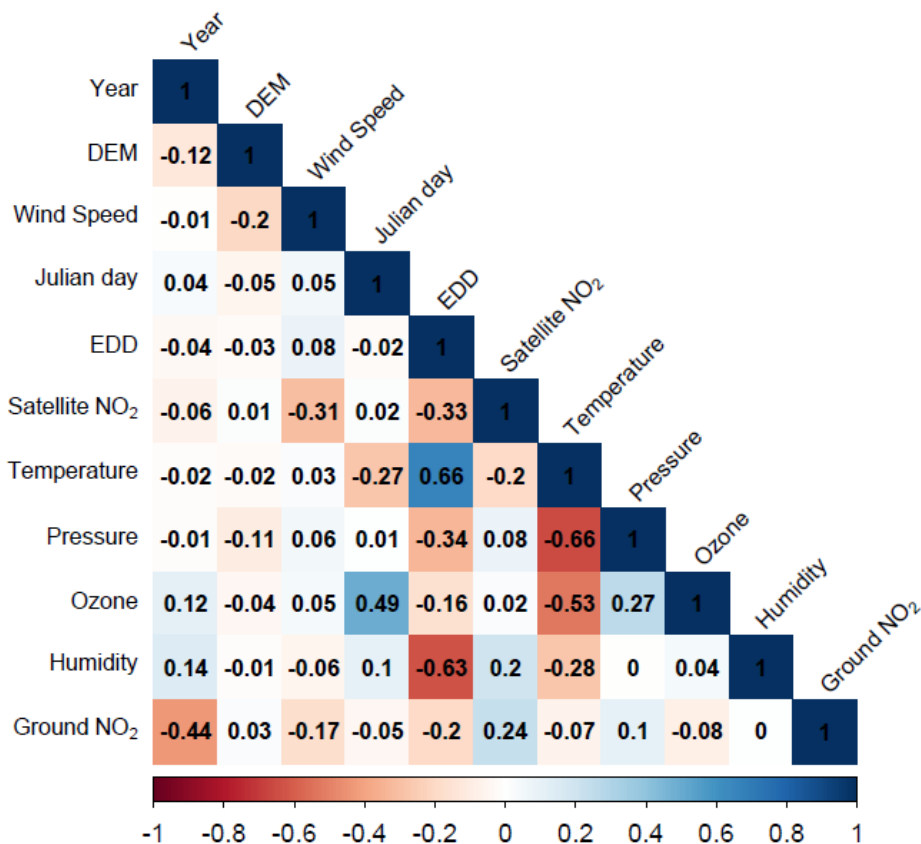
Fig. 4. Correlation matrix of the variables used in the model.
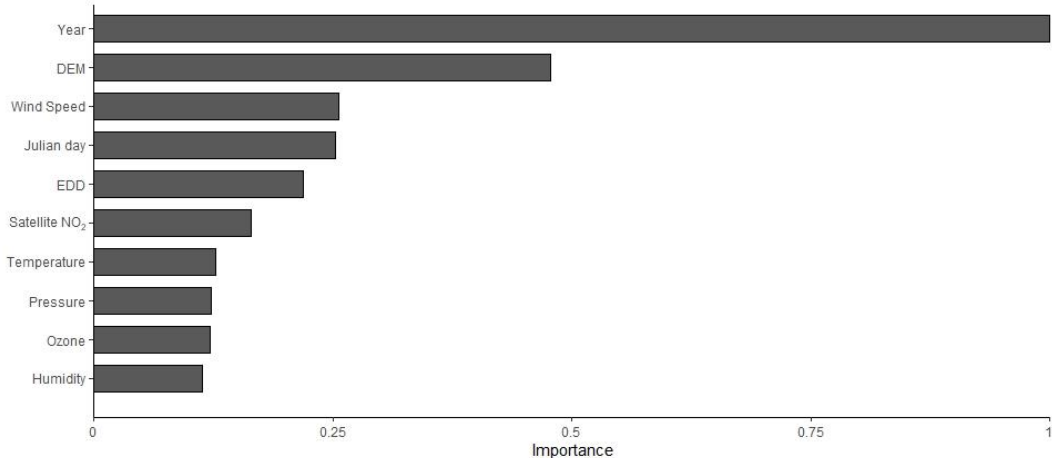
Fig. 5. Relative importance of predictor variables in Random Forest model. The variables are listed in order of importance from top to bottom. The horizontal axis represents the measure of importance.

The categorical variable Year is the most important with a relative value of 1, followed by Elevation (0.5), Wind speed (0.26), Julian day (0.26), Erythemal Daily Dose (0.24), and sixth but not least Satellite NO_2 (0.20). The remaining variables are ranked as less important. It has been reported that the satellite NO_2 (vertical column density) variable can be ranked as one of the most important in most models that use machine learning techniques to predict NO_2 (Araki et al., 2018; Zhu et al., 2019; Qin et al., 2020; Dou et al., 2021; Chan et al., 2021), but some of these studies have shown that this importance varies between geographical areas, and it can become one of the least important variables, contributing in some cases with only 1 % in the prediction. This variation can happen for two reasons, the first one being due to the spatial resolution of this product since variations of NO_2 were averaged out within each cell. The second reason is that the sensitivity of the OMI sensor and of any satellite-based NO_2 measurement increases with altitude, implying that measurements at ground-level are less sensitive due to the scattering of radiation at the surface and through the atmosphere (Lu et al., 2020; Penn and Holloway, 2020; Di et al.,2020).

Results expressing the model performance are presented in Figure 6 as a scatter plot, where the ten-fold cross-validation method yield R^2=0.68, RMSE= 6.43, and MAE= 4.37. The test set validation method used to evaluate the model's performance yield R^2=0.70, indicating the ability of the model to predict unknown data. The model metrics presently reported express a performance similar to those obtained by Dou et al. (2021) and by Qin et al. (2020), which also adopted 0.25⁰ × 0.25⁰ spatial resolutions to estimate ground-level NO_2. We note, however, that in regression models the

adopted spatial resolution of the predictors will depend on the objectives pursued, and for many applications data at a finer ($\leq$1 km^2) spatial resolution are necessary to capture environmental variability that can be partly lost at lower resolutions (Hijmans et al., 2005).
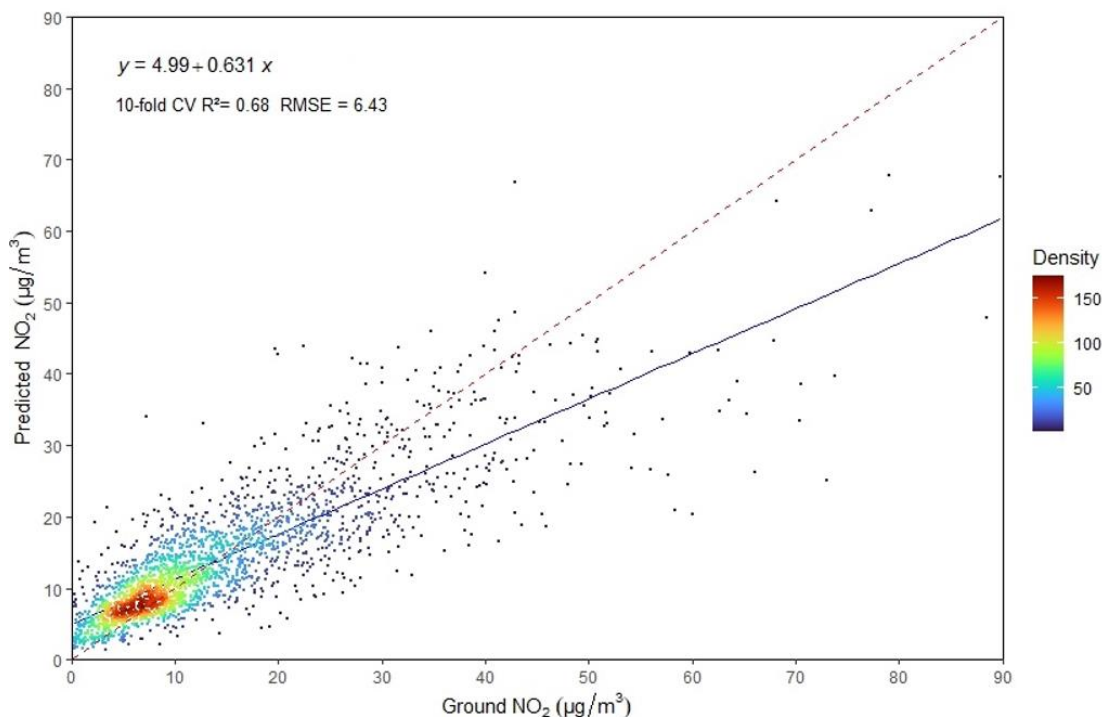
Fig. 6. Scatter plot result for Random Forest model 10-fold cross validation. The red dash line is the 1:1 reference line, the blue solid line is the trend line. The color bar indicates the number of data points.

In models like the one presently developed it has been shown that analysis of the spatio-temporal distribution of a variable with spatial dependencies can suffer from a misinterpretation of certain predictor variables (e.g., coordinates, and elevation), an issue that has been reported as a disadvantage for flexible algorithms (e.g., Random Forest) when predicting beyond the location of the training data (Meyer et al., 2019). In such cases, the predictive performance becomes more sensitive to the sample sizes or absolute values of dependent variables (Zhan et al., 2018; Li et al., 2020). In the case presently investigated, Elevation is one of the most important variables to the final model, which was built from data by nine ground monitoring stations with elevations between 20 to 85 m, while the whole study area displays elevations between 0 and 1400 m; this fact possibly represents a limitation to this analysis, on an extent that has to be evaluated by further studies. However, an additional assessment of this model performance, in the form of a comparison between observed and predicted ground

concentrations for the area covered by the nine monitoring stations, suggests that deviations due to elevation would have low weight, since, as it is presented in Figure 7a, the modeled concentrations closely follow the measurements over the studied period.
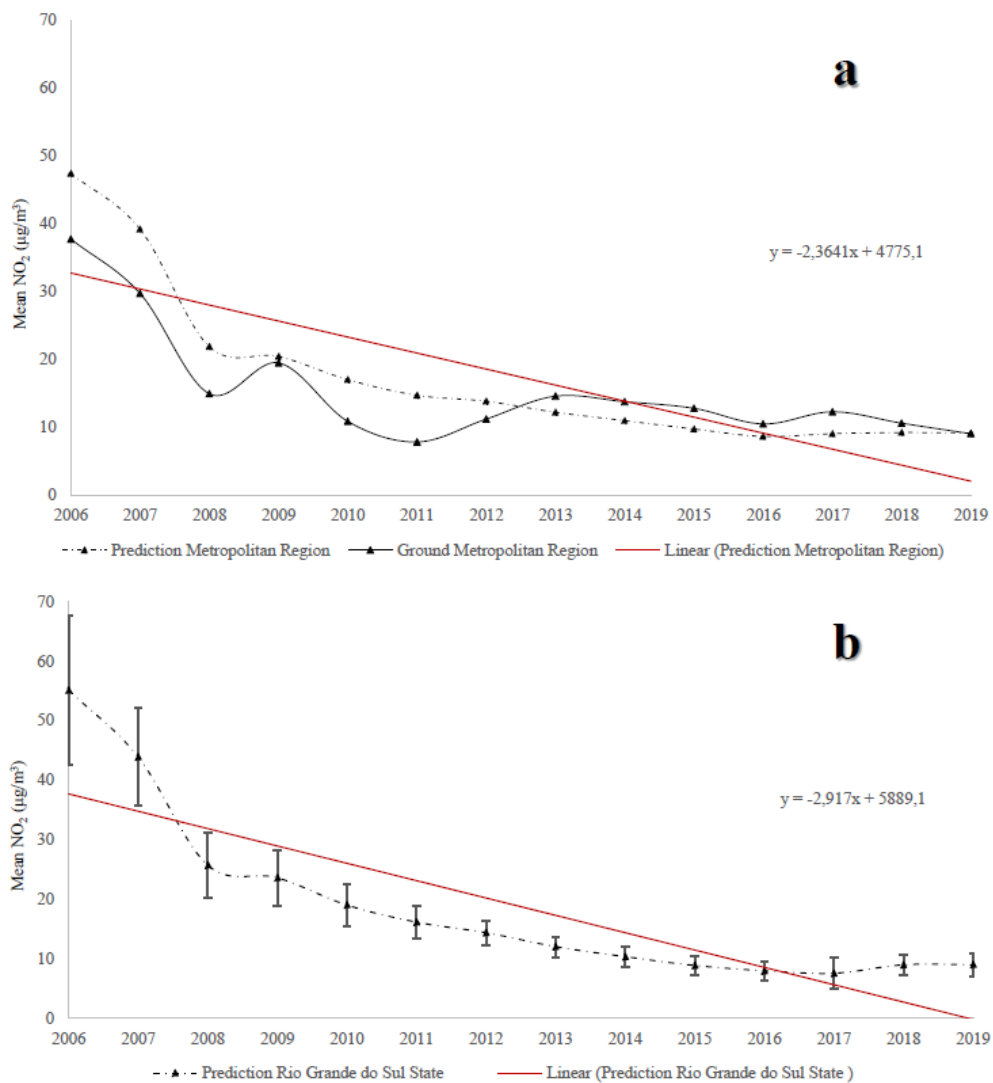
Fig. 7. Time series analysis of the annual mean surface NO_2 from 2006 to 2019 predicted by the model: (a) area covered by the ground monitoring stations; (b) all study area. Red lines are the trends for the period.

Spatial and temporal distribution of ground-level estimated NO_2

Table I presents the total estimated ground-level NO_2 concentrations over the entire state for the period 2006 to 2019. From the RF model, the predicted ground-level NO_2 concentrations across Rio Grande do Sul for this period have a mean of 18.73 µg/m^3, a minimum of 8.67 µg/m^3, and a maximum of 24.94 µg/m^3, with a standard deviation of

3.86 µg∕m^3. From Table I and Figure 7b it can also be noted that the total modeled NO$_2$ concentrations over the entire State showed a decreasing trend from 2006 to 2019.

Table I. Historical modeled means from 2006 to 2019 of Nitrogen Dioxide for Rio Grande do Sul State, Brazil.

		2006	2007	2008	2009	2010	2011	2012	2013	2014	2015	2016	2017	2018	2019
State	Min	18.14	18.28	9.64	9.84	8.97	8.40	8.34	8.14	6.54	6.13	5.56	5.48	4.63	3.25
	Max	65.92	50.64	31.28	28.38	23.42	19.88	17.42	17.27	16.49	15.84	14.64	20.07	14.28	13.61
	Mean	55.10	43.88	25.69	23.57	18.99	16.12	14.34	12.00	10.31	8.84	7.95	7.53	8.95	8.97
	SD	13.68	9.43	6.22	5.25	3.94	3.03	2.29	1.55	1.42	1.14	1.06	1.22	1.62	2.19

This decreasing trend can be expressed by what we presently call the interannual variability, which is the difference between the mean NO$_2$ for each year, *minus* the average for the whole period; considering that year 2006 has the highest mean concentrations, and 2017 the lowest, the interannual variability decreases almost steadily, going from as high as 36.37 µg∕m^3 in 2006 to as low as -11.20 µg∕m^3 in 2017. Considering that burning of biomass and of fossil fuels are the main sources of NO$_2$, this decrease can be at least partly explained, for the fossil fuels, by federal regulations of 1997, reinforced in 2008, making mandatory the installation of catalytic converters in all cars; for biomass burning, fires in crop and grazing fields were outlawed in 1992 in the State, and the legislation were slowly, but steadily enforced since then; we note that, in Rio Grande do Sul State, forest fires are virtually non-existent. A final remark concerning this trend is that similar declines in NO$_2$ concentrations were observed in several countries, having as reference approximately the same periods (UBA, 2020; DEFRA, 2021; EPA, 2021), and for similar reasons.

According to World Health Organization (WHO) guidelines, levels of NO$_2$ should be 40 µg/m^3 for the annual mean (WHO, 2005); in Brazil, regulated levels are higher, with 60 µg/m^3 for the annual average (CONAMA, 2018). The historical annual average for Rio Grande do Sul is well below the recommended levels, being 21.27 µg/m^3 below the world level and 41.27 µg/m^3 below the federal regulation. Besides the more recent, anthropic factors just explained, these State's lower levels are possibly due, historically, to the predominant wind direction in the State, which is Southeast (from the ocean), bringing enhanced dispersion (EMBRAPA, 2003). In addition, polar air masses frequently arriving at the area bring clean air, minimizing the accumulation of this pollutant (Agudelo–Castaneda et al., 2014).

Figures 8 to 10 show the spatial ground-level NO_2 distribution across the State in different time scales. Figure 8 shows the spatial distribution averaged over the entire 2006 to 2019 period, and to better understand this distribution we linked the information on elevation and percentage of urbanized areas in the state (Fig. 2) with the predicted concentrations in Figure 8.
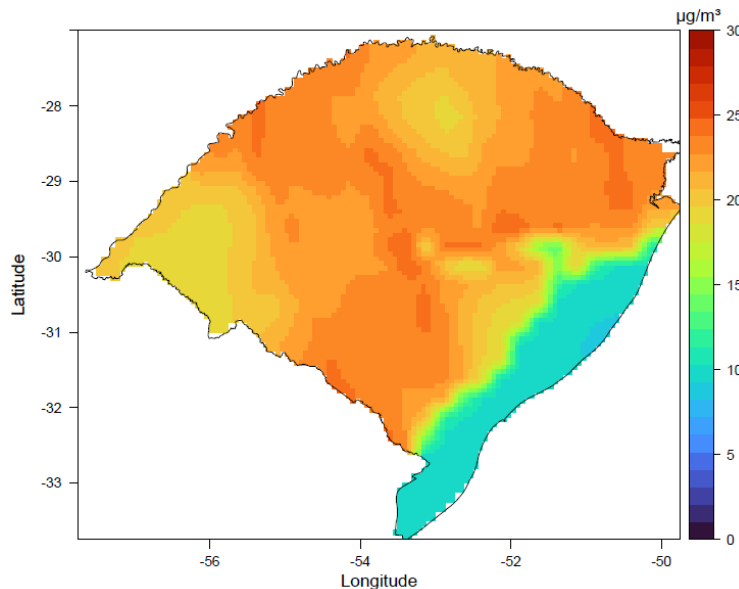
Fig. 8. Satellite-derived historical mean NO_2 concentrations ($\mu g/m^3$) across Rio Grande do Sul from 2006 to 2019.

About elevation, we noted a pattern between the NO_2 concentrations of NO_2 with elevation: up to 100 m, concentrations are between 10−15 $\mu g/m^3$; from 400−600 m, between 15−25 $\mu g/m3$; a decrease is observed between 600−800 m (15−20 $\mu g/m^3$) and finally, from 800−1400 m the increase is continuous. It has been reported that, in general, higher altitudes show lower NO_2 concentrations (Zhu et al., 2019; Chan et al., 2021), since in meteorological situations of inhibited wind transport/advection pollutants can accumulate in depressions (valleys and basins) (Giovannini et al., 2020). However, the atmospheric interactions with the orography at different spatial scales influence the dispersion of atmospheric pollutants, being more complex in rough terrains. As a result, pollutants can be transported by orographic flows to mountainous areas, arriving to significant concentrations in areas where they were not locally emitted. These constraints are reinforced by the fact, that, in Figure 8, higher NO_2 concentrations coincide either with urbanized, industrialized zones (some of which are situated in areas with elevations of about 800 m or higher), or with areas of intensive agriculture (where fertilizers are sources of NO_2, and diesel-powered machines are

heavy NO_2 producers); in some regions both factors are summed up (Guo et al., 2020; Ai et al., 2021).

The NO_2 concentrations are essentially a marker for combustion-related emissions and population, the latter having a direct relationship with urbanization levels. In this study, an inverse relationship was observed of the distribution of NO_2 concentrations with urbanization levels, highlighting the highest concentrations in less urbanized areas <= 70 %, with averages 15−20 µg/m³. This apparently unexpected result, possibly, is because some of the less urbanized areas are dominated by intensive agriculture, which become the major silent source of NOx pollution, because of soil microbes convert fertilizer to nitrogen oxides, emitting about as much of the gases as vehicles. The emissions of these biogenic sources are larger in areas with high N fertilizer applications (Oikawa et al., 2015; Almaraz et al., 2018). In this State, Mossmann Koch et al. (2018) also highlighted that even apparently uncontaminated sites, such as small rural cities with little urbanization and with family farming as the main economic activity, present higher or similar concentrations to urbanized and industrialized areas. In addition to this, combustion emissions in rural regions are by biomass burning (e.g., human-initiated burning for crop preparation (Bechle et al., 2011).
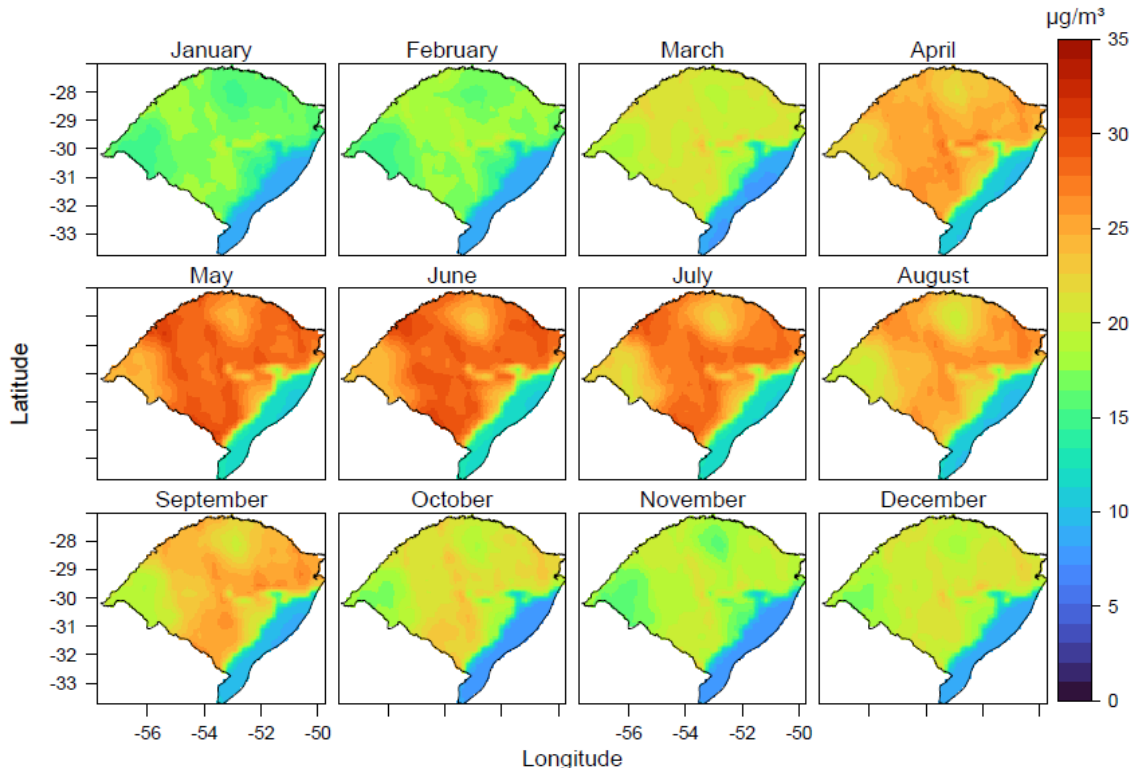
Fig. 9. Satellite-derived monthly mean NO_2 concentrations (µg/m³) across Rio Grande do Sul from 2006 to 2019.

Table II. Monthly means from 2006 to 2019 of Nitrogen Dioxide for Rio Grande do Sul State, Brazil.

		January	February	March	April	May	June	July	August	September	October	November	December
State	Min	8.79	8.28	7.95	10.02	10.82	11.04	11.00	9.75	9.02	7.44	7.72	8.56
	Max	19.79	20.47	23.78	28.23	31.03	31.14	29.50	27.72	26.94	24.26	22.35	23.43
	Mean	15.65	16.08	18.66	22.65	25.44	25.39	24.27	22.30	21.51	19.01	17.32	18.47
	SD	2.62	2.98	3.98	4.57	5.24	5.22	4.94	4.68	4.74	4.44	3.69	3.73
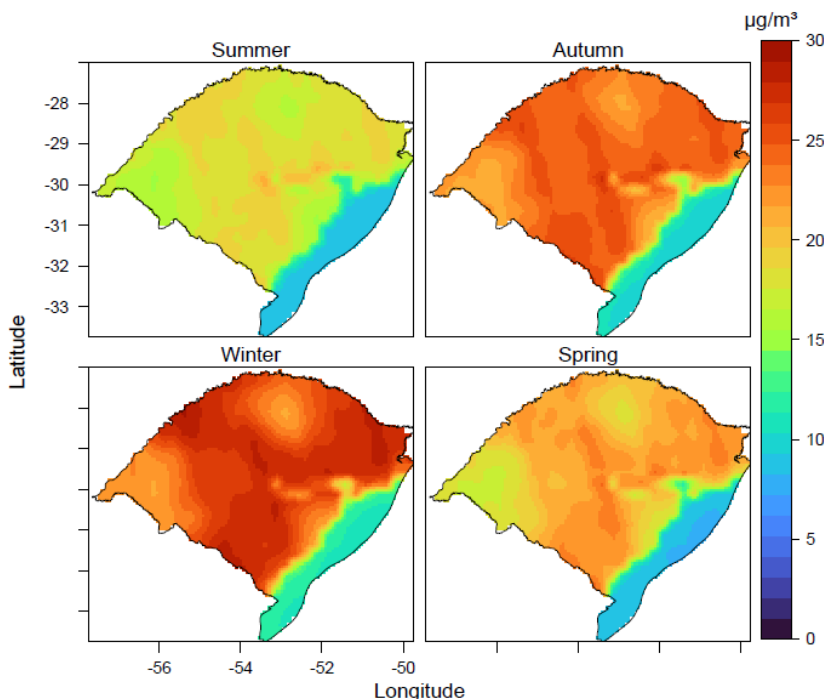
Fig. 10. Satellite-derived season mean NO_2 concentrations (µg/m³) 758 across Rio Grande do Sul from 2006 to -2019.

Table III. Season means from 2006 to 2019 of Nitrogen Dioxide for Rio Grande do Sul State, Brazil.

		Summer	Autumn	Winter	Spring
State	Min	8.58	9.63	10.64	8.09
	Max	21.17	26.97	29.30	23.97
	Mean	16.75	22.12	23.93	19.22
	SD	3.09	4.55	4.91	4.26

With respect to monthly and seasonal distributions (Figs. 9 and 10), these exhibit behavior similar to other studies, with lowest concentrations in January with a mean of 15.65 µg/m³ and standard deviation of 2.62 µg/m³ (Table II); in the spring and summer seasons concentrations assume lower values, the latter with lowest value (mean 16.75

μg∕m^3) (Table III). Highest concentrations were observed in May with a mean of 25.44 μg∕m^3 and standard deviation of 5.24 μg∕m^3 (Table II), while in fall and winter seasons high concentrations were observed, the latter with a higher value (mean 23.93 μg∕m^3) (Table III). In this context, the Rio Grande do Sul State, due to its location, is under the action of a climatic complex that in spring and summer has the predominance of the action of a tropical continental mass, a tropical Atlantic and a polar Atlantic mass, so the high humidity and high temperatures make the climatic conditions warmer, resulting in episodes intense atmospheric convection and frequent precipitation which lead to the dispersion and wet deposition of NO_2, reducing air pollution. Additionally in summer, with longer sunshine durations along with higher temperatures and evaporation, OH (Hydroxide) concentrations are boosted, leading to a lower lifetime of NO_2 which becomes HNO_3 (Nitric acid). In contrast, in autumn and winter, essentially under the control of the equatorial Atlantic, tropical Atlantic, continental tropical and polar masses, there is an intensification of the action of cold fronts in the state, ensuring the cold and reducing humidity (less precipitation and higher atmospheric pressure) than other seasons, conditions that are unfavorable for pollution dispersion (Rossato, 2011; Zhu et al., 2019; Quin et al., 2020; Dou et al., 2021).

4. Conclusions

In our study, the use of Random Forest method, in combination with extensive data collection on multiple parameters from satellite and ground source, was shown to be a valid tool for predicting NO_2 ground level concentrations at spatial low and daily temporal resolution in Rio Grande do Sul, Brazil.

Modeled NO_2 seasonal variations at the troposphere level displayed a higher concentration in winter, followed by autumn and spring, while summer had the lowest values during the fourteen years covered by the study. In this context, such spatiotemporal trend is the combined effect of meteorological, geographical, and anthropogenic factors that, together, determine the increase or decrease of their concentrations.

Although the accuracy of modeled ground-level NO_2 still needs to be improved, especially taking into account elevation variations, the estimates of spatial and temporal presented here can allow the formulation, planning, and implementation of environmental policies considering present and future emission sources. In addition to that, we highlight the need for the design of studies aimed at investigating both short-

term and long-term air pollution, not only in the major cities but also in suburban and rural areas.

Acknowledgments

References

Agudelo–Castaneda D, Calesso E, Norte F. 2014. Time–series analysis of surface ozone and nitrogen oxides concentrations in an urban area at Brazil. Atmospheric Pollution Research 5: 411−420. https://doi.org/10.5094/APR.2014.048

Ai Y., Ge Y., Ran Z., Li X., Xu Z., Chen Y., Miao X., Xu X., Mao H., Shi Z., Jin T. 2021. Quantifying air pollutant emission from agricultural machinery using surveys—A case study in Anhui, China. Atmosphere 12, 440. https://doi.org/10.3390/atmos12040440

Almaraz M, Bai E, Wang C, Trousdell J, Conley S, Faloona I, Houlton B. 2018. Agriculture is a major source of NOx pollution in California. Science Advances 4: 1−8. https://doi.org/10.1126/sciadv.aao3477]

Araki S, Shima M, Yamamoto K. 2018. Spatiotemporal land use random forest model for estimating metropolitan NO_2 exposure in Japan. Science of The Total Environment 634: 1269-1277. https://doi.org/10.1016/j.scitotenv.2018.03.324

Bais AF, Lubin D, Arola A, Bernhard G, Blumthaler M, Chubarova N, Erlick C, Gies HP, Krotkov NA, Lantz K, Mayer B, Mckenzie RL, Piacentini RD, Seckmeyer G, Slusser JR, Zerefos CS. 2007. Surface ultraviolet radiation: past, present, and future. In: Scientific assessment of ozone depletion: 2006. Geneva: World Meteorological Organization, 21.

Bimbaitė V, Girgždienė R. 2007. Evaluation of Lithuanian air quality monitoring data applying synoptical analysis. Journal of Environmental Engineering and Landscape Management 15: 173−181. https://doi.org/10.3846/16486897.2007.9636926

Bechle M, Millet D, Marshall J. 2011. Effects of income and urban form on urban NO_2: Global evidence from satellites. Environmental Science and Technology 45: 4914–4919. https://doi.org/10.1021/es103866b

Beirle S, Platt U, Wenig, M, Wagner, T. 2003. Weekly cycle of NO_2 by GOME measurements: a signature of anthropogenic sources. Atmospheric Chemistry and Physics 3: 2225−2232. https://doi.org/10.5194/acp-3-2225-2003

Bittencourt G, Pinheiro D, Bageston J, Bencherif H, Steffenel L, Vaz Peres L. 2019. Investigation of the behavior of the atmospheric dynamics during occurrences of the ozone hole's secondary effect in southern Brazil. Annals of Geophysics 37, 1049–1061. https://doi.org/10.5194/angeo-37-1049

Bond D, Zhang R, Tie X, Brasseur G, Huffines G, Orville R, Boccippio D. 2001. NOx production by lightning over the continental United States. Journal of Geophysical Research Atmospheres 106, 27701–27710. https://doi.org/10.1029/2000JD000191

Breiman L. Random Forests. 2001. Machine Learning 45: 5–32. https://doi.org/10.1023/A:1010933404324

Chan K, Khorsandi E, Liu S, Baier F, Valks P. 2021. Estimation of surface NO_2 concentrations over Germany from TROPOMI satellite observations using a machine learning method. Remote Sensing 13: 969. https://doi.org/10.3390/rs13050969

CONAMA (Conselho Nacional do Meio Ambiente). 2018. Padrões de qualidade do ar (Resolução nº 491/2018). Diário Oficial da União 223: 155–156.

COREDEs (Conselhos Regionais de Desenvolvimento). 2010. Taxa de urbanização. Available at https://atlassocioeconomico.rs.gov.br/grau-de-urbanizacao (accessed: 2021 July 19).

DEFRA (Department for Environment, Food and Rural Affairs). 2021. National statistics: air quality statistics in the UK, 1987 to 2020−Nitrogen dioxide (NO_2). Available at https://www.gov.uk/government/statistics/air-quality-statistics/ntrogen-dioxide (accessed: 2021 July 19).

Di Q, Amini H, Shi L, Kloog I, Silvern R, Kelly J, Sabath MB, Choirat C, Koutrakis P, Lyapustin A, Wang Y. 2020. Assessing NO_2 concentration and model uncertainty with high spatiotemporal resolution across the contiguous United States using ensemble model averaging. Environmental science & technology 54: 1372−1384. https://doi.org/10.1021/acs.est.9b03358

Dou X, Liao C, Wang H, Huang Y, Tu Y, Huang X, Peng Y, Zhu B, Tan J, Deng Z, Wu N, Sun T, Ke P, Liu Z. 2021. Estimates of daily ground-level NO_2 concentrations in China based on Random Forest model integrated K-means. Advances in Applied Energy 2 :100017. https://doi.org/10.1016/j.adapen.2021.100017

EMBRAPA (Brazilian Agricultural Research Corporation). 2003. Climate of Rio Grande do Sul, Section of Geography, edited by EMBRAPA, Secretary of Agriculture, Porto Alegre (in Portuguese).

EPA (Environmental Protection Agency) .2021. Nitrogen Dioxide trends. Available at https://www.epa.gov/air-trends/nitrogen-dioxide-trends. (accessed: 2021 July 31).

Fajersztajn L, Saldiva P, Pereira L, Leite V, Buehler A. 2017. Short-term effects of fine particulate matter pollution on daily health events in Latin America: a systematic review and meta-analysis. International Journal Public Health 62: 729–738. http://dx.doi.org/10.1007/s00038-017-0960-y

FEPAM (Fundação Estadual de Proteção Ambiental Henrique Luís Roessler). 2021. Rede estadual de monitoramento automático da qualidade do ar. Available at http://www.fepam.rs.gov.br/qualidade/relatorios.asp. (accessed: 2021 March 19).

Gariazzo C, Carlino G, Silibello C, Renzi M, Finardi S, Pepe P, Radice P, Forastiere F, Michelozzi P, Viegi G, Stafoggia M. 2020. A multi-city air pollution population exposure study: Combined use of chemical-transport and random-Forest models with dynamic population data. Science of The Total Environment 724: 138102. https://doi.org/10.1016/j.scitotenv.2020.138102.

Giovannini L, Ferrero E, Karl T, Rotach M, Staquet C, Trini Castelli S, Zardi D. 2020. Atmospheric pollutant dispersion over complex terrain: Challenges and needs for improving air quality measurements and modeling. Atmosphere 11: 646. https://doi.org/10.3390/atmos11060646

Guarnieri RA, Guarnieri FL, Contreira DB, Padilha LF, Echer E, Pinheiro DK, Schuch AMP, Makita K, Schuch NJ. 2004. Ozone and UV-B radiation anticorrelations at fixed solar zenith angles in southern Brazil. Geofísica Internacional 43: 17–22. https://doi.org/10.22201/igeof.00167169p.2004.43.1.209

Guo X., Wu H., Chen D., Ye Z., Shen Y., Liu J., Cheng S. 2020. Estimation and prediction of pollutant emissions from agricultural and construction diesel machinery in the Beijing-Tianjin-Hebei (BTH) region, China, Environmental Pollution 260: 113973. https://doi.org/10.1016/j.envpol.2020.113973.

Hijmans R, Cameron S, Parra J, P, Jarvis A. 2005. Very high-resolution interpolated climate surfaces for global land areas. International Journal of Climatology 25: 1965−1978. https://doi.org/10.1002/joc.1276

Hoek G, Eeftens M, Beelen R, Fischer P, Brunekreef B, Folkert K, Pepijn B. 2015. Satellite NO_2 data improve national land use regression models for ambient NO_2 in a small densely populated country. Atmospheric Environment 05:173-180. https://doi.org/10.1016/j.atmosenv.2015.01.053.

IBGE (Instituto Brasileiro de Geografia e Estatistica). 2021. Cidades. Rio Grande do Sul. Available at http://www.cidades.ibge.gov.br (accessed: 2021 August 10).

Kamińska JA. 2019. A random forest partition model for predicting NO_2 concentrations from traffic flow and meteorological conditions. Science of The Total Environment 651: 475-483. https://doi.org/10.1016/j.scitotenv.2018.09.196.

Kirchhoff VWJH, Echer E, Leme NP, Silva AA. 2000. A variação sazonal da radiação ultravioleta solar biologicamente ativa. Revista Brasileira de Geofísica 18: 63–74. https://doi.org/10.1590/S0102-261X2000000100006

Kuhn, M. 2008. Building predictive models in R using the caret package. Journal of statistical software 28: 1−26. https://doi.org/10.18637/jss.v028.i05

Krotkov N, Carn S, Krueger A, Bhartia P, Yang K. 2006. Band residual difference algorithm for retrieval of SO_2 from the Aura Ozone Monitoring Instrument (OMI). IEEE Transactions on Geosciences and Remote Sensing 44, 1259–1266. https://doi.org/10.1109/TGRS.2005.861932.

Larkin A, Geddes J, Martin R, Xiao Q, Liu Y, Marshall J, Brauer M, Hystad P. 2017. Global land use regression model for nitrogen dioxide air pollution. Environmental Science and Technology 51, 6957–6964. https://doi.org/10.1021/acs.est.7b01148

Levelt P, Van Den Oord G, Dobber M, Mälkki A, Visser H, De Vries J, Stammes P, Lundell J, Saari H. 2006. The ozone monitoring instrument. IEEE Transactions on Geoscience and Remote Sensing 44, 1093–1101. https://doi.org/10.1109/TGRS.2006.872333.

Livi F. 2002. O clima em Porto Alegre no século XX: uma análise de séries temporais. Master's thesis. Federal University of Rio Grande do Sul, Porto Alegre, Brazil.

Liu F, Zhang Q, van der A RJ, Zheng B, Tong D, Yan L, Zheng Y, He K. 2016. Recent reduction in NOx emissions over China: synthesis of satellite observations and emission inventories. Environmental Research Letters 11: 114002. https://doi.org/10.1088/1748-9326/11/11/114002

Li R, Cui L, Liang J, Zhao Y, Zhang Z, Fu H. 2020. Estimating historical SO_2 level across the whole China during 1973–2014 using random forest model. Chemosphere 247: 125839. https://doi.org/10.1016/j.chemosphere.2020.125839

Liu Q, Harris JT, Chiu LS, Sun D, Houser PR, Yu M, Duffy DQ, Little MM, Yang C. 2021. Spatiotemporal impacts of COVID-19 on air pollution in California, USA. Science of The Total Environment 750: 141592. https://doi.org/10.1016/j.scitotenv.2020.141592.

Lu M, Schmitz O, de Hoogh K, Kai Q, Karssenberg D. 2020. Evaluation of different methods and data sources to optimise modelling of NO_2 at a global scale. Environment International 142: 105856. https://doi.org/10.1016/j.envint.2020.105856

Liaw A, Wiener M. 2002. Classification and regression by random Forest. R news 2:18−22.

Meyer H, Reudenbach C, Wöllauer S, Nauss T. 2019. Importance of spatial predictor variable selection in machine learning applications–Moving from data reproduction to spatial prediction. Ecological Modelling 411: 108815. https://doi.org/10.1016/j.ecolmodel.2019.108815

Mostafa MK, Gamal G, Wafiq A. 2021. The impact of COVID 19 on air pollution levels and other environmental indicators - A case study of Egypt. Journal of

Environmental Management 277: 111496. https://doi.org/10.1016/j.jenvman.2020.111496

Mossmann Koch N, Lucheta F, Käffer M, Martins S, Ferrão V. 2018. Air quality assessment in different urban areas from Rio Grande do Sul State, Brazil, using lichen transplants. Annals of the Brazilian Academy of Sciences 90: 2233−2248. http://dx.doi.org/10.1590/0001-3765201820170987

Munzi S, Pisani T, Loppi S. 2009. The integrity of lichen cell membrane as a suitable parameter for monitoring biological effects of acute nitrogen pollution. Ecotoxicology and Environmental Safety 72, 2009–2012. https://doi.org/10.1016/j.ecoenv.2009.05.005

Oikawa P, Ge C, Wang J, Eberwein J, Liang L, Allsman L, Grantz D, Jenerette G. 2015. Unusually high soil nitrogen oxide emissions influence air quality in a high-temperature agricultural region. Nature Communications 6:8753. http://dx.doi.org/10.1038/ncomms9753

Pan Y, Zhao C, Liu Z. 2021. Estimating the daily NO_2 concentration with high spatial resolution in the Beijing–Tianjin–Hebei Region Using an Ensemble Learning Model. Remote Sensing 13: 758. https://doi.org/10.3390/rs13040758

Parra MA, Elustondo D, Bermejo R, Santamaria JM. 2009. Ambient air levels of volatile organic compounds (VOC) and nitrogen dioxide (NO_2) in a medium size city in Northern Spain. Science of the Total Environment 407: 999−1009. https://doi.org/10.1016/j.scitotenv.2008.10.032

Penn E, Holloway T. 2020. Evaluating current satellite capability to observe diurnal change in nitrogen oxides in preparation for geostationary satellite missions. Environmental Research Letters 15: 034038. https://doi.org/10.1088/1748-9326/ab6b36

Qin K, Han X, Li D, Xu J, Loyola D, Xue Y, Zhou X, Li D, Zhang K, Yuan L. 2020. Satellite-based estimation of surface NO_2 concentrations over east-central China: A comparison of POMINO and OMNO2d data. Atmospheric Environment 224: 117322. https://doi.org/10.1016/j.atmosenv.2020.117322

Reboita MS, Gan MA, Rocha RPD, Ambrizzi T. 2010. Regimes de precipitação na América do Sul: uma revisão bibliográfica. Revista Brasileira de Meteorologia 25: 185−204. https://doi.org/10.1590/S0102-77862010000200004

Réquia W, Koutrakis P, Roig H. 2015. Spatial distribution of vehicle emission inventories in the Federal District, Brazil. Atmospheric Environment 112: 32–39. http://dx.doi. org/10.1016/j.atmosenv.2015.04.029

Rienecker M, Suarez M, Gelaro R, Todling R, Bacmeister J, Liu E, Woollen J.2011: MERRA—NASA's Modern-Era Retrospective Analysis for Research and Applications. Journal of climate 24: 3624–3648, https://doi: doi:10.1175/JCLI-D-11-00015.1

Rossato MS. 2011. Os climas do Rio Grande do Sul: variabilidade, tendências e tipologia. Thesis (Doctorate) -Universidad Federal de Rio Grande do Sul. Institute of Geosciences. Graduate Program in Geography, Porto Alegre, Brazil. Available at http://hdl.handle.net/10183/32620 (accessed: 2021 June 01).

Seinfeld J, Pandis S. 1998. Atmospheric Chemistry and Physics: from air pollution to climate change. Wiley Interscience, New York.

Silva J, Honscha J, Brum R, Ramires P, Tavella R, Fernandes C, Penteado J, Bonifácio A, Volcão L, Santos M, Coronas M. 2020. Air quality in cities of the extreme south of Brazil. Ecotoxicology and Environmental Contamination 15 :61-67. https://doi: 10.5132/eec.2020.01.08

Schnitzhofer R, Beauchamp J, Dunkl J, Wisthaler A, Weber A, Hansel A. 2007. Long-term measurements of CO, NO, NO_2, benzene, toluene and PM10 at a motorway location in an Austrian valley. Atmospheric Environment 42: 1012−1024. https://doi.org/10.1016/j.atmosenv.2007.10.004.

Tanskanen A, Krotkov NA, Herman JR, Arola A. 2006. Surface ultraviolet irradiance from OMI. IEEE Transactions on Geoscience and Remote Sensing 44: 1267–1271. https://doi.org/10.1109/TGRS.2005.862203

UBA (German Environment Agency). 2020. Air quality 2019. Available at https://www.umweltbundesamt.de/en/press/pressinformation/air-quality-2019-trend-in-no2-decline-continues (accessed: 2021 August 10).

Wang Q, Su M. 2020. A preliminary assessment of the impact of COVID-19 on environment – A case study of China. Science of the Total Environment 728: 138915. https://doi.org/10.1016/j.scitotenv.2020.138915

WHO (World Health Organization). 2000. Air Quality Guidelines. Available at https://www.euro.who.int/__data/assets/pdf_file/0017/123083/AQG2ndEd_7_1nitro gendioxide.pdf/ (accessed: 2021 June 10).

WHO (World Health Organization). 2005. Air quality guidelines – Global update 2005. Particulate matter, ozone, nitrogen dioxide and sulfur dioxide. World Health Organization.

WHO (World Health Organization). 2018. Air Pollution. Available at http://www.who.int/ airpollution/ (accessed: 2021 August 10).

Wright MN, Ziegler A. 2017. Ranger: A fast implementation of random forests for high dimensional data in C++ and R. Journal of Statistical Software **77**: 1–17. https://doi.org/10.18637/jss.v077.i01

Zhan Y, Luo Y, Deng X, Zhang K, Zhang M, Grieneisen M, Di B. 2018. Satellite-based estimates of daily NO_2 exposure in China using hybrid random forest and spatiotemporal kriging model. Environmental Science & Technology 52: 4180-4189. https://doi.org/10.1021/acs.est.7b05669

Zhan Y, Luo Y, Deng X, Grieneisen M, Zhang M, Di B. 2018. Spatiotemporal prediction of daily ambient ozone levels across China using random forest for human exposure assessment. Environmental Pollution 233: 464e473. https://doi.org/10.1016/j.envpol.2017.10.029

Zhang R, Tie X, Bond D. 2003. Impacts of anthropogenic and natural NOx sources over the U.S. on tropospheric chemistry. Proc. Natl. Acad. Sci. USA 2003, 100, 1505–1509.

Zhu Y, Zhan Y, Wang B, Li Z, Qin Y, Zhang K. 2019. Spatiotemporally mapping of the relationship between NO_2 pollution and urbanization for a megacity in Southwest China during 2005–2016. Chemosphere 220: 155−162. https://doi.org/10.1016/j.chemosphere.2018.12.095

3.3   Artigo 3: Spatiotemporal distributions of ultraviolet radiation from OMI orbital data and relationships with Total O_3 and Total NO_2.

Artigo submetido na Revista Atmósfera— Universidad Nacional Autónoma de México

Spatiotemporal distributions of ultraviolet radiation from OMI orbital data and relationships with Total O_3 and Total NO_2

Adriana BECERRA-RONDÓN[1][*], Jorge DUCATI[1] and Rafael HAAG[2]

[1] *Centro Estadual de Pesquisas em Sensoriamento Remoto e Meteorologia, Universidade Federal do Rio Grande do Sul, Av. Bento Gonçalves, 9500, Porto Alegre, RS, Brazil.*
[2] *Universidade Estadual do Rio Grande do Sul, Av. Bento Gonçalves, 8855, Porto Alegre, RS, Brazil.*

* Corresponding author: abecerrarondon@gmail.com

Ultraviolet radiation spatiotemporal based on OMI dataset 2006–2020

HIGHLIGHTS

- The annual average Erythemal Daily Doses was 3523.18 J/m2, with a long-term decreasing trend in 29.76% of the area.
- During fifteen years, the highest number of days with high erythemal daily doses (EDD90+) was in 2006.
- The correlation between EDD90+ with Total O3 was negative, and with Total NO2 was both positive/negative.

GRAPHICAL ABSTRACT
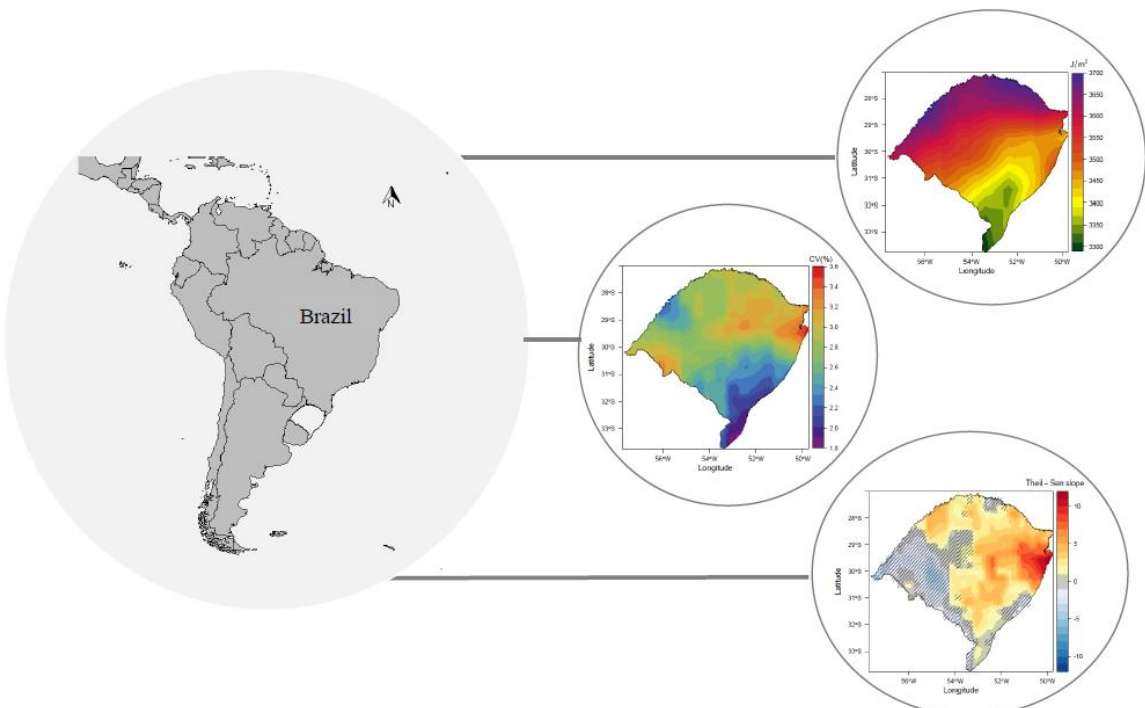
RESUMEN

La radiación ultravioleta (UVR) juega un papel clave en la fotoquímica de la atmósfera, a través de procesos de absorción o dispersión por sus constituyentes (ozono, nubosidad, aerosoles y contaminantes en la troposfera). Cuantificar la RUV de forma espacio-temporal y conocer su relación con las variables moduladoras es importante para el estado de Rio Grande do Sul, una región con una de las tasas de neoplasias cutáneas más altas de Brasil. En este estudio se utilizaron los datos de radiación ultravioleta para la región, adquiridos por el Instrumento de Monitoreo de Ozono (OMI) para el período 2006 a 2020, y expresados en términos de Dosis Diaria Eritematosa (EDD), con el objetivo de cuantificar la incidencia de RUV, su estabilidad en el tiempo y distribución espacial. Nuestros resultados muestran que para esta área de estudio la radiación varía de 3300 a 3700 J/m^2, con un gradiente latitudinal de 66,7 J/m^2 por grado, con máximos registrados en diciembre (6028 J/m^2, verano) y mínimos en junio (1123 J/m^2, invierno). El 29,76% del área tuvo una tendencia decreciente a largo plazo, mientras que el 6,19% del área tuvo una tendencia creciente. Durante el período estudiado de quince años, las ocurrencias de valores altos de Dosis Diaria Eritematosa se correlacionan negativamente con el O_3 Total como relación dominante, registrándose también correlaciones positivas o negativas con el NO_2 Total, dependiendo de la época o región investigada.

ABSTRACT

Ultraviolet radiation (UVR) plays a key role in the photochemistry of the atmosphere, through absorption or dispersion processes by its constituents (ozone, cloudiness, aerosols, and pollutants in the troposphere). Quantifying UVR in a spatial-temporal way and knowing its relationships with modulating variables is important for Rio Grande do Sul State, a region with one of the highest skin neoplasms rates in Brazil. Ultraviolet radiation data for the region, acquired by the Ozone Monitoring Instrument (OMI) for the 2006 to 2020 period, and expressed in terms of Erythemal Daily Dose (EDD), was used in this study, with the objectives of quantifying UVR incidence, its stability in time and spatial distribution. Our results show that for this study area the radiation varies from 3300 to 3700 J/m^2, with a latitudinal gradient of 66.7 J/m^2 per degree, with maxima recorded in in December (6028 J/m^2, summer) and minima in June (1123 J/m^2, winter). 29.76% of the area had a long-term decreasing trend, while 6.19% of the area had an increasing trend. During the studied period of fifteen years,

occurrences of high values of Erythemal Daily Dose are negatively correlated with Total O_3 as the dominant relationship, being also recorded positive or negative correlations with Total NO_2, depending of the investigated epoch or region.

Keywords: Erythemal Daily Dose, Atmospheric constituents. Brazil.

1. Introduction

From the total energy emitted by the Sun, only 8% of what arrives at the top of Earth's atmosphere is ultraviolet radiation, being still reduced to 4% upon arriving at Earth's surface due to physical processes in the atmosphere and to additional—geographical, temporal, astronomical, and others—factors (Iqbal, 1983; Huffman, 1992; Guarnieri et al., 2004; Silva et al., 2008; Fountoulakis et al., 2020). This radiation falls mainly into the UV−A range (315-400 nm) which has low atmospheric absorption, and in UV−B (280−315 nm), which, even if being less intense, is important to several photochemical and biological processes. A third component, UV−C (200−280 nm), is absorbed in the stratosphere during the process of the ozone layer formation (Koller, 1965; Robinson, 1966; Guarnieri et al., 2004; Sliney, 2007; Bilbao et al., 2011; Andrade and Tiba, 2016). Monitoring of UV intensity and its fluctuation is important for biological and human health issues, and one of the most used quantifying parameters is the Erythemal Daily Dose (EDD), expressed in J/m^2 and defined as the integration over the day of the incoming ultraviolet radiation on a horizontal surface weighted with the erythema action spectrum (McKinlay and Diffey, 1987; WMO, 2007).

Since the ozone depletion detection (Farman et al., 1985), efforts have been made to quantify EDD magnitude and to estimate long-term variation trends in ultraviolet radiance, being this variation continuously estimated from satellite measurements, with a large spatial cover and with data records sufficient to produce trend projections and to estimate spatio−temporal changes (Ialongo et al., 2008; Herman, 2010), mostly focused on specific regions. The factors affecting ultraviolet radiation are generally well known, and the importance of each factor varies with latitude, climate, and the amount of atmospheric pollution at each site, giving origin to non-linear interactions involving complex absorption and scattering processes (Koronakis et al., 2002; Kerr and Fioletov, 2008).

The main parameter modulating ultraviolet absorption is stratospheric ozone (90% of total O_3), which presents a seasonal pattern due to natural processes of formation, transport, and destruction; ozone concentrations are at their lowest levels in Fall and

highest in Spring (Wakamatsu et al., 1989; André et al., 2003). However, this variability is influenced by natural phenomena and anthropogenic activities (Fahey and Hegglin, 2011; Bais et al., 2015), the latter being linked to the industrial production of nitrogen dioxide (NO_2) formed from the oxidation of nitrous oxide (N_2O) coming from the troposphere. NO_2 can attain high concentrations in the stratosphere (90% of all NO_2), where it destroys O_3 through catalytic processes by sequestering active radicals (Seinfeld and Pandis, 1998).

The impact of ultraviolet solar radiation on environmental and human health is well known by the scientific community (Davis and Sims, 1983; Caldwell et al., 2003; Tiegte et al., 2007; Cardoso, 2011; Rodriguez, 2017). However, the knowledge of variability and quantity spatio-temporal ultraviolet radiation and its relationship to processes and events in the atmosphere has received considerable attention from research projects (Grant and Heisler, 2000; Alados-Arboleda et al., 2003; Efstathiou et al., 2005; Bais et al., 2007; Kerr and Fioletov, 2008; Meleti et al., 2009; Barnard and Wenny 2010; Elsner et al., 2010; Rieder et al., 2010; Antón et al., 2012; Bernhard et al., 2013; Wolfram et al., 2013; Lopo et al., 2014; Liu et al., 2017; Čížková et al., 2018; Jebar et al., 2019; Becerra-Rondón et al., 2021; Gholamnia et al., 2021; Raptis et al., 2021). In this context, the southern part of South America, being closer to the Antarctic ozone hole, is an area exposed to high levels of ultraviolet radiation throughout the year (Corrêa and Pires 2013; Zaratti et al., 2014), making this region important (Diaz et al., 2006) at a global scale for UV studies.

While stratospheric ozone is the major atmospheric absorber of ultraviolet radiation, local changes in air pollutants may mask an ultraviolet radiation increase associated with low total ozone episodes (Meleti et al., 2009). This confusing factor may be taken into account by analyzing each pixel as its time series, helping to understand UV relationships with pollutants. Besides, taking into account that for southern Brazil ultraviolet fluxes show significant variability between seasons (Kirchhoff et al., 2000; Guarnieri et al., 2004; Kerr and Fioletov, 2008), quantifying UV variability becomes important on decision-making processes aiming to mitigate effects from exposition to ultraviolet radiation. Based on these perceptions, the objective of this research was: a) to perform an evaluation, at pixel scale, of the long-term UV variability in Rio Grande do Sul State; b) to estimate time trends in this variability and c) to investigate possible relationships between UV higher values with total O_3 and total NO_2. To this end,

satellite data will be our primary source of information, and our research will be presented in the following Sections.

2. Material and methods

2.1. Study area

Rio Grande do Sul is the Brazilian southernmost state, having international borders with Argentina to the West and with Uruguay to the South (Fig.1). Its area is 281,707 km², and with more than 11.5 million inhabitants it is the fifth most populated state in the country. The region has a humid subtropical climate with a large seasonal variation with hot summers and well-defined, cold winters. Mean temperatures vary from 15 to 18 °C, with lows of as much as -10 °C (June and July) and highs going up to 40°C (December to March) (Livi, 2002). The surface elevation ranges from sea level up to 1200 m with the highest points northeast of the state (Fig. 1).
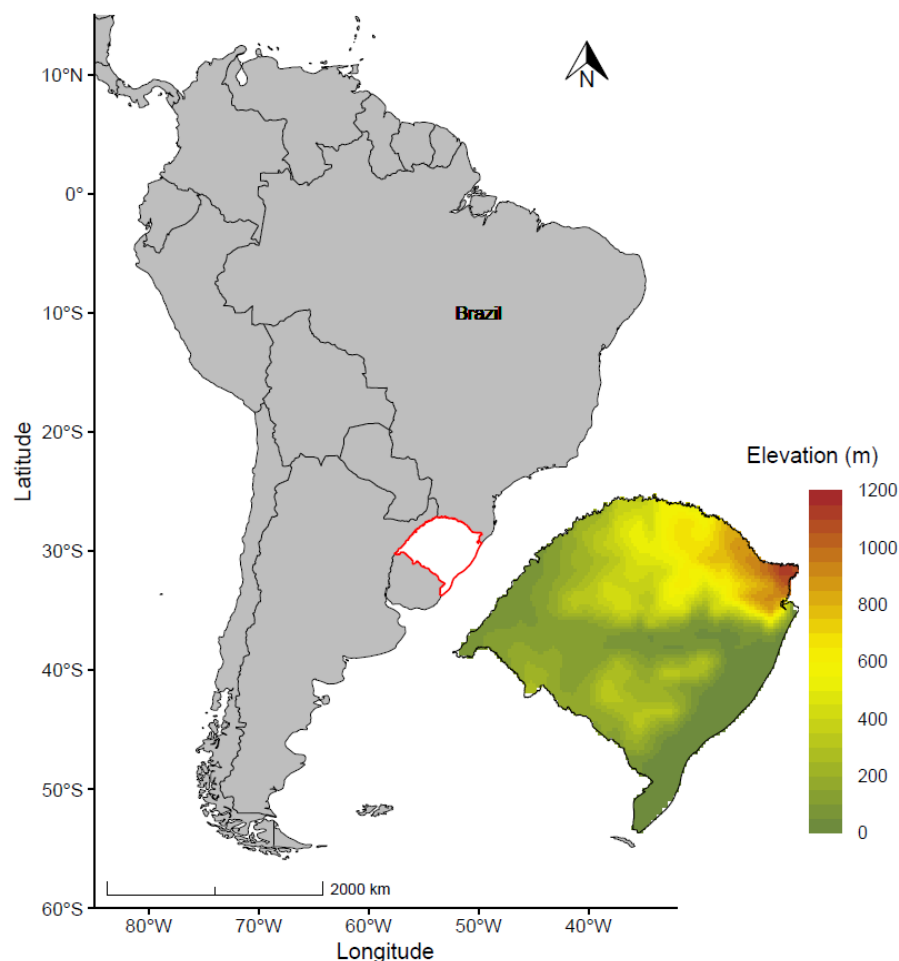
Fig. 1. Map with the State of Rio Grande do Sul, Brazil location (red contour) and its topographic representation (right).

2.2. Data source

This research was performed from data acquired by the sensor OMI (Ozone Monitoring Instrument) aboard satellite Aura. This instrument is equipped with a spectrometer pointed to the nadir which measures the ultraviolet light (264–504 nm) coming from the Sun and back-scattered by the atmosphere. The algorithms Differential Optical Absorption Spectroscopy (DOAS) and Total Ozone Mapping Spectrometer (TOMS) were developed to derive several products (Levelt et al., 2006), of which we used nitrogen dioxide (OMNO2d), total ozone (OMTO3d), and Erythemal Daily Dose (OMUVBd) (Krotkov et al., 2006; Tanskanen et al., 2006). For product OMNO2d (total column density) the data is provided in molecules/cm^2, at a spatial resolution of 0.25^0 × 0.25^0 (Lat/Lon), and with a daily frequency; product OMTO3d (total column density) is also daily, but with 1.0^0 x 1.0^0 (Lat/Lon) spatial resolution and in Dobson Units (where 1 DU = 2.7 x 1018 molecules O_3/cm^2); product OMUVBd (cumulative daily dose) is in J/m^2.

In this study, information of fifteen years (2006–2020) with 5452 images with daily measurements (99% of the series) were used to assess and analyze Erythemal Daily Dose distributions above the study area. This data was acquired from the data provider GES-DISC (https://urs.earthdata.nasa.gov) and processed using free software RStudio. The spatial resolution of products OMUVBd and OMTO3d was resampled to 0.25^0 to have uniformity with product OMNO2d. For this 0.25^0 resolution, the study area is covered by 420 cells.

2.3. Analysis

The spatio-temporal analysis of the long-term (2006-2020) Erythemal Daily Dose (EDD) consisted of two parts: (1) variation and trend, and (2) relationships of Total O_3 and Total NO_2 with higher values of Erythemal Daily Dose. All the statistical analyzes and maps have been processed using the software R, version 4.0.5 (http://R-project.org).

To analyze the spatio-temporal variation and trends in the study area, we performed the following calculations:

- The average per cell for all 420 cells of the study area for three periods (yearly, monthly and seasonal), using their daily values, is as follows:

$$Var_{i=} \frac{\sum_t {}_{end\ date}^{start\ date} Var_{i,t}}{n} \tag{1}$$

where Var*i* is the average of the variable in each cell for the respective period; start date and end date correspond to the first and last date of each period; n is the number of days in the period.

- Coefficient of variation (CV), which is a statistical measure of the dispersion of data points in a data series around the mean, expressed as:

$$CV = \frac{\sigma}{\mu} * 100 \qquad (2)$$

- From annual means of EDD, the spatiotemporal trend was determined using the Mann-Kendall trend test and Theil-Sen's slope estimator (Mann, 1945; Kendall, 1975), both of them being nonparametric tests. The Mann-Kendall test indicates trend and Theil-Sen's slope estimator indicates the slope of this trend as follows:

$$Q = \frac{EDD_i - EDD_j}{T_i - T_j} \qquad (3)$$

where EDD_i and EDD_j indicate the sequential data values of the time series in the year's T_i and T_j, respectively, with $j > i$. The calculated Q is the estimated magnitude of the trend slope in the time series of the data, where negative values indicate a downward trend and positive values indicate an upward trend.
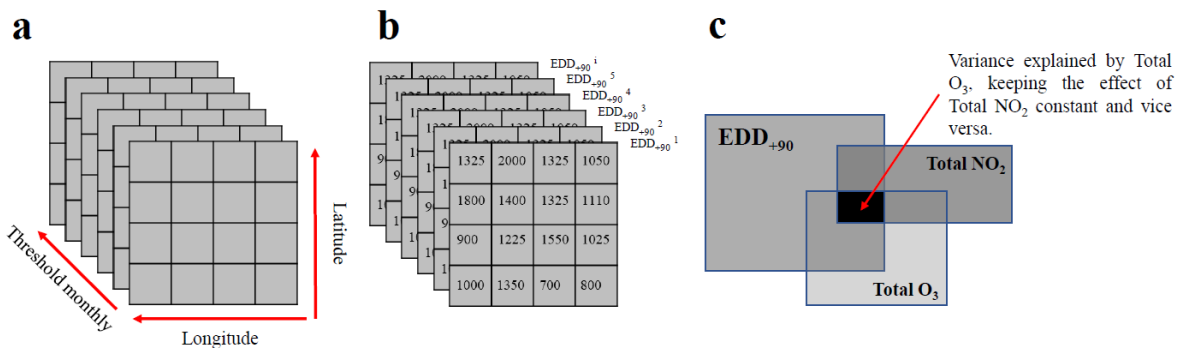
Fig. 2. Stages to evaluate the relationships with higher values of Erythemal Daily Doses.

To evaluate the relationships between the higher values of Erythemal Daily Doses with variables Total O_3 and Total NO_2, we compiled the spatial and temporal distribution of Erythemal Daily Doses at each month for the period 2006 to 2020 (Fig. 2a), being then able to establish the 90th percentile (EDD_{90+}) by pixel in each month (Fig. 2b). Once identified the EDD_{90+} days and selected the values of Total O_3 and Total NO_2 corresponding to these higher UV values for the concerned pixels, we performed a partial correlation (rpartial) and we valued only those results with a level of statistical significance α≤ 0.05. This method allowed evaluating the correlation

between two variables considering the effect (variance) of a third (Fig. 2c) and is typically applied when there is reasonable evidence of correlations between the considered variables, which is the case involving UV, NO_2, and O_3. Therefore, presently we applied this method successively for both Total O_3 and Total NO_2, in this way obtaining the respective correlations with EDD_{90+} while the other variable remained constant. To better understand and describe the results, classification criteria according to the type of correlation and the respective level of significance were established.

Additionally, having generated monthly EDD_{90+} thresholds, these results were grouped by year to estimate a) the number of times (frequency) that a pixel is repeated under this condition each year; b) the number of days per year that registered this condition.

3. Results

3.1. Spatial and temporal distribution over Rio Grande do Sul State

The average daily ultraviolet erythemal irradiance for Rio Grande do Sul State, derived from OMI observations for the 15-years studied period, is presented in Figure 3a. Values vary from 3300 to 3700 J/m^2, with an average, steady gradient in longitude of about 66.7 J/m^2. degree. The long-term spatio-temporal variations are presented in Figure 3b, with values from 1.8% to 3.6%, a fluctuation that approximately follows the gradient shown in Figure 3a. Figure 3c shows that 29.76% of the area had a long-term decreasing trend, while 6.19% of the area had a long-term increasing trend; the remaining State's area didn't record significant ($\alpha > 0.05$) trends.
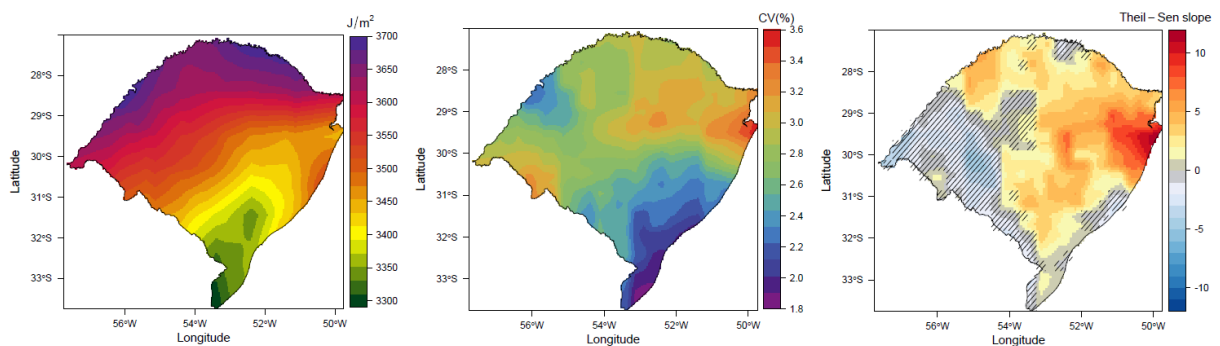
Fig. 3. Spatial distribution: a) multi-year average Erythemal Daily Dose from 2006 to 2020 (unit: J/m^2); b) coefficients of variations (CV%); c) long-term trends (Theil-Sens's slope value). Significant trends ($\alpha \leq 0.05$) are shown as hatched areas, where trends to increase are displayed as red gradients and to decrease as blue gradients.

Table I. Historical means calculated from 2006 to 2020 of Erythemal Daily Dose (J/m^2) for Rio Grande do Sul State, Brazil. Obtained from the OMI dataset.

		2006	2007	2008	2009	2010	2011	2012	2013	2014	2015	2016	2017	2018	2019	2020	Average
	Min	3268.80	3150.66	3147.99	3047.56	3062.55	2923.35	3144.24	3127.65	3062.54	3038.59	3107.56	3098.80	3103.57	3066.23	3258.64	
	Max	4048.69	3816.12	3890.14	3834.19	3938.40	3817.10	3948.04	3980.54	3766.24	3817.86	3938.17	3898.87	3950.04	3832.75	4047.60	
	Avg	3682.38	3448.17	3557.41	3455.17	3519.18	3423.95	3579.51	3592.31	3445.45	3388.14	3539.02	3526.36	3538.92	3478.90	3672.87	3523.18
	SD	169.21	140.71	155.85	167.83	191.46	180.91	164.58	186.94	152.03	169.42	178.87	168.47	185.78	155.05	181.05	
	Min	5488.48	5939.72	5617.14	5504.68	4961.95	4994.64	6129.48	5905.89	5352.54	5365.28	5844.16	5643.63	5064.32	4578.50	5716.81	
January	Max	6429.91	6797.85	6359.55	6183.63	6557.13	6215.91	6800.09	6674.06	6503.99	6242.56	6679.80	6385.24	6298.20	6154.74	6395.92	
	Avg	5894.54	6279.19	6080.60	5856.46	5843.93	5718.32	6452.78	6283.06	6005.87	5741.27	6237.72	5908.81	5681.96	5431.39	6010.57	5961.76
	Min	5131.20	5251.41	4581.02	5082.78	4674.11	4193.23	4538.52	4412.04	4767.73	4971.58	4879.41	4871.09	5434.91	4965.13	5298.93	
February	Max	5907.30	6044.07	5697.91	6044.57	6082.00	5348.34	6213.93	5603.45	5808.65	6007.45	5841.39	5684.70	6162.54	5623.77	5875.65	
	Avg	5608.42	5558.54	5372.52	5590.69	5531.27	5005.12	5423.73	5091.80	5335.45	5317.14	5479.22	5292.31	5883.53	5365.86	5600.85	5430.43
	Min	3916.93	3546.14	3833.16	3834.76	4105.68	3793.35	3690.78	3638.05	3864.86	4158.70	3551.23	3636.17	3938.33	3722.94	4022.40	
March	Max	4759.97	4738.58	4565.17	4866.91	4760.19	4438.87	4823.19	4177.45	4381.57	4527.89	4273.16	4464.31	4847.67	4322.19	5116.54	
	Avg	4410.86	4025.67	4255.23	4373.04	4456.69	4157.43	4495.57	3954.00	4129.94	4346.50	3868.19	4232.09	4390.95	4046.54	4641.13	4252.25
	Min	2326.92	2455.26	2462.56	2552.55	2464.89	2279.12	2342.64	2412.18	2336.02	2585.23	1657.28	2164.06	2279.33	2382.82	2447.82	
April	Max	3510.89	3172.53	3097.19	3580.86	3049.51	3114.04	3120.64	3500.83	3072.16	3155.04	3092.69	3185.53	3400.84	3191.08	3471.86	
	Avg	2975.73	2800.14	2846.04	3093.56	2685.01	2756.59	2762.93	2936.22	2719.92	2925.25	2336.12	2615.73	2918.77	2727.55	3078.20	2811.85
	Min	1405.48	1261.47	1302.16	1417.23	1256.34	1287.07	1447.21	1319.54	1249.94	1356.93	1186.56	1256.72	1328.20	1337.50	1530.71	
May	Max	2358.26	1764.32	2045.70	1937.72	1646.95	2037.09	2150.80	2002.00	1903.50	1931.15	1733.36	1687.89	2001.26	1627.08	2025.22	
	Avg	1804.05	1564.14	1717.16	1707.28	1417.34	1698.00	1857.55	1660.58	1547.57	1649.24	1530.44	1462.03	1583.99	1534.18	1763.86	1633.16
	Min	913.73	804.79	885.78	824.74	865.82	879.28	826.25	975.40	791.18	940.61	782.16	998.74	852.47	802.04	857.91	
June	Max	1479.06	1185.81	1289.37	1322.81	1427.01	1219.37	1328.42	1381.97	1177.11	1529.54	1357.12	1356.21	1223.61	1595.85	1286.04	
	Avg	1206.58	996.13	1099.70	1161.73	1094.31	1101.48	1074.86	1222.13	987.52	1182.22	1131.44	1153.66	1069.88	1287.23	1081.01	1123.32
	Min	992.79	892.97	1073.82	1017.59	894.56	902.76	1064.08	1007.08	836.25	1002.54	892.31	928.12	743.58	933.30	996.78	
July	Max	1724.80	1306.05	1868.98	1376.06	1493.15	1444.95	1391.53	1772.42	1420.21	1417.55	1682.35	1773.31	1521.86	1512.09	1556.63	
	Avg	1364.39	1139.92	1358.41	1254.90	1233.95	1122.99	1278.12	1425.48	1205.34	1159.73	1347.39	1495.27	1072.57	1215.55	1319.58	1266.24
	Min	1393.45	1142.04	1570.57	1410.61	1446.86	1240.69	1380.80	1449.65	1611.09	1257.35	1467.05	1294.07	1396.50	1467.94	1519.99	
August	Max	2025.51	1820.27	1919.62	1888.74	2029.95	1788.92	2154.31	1991.12	2177.76	2252.10	1976.43	2094.30	1932.47	2248.12	2216.56	
	Avg	1796.03	1448.47	1752.28	1615.48	1705.71	1564.51	1789.24	1715.54	1924.75	1793.68	1788.36	1829.37	1645.72	1861.23	1967.97	1746.56
	Min	2666.08	2157.96	2172.60	2117.35	2226.36	2372.50	2319.42	2138.77	2369.27	2299.69	2441.69	2295.98	2178.74	2521.37	2228.43	
September	Max	3089.37	3049.60	2924.10	2606.62	3162.04	3094.03	3078.70	3008.47	2747.02	3205.11	3392.04	3236.68	2814.52	2997.93	3217.45	
	Avg	2881.63	2528.25	2579.68	2398.34	2582.10	2633.46	2668.19	2647.56	2527.15	2729.82	2984.77	2694.28	2565.38	2947.72	2630.15	2666.57
	Min	3932.25	3218.74	3429.20	3606.20	3916.43	3174.74	3424.19	3811.28	3553.57	3442.41	3638.36	3267.41	3352.05	3139.08	3586.36	
October	Max	4534.77	3796.06	3944.03	4604.51	4756.67	4794.01	3964.24	4667.41	4425.30	4133.68	4664.19	4060.87	4321.33	4004.53	5037.91	
	Avg	4342.24	3401.74	3687.50	4130.93	4332.84	4083.44	3615.90	4249.34	4001.07	3783.76	4073.70	3640.47	3917.30	3595.26	4325.11	3945.37
	Min	4811.50	5289.39	4943.70	3938.55	4630.76	4984.41	5322.94	4970.05	4824.56	4360.12	5352.40	5117.16	5193.20	4940.17	4884.87	
November	Max	5904.39	5866.41	6287.10	5099.73	5817.45	5901.41	5989.90	6207.80	5637.73	5246.93	6067.33	6268.46	6094.22	5744.24	5839.23	
	Avg	5381.80	5573.39	5749.70	4365.35	5251.96	5473.05	5742.53	5486.37	5391.29	4770.12	5674.64	5852.64	5767.54	5361.81	5336.20	5411.89
	Min	6246.74	5848.03	5904.21	5263.71	5306.82	4978.41	5244.60	5491.89	5193.51	4722.65	5598.16	5712.44	5481.18	6004.03	6012.68	
December	Max	6860.07	6251.92	6682.90	6498.12	6478.56	6408.23	6360.69	6779.48	5939.91	6165.36	6498.18	6588.90	6782.01	6671.44	6532.23	
	Avg	6522.29	6062.50	6190.04	5914.31	6095.00	5772.99	5792.72	6435.61	5569.49	5258.93	6016.23	6139.60	5969.40	6372.44	6319.77	6028.75
	Min	5622.14	5679.72	5367.46	5283.72	4980.96	4722.10	5304.20	5269.94	5104.59	5019.84	5440.58	5409.05	5326.80	5182.55	5676.14	
Summer	Max	6399.09	6364.61	6246.79	6242.11	6372.56	5990.83	6458.24	6352.33	6084.18	6138.46	6339.79	6219.61	6414.25	6149.98	6267.93	
	Avg	6008.42	5966.74	5881.05	5787.15	5823.40	5498.81	5889.74	5936.82	5636.94	5439.11	5911.05	5780.24	5844.96	5723.23	5977.07	5806.98
	Min	2549.78	2420.96	2532.63	2601.51	2608.97	2453.18	2493.54	2456.59	2483.60	2700.29	2131.69	2352.32	2515.29	2481.09	2666.98	
Fall	Max	3543.04	3225.14	3236.02	3461.83	3152.22	3196.67	3364.88	3226.76	3119.08	3204.70	3033.07	3112.57	3416.59	3046.78	3537.87	
	Avg	3063.55	2796.65	2939.48	3057.96	2853.01	2870.67	3038.68	2850.27	2799.14	2973.67	2578.25	2769.95	2964.57	2769.43	3161.07	2899.09
	Min	1099.99	946.60	1176.72	1084.31	1069.08	1007.58	1090.37	1144.04	1079.51	1066.84	1047.17	1073.64	997.51	1067.76	1124.89	
Winter	Max	1743.13	1437.38	1692.66	1529.20	1650.03	1484.41	1624.75	1715.17	1591.69	1733.06	1671.97	1741.28	1559.31	1785.35	1686.41	
	Avg	1455.66	1194.84	1403.47	1344.04	1344.66	1262.99	1380.74	1454.39	1372.54	1378.54	1422.40	1492.77	1262.72	1454.67	1456.19	1378.71
	Min	3803.28	3555.36	3515.17	3220.70	3591.18	3510.55	3688.85	3640.03	3582.47	3367.41	3810.82	3560.19	3574.66	3533.54	3566.55	
Spring	Max	4509.51	4237.36	4385.07	4103.62	4578.79	4596.48	4344.28	4627.89	4270.02	4195.24	4707.86	4522.00	4410.02	4348.90	4698.20	
	Avg	4201.89	3834.46	4005.63	3631.54	4055.64	4063.32	4008.87	4127.75	3973.17	3761.23	4244.37	4062.46	4083.41	3968.26	4097.15	4007.94

Monthly averages had values as high as 6028 J/m^2 in December and as low as 1123 J/m^2 in June (Figure 4 and Table I). Besides, it was observed that April and August were the months with the largest changes in ultraviolet erythemal irradiance, dropping from 2811 J/m^2 to 1633 J/m^2 from April to May and the inverse between August and September (1746 J/m^2 to 2666 J/m^2 (Figure 4, Tab. I). Regarding seasonal variations, these are more intense in the spring-summer period (4007 J/m^2 to 5411 J/m^2) rather than in the autumn-winter period (1378 J/m^2 to 2899 J/m^2) (Tab. I).
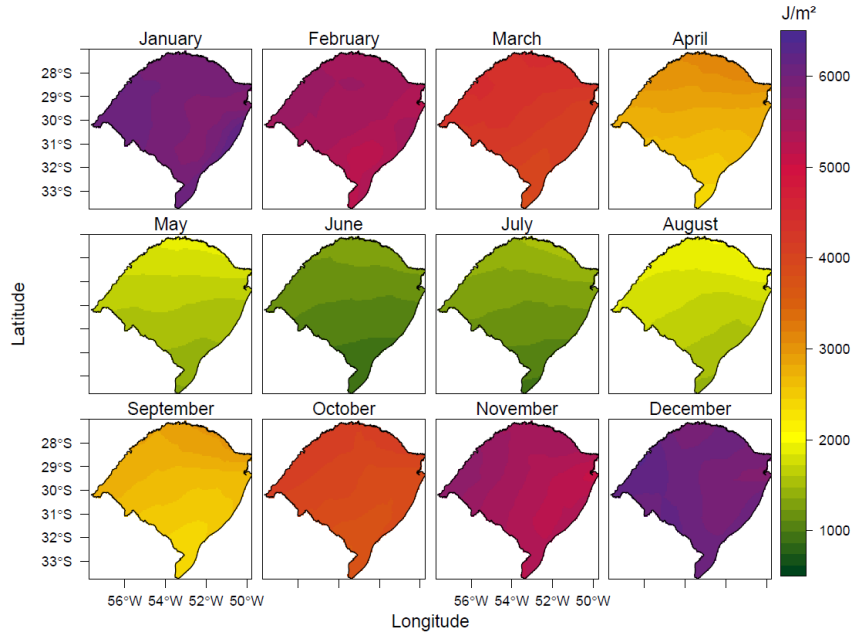
Fig. 4. Spatial-temporal distribution of the monthly Erythemal Daily Dose (J/m^2) in Rio Grande do Sul from 2006 to 2020.

Considering that the ultraviolet erythemal irradiance in Rio Grande do Sul has a defined spatial and temporal pattern (Fig. 3 and Fig. 4) and based on the 90th percentile for each pixel in each month (see Table I of the supplementary material), we derived that in 2006 there was the highest incidence of high values of ultraviolet erythemal irradiance (maximum 67 occurrences per pixel and a total of 157 days), and in 2011 the lowest incidence (maximum 20 occurrences per pixel and a total of 49 days) (Fig. 5).
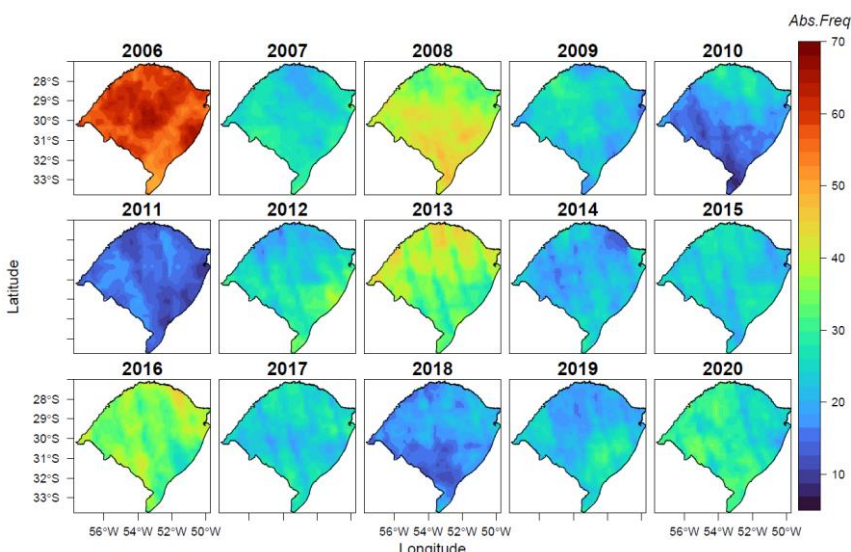
Fig. 5. Occurrence spatial-temporal distribution of high erythemal daily dose values above the 90th percentile (EDD_{90+}).

The temporal relationships of Total O_3 and Total NO_2 with the higher values of ultraviolet erythemal irradiance are presented in Figure 6. It is observed that ultraviolet erythemal irradiance and Total NO_2 present a similar pattern throughout the year with a minimum between the months that correspond to winter and maximum between the months that correspond to summer (Fig. 6a and 6c); in the meanwhile, Total O_3 presents minimum in summer and maximum in spring (Fig6. b).
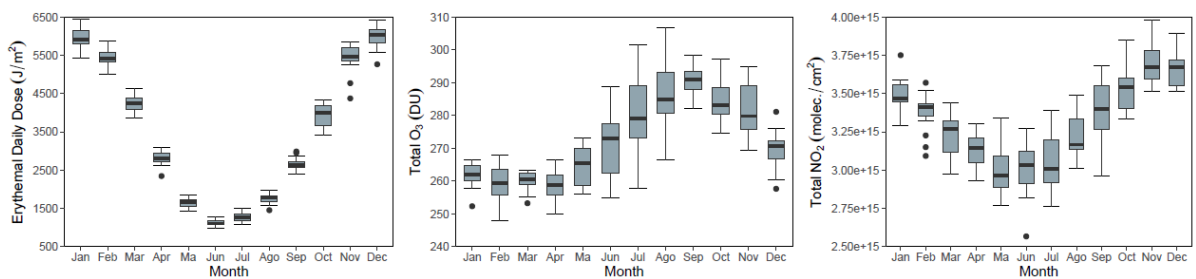
Fig. 6. The mean monthly of (a) Erythemal Daily Dose, (b) Total Ozone, and (c) Total Nitrogen Dioxide at Rio Grande do Sul for the period 2006–2020.

The partial ($r_{partial}$) pixel-to-pixel relationships between EDD_{90+} with Total O_3 and Total NO_2 vary by month (Table II to Table XIII in Appendix). In particular, we observed that occurrences of EDD_{90+} can be grouped in five situations (Table II), as follows: (a) pixels where there is a dominant negative correlation of EDD_{90+} both with Total O_3 and with Total NO_2, (b) pixels where there is a negative correlation with Total O_3 and a positive one with Total NO_2, (c) negative correlation predominates with Total NO_2, (d) negative correlation predominates with Total O_3 and, (e) cases where EDD_{90+} occurrence is not explained by its correlation neither with Total O_3 nor Total NO_2.

Table II. Classes according to partial correlation coefficients (r_{part}). [a] Total NO_2 (TNO_2), [b] Total O_3(TO_3).

Classification criteria	Class
$r_{partial}^{a} \leq 0$ & $r_{partial}^{b} \leq 0$; $pvalue^{a} \leq 0.05$ & $pvalue^{b} \leq 0.05$	$TO_3 - TNO_2$
$r_{partial}^{a} \geq 0$ & $r_{partial}^{b} \leq 0$; $pvalue^{a} \leq 0.05$ & $pvalue^{b} \leq 0.05$	$TO_3 - TNO_2$
$r_{partial}^{b} \leq 0$; $pvalue^{a} \geq 0.05$ & $pvalue^{b} \leq 0.05$	TO_3
$r_{partial}^{a} \leq 0$; $pvalue^{a} \leq 0.05$ & $pvalue^{b} \geq 0.05$	TNO_2
$pvalue^{a} \geq 0.05$ & $pvalue^{b} \geq 0.05$	Unexplained

How these five situations are distributed both temporally and spatially is shown in Figures 7a and 7b, in terms of the percentages which explain the EDD_{90+} observations. From the analysis of results presented in Figures 7, it is suggested that Total O_3 is the

main factor explaining EDD_{90+} observations for all months, having a weight ranging from 25% (April) to 93% (November), with the notable exception of May, where its contribution (and of all other considered factors) is not significant. Synergies, either positive or negative, of Total O_3 and NO_2 did not seem to play significant roles in EDD_{90+} observations, while Total NO_2 explains EDD_{90+} observations at most for 4% of all pixels. On the other hand, between 5% to 96 of pixels with EDD_{90+} seem not to be linked neither to O_3 nor to NO_2, with higher frequenciesin January (40% of the area) and May (96% of the area); EDD_{90+} data for these months remains mostly unexplained by our approach.
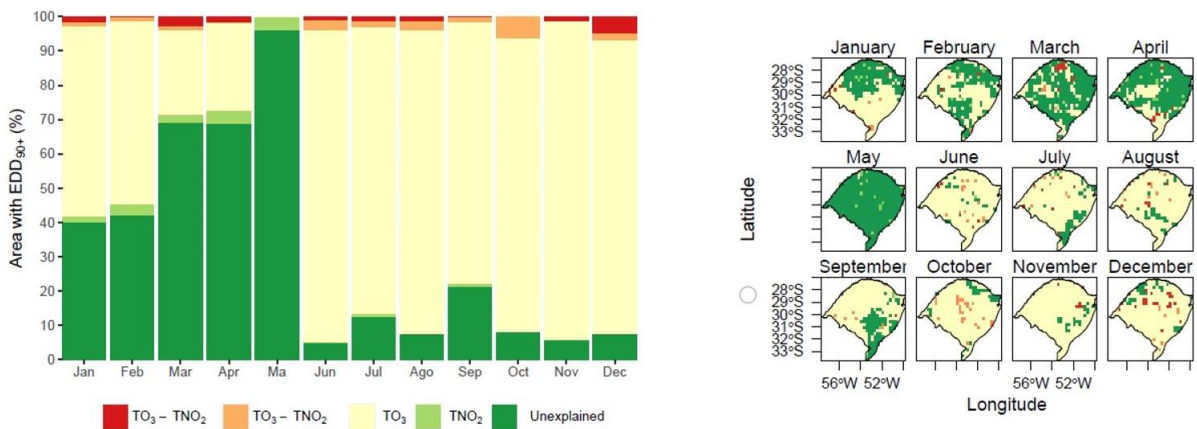
Fig. 7. Factors affecting the EDD_{90+} spatio-temporal variability in Rio Grande do Sul: a) Monthly percentage of area explained by each factor Total O_3 or Total NO_2, and their combinations, b) and its spatial location

4. Discussion

4.1. Spatial and temporal distribution over the Rio Grande do Sul State

The latitude dependence of ultraviolet erythemal irradiance within Rio Grande do Sul State shown in Figure 3a is part of an ampler dependence already reported (Corrêa 2015); even if the overall ultraviolet irradiance in south Brazil, and especially in Rio Grande do Sul, present lower values if compared with northern regions, detailed knowledge of its magnitude and distribution is of interest by demographical reasons: the State presents the country's highest rates of melanoma cancer, a fact that is attributed to a higher percentage of people of Caucasian or European origins, who exposed to UV radiation presents a greater predisposition to develop this pathology (Lee-Taylor et al., 2010; Corrêa, 2015; INCA, 2020). From Figure 3a it can be seen that UV erythemal irradiance varies significantly across the State, a perception that is reinforced by what is presented in Figure 3b, and especially from Figure 3c, which

suggests that irradiance had a positive time variation in a non-negligible fraction of the State's area during the period covered by our data. Presently, information on skin cancer incidence in different regions of the State is still lacking, and this study provides useful information for the understanding of the data which eventually will be available, and the corresponding management. It is also important to note that the erythemal ultraviolet irradiance received in the fall of 2020 (with 3161 J/m^2) was higher than in the autumns of the previous fourteen years, in agreement with what was reported by Becerra-Rondón et al. (2021) on increases in the ultraviolet radiation index for that season in previous years. Additionally, we also note that the highest EDD values, which have been measured in 2006, coincide with a year of very low solar activity, as measured by the number of solar spots, while the lowest EDDs have been measured in 2011, that is, about half solar cycle after 2006 (Rampelotto et al., 2009; Valachovic and Zurbenko, 2014; BOM, 2021)

Presently we observe that the northeast part of the study area has the lowest latitudes and the highest altitudes, associated with the highest radiation values and with changes in intensity according to the period (for the monthly and seasonal case) (Fig. 4). This behavior is due, at least in part, to the fact that at higher sites the path through the atmosphere is shorter and scattering processes (Rayleigh and Mie) are not as important compared to sites lower, where radiation is reduced by increasing density and atmospheric components, which promotes greater attenuation (Ziemke et al. 2000); this effect is intensified when combined with the variation of the solar zenith angles (geographical and astronomical effects) (Schmucki and Philipona, 2002). Although these two aforementioned effects establish a spatial and temporal distribution pattern in our study area, changes in cloud cover, temperature, secondary effects of the Antarctic ozone hole, and other variables (eg ozone, aerosols, and air pollutants) also greatly influence short- and long-term variations (Kirchhoff et al., 1996; Koronakis et al., 2002; Schmucki and Philipona, 2002; Guarnieri et al., 2004; Kerr and Fioletov, 2008; Salgado et al. ., 2010; Schmalfuss et al., 2014; Nunes et al., 2020).

4.2. Relationships of Total O_3 and Total NO_2 with high values of Erythemal Daily Dose
Even if the temporal behavior of Total O_3 and Total NO_2, factors that affect ultraviolet radiation (Fig. 6b, 6c) is well defined, the simultaneous presence of more than one of them can lead to non-linear interactions involving complex absorption and scattering processes (Kirchhoff et al., 2000; Krotkov et al., 2001; Koronakis et al., 2002).

Moreover, the magnitude of the ultraviolet intensity varies in function of the chosen period (daily, monthly, and annual mean), and from geographical characteristics (Kerr, 2005; Ialongo et al. 2011; Cížková et al., 2018). From these perceptions, and considering the atmospheric processes and associated health hazards characteristic of our study area, we highlighted where higher values of ultraviolet radiation occurred, spatially and temporally (EDD_{90+}) (Fig. 5). From these results, the relationships of the two modulating factors Total O_3 and Total NO_2 with respect to EDD_{90+} were investigated.

We found that for nine months of an average year (from June to February) between 53% to 93% of the study area have EDD_{90+} primarily associated with Total O_3 in the form of a negative correlation (Fig. 7a and 7b). This behavior has also been reported in other works under all weather conditions (Kerr and McElroy, 1993; Guarnieri et al. 2004; Fioletov et al., 1997; Rieder et al., 2010; Bernhard et a., 2013; Lopo et al., 2014; Cížková et al., 2018; Raptis et al., 2021). In the remaining months (March to May) from 70% to 96% of the area have EDD_{90+} unexplained by Total O_3 and/or Total NO_2, being therefore attributed to variables not considered in this study. A large inversion of the Total O_3 weight between May and June was observed; while it is true that Total O_3 is the main driver of long-term variations in ultraviolet radiation intensities, it can also be argued that the solar zenith angle (SZA) and cloud cover are non-negligible factors in the short term, gaining more importance during autumn and summer respectively (Lopo et al., 2014; De Bock et al., 2014; Cížková et al., 2018). In this context and considering the complexity of interactions with ultraviolet radiation, the Rio Grande do Sul state, during autumn and winter, is also under the effect of atmospheric circulation patterns (equatorial Atlantic mass, tropical Atlantic, continental tropical, and polar), that promote the transport of flows of ozone-poor air from the tropics towards high latitudes, accompanied by higher air pressures that lead to clear or partially cloudy skies, leading to the incidences of EDD_{90+} (Stick et al., 2006; Rossato, 2011).

Meanwhile, although in a smaller proportion of the studied area (between 0.2−6.4%) throughout the year, the relationship of Total NO_2 with EDD_{90+} values exists in three situations (Table II), depending of the pixels (regions) considered, in an example of how the complexity of the interaction of more than one variable in time and space generates the same effect.

Associating our results and their derived perceptions to what has been reported elsewhere (Rieder et al., 2010; Cížková et al., 2018), high values of ultraviolet radiation

tend to be associated to low Total O_3 levels and with the absence of clouds or with partly cloudy skies. Furthermore, the influence of air pollutants (e.g NO_2) over ultraviolet radiation is significant, acting in complex ways, even on cloudy days when the prevailing effect of clouds was expected; it was reported that two of these influences are that both high and low concentrations of NO_2 lead to higher ultraviolet radiation (Dickerson et al., 2004; WMO, 2020; Musiolková et al., 2021). This strongly suggests that although there are specific patterns for each variable depending on the season and cloud cover, the latter is possibly the most important, since it plays a crucial role in the influence of incident solar radiation during the day (Krotkov et al., 2001; Alados-Arboledas et al., 2003; Musiolková et al., 2021)

5. Conclusions

Human exposure to solar ultraviolet radiation has important public health implications, and evidences of hazards associated with UV overexposure have been reported in many investigations. Starting from these perceptions and taking them as motivation, this study used remote sensing data to analyze the spatio-temporal characteristics of the daily erythemal doses in Rio Grande do Sul, a region where this important information is still lacking. Our results showed that (1) the annual average of the daily accumulated Erythemal Daily Doses was 3523.18 J/m^2, with a long-term decreasing trend in 29.76% of the state's area; (2) places located in lower latitudes and higher altitudes had higher incidences of EDD; (3) there is a well defined temporal pattern, with a higher average value in summer (5806.98 J/m^2) and a lower average value in winter (1378.71 J/m^2); (4) during the fifteen years of the study (2006 to 2020), the highest number of days with high erythemal daily doses was in 2006, a year of lower solar activity; and 5) the incidence of EDD_{90+}, the occasions of incidence of the more intense radiation for the whole studied period, showed a negative correlation with Total O_3, and in a few cases either positive or negative correlations with Total NO_2; however, the lack of correlations of EDD_{90+} with both Total O_3 and Total NO_2 in many instances (places and dates) is an indication that there are variables not considered in this study. Even if part of our generated EDD_{90+} data remains unexplained, our results on the spatiotemporal distribution of the highest incidence of this radiation can be of relevant utility to official policies concerning the regional prevention of skin neoplasmas, which are already among the highest in Brazil.

References

André IRN, Ferreira NJ, Conforte JC. 2003. Análise do comportamento do ozônio estratosférico na América do Sul e vizinhanças utilizando-se imagens do satélite NIMBUS7/TOMS. In: Proceedings of the 11th Brazilian Symposium on Remote Sensing, Belo Horizonte. 1117–1124.

Alados-Arboledas L, Alados I, Foyo-Moreno I, Olmo FJ, Alcántara, A. 2003. The influence of clouds on surface UV erythemal irradiance, Atmospheric Research 66, 273–290. https://doi.org/10.1016/S0169-8095(03)00027-9

Andrade R, Tiba C. 2016. Extreme global solar irradiance due to cloud enhancement in northeastern Brazil. Renewable Energy 86, 1433–1441. https://doi.org/10.1016/j.renene.2015.09.012

Antón M, Piedehierro AA, Alados-Arboledas L, Wolfran E, Olmo FJ. 2012. Extreme ultraviolet index due to broken clouds at a midlatitude site, Granada (southeastern Spain). Atmospheric Research 118, 10−14. https://doi.org/10.1016/j.atmosres.2012.06.007

Bais AF, Lubin D, Arola A, Bernhard G, Blumthaler M, Chubarova N, Erlick C, Gies HP, Krotkov NA, Lantz K, Mayer B, Mckenzie RL, Piacentini RD, Seckmeyer G, Slusser JR, Zerefos CZ. 2007. Surface ultraviolet radiation: past, present, and future. In: Scientific assessment of ozone depletion 2006. Geneva: World Meteorological Organization, 21.

Bais AF, Mckenzie RL, Bernhard G, Aucamp PJ, Ilysa M, Madronich S, Tourpali K. 2015. Ozone depletion and climate change: Impacts on UV radiation, Photochemical and Photobiological Sciences 14, 19–52. https://doi.org/10.1039/C4PP90032D

Barnard WF, Wenny BN. 2010. Ultraviolet Radiation and Its Interaction with Air Pollution. In: Gao W, Slusser JR, Schmoldt DL, eds. UV Radiation in Global Climate Change. Berlin: Springer, 290–330. https://doi.org/10.1007/978-3-642-03313-1_11

Becerra-Rondón, A, Ducati J, Haag R. 2021. Partial COVID-19 lockdown effect in atmospheric pollutants and indirect impact in UV radiation in Rio Grande do Sul, Brazil. Atmósfera. https://doi.org/10.20937/ATM.53027

Bernhard G, Dahlback A, Fioletov V, Heikkilä A, Johnsen B, Koskela T, Lakkala K, Svendby T. 2013. High levels of ultraviolet radiation observed by ground-based instruments below the 2011 Arctic ozone hole. Atmospheric Chemistry and Physics 13, 10573–10590. https://doi.org/10.5194/acp-13-10573-2013.

Bilbao J, Román R, de Miguel A, Mateos D. 2011. Long-term solar erythemal UV irradiance data reconstruction in Spain using a semiempirical method. Journal of Geophysical Research Atmospheres 116, D22211. https://doi.org/10.1029/2011JD015836

BOM. 2021. Bureau of Meteorology. Space Weather Services: The Sun and Solar Activity. Available at https://www.sws.bom.gov.au/Educational/2/3/6 (accessed 2021 December 21).

Cardoso V. 2011. Efeitos da radiação ultravioleta-A e ultravioleta-B sobre os embriões do camarão de água-doce *Macrobrachium olfersii* (Crustacea, Decapoda) e o papel da radiação ultravioleta-A na fotorreativação. Master's thesis, Federal University of Santa Catarina, Florianópolis, Brazil.

Caldwell M, Ballaré C, Bornman J, Flint S, Björn L, Teramura A, Kulandaivelu G, Tevini M. 2003. Terrestrial ecosystems, increased solar ultraviolet radiation and interactions with other climatic change factors. Photochemical and Photobiological Sciences 2, 29–38. https://doi.org/10.1039/B211159B

Caldwell MM, Bornman JF, Ballaré CL, Flint SD, Kulandaivelu G. 2007. Terrestrial ecosystems, increased solar ultraviolet radiation, and interactions with other climate change factors. Photochemical & Photobiological Sciences 6, 252–266. https://doi.org/10.1039/b700019g

Corrêa M, Pires L. 2013. Doses of erythemal ultraviolet radiation observed in Brazil. International Journal of Dermatology 52, 966−973. https://doi.org/10.1111/j.1365-4632.2012.05834.x

Corrêa MP, Dubuisson P, Plana-Fattori A. 2003. An Overview of the Ultraviolet Index and the Skin Cancer Cases in Brazil. Photochemistry and Photobiology 78, 49–54. https://doi.org/10.1562/0031-8655(2003)0780049AOOTUI2.0.CO2

Čížková K, Láska K, Metelka L, Staněk M. 2018. Reconstruction and analysis of erythemal UV radiation time series from Hradec Králové (Czech Republic) over the past 50 years. Atmospheric Chemistry and Physics18, 1805–1818. https://doi.org/10.5194/acp-18-1805-2018

Davis A, Sims D. 1983. Weathering of Polymers. Applied Science Publishers, England. https://doi.org/10.1002/pol.1984.130220709

De Bock V, De Backer H, Van Malderen R, Mangold A, Delcloo A. 2014. Relations between erythemal UV dose, global solar radiation, total ozone column and aerosol optical depth at Uccle, Belgium. Atmospheric Chemistry and Physics 14, 12251–12270. https://doi.org/10.5194/acp-14-12251-2014.

Diffey BL. 1991. Solar ultraviolet radiation effects on biological systems. Physics in Medicine & Biology 36, 299–328. https://doi.org/10.1088/0031-9155/36/3/001

Dickerson RR, Kondragunta S, Stenchikov G, Civerolo KL, Doddridge BG, Holben B. N. 1997. The impact of aerosols on solar ultraviolet radiation and photochemical smog. Science 278, 827−830. https://doi.org/10.1126/science.278.5339.827

Diaz S, Camilión C, Deferrari G, Fuenzalida H, Armstrong R, Booth C Paladini A, Cabrera S, Casiccia C, Lovengreen C, Pedroni J, Rosales A, Zagarese H, Vernet M. 2006. Ozone and UV Radiation over Southern South America: Climatology and Anomalies. Photochemistry and Photobiology 82, 0031−8655. https://doi.org/10.1562/2005-09-26-RA-697

Efstathiou MN, Feretis H, Tzanis C, Christodoulakis J. 2005. Observed association between air pollution and the biologically effective solar ultraviolet irradiance. International Journal of Remote Sensing 26, 3487−3495. https://doi.org/10.1080/01431160500076566

Elsner JB, Jagger TH, Hodges RE. 2010. Daily tropical cyclone intensity response to solar ultraviolet radiation. Geophysical Research Letters 37, L09701. https://doi.org/10.1029/2010GL043091

Fahey DW, Hegglin ML. 2011. Twenty questions and answers about the ozone layer: 2010 update. In: Scientific assessment of ozone depletion 2010. Geneva: World Meteorological Organization, 516.

Farman JC, Gardiner BG, Shanklin JD. 1985. Large losses of total ozone in Antarctica reveal seasonal ClO x/NO x interaction. Nature 315, 207−210. https://doi.org/10.1038/315207a0

Fioletov VE, Kerr JB, Wardle DI. 1997. The relationship between total ozone and spectral UV irradiance and its use for deriving total ozone from UV measurements. Geophysical Research Letters 24, 2997–3000. https://doi.org/10.1029/97GL53153

Fountoulakis I, Diémoz H, Siani AM, Laschewski G, Filippa G, Arola A, Bais AF, De Backer H, Lakkala K, Webb AR, De Bock V, Karppinen T, Garane K, Kapsomenakis J, Koukouli ME, Zerefos CS. 2020. Solar UV Irradiance in a Changing Climate: Trends in Europe and the Significance of Spectral Monitoring in Italy. Environments 7, 1. https://doi.org/10.3390/environments7010001

Guarnieri RA, Guarnieri FL, Contreira DB, Padilha LF, Echer E, Pinheiro DK, Schuch AMP, Makita K, Schuch NJ. 2004. Ozone and UVB radiation anticorrelations at fixed solar zenith solar angles in southern Brazil. Geofísica Internacional 43, 17–22.

Gholamnia R, Abtahi M, Dobaradaran S, Koolivand A, Jorfi S, Khaloo S, Bagheri A, Hossein Vaziri M, Atabaki J, Alhouei F,Saeedi, R. 2021. Spatiotemporal analysis of solar ultraviolet radiation based on Ozone Monitoring Instrument dataset in Iran, 2005–2019. Environmental Pollution 287, 117643. https://doi.org/10.1016/j.envpol.2021.117643

Grant RH, Heisler GM. 2000. Estimation of ultraviolet-B irradiance under variable cloud conditions. Journal of Applied Meteorology 39, 904−916. https://doi.org/10.1175/1520-0450(2000)039<0904:EOUBIU>2.0.CO;2

Guarnieri RA, Guarnieri FL, Contreira DB, Padilha LF, Echer E, Pinheiro DK, Schuch AMP, Makita K, Schuch NJ. 2004. Ozone and UVB radiation anticorrelations at fixed solar zenith solar angles in southern Brazil. Geofísica Internacional 43, 17–22.

Herman J. 2010. Changes in ultraviolet and visible solar irradiance 1979 to 2008. Changes in Ultraviolet and Visible Solar Irradiance 1979 to 2008. In: Gao W., Slusser J.R., Schmoldt D.L. (eds). UV Radiation in Global Climate Change. Springer, Berlin, Heidelberg. https://doi.org/10.1007/978-3-642-03313-1_5

Huffman RE. 1992. Atmospheric ultraviolet remote sensing. Academic Press, California.

Ialongo I, Arola A, Kujanpää J, Tamminen J. 2011. Use of satellite erythemal UV products in analysing the global UV changes. Atmospheric Chemistry and Physics 11, 9649−9658. https://doi.org/10.5194/acp-11-9649-2011

Ialongo I, Casale GR, Siani A.M. 2008. Comparison of total ozone and erythemal UV data from OMI with ground-based measurements at Rome station. Atmospheric Chemistry and Physics 8, 3283−3289. https://doi.org/10.5194/acp-8-3283-2008

Iqbal M, 1983. An introduction to solar radiation. Academic Press, Toronto, New York, London.

INCA. 2020. The cancer incidence in Brazil, National Institute of Cancer José Alencar Gomes (INCA). Available at https://www.inca.gov.br/sites/ufu.sti.inca.local/files//media/document//estimativa-2020-incidencia-de-cancer-no-brasil.pdf (accessed 2021 August 10).

Jebar MAA, Parisi AV, Downs NJ, Turner J .2020. Influence of clouds on OMI satellite total daily UVA exposure over a 12-year period at a southern hemisphere site, International Journal of Remote Sensing 41, 272−283. https://doi.org/10.1080/01431161.2019.1641243

Kerr JB. 2005. Understanding the factors that affect surface ultraviolet radiation. Optical Engineering 44, 041002. https://doi.org/10.1117/1.1886817, 2005.

Kerr JB, Mcelroy CT. 1993. Evidence for large upward trends of ultraviolet- B radiation linked to ozone depletion. Science 262, 1032–1034. https://doi.org/10.1126/science.262.5136.1032

Kerr JB, Fioletov VE. 2008. Surface ultraviolet radiation. Atmospheric Ocean 46, 159–184. https://doi.org/10.3137/ao.460108

Kirchhoff VWJH, Schuch NJ, Pinheiro DK, Harris JM. 1996. Evidence for an Ozone Hole Perturbation at 30° South. Atmospheric Environment 30, 1481–1488. 379 https://doi.org/10.1016/1352-2310(95)00362-2

Kirchhoff VWJH, Echer E, Leme NP, Silva AA. 2000. A variação sazonal da radiação ultravioleta solar biologicamente ativa. Revista Brasileira de Geofísica 18, 63–74.https://doi.org/10.1590/S0102-261X2000000100006

Koronakis PS, Sfantosa GK, Paliatsosb AG, JKaldellisc K, Garofalakisd JE, Koronakie IP. 2002. Interrelations of UV-global/global/diffuse solar irradiance components and UV-global attenuation on air pollution episode days in Athens, Greece. Atmospheric Environment 36, 3173–3181. https://doi.org/10.1016/S1352-2310(02)00233-9

Koller LR. 1965. Ultraviolet Radiation. John Wiley and Sons. New York.

Krotkov NA, Herman JR, Bhartia PK, Fioletov V, Ahmad Z. 2001. Satellite estimation of spectral UV irradiance. Effects of homogeneous clouds and snow. Journal of Geophysical Research 106, 11743–11759. https://doi.org/10.1029/2000JD900721

Liu H, Hu B, Zhang L, Zhao XJ, Shang KZ, Wang YS, Wang J. 2017. Ultraviolet radiation over China: Spatial distribution and trends. Renewable and Sustainable Energy Reviews 76, 1371−1383. https://doi.org/10.1016/j.rser.2017.03.102

Lopo AB, Spyrides MHC, Lucio PS, da Silva SMP. 2014. UV extreme events in Northeast of Brazil. Ciência e Natura 36, 482−490. https://doi.org/10.5902/2179460X12816

Lucas RM, Yazar S, Young AR, Norval M, De Gruijl FR, Takizawa Y, Rhodes LE, Sinclair CA, Neale RE. 2019. Human health in relation to exposure to solar ultraviolet radiation under changing stratospheric ozone and climate. Photochemical & Photobiological Sciences 18, 641−680. https://doi.org/10.1039/C8PP90060D

Meleti C, Bais AF, Kazadzis S, Kouremeti N, Garane K, Zerefos C. 2009. Factors affecting solar ultraviolet irradiance measured since 1990 at Thessaloniki, Greece, International Journal of Remote Sensing 30, 4167−4179, https://doi.org/10.1080/01431160902822864

Musiolková M, Huszár P, Navrátil M, Špunda V. 2021. Impact of season, cloud cover, and air pollution on different spectral regions of ultraviolet and visible incident solar radiation at the surface. Quarterly Journal of the Royal Meteorological Society 147, 2834−2849. https://doi.org/10.1002/qj.4102

McKinlay AF, Diffey BL. 1987.A reference action spectrum for ultraviolet induced erythemal in human skin.Human Exposure to Ultraviolet Radiation: Risks and Regulations,W. R. Passchler and B. F. M. Bosnajakovic, Eds., Elsevier, 83–87.

Nunes MD, Mariano GL, Alonso MF. 2020. Variabilidade espaço-temporal da coluna total de ozônio e sua relação com a radiação ultravioleta na América do Sul. Revista Brasileira de Geografia Física 13, 2053−2073.

Rampelotto PH, da Rosa MB, Schuch NJ. 2009. Solar cycle and UV-B comparison for South America—South of Brazil (29° S, 53° W). In AIP Conference Proceedings. American Institute of Physics 1100, 490−493. https://doi.org/10.1063/1.3117028

Raptis IP, Eleftheratos K, Kazadzis S, Kosmopoulos P. 2021. The Effect of Ozone and Aerosols on Erythemal Irradiance in a Low Ozone Event. Atmosphere 12, 145. https://doi.org/10.3390/atmos12020145

Rieder HE, Staehelin J, Weihs P, Vuilleumier L, Maeder JA, Holawe F, Blumthalere M, Lindfors A, Peter T, Simic S, Spichtinger P, Wagner JW, Walker D, Ribatet M. 2010. Relationship between high daily erythemal UV doses, total ozone, surface albedo and cloudiness: An analysis of 30 years of data from Switzerland and Austria. Atmospheric Research 98, 9−20. https://doi.org/10.1016/j.atmosres.2010.03.006.

Robinson N. 1966. Solar Radiation. Elsevier. Amsterdam.

Rodriguez J. 2017. Características da Radiação Ultravioleta Solar e seus efeitos na saúde humana nas cidades de La Paz – Bolívia e Natal – Brasil. Doctoral thesis, Federal University of Rio Grande do Norte, Natal, Brazil.

Rossato MS. 2011. Os climas do Rio Grande do Sul: variabilidade, tendências e tipologia. Thesis (Doctorate) -Universidad Federal de Rio Grande do Sul. Institute of Geosciences. Graduate Program in Geography, Porto Alegre, Brazil. Available at http://hdl.handle.net/10183/32620 (accessed: 2021 June 01).

Salgado CAC, Paes Leme NM, Zamorano F, Quel EJ, Viana R. 2010. Influence of the ozone hole on the American. South Cone 1992−2009. In: Proceedings of the Meeting of the Americas, Foz do Iguaçu, Brazil.

Seinfeld JH, Pandis SN. 1998. Atmospheric Chemistry and Physics: from air pollution to climate change. Wiley Interscience, New York.

Silva F, Oliveira H, Marinho G. 2008. Variação do índice de radiação solar ultravioleta em Natal-RN entre 2001 e 2007. In: Brazilian Solar Energy Congress and III ISES Latin American Regional Conference, Florianópolis, Brazil.

Schmalfuss LSM, Mariano GL, Pinheiro DK, Peres LV. 2014. Análise dos dois principais fatores de decaimento da Coluna Total de Ozônio sobre o sul da América do Sul. Ciência e Natura 36, 415–422.

Schmucki DA, Philipona R. 2002. UV radiation in the Alps: the altitude effect. Proceedings of SPIE 4482, 234−239. https://doi.org/10.1117/12.452923

Sliney DH. 2007. Radiometric quantities and units used in photobiology and photochemistry: recommendations of the commission internationale de L'eclairage. Photochemistry and Photobiology 83, 425−432. https://doi.org/10.1562/2006-11-14-RA-1081

Stick C, Krüger K, Schade NH, Sandmann H, Macke A. 2006. Episode of unusual high solar ultraviolet radiation over central Europe due to dynamical reduced total ozone in May 2005. Atmospheric Chemistry and Physics 6, 1771–1776. https://doi.org/10.5194/acp- 6-1771-2006.

Tiegte JE, Diamond SA, Ankley GT, DeFoe DL, Holcombe GW, Jensen KM, Degitz SJ, Elonen GH, Hammer E. 2007. Ambient solar UV radiation causes mortality in larvae of three species of rana under controlled exposure conditions. Photochemistry and Photobiology 74, 261–268. https://doi.org/10.1562/0031-8655(2001)0740261ASURCM2.0.CO2

Valachovic E, Zurbenko I. 2014. Skin cancer, irradiation, and sunspots: the solar cycle effect. BioMed research international, 538574. https://doi.org/10.1155/2014/538574

Varotsos C, Feretis E. 1997. Health effects on human eye resulting from the increased ambient solar ultraviolet radiation. Toxicological & Environmental Chemistry 61, 43−68. https://doi.org/10.1080/02772249709358473

Wakamatsu S, Uno I, Veda H, Uehara K, Tateishh H. 1989. Observational study of stratospheric ozone intrusions into the lower troposphere. Atmospheric Environment 23, 1815–1826. https://doi.org/10.1016/0004-6981(89)90065-6

Wolfram EA, Salvador J, Orte F, Bulnes D, D'Elia R, Antón M, Alados-Arboledas L, Quel, E. 2013. Study of cloud enhanced surface UV radiation at the atmospheric observatory of Southern Patagonia, Río Gallegos, Argentina. In AIP Conference Proceedings 1531, 907. https://doi.org/10.1063/1.4804918

WMO. 2020. World Meteorological Organization. Available at https://public.wmo.int/en/media/news/arctic-ozone-depletion-reached-record-level (accessed 2020 August 10).

WMO (World Meteorological Organization). 2007. Scientific Assessment of Ozone Depletion: 2006, Global Ozone, Research and Monitoring Project−Report 50, Geneva, Switzerland.

Zaratti F, Piacentini RD, Guillén HA, Cabrera SH, Liley JB, McKenzie RL. 2014. Proposal for a modification of the UVI risk scale. Photochemical & Photobiological Sciences 13, 980−985. https://doi.org/10.1039/C4PP00006D

Ziemke JR, Chandra S, Herman J, Varotsos C. 2000. Erythemal Weighted Ultraviolet Trends Over Northern Latitudes. Radiation Protection Dosimetry 91, 157–160. https://doi.org/10.1093/oxfordjournals.rpd.a033188

APPENDIX

Table I. Threshold values for each pixel with EDD$_{90+}$per month for all period (unit: J/m^2).

Pixel	January	February	March	April	May	June	July	August	September	October	November	December
1	7431.75	6636.11	5083.81	3270.95	1856.70	1169.57	1365.59	2213.14	3354.52	5043.16	6618.57	7527.05
2	7343.86	6650.97	5089.88	3281.90	1870.50	1178.94	1367.84	2216.82	3336.07	5042.95	6623.39	7465.37
3	7358.40	6649.81	5037.83	3274.83	1870.84	1170.49	1369.81	2206.75	3346.96	4989.79	6575.10	7487.82
4	7338.57	6672.44	5086.56	3274.71	1890.66	1195.73	1376.77	2230.20	3367.46	5006.95	6624.77	7461.35
5	7320.87	6661.10	5053.17	3283.71	1892.50	1192.72	1382.75	2211.99	3376.92	4990.26	6593.38	7457.15
6	7322.95	6655.89	5070.29	3279.06	1883.11	1178.33	1387.58	2188.06	3361.78	4981.26	6558.56	7408.69
7	7336.42	6624.03	5097.70	3268.74	1925.09	1207.86	1402.75	2239.55	3371.72	5010.23	6571.92	7453.98
8	7310.73	6628.07	5070.61	3291.78	1906.05	1196.84	1404.18	2213.99	3385.84	4997.84	6618.13	7407.73
9	7299.65	6607.80	5067.06	3298.06	1900.90	1190.86	1405.39	2191.59	3392.77	4994.67	6616.80	7416.85
10	7333.57	6621.68	5193.05	3326.62	1934.47	1238.82	1436.79	2250.95	3402.28	5030.47	6618.69	7428.14
11	7312.97	6634.63	5147.27	3335.65	1923.93	1220.26	1426.56	2244.16	3401.13	5022.98	6628.13	7400.38
12	7304.44	6601.02	5099.78	3323.25	1913.03	1224.45	1407.01	2226.69	3412.23	5020.69	6618.65	7427.06
13	7362.06	6644.24	5199.63	3331.96	1982.12	1254.74	1471.67	2295.31	3479.96	5124.52	6682.94	7486.62
14	7352.44	6657.49	5177.64	3340.19	1985.22	1261.47	1459.11	2302.29	3467.00	5100.36	6653.84	7473.11
15	7354.32	6613.64	5203.27	3344.73	1979.05	1260.00	1456.25	2283.21	3441.00	5065.09	6670.20	7430.89
16	7334.64	6648.87	5160.89	3361.19	1947.96	1257.85	1445.38	2268.10	3440.03	5057.54	6637.12	7420.46
17	7320.08	6614.65	5156.73	3359.93	1950.88	1250.54	1429.42	2253.52	3435.68	5061.23	6638.40	7405.40
18	7313.19	6641.73	5170.02	3402.81	1951.75	1246.10	1422.36	2252.46	3434.95	5090.71	6611.49	7397.98
19	7375.93	6625.89	5232.18	3387.99	2011.77	1286.34	1506.62	2332.50	3505.62	5154.91	6714.79	7505.90
20	7381.09	6656.12	5209.99	3395.26	2010.76	1286.62	1493.02	2325.14	3481.62	5139.89	6717.58	7484.76
21	7378.09	6667.15	5212.30	3406.13	2007.24	1288.92	1486.10	2300.99	3468.19	5123.70	6687.17	7449.93
22	7354.68	6647.96	5197.31	3390.61	1994.50	1287.03	1473.61	2266.95	3460.19	5088.82	6683.27	7436.36
23	7331.34	6633.43	5183.26	3387.55	1976.28	1278.63	1455.09	2301.43	3461.09	5085.84	6667.47	7399.64
24	7325.79	6650.32	5201.71	3414.64	1962.90	1270.72	1450.08	2290.27	3439.32	5117.29	6629.72	7415.84
25	7308.15	6668.96	5173.16	3432.16	1971.35	1273.88	1448.54	2275.46	3439.76	5101.15	6619.54	7401.67
26	7417.59	6739.68	5346.74	3424.12	2057.07	1320.52	1549.58	2339.31	3572.80	5208.81	6781.83	7518.71
27	7394.37	6677.11	5316.70	3406.28	2053.60	1318.92	1546.88	2344.88	3541.89	5190.32	6758.70	7502.07
28	7389.28	6679.67	5265.30	3421.29	2041.36	1315.44	1535.09	2358.21	3507.86	5149.93	6725.47	7492.34
29	7387.69	6643.42	5250.75	3427.71	2043.79	1308.14	1526.04	2348.65	3507.10	5147.76	6706.36	7467.26
30	7387.11	6642.23	5235.49	3455.43	2038.77	1312.99	1518.46	2328.10	3467.55	5152.40	6718.85	7454.17
31	7355.31	6613.79	5171.24	3430.08	2027.44	1309.56	1493.73	2325.00	3447.67	5135.36	6701.59	7415.63
32	7348.57	6636.56	5202.32	3432.60	1997.75	1302.78	1488.11	2324.91	3455.63	5117.17	6691.16	7383.31
33	7331.99	6628.99	5206.19	3423.78	1979.84	1292.08	1485.61	2317.47	3449.11	5156.96	6686.71	7377.77
34	7324.42	6637.28	5210.18	3420.24	1973.17	1288.92	1477.97	2306.33	3450.05	5122.33	6617.71	7371.32
35	7336.71	6659.90	5212.18	3441.23	1989.58	1289.65	1475.07	2272.49	3475.55	5143.33	6684.69	7390.21
36	7448.75	6792.42	5363.49	3513.24	2092.77	1349.38	1583.60	2360.53	3589.79	5238.09	6840.44	7515.60
37	7438.15	6760.38	5381.08	3482.42	2084.73	1348.85	1581.42	2347.80	3610.83	5232.64	6818.98	7510.96
38	7433.63	6703.35	5378.14	3452.98	2081.18	1340.88	1570.27	2334.03	3566.63	5226.12	6784.09	7480.31
39	7418.11	6670.44	5333.75	3466.37	2075.34	1341.66	1573.73	2367.66	3531.28	5207.96	6765.41	7464.84
40	7428.60	6645.95	5323.42	3513.64	2069.43	1340.23	1585.48	2358.90	3532.73	5192.65	6757.94	7458.10
41	7401.11	6628.25	5249.95	3485.95	2058.62	1344.51	1568.12	2344.16	3496.31	5199.08	6750.28	7444.36
42	7379.52	6626.14	5207.45	3432.17	2034.97	1339.97	1541.45	2332.78	3476.92	5185.66	6723.11	7413.62
43	7355.42	6634.62	5222.38	3468.17	2019.49	1328.39	1540.76	2344.82	3466.74	5169.84	6696.24	7389.25
44	7350.01	6620.29	5242.11	3463.32	2010.39	1323.20	1524.85	2346.25	3464.07	5176.84	6675.80	7365.19
45	7347.63	6629.24	5268.82	3463.05	1989.89	1316.93	1516.40	2332.07	3472.45	5171.56	6681.95	7360.24
46	7346.59	6631.54	5266.79	3494.68	1998.22	1314.11	1507.18	2317.89	3490.41	5180.67	6720.07	7369.66
47	7339.51	6649.75	5248.55	3492.33	2022.84	1317.15	1509.08	2320.56	3505.73	5182.50	6701.10	7402.41
48	7367.84	6688.80	5253.24	3531.40	2025.81	1312.84	1490.30	2316.66	3534.96	5180.05	6683.18	7438.56
49	7471.84	6793.43	5338.89	3576.61	2127.95	1381.97	1573.49	2420.73	3639.74	5269.23	6907.38	7539.62
50	7467.23	6781.01	5401.04	3575.90	2117.34	1381.64	1602.62	2416.67	3621.48	5258.96	6891.87	7510.55
51	7451.40	6803.57	5424.38	3568.70	2126.92	1385.59	1611.39	2358.23	3616.33	5236.86	6860.70	7515.88
52	7452.48	6773.06	5410.29	3538.50	2122.45	1376.51	1616.73	2373.16	3604.30	5238.21	6828.27	7504.70
53	7464.72	6740.25	5400.55	3521.46	2112.53	1373.77	1614.32	2365.37	3607.95	5274.64	6833.78	7499.25
54	7447.66	6722.85	5357.15	3505.86	2101.78	1375.38	1614.78	2386.59	3587.76	5242.42	6810.18	7470.39
55	7461.97	6710.01	5336.56	3557.32	2094.79	1376.91	1620.10	2378.34	3588.12	5238.70	6781.53	7479.55
56	7452.88	6678.41	5286.49	3515.42	2090.33	1376.86	1596.34	2367.06	3545.47	5232.86	6784.18	7459.75
57	7424.01	6650.02	5264.03	3514.64	2072.78	1373.88	1579.39	2376.49	3525.98	5224.18	6770.10	7423.01
58	7396.09	6664.13	5240.14	3536.59	2055.68	1359.41	1576.25	2379.57	3501.67	5218.63	6748.59	7400.83
59	7361.59	6629.63	5260.63	3544.72	2049.63	1351.51	1559.11	2382.21	3496.89	5221.35	6725.12	7387.10
60	7358.16	6637.79	5269.99	3528.62	2032.32	1346.14	1550.73	2369.05	3499.81	5199.61	6707.63	7385.00
61	7367.06	6621.38	5274.31	3522.14	2034.29	1345.30	1539.30	2355.23	3508.23	5216.29	6752.09	7373.26
62	7366.97	6632.13	5274.87	3514.01	2038.89	1333.87	1529.78	2345.76	3504.37	5193.70	6709.60	7374.80
63	7374.93	6632.26	5273.24	3513.16	2055.34	1328.84	1527.32	2339.56	3527.19	5178.69	6702.99	7410.12
64	7428.38	6680.41	5293.21	3526.41	2067.71	1338.33	1518.94	2337.55	3539.39	5208.29	6714.78	7424.41
65	7490.73	6820.25	5361.58	3607.30	2154.24	1408.79	1628.56	2437.04	3695.76	5327.70	6949.28	7549.51
66	7490.24	6803.75	5366.34	3619.17	2153.99	1407.78	1625.03	2433.86	3673.45	5306.64	6879.75	7516.28
67	7465.40	6781.97	5401.69	3610.15	2149.02	1409.55	1628.49	2408.70	3664.21	5293.25	6907.47	7511.78
68	7447.88	6802.87	5402.32	3606.80	2149.57	1408.48	1635.59	2393.38	3645.40	5273.25	6878.38	7546.81
69	7440.96	6776.24	5398.23	3580.40	2143.97	1395.65	1630.01	2416.80	3640.62	5266.05	6874.19	7524.81
70	7451.73	6768.14	5363.12	3566.20	2137.70	1395.73	1626.21	2398.70	3628.41	5269.81	6859.13	7493.15
71	7452.06	6752.60	5336.89	3549.56	2120.26	1403.82	1645.66	2399.52	3632.42	5263.26	6830.61	7468.72
72	7491.61	6734.42	5327.58	3601.47	2114.17	1398.97	1648.55	2391.67	3615.74	5240.54	6809.21	7466.26
73	7481.28	6706.33	5284.42	3561.43	2109.22	1405.04	1618.08	2402.52	3597.79	5250.22	6807.64	7477.24
74	7435.13	6680.52	5280.98	3583.41	2098.85	1394.73	1632.82	2400.57	3575.61	5263.64	6797.39	7411.99
75	7380.36	6676.68	5286.65	3580.55	2100.43	1398.09	1631.90	2405.22	3551.69	5241.08	6781.35	7403.97
76	7401.23	6648.94	5251.55	3547.26	2093.08	1388.94	1632.66	2399.46	3567.53	5255.85	6745.06	7387.47
77	7364.30	6641.30	5266.39	3552.25	2081.65	1385.29	1619.81	2381.69	3569.84	5241.10	6740.74	7359.51
78	7366.00	6625.59	5296.36	3576.80	2072.83	1375.02	1600.09	2370.21	3559.88	5234.06	6756.42	7361.39
79	7357.75	6634.97	5291.16	3586.41	2070.34	1362.42	1589.73	2355.08	3553.70	5196.83	6714.78	7361.76
80	7361.07	6625.10	5280.85	3591.97	2063.27	1349.12	1572.03	2355.23	3546.23	5150.61	6706.01	7389.92
81	7420.01	6622.49	5273.51	3566.33	2066.07	1346.91	1554.33	2352.04	3561.18	5211.77	6719.31	7385.73
82	7439.74	6640.55	5296.26	3590.07	2048.76	1352.15	1553.63	2357.87	3595.71	5246.22	6744.51	7441.00
83	7496.64	6859.38	5423.07	3589.44	2164.20	1436.94	1642.19	2455.74	3749.49	5356.69	6991.82	7637.71
84	7501.37	6842.57	5372.50	3634.83	2177.03	1433.03	1650.60	2444.24	3728.45	5361.98	6949.47	7576.40

Table I. (Continuation)

Pixel	January	February	March	April	May	June	July	August	September	October	November	December
85	7488.01	6823.23	5370.92	3643.93	2171.11	1436.17	1645.26	2456.68	3715.48	5342.32	6940.53	7529.36
86	7476.55	6795.97	5380.10	3626.71	2163.54	1427.91	1642.89	2429.06	3700.65	5336.58	6927.88	7527.57
87	7456.34	6778.81	5367.70	3642.77	2162.20	1435.95	1640.79	2422.19	3691.44	5317.74	6920.69	7533.84
88	7448.57	6794.45	5361.62	3640.40	2158.79	1432.00	1642.57	2418.74	3686.03	5310.13	6903.24	7540.32
89	7453.15	6781.86	5364.97	3633.23	2160.23	1429.12	1639.47	2412.01	3672.66	5290.48	6877.40	7535.82
90	7447.30	6808.02	5361.57	3605.19	2150.52	1429.30	1632.51	2413.46	3664.44	5288.78	6852.40	7503.60
91	7462.54	6762.70	5350.46	3613.20	2141.25	1421.29	1647.80	2412.97	3655.47	5291.71	6840.11	7471.84
92	7455.99	6756.15	5326.87	3629.82	2138.71	1426.30	1663.33	2407.56	3636.99	5277.05	6797.53	7472.58
93	7423.63	6733.03	5300.29	3594.22	2139.02	1421.75	1631.92	2410.70	3617.60	5288.16	6828.78	7455.02
94	7398.25	6716.64	5305.01	3598.95	2122.69	1411.65	1670.42	2415.02	3609.31	5293.88	6799.52	7414.56
95	7391.62	6682.62	5262.91	3586.29	2113.42	1417.98	1656.25	2402.55	3598.81	5285.81	6790.85	7391.25
96	7381.99	6664.64	5267.92	3581.09	2106.26	1417.39	1659.69	2401.42	3609.94	5291.64	6766.50	7382.86
97	7361.55	6660.74	5276.18	3563.27	2099.85	1413.15	1653.81	2389.40	3604.63	5251.71	6759.61	7361.99
98	7340.69	6627.53	5290.63	3600.60	2106.76	1398.86	1640.23	2392.20	3605.37	5245.38	6789.25	7355.13
99	7328.15	6660.51	5284.92	3618.99	2092.91	1382.00	1629.02	2378.42	3614.59	5185.92	6738.99	7356.82
100	7347.07	6616.28	5257.44	3601.84	2087.88	1373.06	1617.10	2379.57	3578.84	5203.02	6728.26	7353.89
101	7387.95	6663.53	5254.65	3604.33	2080.52	1370.88	1598.11	2373.05	3581.43	5213.76	6760.29	7359.82
102	7420.42	6683.67	5259.28	3611.63	2061.84	1375.87	1591.61	2380.64	3617.82	5243.38	6760.05	7402.50
103	7452.36	6694.07	5274.56	3632.91	2066.66	1380.05	1586.70	2389.65	3670.81	5277.74	6801.09	7413.30
104	7511.75	6897.94	5505.26	3635.59	2186.95	1461.94	1669.28	2484.50	3804.44	5399.18	6990.54	7641.88
105	7495.46	6876.63	5423.64	3647.40	2201.27	1465.22	1671.14	2462.06	3770.15	5399.77	6974.07	7629.00
106	7498.64	6840.38	5394.51	3666.14	2191.80	1454.60	1663.76	2455.49	3755.31	5400.08	6985.07	7612.92
107	7495.54	6855.81	5391.49	3667.66	2195.75	1467.24	1668.94	2448.84	3745.33	5393.16	6975.75	7597.59
108	7480.67	6825.23	5393.79	3674.42	2194.33	1464.59	1661.33	2451.77	3740.21	5389.17	6947.18	7560.33
109	7468.27	6811.54	5416.29	3658.26	2184.44	1465.36	1664.16	2450.05	3726.92	5365.76	6945.09	7558.83
110	7461.75	6810.40	5426.16	3681.85	2182.13	1465.25	1669.63	2438.14	3726.86	5341.47	6922.08	7551.66
111	7453.49	6822.45	5407.44	3680.96	2183.08	1458.03	1672.76	2418.17	3716.82	5322.17	6916.92	7543.21
112	7453.55	6832.51	5407.10	3669.04	2183.85	1454.41	1645.20	2428.38	3722.62	5318.97	6893.58	7529.11
113	7435.25	6804.36	5393.12	3648.94	2177.46	1457.19	1652.56	2427.96	3716.29	5318.78	6875.00	7500.99
114	7437.97	6778.92	5378.34	3665.35	2169.29	1457.45	1662.86	2429.76	3705.79	5311.46	6846.65	7461.66
115	7440.29	6783.94	5369.39	3611.16	2182.42	1452.83	1657.48	2434.37	3698.13	5313.01	6808.16	7462.44
116	7444.23	6782.04	5359.28	3633.25	2178.78	1450.92	1648.42	2427.27	3670.27	5333.22	6820.76	7447.82
117	7439.48	6726.06	5344.67	3643.40	2148.02	1441.38	1687.67	2423.31	3655.01	5335.41	6803.11	7407.15
118	7404.28	6726.32	5321.99	3656.97	2137.15	1433.89	1694.55	2416.81	3659.55	5331.54	6787.55	7381.80
119	7407.73	6696.81	5316.91	3641.52	2126.08	1435.25	1694.21	2428.80	3664.90	5326.54	6799.52	7370.25
120	7378.91	6679.79	5312.42	3636.88	2127.84	1432.00	1691.33	2419.64	3650.57	5283.62	6790.49	7349.93
121	7343.83	6666.43	5295.37	3654.28	2118.87	1415.54	1666.71	2411.50	3668.61	5275.13	6748.63	7354.24
122	7329.75	6662.99	5285.06	3629.18	2106.66	1406.54	1663.92	2382.48	3666.57	5263.49	6752.38	7352.24
123	7355.87	6638.83	5289.73	3638.95	2107.25	1398.27	1652.08	2380.66	3657.79	5253.65	6754.09	7360.92
124	7380.51	6678.38	5279.40	3635.10	2106.64	1399.51	1646.39	2392.66	3639.19	5257.72	6785.57	7365.68
125	7415.30	6704.64	5279.05	3649.61	2088.74	1405.23	1634.26	2402.63	3670.75	5259.19	6791.19	7365.07
126	7442.75	6738.90	5277.73	3672.29	2104.61	1401.10	1627.47	2417.00	3671.21	5290.69	6797.33	7377.85
127	7536.78	6869.41	5504.88	3669.92	2217.73	1487.84	1715.88	2506.44	3812.97	5413.13	7041.49	7650.83
128	7529.37	6887.88	5522.87	3682.32	2227.01	1497.47	1695.83	2495.75	3826.82	5420.33	7025.51	7627.50
129	7517.65	6899.46	5487.35	3696.38	2218.64	1497.94	1698.87	2477.21	3811.40	5419.42	7013.98	7598.36
130	7505.58	6835.47	5478.91	3693.90	2220.36	1489.37	1695.25	2461.53	3791.88	5432.32	7002.68	7597.65
131	7499.60	6866.78	5463.24	3704.31	2222.04	1487.92	1697.21	2460.49	3758.20	5438.29	6996.57	7583.18
132	7475.24	6839.94	5444.00	3702.88	2217.26	1491.16	1707.16	2466.39	3752.21	5445.81	6979.21	7548.79
133	7470.93	6826.43	5450.00	3717.47	2218.64	1489.39	1696.82	2471.76	3754.01	5424.41	6960.88	7556.31
134	7462.25	6862.32	5481.22	3734.37	2216.17	1490.79	1706.85	2447.37	3758.52	5387.71	6937.18	7562.29
135	7475.30	6827.10	5482.57	3710.16	2213.22	1484.18	1692.66	2439.26	3746.73	5392.89	6946.28	7549.45
136	7466.64	6845.46	5447.26	3701.74	2211.29	1484.55	1669.15	2429.38	3752.33	5370.98	6938.54	7535.61
137	7471.10	6812.60	5434.78	3697.79	2207.57	1478.75	1664.97	2430.41	3755.40	5358.23	6902.26	7529.98
138	7472.64	6800.00	5421.95	3688.85	2201.81	1473.57	1679.02	2442.30	3750.31	5352.13	6865.44	7499.16
139	7463.85	6768.49	5413.88	3677.71	2212.54	1471.06	1675.33	2452.05	3729.91	5360.06	6848.60	7510.80
140	7469.07	6805.46	5416.81	3691.10	2221.49	1468.68	1709.14	2452.02	3739.78	5393.70	6850.28	7462.43
141	7437.34	6748.49	5401.78	3693.72	2182.09	1463.76	1707.99	2441.46	3728.69	5391.90	6809.52	7419.94
142	7425.23	6750.88	5378.49	3693.48	2172.56	1458.12	1719.99	2425.13	3709.43	5357.85	6806.02	7399.66
143	7404.17	6767.40	5340.03	3693.49	2159.81	1451.40	1727.25	2432.74	3725.16	5341.28	6791.53	7374.82
144	7411.03	6748.43	5343.04	3711.16	2174.50	1463.06	1721.02	2443.76	3724.25	5330.51	6817.26	7363.77
145	7376.41	6722.36	5348.99	3690.62	2165.18	1441.29	1711.88	2418.06	3729.65	5289.24	6792.72	7371.22
146	7378.60	6687.23	5335.20	3670.22	2122.61	1436.47	1696.11	2392.59	3725.66	5291.18	6798.26	7355.72
147	7389.48	6706.68	5329.83	3662.05	2120.48	1431.10	1687.95	2406.91	3701.91	5292.95	6776.20	7376.86
148	7398.57	6733.52	5320.97	3685.74	2127.67	1426.89	1681.94	2431.66	3704.40	5301.12	6811.72	7388.33
149	7416.43	6759.05	5327.49	3693.19	2130.81	1429.72	1672.85	2449.14	3701.97	5341.35	6811.82	7354.27
150	7445.29	6781.30	5313.85	3715.87	2133.51	1430.74	1667.58	2442.89	3707.31	5336.85	6800.80	7385.76
151	7517.34	6837.40	5350.97	3717.80	2134.62	1440.16	1658.76	2439.40	3688.60	5354.68	6849.09	7416.80
152	7500.23	6886.96	5545.13	3785.87	2308.81	1529.65	1767.49	2581.12	3794.23	5484.87	7081.72	7682.25
153	7507.98	6888.23	5547.28	3769.42	2296.45	1527.19	1764.29	2566.57	3805.00	5473.80	7064.57	7654.22
154	7513.50	6919.22	5551.96	3757.94	2284.79	1522.90	1762.23	2540.22	3826.12	5464.40	7055.00	7601.05
155	7519.99	6941.78	5559.91	3772.24	2290.10	1521.36	1741.68	2524.54	3836.88	5474.35	7049.15	7600.70
156	7521.75	6913.69	5548.01	3743.79	2285.16	1520.64	1752.78	2501.58	3824.16	5470.02	7034.01	7600.85
157	7515.26	6885.84	5530.73	3751.70	2272.81	1521.90	1740.88	2500.61	3803.49	5467.50	7019.75	7594.09
158	7514.17	6865.37	5526.11	3741.21	2274.66	1520.33	1741.63	2496.70	3775.34	5471.44	7018.64	7593.92
159	7504.17	6872.80	5536.73	3778.52	2282.23	1519.05	1740.92	2479.70	3772.25	5479.08	7022.23	7572.60
160	7499.40	6861.21	5543.73	3768.19	2285.18	1513.84	1741.22	2457.87	3769.74	5484.14	6996.40	7572.75
161	7488.45	6898.95	5542.82	3809.91	2285.72	1520.63	1734.62	2444.17	3781.24	5468.54	7003.67	7570.38
162	7464.55	6839.41	5534.31	3779.45	2286.18	1527.42	1745.52	2450.53	3778.46	5474.60	7022.86	7558.77
163	7505.34	6834.75	5547.11	3774.84	2295.21	1523.84	1733.25	2448.00	3792.60	5484.90	7025.20	7560.28
164	7500.11	6844.69	5538.36	3773.57	2315.65	1523.86	1738.58	2471.96	3799.60	5473.80	7011.60	7538.39
165	7490.11	6839.99	5500.10	3772.53	2289.99	1516.37	1746.96	2474.48	3794.46	5466.77	6972.19	7526.62
166	7470.32	6793.71	5486.53	3741.14	2283.52	1514.94	1729.84	2493.73	3795.68	5433.79	6916.47	7522.28
167	7490.53	6830.36	5489.99	3751.53	2284.80	1512.05	1716.85	2499.08	3776.28	5446.49	6912.28	7514.12
168	7481.97	6832.61	5478.30	3768.13	2279.26	1515.54	1760.92	2504.52	3793.10	5437.91	6892.79	7494.04

Table I. (Continuation)

Pixel	January	February	March	April	May	June	July	August	September	October	November	December
169	7444.16	6833.30	5444.25	3748.59	2266.25	1508.00	1761.66	2499.32	3768.82	5422.61	6871.55	7450.45
170	7429.86	6846.52	5434.30	3758.29	2251.66	1509.58	1761.76	2493.95	3771.40	5409.87	6879.74	7416.02
171	7423.96	6837.63	5424.44	3758.24	2247.64	1507.20	1760.96	2488.91	3759.97	5386.92	6861.33	7402.74
172	7427.23	6839.58	5432.89	3745.59	2254.34	1507.92	1746.30	2486.59	3795.81	5378.11	6879.09	7392.23
173	7429.13	6812.94	5441.40	3739.25	2245.15	1496.01	1718.99	2471.76	3793.19	5350.81	6867.61	7384.74
174	7440.29	6786.31	5442.94	3747.76	2207.78	1497.55	1732.10	2483.62	3775.32	5371.59	6865.87	7382.16
175	7450.10	6779.58	5428.68	3759.82	2200.52	1495.40	1742.98	2507.26	3776.30	5350.60	6845.55	7392.87
176	7472.83	6760.84	5401.86	3774.86	2196.81	1498.13	1739.27	2512.41	3777.39	5356.66	6854.65	7374.01
177	7482.22	6762.21	5385.00	3781.56	2197.31	1501.83	1729.46	2536.07	3767.30	5370.42	6883.89	7380.63
178	7491.17	6766.60	5386.41	3799.52	2222.77	1506.95	1726.95	2542.83	3745.75	5367.13	6890.90	7411.20
179	7499.18	6789.28	5395.88	3790.09	2246.87	1514.78	1730.61	2523.24	3759.44	5341.55	6899.08	7403.30
180	7522.70	6865.27	5572.71	3804.75	2313.98	1545.64	1781.66	2580.10	3827.17	5497.26	7102.06	7659.78
181	7522.56	6875.68	5555.15	3802.79	2310.78	1540.70	1782.36	2557.90	3802.54	5475.72	7078.27	7652.15
182	7518.66	6930.06	5568.04	3797.06	2318.12	1545.48	1784.64	2543.01	3815.42	5479.15	7087.99	7629.41
183	7527.32	6955.15	5594.18	3789.34	2332.08	1546.42	1784.60	2535.47	3826.30	5441.10	7063.49	7637.58
184	7529.51	6946.47	5587.17	3798.90	2316.50	1545.45	1783.12	2518.85	3808.14	5464.33	7056.52	7633.54
185	7522.52	6929.84	5567.79	3787.22	2303.44	1541.57	1773.74	2513.41	3803.54	5471.95	7060.13	7598.48
186	7519.65	6894.91	5576.96	3807.46	2306.65	1537.84	1770.63	2480.91	3793.88	5476.81	7064.76	7587.65
187	7520.97	6890.04	5575.40	3807.71	2314.95	1533.44	1772.35	2466.20	3785.59	5475.31	7061.91	7595.58
188	7519.58	6900.00	5569.48	3831.21	2322.63	1536.11	1761.61	2453.94	3794.05	5492.33	7042.26	7620.07
189	7495.85	6903.16	5583.06	3856.05	2321.14	1539.89	1761.88	2444.72	3789.10	5486.41	7046.28	7610.48
190	7495.31	6857.53	5589.25	3795.61	2323.23	1540.39	1754.34	2451.57	3799.26	5487.92	7036.95	7589.73
191	7505.41	6840.09	5584.32	3795.79	2332.59	1540.39	1748.20	2463.25	3806.12	5479.84	7056.19	7583.56
192	7505.47	6857.26	5576.54	3804.34	2338.57	1545.79	1755.72	2495.08	3813.65	5482.76	7035.80	7550.97
193	7505.94	6851.83	5551.59	3787.58	2322.41	1542.49	1756.28	2512.28	3810.40	5455.31	7035.31	7534.84
194	7516.05	6823.88	5514.02	3767.86	2314.67	1539.44	1754.06	2520.12	3791.78	5485.37	6988.42	7521.75
195	7535.99	6854.67	5514.74	3820.80	2321.30	1534.75	1781.18	2516.50	3813.13	5465.53	6979.04	7507.65
196	7532.15	6854.45	5495.78	3819.00	2322.29	1535.80	1782.78	2515.21	3813.99	5459.76	6951.96	7495.17
197	7498.87	6847.87	5492.97	3824.38	2315.51	1532.39	1782.81	2509.24	3814.58	5420.33	6941.64	7472.81
198	7481.32	6866.12	5478.86	3810.04	2302.16	1531.01	1781.49	2513.97	3814.39	5383.90	6920.66	7457.88
199	7497.66	6864.23	5484.50	3794.46	2297.79	1529.43	1777.15	2499.77	3816.04	5412.98	6921.89	7434.06
200	7479.23	6869.95	5499.57	3789.01	2299.91	1531.45	1770.58	2507.75	3826.55	5421.46	6919.79	7445.89
201	7470.90	6831.51	5515.51	3794.93	2284.52	1528.41	1768.69	2502.22	3819.22	5412.07	6877.17	7430.07
202	7464.08	6839.45	5476.83	3800.45	2274.30	1532.08	1761.37	2508.08	3805.16	5401.88	6867.60	7428.76
203	7496.25	6821.46	5448.93	3800.34	2271.44	1536.81	1767.55	2536.60	3814.36	5405.77	6884.63	7427.81
204	7498.06	6848.54	5428.79	3806.85	2263.65	1536.76	1767.08	2565.48	3804.34	5408.21	6913.07	7422.81
205	7508.22	6804.65	5432.10	3818.30	2264.34	1538.37	1766.88	2576.12	3792.06	5402.31	6931.70	7442.12
206	7474.29	6777.43	5439.88	3835.90	2281.40	1547.01	1771.64	2581.26	3789.98	5368.89	6926.47	7440.91
207	7510.56	6821.37	5457.17	3844.20	2299.22	1554.18	1770.32	2576.55	3776.62	5413.89	6935.69	7414.43
208	7540.70	6882.66	5465.61	3857.21	2319.31	1555.69	1777.20	2588.19	3765.75	5441.28	6918.24	7443.11
209	7555.48	6925.76	5593.67	3847.94	2344.16	1551.01	1803.79	2567.29	3831.30	5497.57	7101.38	7669.98
210	7540.19	6969.02	5604.84	3821.57	2354.01	1568.11	1804.58	2566.82	3833.95	5477.40	7101.91	7646.47
211	7532.95	6971.44	5612.62	3837.95	2340.62	1562.98	1806.52	2564.18	3833.25	5476.54	7086.07	7667.59
212	7540.94	6984.34	5617.72	3846.07	2338.46	1560.66	1804.58	2530.16	3827.60	5468.88	7092.81	7653.02
213	7532.32	6936.40	5604.47	3839.92	2353.49	1554.10	1802.05	2522.92	3825.07	5489.70	7086.51	7652.84
214	7523.93	6924.00	5606.73	3864.88	2344.17	1552.05	1796.60	2507.72	3819.81	5488.07	7072.62	7625.18
215	7535.10	6933.12	5623.51	3888.26	2354.02	1556.82	1793.92	2466.46	3820.10	5502.19	7076.29	7643.06
216	7537.42	6922.17	5634.50	3889.37	2359.47	1564.42	1793.87	2467.87	3819.28	5514.99	7097.07	7640.93
217	7529.84	6893.67	5640.11	3858.82	2355.27	1558.08	1781.40	2456.93	3824.52	5505.88	7105.78	7629.05
218	7523.23	6886.44	5636.43	3824.32	2354.76	1562.79	1782.28	2469.76	3826.47	5507.08	7094.79	7604.81
219	7550.39	6882.32	5625.86	3822.80	2374.64	1558.02	1782.03	2485.49	3830.54	5514.78	7103.69	7584.31
220	7560.15	6870.52	5638.38	3837.21	2367.59	1565.06	1790.51	2518.03	3837.43	5516.57	7098.62	7552.27
221	7542.26	6882.79	5642.27	3858.51	2364.20	1562.35	1800.16	2526.67	3836.20	5471.62	7068.95	7545.92
222	7556.51	6887.24	5585.52	3807.79	2342.83	1563.04	1772.23	2537.10	3825.05	5484.50	7059.32	7576.74
223	7591.91	6897.21	5590.58	3875.95	2353.66	1562.83	1805.93	2530.49	3842.42	5489.55	7036.37	7547.78
224	7566.28	6886.05	5544.50	3874.55	2355.44	1557.02	1801.53	2525.64	3839.00	5482.77	6998.95	7560.24
225	7567.78	6877.12	5550.71	3870.63	2352.31	1552.60	1796.43	2543.56	3843.51	5453.42	7009.68	7532.66
226	7559.75	6871.96	5545.55	3867.28	2346.83	1548.62	1796.02	2547.67	3847.88	5432.04	6989.18	7519.07
227	7526.50	6897.03	5589.10	3859.90	2350.17	1558.61	1801.19	2552.52	3848.74	5446.73	6980.70	7488.86
228	7539.11	6882.64	5559.30	3854.58	2347.64	1565.78	1798.16	2551.42	3850.42	5447.78	6962.98	7486.08
229	7527.71	6879.44	5559.37	3863.00	2341.91	1570.15	1797.13	2547.40	3832.14	5457.13	6945.09	7480.14
230	7505.43	6897.94	5544.00	3862.68	2342.28	1570.29	1795.66	2558.22	3832.92	5461.95	6929.32	7466.56
231	7531.63	6919.23	5564.77	3860.84	2351.86	1571.60	1793.23	2574.51	3848.26	5447.37	6924.77	7524.23
232	7523.35	6873.73	5509.97	3871.04	2344.75	1575.90	1797.51	2586.36	3844.35	5454.54	6956.09	7497.17
233	7522.08	6850.36	5506.07	3885.88	2350.85	1575.61	1800.22	2601.35	3842.20	5446.01	6933.10	7487.02
234	7517.42	6804.74	5505.93	3874.68	2346.09	1589.62	1802.89	2609.84	3853.51	5437.95	6944.78	7490.42
235	7531.46	6868.13	5516.97	3890.21	2356.31	1593.40	1808.95	2622.80	3822.60	5503.72	6953.90	7521.76
236	7536.62	6899.33	5519.27	3895.07	2362.16	1597.93	1813.04	2630.78	3809.57	5532.10	6961.56	7539.81
237	7544.61	7020.94	5633.99	3878.16	2383.62	1576.51	1827.51	2579.02	3843.79	5502.50	7126.42	7655.41
238	7540.21	7009.82	5647.67	3880.90	2379.66	1576.12	1827.79	2560.62	3840.30	5500.43	7117.06	7668.32
239	7541.02	6985.88	5650.10	3884.24	2373.32	1575.97	1825.96	2544.43	3849.93	5488.30	7111.56	7654.76
240	7525.09	6964.98	5628.77	3906.31	2379.73	1569.78	1818.63	2541.19	3849.33	5495.32	7108.71	7661.19
241	7521.38	6961.18	5627.53	3916.88	2382.39	1574.79	1816.49	2538.72	3841.75	5505.97	7112.87	7653.82
242	7535.34	6960.69	5650.47	3926.85	2384.76	1577.62	1819.80	2506.40	3847.46	5519.18	7113.88	7641.96
243	7525.08	6947.33	5669.17	3926.40	2385.65	1581.91	1815.54	2472.41	3847.55	5522.77	7122.37	7629.43
244	7514.38	6907.19	5661.56	3875.48	2377.88	1582.29	1805.10	2482.43	3848.01	5531.84	7121.85	7626.37
245	7534.37	6909.76	5665.43	3866.26	2387.30	1576.94	1810.14	2476.98	3848.79	5514.00	7121.95	7601.39
246	7546.68	6894.70	5656.51	3870.35	2403.01	1578.62	1812.44	2517.15	3849.83	5507.59	7119.89	7604.71
247	7560.61	6903.35	5648.43	3870.48	2408.06	1581.14	1815.55	2539.18	3860.36	5516.05	7129.27	7585.32
248	7576.35	6910.73	5665.71	3901.62	2402.08	1578.29	1810.47	2546.11	3864.26	5501.56	7107.89	7570.82
249	7584.87	6938.37	5624.20	3864.04	2382.70	1579.89	1801.47	2559.86	3850.61	5495.45	7100.53	7579.76
250	7603.82	6943.72	5638.89	3912.38	2382.57	1574.28	1824.22	2556.90	3870.92	5503.97	7090.06	7582.16
251	7606.49	6924.80	5638.47	3882.81	2382.80	1578.08	1818.04	2572.63	3872.45	5503.11	7070.10	7567.92
252	7602.24	6918.66	5615.41	3888.30	2388.29	1576.82	1819.66	2570.80	3888.67	5485.78	7036.03	7586.31

Table I. (Continuation)

Pixel	January	February	March	April	May	June	July	August	September	October	November	December
253	7572.33	6913.06	5593.29	3875.83	2392.67	1579.55	1823.39	2566.72	3884.29	5483.46	7049.56	7565.56
254	7531.60	6949.30	5587.70	3870.97	2395.09	1587.94	1825.05	2571.05	3891.80	5485.31	7038.22	7567.06
255	7549.65	6886.93	5578.58	3888.58	2401.14	1602.16	1822.95	2575.35	3889.95	5479.92	7027.19	7525.18
256	7546.42	6937.98	5565.40	3912.17	2372.55	1599.41	1822.81	2589.27	3876.90	5508.69	6992.20	7513.98
257	7539.18	6965.20	5540.98	3886.25	2372.05	1600.60	1826.60	2606.57	3884.18	5512.81	6996.76	7513.76
258	7523.89	6956.66	5547.68	3889.59	2360.52	1602.38	1830.16	2618.02	3895.09	5471.50	6987.82	7519.97
259	7565.35	6917.79	5565.89	3937.45	2387.13	1608.61	1832.26	2630.90	3888.11	5523.33	7002.82	7542.43
260	7537.42	6848.84	5575.74	3939.82	2385.62	1617.44	1835.45	2639.80	3887.55	5541.70	7017.20	7543.68
261	7528.64	6786.53	5582.10	3944.27	2391.72	1624.76	1831.60	2641.16	3891.49	5499.43	7022.61	7545.09
262	7552.11	6868.72	5558.60	3975.56	2402.37	1627.43	1835.47	2645.81	3867.86	5560.45	7044.61	7577.01
263	7562.13	6858.63	5548.36	3981.79	2423.91	1630.38	1839.82	2653.86	3862.06	5584.95	7064.25	7593.80
264	7593.75	6884.26	5548.32	3991.45	2430.02	1637.50	1847.00	2666.67	3876.12	5583.25	7072.41	7614.23
265	7527.14	7007.00	5656.80	3906.28	2421.43	1590.76	1844.59	2570.44	3862.43	5538.46	7143.41	7644.76
266	7516.08	7007.98	5640.19	3902.22	2409.34	1595.28	1837.51	2560.67	3862.79	5527.61	7131.71	7643.27
267	7510.40	6982.22	5636.31	3917.86	2407.10	1595.15	1825.96	2555.86	3857.06	5509.25	7107.89	7641.83
268	7516.94	6961.27	5617.90	3919.22	2408.55	1594.71	1827.97	2546.00	3848.57	5497.79	7106.54	7644.92
269	7520.12	6960.57	5639.48	3925.86	2411.81	1596.46	1839.12	2520.76	3856.66	5494.47	7129.07	7628.41
270	7513.57	6939.10	5645.47	3929.19	2406.65	1601.27	1837.47	2482.84	3847.33	5498.42	7120.28	7621.43
271	7519.20	6913.80	5651.21	3912.72	2411.02	1595.69	1830.51	2495.07	3851.26	5514.19	7117.73	7600.83
272	7531.80	6909.05	5651.14	3911.74	2420.20	1592.53	1833.27	2500.92	3862.91	5507.05	7102.93	7595.95
273	7551.25	6881.70	5653.98	3914.23	2423.05	1596.16	1838.09	2528.12	3868.07	5515.40	7104.51	7599.05
274	7586.78	6906.81	5660.84	3928.85	2418.60	1598.91	1836.52	2546.61	3887.45	5513.10	7097.20	7590.76
275	7597.01	6892.66	5644.64	3921.74	2417.07	1596.25	1838.29	2553.29	3892.73	5504.33	7123.33	7590.74
276	7590.42	6942.05	5648.64	3910.56	2413.37	1596.98	1839.89	2566.50	3890.55	5516.16	7117.49	7577.42
277	7604.02	6931.51	5610.55	3909.57	2407.20	1600.79	1838.61	2586.46	3901.50	5524.47	7113.46	7573.74
278	7591.65	6905.29	5619.46	3909.79	2414.23	1595.90	1843.62	2595.29	3904.46	5515.64	7075.82	7563.20
279	7589.10	6903.21	5629.94	3912.53	2414.83	1596.79	1849.21	2586.08	3918.65	5495.38	7038.79	7528.73
280	7556.26	6882.39	5618.18	3882.74	2419.00	1607.57	1858.81	2586.47	3897.93	5519.50	7039.05	7538.97
281	7551.60	6907.04	5632.24	3899.94	2424.93	1618.82	1855.85	2599.25	3897.93	5520.63	7050.65	7542.43
282	7563.49	6905.93	5579.82	3914.07	2427.99	1621.81	1851.96	2611.36	3915.06	5557.69	7048.07	7547.72
283	7558.14	6936.50	5570.63	3933.11	2425.18	1625.47	1857.07	2624.26	3905.56	5561.04	7039.14	7528.80
284	7541.79	6932.24	5575.01	3939.79	2425.86	1625.25	1868.49	2633.09	3926.30	5561.01	7046.71	7530.22
285	7554.08	6954.20	5590.88	3943.78	2430.22	1639.67	1872.57	2654.82	3941.69	5556.60	7053.66	7533.35
286	7579.30	6915.69	5621.32	3958.97	2434.14	1644.73	1872.18	2668.45	3938.35	5566.53	7062.91	7556.72
287	7547.91	6759.46	5642.71	3971.08	2442.46	1650.24	1875.74	2678.16	3935.51	5546.88	7066.95	7563.67
288	7527.15	6735.56	5627.45	3998.67	2449.56	1653.52	1871.48	2663.09	3938.39	5520.31	7079.62	7557.76
289	7525.18	6758.23	5603.88	4016.09	2475.26	1658.64	1868.60	2668.60	3943.05	5589.32	7106.54	7574.02
290	7528.69	6793.11	5583.82	4045.26	2484.63	1664.49	1875.63	2680.13	3935.15	5583.92	7107.32	7594.20
291	7522.88	7011.30	5644.68	3930.84	2446.79	1611.99	1862.20	2565.56	3874.16	5581.84	7160.83	7645.33
292	7515.40	7002.28	5635.10	3932.93	2444.20	1610.30	1863.23	2566.07	3865.36	5555.54	7149.65	7645.34
293	7502.79	6986.92	5617.89	3922.75	2442.82	1612.04	1868.63	2544.76	3865.73	5539.04	7128.77	7607.26
294	7516.21	6974.44	5665.93	3963.58	2452.92	1630.15	1868.06	2511.87	3862.38	5512.34	7140.42	7647.26
295	7509.29	6944.26	5670.28	3958.55	2443.13	1616.56	1862.72	2510.30	3865.42	5545.57	7151.74	7642.56
296	7534.32	6920.75	5668.21	3969.19	2445.05	1615.11	1863.56	2525.64	3866.60	5522.04	7120.91	7605.06
297	7528.58	6905.34	5669.95	3959.04	2448.17	1612.18	1854.87	2528.76	3877.58	5513.74	7127.27	7584.16
298	7561.84	6947.78	5671.74	3951.55	2447.15	1621.14	1859.19	2551.30	3897.14	5519.31	7122.08	7570.45
299	7590.18	6935.40	5682.98	3964.72	2448.78	1624.46	1858.93	2562.04	3903.43	5521.77	7104.70	7586.39
300	7574.98	6921.28	5660.55	3952.31	2444.78	1617.03	1864.16	2575.42	3917.08	5511.17	7127.40	7591.53
301	7595.68	6906.92	5661.65	3957.23	2439.32	1614.78	1864.28	2597.15	3916.35	5523.24	7119.31	7581.39
302	7597.46	6878.73	5633.95	3954.09	2436.49	1615.43	1866.37	2600.19	3924.41	5527.43	7112.61	7557.41
303	7594.54	6887.92	5603.27	3949.84	2439.99	1614.19	1871.21	2622.20	3926.33	5546.36	7095.35	7555.93
304	7568.82	6888.20	5628.86	3917.64	2455.86	1628.38	1887.38	2614.61	3931.13	5527.37	7060.02	7533.31
305	7557.49	6885.70	5627.71	3925.94	2456.43	1639.21	1898.67	2624.49	3911.00	5545.51	7060.91	7551.20
306	7539.94	6888.85	5667.50	3930.27	2460.66	1642.81	1899.88	2627.44	3918.28	5553.88	7098.28	7556.87
307	7578.56	6900.55	5677.00	3941.13	2475.27	1647.71	1902.50	2636.80	3924.03	5638.36	7102.03	7558.50
308	7591.07	6898.33	5634.48	3945.14	2468.08	1658.86	1902.46	2655.14	3942.74	5631.27	7090.88	7561.78
309	7568.81	6935.70	5635.64	3951.23	2464.78	1669.65	1899.45	2677.46	3972.39	5631.99	7096.66	7595.12
310	7612.92	6937.15	5651.75	3952.35	2487.53	1677.13	1907.80	2688.83	3994.46	5644.10	7110.04	7599.38
311	7613.78	6919.89	5663.83	4028.43	2479.78	1676.90	1910.06	2710.22	3986.81	5597.29	7115.76	7610.77
312	7561.39	6795.37	5653.67	4027.87	2516.69	1680.12	1907.91	2706.94	3999.89	5614.87	7157.89	7615.60
313	7534.60	6779.69	5673.04	4076.00	2520.79	1682.74	1910.79	2709.35	4011.67	5629.16	7131.37	7592.47
314	7548.92	6765.52	5637.49	4057.06	2525.52	1693.40	1916.16	2717.61	4025.68	5637.77	7138.75	7593.15
315	7575.41	6781.92	5616.56	4080.08	2534.96	1698.64	1918.95	2727.20	4028.73	5639.76	7148.23	7610.97
316	7528.10	7020.90	5643.02	3942.86	2475.60	1638.71	1874.06	2582.25	3883.44	5571.40	7160.40	7617.29
317	7510.68	7015.97	5685.32	3946.96	2480.89	1639.22	1884.83	2569.33	3891.82	5567.93	7146.09	7621.92
318	7510.50	6996.01	5714.08	3974.89	2487.60	1644.36	1891.16	2534.77	3884.49	5596.44	7146.07	7633.21
319	7525.35	6959.94	5692.21	3971.26	2486.32	1635.20	1885.69	2535.88	3883.57	5561.15	7131.92	7632.00
320	7539.89	6950.56	5686.26	4012.20	2485.44	1643.89	1881.02	2543.39	3881.80	5525.55	7133.98	7628.79
321	7528.45	6937.97	5698.32	3990.21	2489.45	1648.99	1877.85	2557.99	3891.00	5528.21	7137.48	7617.97
322	7547.25	6971.88	5698.79	3984.04	2483.29	1649.53	1879.36	2571.96	3897.87	5510.87	7147.11	7587.20
323	7567.85	6981.78	5690.86	3996.82	2483.73	1647.10	1893.29	2605.49	3911.38	5537.12	7149.50	7564.96
324	7565.93	6957.00	5610.42	3972.37	2473.61	1652.70	1891.82	2616.21	3922.17	5526.31	7149.41	7600.52
325	7592.90	6967.39	5696.15	4001.67	2459.61	1653.76	1892.60	2622.66	3942.93	5528.01	7130.66	7576.88
326	7594.29	6958.11	5656.28	3994.13	2470.56	1660.14	1893.25	2625.36	3934.36	5570.91	7134.22	7554.92
327	7580.59	6970.06	5659.26	3992.71	2480.94	1665.65	1902.18	2628.34	3965.20	5566.06	7103.13	7559.50
328	7576.23	6929.56	5638.83	3969.68	2499.70	1666.23	1920.90	2636.54	3955.30	5562.57	7086.33	7558.94
329	7565.42	6892.81	5647.42	3957.16	2503.04	1665.49	1936.28	2671.70	3974.42	5584.60	7112.98	7586.03
330	7572.78	6896.97	5682.44	3959.26	2519.92	1674.65	1937.22	2668.89	3973.13	5614.44	7141.64	7602.31
331	7618.04	6910.77	5686.64	3968.61	2530.96	1681.03	1944.80	2679.35	3964.14	5678.15	7141.91	7615.13
332	7649.95	6942.15	5709.29	3985.57	2531.93	1686.07	1944.07	2697.16	4000.11	5671.12	7145.55	7629.16
333	7631.37	6941.57	5717.28	4003.85	2534.00	1698.73	1945.21	2725.58	4036.91	5683.16	7195.91	7628.22
334	7639.08	6954.45	5759.18	4019.35	2544.94	1708.38	1948.92	2738.08	4049.23	5716.17	7193.17	7661.54
335	7655.05	6917.78	5749.62	4049.55	2553.70	1705.71	1951.96	2764.19	4037.23	5713.75	7219.42	7661.08
336	7597.08	6840.90	5748.73	4072.01	2574.81	1715.70	1948.88	2763.99	4079.53	5678.47	7171.04	7657.66

Table I. (Continuation)

Pixel	January	February	March	April	May	June	July	August	September	October	November	December
337	7586.33	6839.24	5700.44	4120.64	2568.14	1712.50	1955.88	2778.78	4084.71	5688.91	7161.38	7640.64
338	7601.25	6819.91	5692.17	4130.29	2573.14	1723.23	1963.52	2796.89	4084.99	5694.61	7185.37	7630.05
339	7620.27	6804.66	5712.02	4135.77	2590.54	1732.60	1966.13	2805.17	4092.67	5727.34	7189.83	7656.42
340	7646.77	6844.99	5731.65	4186.12	2592.23	1739.05	1972.04	2812.33	4099.63	5756.49	7244.42	7686.15
341	7529.63	7027.31	5669.89	3978.02	2517.61	1663.14	1885.24	2594.11	3875.62	5594.79	7155.08	7626.15
342	7511.57	7028.74	5711.34	3969.52	2522.40	1662.78	1897.32	2582.06	3882.44	5566.33	7154.46	7628.09
343	7496.75	6968.37	5750.05	4007.08	2517.99	1662.12	1901.26	2564.13	3867.99	5567.21	7181.22	7621.32
344	7504.04	6962.46	5720.84	4018.28	2513.87	1662.10	1904.09	2568.63	3875.37	5571.20	7152.94	7620.39
345	7494.77	6964.76	5686.03	4010.76	2521.01	1659.49	1902.64	2565.41	3884.42	5528.25	7167.68	7617.46
346	7504.36	6958.97	5675.54	4026.37	2524.15	1661.92	1899.34	2585.10	3900.09	5532.33	7154.86	7609.57
347	7516.49	6971.61	5687.73	4015.06	2521.07	1658.89	1906.75	2592.45	3910.21	5509.11	7142.29	7595.81
348	7554.20	6995.61	5644.03	4016.13	2527.56	1669.65	1915.48	2623.97	3924.90	5549.81	7135.56	7589.13
349	7524.64	6985.79	5616.97	4000.44	2498.06	1665.98	1916.04	2650.62	3942.83	5550.69	7134.94	7589.19
350	7594.96	7006.25	5706.55	4040.13	2509.36	1680.50	1931.80	2688.49	3976.19	5562.43	7123.39	7545.17
351	7593.47	7020.36	5711.23	4034.01	2523.49	1692.22	1931.60	2682.83	4004.60	5584.97	7123.50	7514.70
352	7605.34	7027.56	5713.35	4031.14	2530.57	1694.83	1946.89	2660.53	4026.25	5601.10	7099.83	7552.46
353	7588.71	6995.12	5681.29	3986.55	2541.23	1683.34	1955.99	2675.04	4013.28	5611.64	7104.47	7549.48
354	7567.38	6921.19	5680.93	3983.42	2551.73	1686.42	1960.29	2704.85	4008.65	5641.88	7113.63	7561.65
355	7635.34	6930.87	5690.53	3994.60	2564.13	1703.30	1963.22	2712.94	4004.34	5664.18	7120.28	7589.10
356	7650.67	6921.82	5707.57	4014.03	2569.23	1708.00	1968.63	2720.60	4010.72	5681.97	7137.95	7603.18
357	7648.18	6938.07	5744.76	4026.63	2581.56	1706.14	1974.39	2741.19	4051.08	5686.87	7217.18	7620.96
358	7641.63	6931.82	5743.49	4042.15	2578.51	1715.29	1976.16	2758.77	4070.59	5692.11	7242.69	7646.70
359	7670.11	6926.04	5753.94	4054.70	2597.36	1721.21	1984.30	2768.15	4076.88	5745.29	7265.72	7662.26
360	7655.48	6905.14	5808.80	4090.24	2605.26	1742.56	1981.53	2775.92	4091.78	5715.32	7242.02	7691.20
361	7592.32	6867.83	5790.18	4123.24	2610.14	1736.28	1984.43	2790.48	4118.09	5705.39	7178.01	7669.44
362	7519.74	6999.70	5724.99	4000.74	2553.04	1674.83	1903.10	2597.43	3885.24	5540.91	7207.84	7617.03
363	7494.76	6992.25	5681.34	4025.38	2545.87	1677.50	1912.18	2605.90	3869.96	5520.00	7155.92	7602.00
364	7484.44	6980.53	5670.62	4022.76	2546.61	1669.67	1909.22	2601.90	3896.79	5517.35	7178.83	7603.95
365	7487.68	6981.72	5661.01	4032.25	2549.09	1671.02	1912.67	2606.39	3910.15	5511.83	7143.71	7572.23
366	7470.26	7000.79	5645.06	4035.74	2558.03	1672.93	1926.15	2620.66	3905.39	5507.94	7135.25	7562.94
367	7470.80	7006.69	5649.43	4038.46	2563.69	1671.33	1930.83	2657.55	3932.00	5530.27	7134.25	7534.58
368	7485.03	7031.90	5655.67	4035.50	2546.89	1687.85	1928.88	2683.88	3947.69	5536.08	7111.11	7533.08
369	7509.54	7013.87	5671.43	4069.75	2549.11	1685.53	1936.62	2709.82	3988.83	5561.84	7101.20	7513.94
370	7531.08	6993.78	5682.88	4074.01	2551.90	1695.42	1951.32	2709.34	3996.15	5594.21	7092.34	7523.07
371	7547.69	7006.28	5690.99	4051.42	2556.69	1707.06	1963.83	2697.14	4021.98	5606.68	7082.90	7545.87
372	7542.57	6969.29	5696.55	4043.44	2553.23	1709.38	1970.00	2700.70	4023.59	5603.83	7085.42	7525.63
373	7552.83	6897.89	5703.05	4033.99	2572.83	1695.86	1974.88	2722.95	4027.49	5623.91	7098.97	7540.38
374	7604.73	6916.27	5718.44	4031.04	2582.07	1707.13	1980.29	2724.48	4029.45	5656.18	7119.22	7556.65
375	7616.52	6914.66	5736.66	4044.84	2593.21	1717.35	1985.34	2735.60	4026.51	5666.86	7130.20	7592.10
376	7632.08	6895.10	5717.09	4055.92	2600.22	1716.93	1989.50	2755.28	4042.12	5656.35	7147.69	7621.91
377	7653.76	6881.02	5750.73	4059.90	2602.87	1726.64	1996.93	2763.57	4070.59	5668.29	7206.95	7629.69
378	7650.22	6877.34	5797.82	4073.46	2611.06	1735.19	1997.77	2779.51	4091.27	5729.82	7225.53	7635.50
379	7542.06	6867.46	5842.50	4079.52	2638.42	1750.03	2006.43	2790.39	4130.38	5715.31	7237.22	7650.97
380	7562.14	6807.92	5810.98	4136.30	2620.78	1743.88	2011.05	2802.02	4125.91	5689.00	7186.75	7630.25
381	7469.60	6972.69	5692.86	4030.87	2576.07	1694.02	1926.82	2622.73	3902.40	5541.24	7173.28	7607.44
382	7463.51	6972.62	5672.62	4039.91	2588.09	1699.31	1918.84	2626.39	3910.39	5541.35	7170.35	7565.39
383	7434.38	7004.10	5673.63	4036.41	2592.14	1695.46	1933.07	2630.94	3910.60	5526.39	7150.69	7559.91
384	7419.79	7027.64	5672.03	4055.13	2595.93	1696.81	1954.79	2641.46	3919.06	5536.18	7151.08	7542.25
385	7424.45	7066.06	5667.41	4054.92	2604.79	1698.04	1957.17	2687.51	3939.81	5532.28	7108.21	7541.09
386	7447.44	7035.80	5670.03	4077.69	2594.45	1699.45	1964.22	2705.69	3922.12	5542.92	7066.53	7535.10
387	7497.03	6984.31	5697.24	4099.03	2586.35	1702.25	1964.11	2725.00	3970.27	5561.57	7068.01	7521.35
388	7512.66	6994.14	5710.78	4113.36	2588.38	1706.07	1976.29	2731.52	4024.68	5597.10	7094.28	7523.80
389	7524.57	7013.71	5723.34	4102.58	2587.99	1719.23	1994.50	2726.65	4039.88	5614.77	7094.85	7563.10
390	7516.01	6929.50	5743.65	4097.80	2595.87	1708.52	1990.54	2729.17	4041.81	5602.36	7101.87	7556.45
391	7520.92	6903.00	5746.53	4088.12	2597.20	1720.73	1993.66	2740.49	4016.59	5621.94	7112.31	7573.97
392	7596.38	6909.53	5766.08	4075.97	2618.89	1723.20	1999.62	2747.31	4014.82	5660.52	7108.83	7583.73
393	7592.91	6892.65	5771.89	4086.87	2624.10	1731.61	2005.43	2757.00	4041.57	5649.65	7101.98	7584.22
394	7587.98	6875.80	5756.98	4090.94	2628.89	1733.64	2005.92	2769.76	4082.74	5652.89	7130.58	7633.78
395	7625.84	6871.69	5815.71	4103.35	2633.94	1740.47	2013.94	2778.38	4114.09	5666.26	7167.04	7636.77
396	7587.58	6871.36	5829.96	4116.34	2647.65	1752.61	2026.49	2804.39	4142.51	5701.78	7191.83	7642.04
397	7540.72	6846.12	5851.61	4126.87	2663.67	1769.56	2029.03	2807.79	4161.30	5723.88	7233.81	7657.08
398	7432.92	6998.11	5682.70	4084.55	2637.97	1718.23	1955.97	2656.74	3923.72	5573.19	7124.98	7545.81
399	7420.29	7020.42	5680.04	4091.58	2644.71	1715.41	1974.08	2691.24	3907.13	5580.46	7121.34	7517.76
400	7421.13	7021.51	5717.04	4112.84	2643.38	1719.54	1973.49	2718.84	3937.88	5573.74	7098.33	7555.43
401	7444.71	7025.65	5703.58	4119.74	2634.62	1717.62	1994.80	2731.08	3969.45	5573.28	7094.47	7523.72
402	7487.78	6999.29	5724.42	4129.88	2626.61	1717.50	2001.90	2743.93	3990.92	5610.67	7090.27	7522.12
403	7496.42	7025.58	5736.65	4152.07	2620.86	1726.54	2006.26	2748.86	4030.85	5627.51	7125.96	7548.81
404	7509.11	7000.89	5758.47	4131.78	2628.39	1726.00	2014.71	2755.01	4048.78	5617.02	7106.13	7563.02
405	7501.60	6971.36	5777.00	4117.70	2630.59	1726.56	2017.85	2757.81	4052.94	5630.23	7133.67	7559.54
406	7530.93	6931.09	5790.45	4126.13	2643.54	1744.49	2018.17	2762.65	4056.12	5649.25	7123.93	7581.44
407	7558.90	6939.14	5811.56	4130.67	2647.03	1754.54	2023.07	2778.44	4051.64	5637.25	7127.28	7605.68
408	7597.59	6874.52	5813.30	4137.80	2654.12	1757.65	2026.59	2799.24	4074.04	5656.17	7156.35	7626.65
409	7606.01	6878.65	5815.47	4138.27	2664.21	1758.35	2029.82	2823.18	4126.14	5646.23	7185.27	7639.40
410	7617.62	6907.70	5843.62	4140.59	2666.41	1768.15	2046.17	2828.30	4134.02	5672.92	7180.97	7631.69
411	7431.11	7003.53	5764.37	4166.24	2679.20	1748.46	2001.18	2753.88	3969.45	5601.34	7151.79	7567.89
412	7445.57	7008.80	5755.28	4166.22	2677.29	1744.82	2022.83	2756.76	3999.46	5609.41	7131.96	7536.06
413	7476.30	7003.31	5767.17	4160.50	2675.80	1741.31	2032.61	2764.56	4025.14	5621.26	7138.53	7547.28
414	7533.11	7000.09	5790.03	4200.81	2691.21	1745.37	2038.39	2774.70	4053.30	5616.64	7145.12	7592.17
415	7546.85	6998.91	5804.28	4185.61	2690.70	1754.37	2051.38	2778.02	4070.42	5629.33	7135.97	7605.33
416	7523.32	6963.35	5810.75	4160.20	2694.95	1763.42	2041.40	2777.39	4080.09	5655.52	7180.27	7603.75
417	7570.83	6918.59	5840.96	4167.73	2687.63	1773.29	2042.50	2779.86	4099.22	5662.70	7134.82	7618.99
418	7588.60	6932.49	5867.37	4174.22	2686.31	1778.93	2053.79	2800.60	4101.40	5678.98	7161.01	7642.06
419	7623.56	6867.22	5880.47	4188.63	2679.29	1792.69	2061.79	2819.17	4133.27	5678.69	7194.19	7661.48
420	7579.00	7045.52	5851.02	4260.68	2752.42	1774.31	2081.26	2801.57	4073.73	5658.63	7178.68	7605.56

Table II. Partial correlation coefficients of Total NO₂ and Total O₃ on Erythemal daily doses high values for January; asterisks mark statistically significant correlations.

Pixel	Total NO₂ $r_{partial}$	α	Total O₃ $r_{partial}$	α	Class	Pixel	Total NO₂ $r_{partial}$	α	Total O₃ $r_{partial}$	α	Class	Pixel	Total NO₂ $r_{partial}$	α	Total O₃ $r_{partial}$	α	Class	Pixel	Total NO₂ $r_{partial}$	α	Total O₃ $r_{partial}$	α	Class	Pixel	Total NO₂ $r_{partial}$	α	Total O₃ $r_{partial}$	α	Class
1	0.06		-0.46	**	3	85	-0.20		-0.53	***	3	169	0.13		-0.39	*	3	253	-0.04		-0.18		5	337	-0.14		-0.17		5
2	0.05		-0.73	***	3	86	-0.13		-0.51	**	3	170	0.04		-0.46	**	3	254	-0.19		-0.42	*	3	338	-0.27		-0.08		5
3	0.26		-0.64	***	3	87	-0.02		-0.45	**	3	171	0.28		-0.51	**	3	255	-0.06		-0.34	*	3	339	0.03		-0.23		5
4	0.21		-0.76	***	3	88	0.12		-0.45	**	3	172	0.26		-0.53	**	3	256	-0.06		-0.35	*	3	340	-0.16		-0.21		5
5	0.19		-0.69	***	3	89	-0.14		-0.48	**	3	173	0.21		-0.58	***	3	257	0.01		-0.39	*	3	341	0.06		-0.38	*	3
6	-0.12		-0.61	***	3	90	-0.09		-0.45	**	3	174	0.13		-0.52	**	3	258	-0.02		-0.35	*	3	342	0.12		-0.23		5
7	0.34	*	-0.74	***	2	91	0.29	.	-0.43	*	3	175	0.13		-0.47	**	3	259	0.22		-0.37	*	3	343	0.04		-0.29		5
8	0.35	*	-0.71	***	2	92	0.27		-0.39	*	3	176	0.11		-0.45	**	3	260	0.13		-0.20		5	344	0.12		-0.22		5
9	0.04		-0.63	***	3	93	0.00		-0.47	**	3	177	-0.02		-0.46	**	3	261	-0.10		-0.33	.	5	345	0.28	.	-0.27		5
10	0.40	*	-0.69	***	2	94	0.14		-0.45	**	3	178	0.05		-0.48	**	3	262	0.02		-0.23		5	346	-0.07		-0.23		5
11	0.41	*	-0.72	***	2	95	0.10		-0.41	*	3	179	0.19		-0.39	*	3	263	-0.05		-0.31	.	5	347	-0.05		-0.25		5
12	0.21		-0.71	***	3	96	0.21		-0.48	**	3	180	-0.16		-0.42	*	3	264	-0.09		-0.11		5	348	-0.03		-0.09		5
13	0.16		-0.72	***	3	97	0.01		-0.52	**	3	181	-0.47	**	-0.59	***	1	265	0.01		-0.39	*	3	349	-0.09		-0.13		5
14	0.05		-0.62	***	3	98	0.11		-0.54	***	3	182	-0.29	.	-0.57	***	3	266	0.04		-0.41	*	3	350	-0.05		-0.12		5
15	0.24		-0.63	***	3	99	-0.03		-0.49	**	3	183	-0.22		-0.54	**	3	267	-0.02		-0.40	*	3	351	-0.19		-0.10		5
16	0.21		-0.59	***	3	100	0.09		-0.49	**	3	184	-0.13		-0.57	***	3	268	-0.04		-0.31	.	5	352	-0.01		-0.25		5
17	0.22		-0.66	***	3	101	-0.14		-0.47	**	3	185	0.13		-0.50	**	3	269	-0.03		-0.30	.	5	353	-0.08		-0.18		5
18	0.14		-0.77	***	3	102	0.09		-0.51	**	3	186	0.27		-0.51	**	3	270	-0.02		-0.30	.	5	354	0.00		-0.22		5
19	0.14		-0.64	***	3	103	-0.07		-0.50	**	3	187	0.17		-0.47	**	3	271	0.12		-0.36	*	3	355	0.00		-0.10		5
20	0.05		-0.48	**	3	104	-0.14		-0.63	***	3	188	0.02		-0.40	*	3	272	0.05		-0.28	.	5	356	0.09		-0.14		5
21	0.14		-0.63	***	3	105	0.09		-0.58	***	3	189	-0.30	.	-0.45	**	3	273	0.00		-0.14		5	357	0.05		-0.25		5
22	0.17		-0.68	***	3	106	-0.10		-0.60	***	3	190	0.00		-0.30		5	274	0.07		-0.12		5	358	-0.14		-0.28	.	5
23	-0.01		-0.71	***	3	107	-0.22		-0.50	**	3	191	0.16		-0.21		5	275	-0.04		-0.06		5	359	-0.36	*	-0.39	*	1
24	0.16		-0.73	***	3	108	-0.15		-0.47	**	3	192	0.26		-0.18		5	276	0.05		-0.21		5	360	-0.16		-0.40	*	3
25	-0.01		-0.77	***	3	109	-0.32	.	-0.46	**	3	193	0.20		-0.21		5	277	-0.03		-0.35	*	3	361	-0.01		-0.17		5
26	0.01		-0.60	***	3	110	-0.10		-0.35	*	3	194	0.01		-0.36	*	3	278	0.00		-0.23		5	362	-0.09		-0.18		5
27	0.02		-0.61	***	3	111	-0.08		-0.38	*	3	195	0.14		-0.35	*	3	279	-0.17		-0.30	.	5	363	-0.09		-0.22		5
28	0.10		-0.55	***	3	112	-0.22		-0.44	**	3	196	0.12		-0.41	*	3	280	-0.11		-0.34	*	3	364	-0.01		-0.13		5
29	0.08		-0.52	**	3	113	-0.01		-0.44	**	3	197	0.01		-0.33	.	5	281	0.01		-0.32	.	5	365	0.07		-0.11		5
30	0.09		-0.57	***	3	114	-0.08		-0.40	*	3	198	0.09		-0.37	*	3	282	0.03		-0.39	*	3	366	-0.05		-0.04		5
31	0.24		-0.65	***	3	115	0.20		-0.44	**	3	199	0.09		-0.35	*	3	283	-0.16		-0.33	.	5	367	-0.21		-0.07		5
32	0.17		-0.64	***	3	116	0.36	*	-0.53	**	2	200	0.07		-0.47	**	3	284	0.04		-0.29	.	5	368	-0.17		-0.15		5
33	0.03		-0.69	***	3	117	0.17		-0.45	**	3	201	-0.09		-0.49	**	3	285	-0.04		-0.18		5	369	-0.10		-0.27		5
34	0.12		-0.72	***	3	118	0.03		-0.37	*	3	202	-0.25		-0.54	***	3	286	-0.12		-0.20		5	370	-0.07		-0.18		5
35	0.22		-0.76	***	3	119	0.18		-0.46	**	3	203	-0.21		-0.46	**	3	287	-0.15		-0.38	*	3	371	0.18		-0.23		5
36	-0.22		-0.60	***	3	120	-0.06		-0.44	**	3	204	-0.01		-0.44	**	3	288	-0.13		-0.33	.	5	372	-0.16		-0.23		5
37	-0.22		-0.57	***	3	121	0.15		-0.50	**	3	205	-0.04		-0.47	**	3	289	-0.21		-0.37	*	3	373	-0.13		-0.33	.	5
38	-0.26		-0.49	**	3	122	0.01		-0.42	*	3	206	-0.10		-0.32	.	5	290	0.07		-0.23		5	374	-0.19		-0.15		5
39	0.10		-0.50	**	3	123	-0.02		-0.47	**	3	207	-0.07		-0.27		5	291	0.14		-0.48	**	3	375	-0.19		-0.29	.	5
40	0.16		-0.42	*	3	124	-0.06		-0.47	**	3	208	-0.05		-0.19		5	292	0.05		-0.41	*	3	376	-0.14		-0.29	.	5
41	0.02		-0.61	***	3	125	0.04		-0.47	**	3	209	-0.41	*	-0.44	**	1	293	-0.32	.	-0.39	*	3	377	-0.31	.	-0.18		5
42	0.24		-0.69	***	3	126	0.00		-0.50	**	3	210	-0.29		-0.53	**	3	294	-0.23		-0.28		5	378	-0.26		-0.23		5
43	0.23		-0.68	***	3	127	-0.25		-0.58	***	3	211	-0.35	*	-0.59	***	1	295	0.12		-0.30	.	5	379	-0.14		-0.16		5
44	0.04		-0.66	***	3	128	0.08		-0.58	***	3	212	-0.31	.	-0.53	***	3	296	0.17		-0.32	.	5	380	-0.18		-0.30	.	5
45	0.09		-0.68	***	3	129	0.23		-0.58	***	3	213	-0.23		-0.51	**	3	297	0.03		-0.14		5	381	-0.10		-0.10		5
46	0.06		-0.68	***	3	130	0.25		-0.61	***	3	214	0.12		-0.40	*	3	298	-0.32	.	-0.15		5	382	-0.19		0.04		5
47	0.16		-0.68	***	3	131	-0.06		-0.62	***	3	215	0.04		-0.36	*	3	299	-0.45	**	-0.21		4	383	0.22		-0.39	*	3
48	0.03		-0.65	***	3	132	-0.24		-0.64	***	3	216	-0.02		-0.31		5	300	-0.22		-0.10		5	384	0.06		-0.20		5
49	-0.17		-0.62	***	3	133	-0.19		-0.44	**	3	217	-0.19		-0.31	.	5	301	-0.06		-0.12		5	385	-0.15		-0.23		5
50	-0.36	*	-0.60	***	1	134	-0.17		-0.42	*	3	218	-0.12		-0.27		5	302	-0.11		-0.22		5	386	0.13		-0.14		5
51	0.01		-0.62	***	3	135	-0.15		-0.30	.	5	219	0.03		-0.09		5	303	-0.09		-0.30	.	5	387	0.13		-0.19		5
52	-0.19		-0.57	***	3	136	-0.05		-0.41	*	3	220	-0.30		-0.15		5	304	-0.10		-0.30	.	5	388	-0.01		-0.14		5
53	-0.27		-0.42	*	3	137	-0.03		-0.42	*	3	221	-0.13		-0.16		5	305	-0.16		-0.40	*	3	389	0.36	*	-0.29	.	4
54	-0.22		-0.44	**	3	138	-0.05		-0.45	**	3	222	-0.03		-0.29		5	306	0.13		-0.40	*	3	390	-0.20		-0.24		5
55	0.08		-0.43	*	3	139	-0.03		-0.54	**	3	223	0.04		-0.27		5	307	0.26		-0.41	*	3	391	0.03		-0.23		5
56	-0.09		-0.53	**	3	140	0.01		-0.56	***	3	224	-0.12		-0.31	.	5	308	-0.17		-0.31	.	5	392	0.22		-0.33	*	3
57	-0.12		-0.57	***	3	141	-0.10		-0.41	*	3	225	-0.19		-0.25		5	309	0.07		-0.27		5	393	0.18		-0.37	*	3
58	0.19		-0.60	***	3	142	-0.17		-0.38	*	3	226	-0.03		-0.19		5	310	-0.02		-0.17		5	394	0.13		-0.37	*	3
59	0.12		-0.62	***	3	143	0.09		-0.44	**	3	227	0.18		-0.29	.	5	311	-0.19		-0.26		5	395	-0.28		-0.18		5
60	-0.07		-0.63	***	3	144	0.34	*	-0.47	**	2	228	0.14		-0.36	*	3	312	-0.30	.	-0.31	.	5	396	-0.01		-0.32	.	5
61	0.16		-0.60	***	3	145	0.26		-0.50	**	3	229	-0.27		-0.44	**	3	313	-0.12		-0.35	*	3	397	0.24		-0.17		5
62	0.10		-0.66	***	3	146	0.08		-0.48	**	3	230	-0.18		-0.46	**	3	314	-0.12		-0.19		5	398	0.15		-0.20		5
63	-0.10		-0.60	***	3	147	0.06		-0.39	*	3	231	-0.12		-0.41	**	3	315	0.00		-0.24		5	399	0.13		-0.24		5
64	0.18		-0.55	***	3	148	0.10		-0.41	*	3	232	0.00		-0.38	*	3	316	0.09		-0.42	**	3	400	-0.12		-0.06		5
65	-0.29	.	-0.63	***	3	149	0.06		-0.52	**	3	233	-0.03		-0.42	**	3	317	-0.15		-0.35	*	3	401	0.21		-0.16		5
66	-0.11		-0.53	***	3	150	0.03		-0.41	*	3	234	-0.11		-0.32	.	5	318	-0.27		-0.30	.	5	402	0.37	*	-0.04		4
67	-0.19		-0.51	**	3	151	0.12		-0.32	.	5	235	0.07		-0.25		5	319	-0.01		-0.30	.	5	403	0.06		-0.12		5
68	-0.19		-0.58	***	3	152	-0.09		-0.44	**	3	236	-0.02		-0.05		5	320	0.17		-0.18		5	404	0.17		-0.14		5
69	-0.12		-0.52	**	3	153	0.13		-0.55	***	3	237	-0.38	*	-0.61	***	1	321	-0.13		-0.23		5	405	0.10		-0.20		5
70	-0.03		-0.40	*	3	154	-0.11		-0.64	***	3	238	-0.30		-0.52	**	3	322	-0.40	*	-0.14		4	406	0.28		-0.27		5
71	0.05		-0.51	**	3	155	-0.34	.	-0.67	***	3	239	-0.16		-0.45	**	3	323	-0.28	.	-0.12		5	407	-0.03		-0.18		5
72	0.21		-0.44	**	3	156	-0.21		-0.65	***	3	240	-0.35	*	-0.56	***	1	324	-0.45	**	-0.23		4	408	-0.08		-0.25		5
73	-0.17		-0.50	**	3	157	0.15		-0.58	***	3	241	0.08		-0.33		5	325	0.09		-0.23		5	409	-0.22		-0.25		5
74	0.06		-0.52	**	3	158	0.08		-0.59	***	3	242	0.00		-0.30	.	5	326	-0.34	*	-0.11		4	410	-0.33	*	-0.24		4
75	-0.03		-0.47	**	3	159	0.06		-0.59	***	3	243	-0.11		-0.28		5	327	-0.25		-0.21		5	411	-0.01		-0.05		5
76	0.09		-0.51	**	3	160	0.06		-0.53	**	3	244	0.14		-0.41	*	3	328	-0.24		-0.27		5	412	0.05		0.03		5
77	0.05		-0.55	***	3	161	0.07		-0.45	**	3	245	0.09		-0.17		5	329	-0.06		-0.26		5	413	-0.19		-0.13		5
78	0.06		-0.55	***	3	162	0.12		-0.42	*	3	246	0.00		-0.13		5	330	0.14		-0.29	.	5	414	-0.29	.	-0.25		5
79	0.02		-0.50	**	3	163	0.13		-0.26		5	247	-0.11		-0.18		5	331	0.11		-0.20		5	415	0.01		-0.04		5
80	-0.05		-0.45	**	3	164	0.11		-0.28		5	248	-0.10		-0.19		5	332	-0.03		-0.26		5	416	-0.25		-0.01		5
81	0.09		-0.48	**	3	165	0.19		-0.26		5	249	0.23		-0.26		5	333	0.01		-0.20		5	417	-0.05		-0.04		5
82	0.20		-0.39	*	3	166	0.10		-0.37	*	3	250	-0.01		-0.28	.	5	334	-0.10		-0.28		5	418	-0.20		-0.11		5
83	-0.14		-0.67	***	3	167	0.21		-0.43	*	3	251	0.11		-0.32	.	5	335	0.08		-0.36	*	3	419	-0.36	*	-0.10		4
84	0.01		-0.56	***	3	168	0.23		-0.47	**	3	252	-0.09		-0.20		5	336	-0.12		-0.23		5	420	-0.06		0.04		5

Table III. Partial correlation coefficients of Total NO$_2$ and Total O$_3$ on Erythemal daily doses high values for February; asterisks mark statistically significant correlations.

Pixel	NO₂ $r_{partial}$	α	O₃ $r_{partial}$	α	Class	Pixel	NO₂ $r_{partial}$	α	O₃ $r_{partial}$	α	Class	Pixel	NO₂ $r_{partial}$	α	O₃ $r_{partial}$	α	Class	Pixel	NO₂ $r_{partial}$	α	O₃ $r_{partial}$	α	Class	Pixel	NO₂ $r_{partial}$	α	O₃ $r_{partial}$	α	Class
1	-0.14		-0.39	*	3	85	-0.26		-0.43	*	3	169	0.05		-0.56	***	3	253	-0.04		-0.42	*	3	337	0.07		-0.25		5
2	-0.39	*	-0.18		4	86	-0.25		-0.37	*	3	170	0.08		-0.56	***	3	254	-0.15		-0.48	**	3	338	-0.17		-0.25		5
3	-0.17		-0.08		5	87	0.01		-0.32	.	5	171	0.22		-0.53	**	3	255	-0.18		-0.44	*	3	339	0.05		-0.13		5
4	-0.04		-0.08		5	88	-0.27		-0.29		5	172	0.27		-0.56	**	3	256	-0.33	.	-0.45	**	3	340	0.02		0.11		5
5	-0.06		-0.27		5	89	-0.12		-0.25		5	173	0.08		-0.40	*	1	257	-0.31	.	-0.54	**	3	341	0.18		-0.72	***	3
6	0.03		-0.22		5	90	0.06		-0.18		5	174	0.07		-0.37	*	3	258	-0.21		-0.51	**	3	342	-0.03		-0.59	***	3
7	0.11		-0.22		5	91	-0.21		-0.32		5	175	-0.04		-0.46	**	3	259	0.13		-0.28		5	343	0.18		-0.65	***	3
8	0.28		-0.15		5	92	-0.20		-0.32	.	5	176	-0.12		-0.43	*	3	260	-0.06		-0.33	.	5	344	0.18		-0.64	***	3
9	0.41	*	-0.42	*	2	93	0.03		-0.32	.	5	177	0.00		-0.42	*	3	261	0.09		-0.33	.	5	345	0.25		-0.56	***	3
10	0.08		-0.26		5	94	0.20		-0.26		5	178	0.03		-0.31	.	5	262	0.21		-0.45	**	3	346	0.18		-0.54	**	3
11	-0.12		-0.47	**	3	95	0.35	*	-0.28		4	179	-0.11		-0.32	.	5	263	0.05		-0.35	*	3	347	0.05		-0.39	*	3
12	0.05		-0.32	.	5	96	-0.02		-0.39	*	3	180	0.07		-0.48	**	3	264	0.16		-0.28		5	348	-0.01		-0.47	**	3
13	0.12		-0.19		5	97	-0.13		-0.47	**	3	181	0.07		-0.48	**	3	265	-0.09		-0.52	**	3	349	0.11		-0.32	.	5
14	-0.19		-0.27		5	98	0.22		-0.47	**	3	182	-0.33	.	-0.38	*	3	266	0.04		-0.48	**	3	350	0.43	*	-0.56	***	2
15	-0.16		-0.41	*	3	99	0.19		-0.30		5	183	-0.08		-0.52	**	3	267	-0.15		-0.53	**	3	351	0.17		-0.44	*	3
16	-0.21		-0.36	*	3	100	0.04		-0.37	*	3	184	-0.17		-0.49	**	3	268	-0.02		-0.46	**	3	352	0.10		-0.29		5
17	-0.24		-0.27		5	101	-0.15		-0.40	*	3	185	-0.05		-0.46	**	3	269	-0.10		-0.57	***	3	353	0.08		-0.21		5
18	-0.12		-0.40	*	3	102	-0.14		-0.41	*	3	186	0.09		-0.29		5	270	-0.06		-0.57	***	3	354	0.20		-0.33	.	5
19	0.01		-0.18		5	103	-0.11		-0.48	**	3	187	-0.30	.	-0.38	*	3	271	0.32	.	-0.53	**	3	355	0.12		-0.34	.	5
20	-0.28		-0.24		5	104	0.14		-0.62	***	3	188	0.02		-0.41	*	3	272	0.18		-0.54	**	3	356	-0.20		-0.34	.	5
21	-0.21		-0.36	*	3	105	0.08		-0.61	***	3	189	0.08		-0.56	**	3	273	-0.16		-0.43	*	3	357	-0.38	*	-0.36	*	1
22	-0.27		-0.45	*	3	106	0.05		-0.62	***	3	190	0.02		-0.64	***	3	274	-0.33	.	-0.45	**	3	358	-0.21		-0.27		5
23	-0.23		-0.29		5	107	0.29	.	-0.70	***	3	191	0.13		-0.58	***	3	275	-0.13		-0.33	.	5	359	-0.21		-0.11		5
24	0.12		-0.46	**	3	108	0.04		-0.52	**	3	192	0.24		-0.51	**	3	276	-0.17		-0.29		5	360	-0.29		0.01		5
25	-0.11		-0.37	*	3	109	-0.19		-0.38	*	3	193	0.18		-0.47	**	3	277	-0.03		-0.28		5	361	0.10		-0.12		5
26	-0.14		-0.41	*	3	110	0.15		-0.31	.	5	194	-0.15		-0.39	*	3	278	-0.44	**	-0.26		4	362	-0.16		-0.47	**	3
27	0.01		-0.17		5	111	-0.18		-0.20		5	195	-0.21		-0.56	***	3	279	-0.29		-0.23		5	363	0.11		-0.41	*	3
28	-0.08		-0.23		5	112	-0.06		-0.22		5	196	-0.22		-0.52	**	3	280	-0.32	.	-0.31	.	5	364	0.04		-0.40	*	3
29	0.01		-0.36	*	3	113	0.05		-0.31	.	5	197	-0.20		-0.52	**	3	281	-0.11		-0.28		5	365	0.11		-0.42	*	3
30	0.01		-0.34	*	3	114	-0.16		-0.32	.	5	198	-0.12		-0.48	**	3	282	0.08		-0.34	.	5	366	-0.02		-0.29	.	5
31	0.04		-0.31	.	5	115	-0.35	.	-0.31	.	5	199	0.14		-0.48	**	3	283	-0.12		-0.41	*	3	367	0.02		-0.13		5
32	-0.05		-0.36	*	3	116	-0.05		-0.33	.	5	200	0.16		-0.58	***	3	284	-0.27		-0.19		5	368	-0.03		-0.28		5
33	0.01		-0.46	**	3	117	0.04		-0.33	.	5	201	-0.10		-0.52	**	3	285	-0.40	*	-0.13		4	369	0.22		-0.33	.	5
34	0.06		-0.46	**	3	118	0.05		-0.26		5	202	0.03		-0.58	***	3	286	0.03		-0.27		5	370	-0.02		-0.25		5
35	-0.11		-0.28		5	119	-0.08		-0.43	*	3	203	-0.27		-0.51	**	3	287	-0.05		-0.24		5	371	0.14		-0.22		5
36	0.00		-0.17		5	120	-0.10		-0.51	**	3	204	-0.01		-0.50	**	3	288	-0.19		-0.36	*	3	372	-0.04		-0.25		5
37	-0.07		-0.20		5	121	-0.08		-0.37	*	3	205	-0.26		-0.44	*	3	289	0.16		-0.35	.	5	373	-0.03		-0.26		5
38	-0.20		-0.07		5	122	0.16		-0.33	.	5	206	-0.26		-0.33	.	5	290	0.09		-0.39	*	3	374	0.02		-0.32	.	5
39	0.08		-0.17		5	123	0.17		-0.53	**	3	207	0.00		-0.29		5	291	0.03		-0.53	**	3	375	0.15		-0.32	.	5
40	-0.02		-0.30	.	5	124	0.08		-0.40	*	3	208	-0.05		-0.27		5	292	-0.10		-0.56	***	3	376	0.07		-0.27		5
41	-0.15		-0.34	.	5	125	0.15		-0.45	**	3	209	0.04		-0.31	.	5	293	-0.07		-0.64	***	3	377	-0.12		-0.29		5
42	0.00		-0.26		5	126	0.09		-0.46	**	3	210	-0.19		-0.56	**	3	294	-0.27		-0.66	***	3	378	-0.35	*	-0.13		4
43	0.11		-0.36	*	3	127	0.02		-0.45	*	3	211	-0.08		-0.51	**	3	295	-0.10		-0.57	***	3	379	-0.34	.	-0.19		5
44	0.05		-0.42	*	3	128	0.13		-0.57	**	3	212	-0.20		-0.44	*	3	296	0.14		-0.63	***	3	380	-0.09		-0.19		5
45	0.03		-0.37	*	3	129	0.09		-0.63	***	3	213	-0.03		-0.38	*	3	297	0.16		-0.59	***	3	381	-0.10		-0.36	*	3
46	-0.01		-0.54	**	3	130	0.07		-0.64	***	3	214	-0.10		-0.25		5	298	0.09		-0.56	***	3	382	-0.27		-0.28		5
47	0.06		-0.39	*	3	131	0.23		-0.50	**	3	215	-0.38	*	-0.50	**	3	299	-0.18		-0.55	***	3	383	-0.29		-0.22		5
48	0.44	*	-0.33	.	4	132	0.22		-0.38	*	3	216	-0.31	.	-0.36	.	5	300	0.35	.	-0.37	*	3	384	-0.27		-0.26		5
49	0.34	.	-0.39	*	3	133	-0.02		-0.40	*	3	217	0.06		-0.53	**	3	301	0.27		-0.35	*	3	385	-0.22		-0.20		5
50	0.31	.	-0.31	.	5	134	0.20		-0.16		5	218	0.20		-0.16		5	302	0.31	.	-0.37	*	3	386	-0.38	*	-0.05		4
51	0.10		-0.31		5	135	0.37	*	-0.29	.	4	219	0.34	.	-0.45	**	3	303	0.16		-0.26		5	387	-0.04		-0.19		5
52	0.08		-0.38	*	3	136	-0.01		-0.24		5	220	0.33	.	-0.41	*	3	304	0.26		-0.35	*	3	388	-0.03		-0.23		5
53	0.12		-0.10		5	137	0.14		-0.42	*	3	221	-0.07		-0.42	*	3	305	0.06		-0.26		5	389	0.21		-0.22		5
54	-0.23		-0.25		5	138	0.15		-0.55	**	3	222	-0.10		-0.29		5	306	-0.08		-0.12		5	390	0.15		-0.24		5
55	-0.14		-0.27		5	139	-0.37	*	-0.27		4	223	-0.10		-0.53	**	3	307	-0.04		-0.17		5	391	-0.23		-0.19		5
56	-0.17		-0.29		5	140	-0.21		-0.41	*	3	224	-0.33	.	-0.62	***	3	308	0.06		-0.27		5	392	-0.17		-0.34	.	5
57	-0.32	.	-0.16		5	141	-0.19		-0.26		5	225	-0.17		-0.50	**	3	309	-0.31	.	-0.21		5	393	-0.14		-0.33	.	5
58	0.03		-0.25		5	142	-0.06		-0.28		5	226	-0.19		-0.44	*	3	310	-0.24		-0.24		5	394	0.05		-0.33	.	5
59	0.14		-0.38	*	3	143	-0.20		-0.45	*	3	227	-0.02		-0.44	*	3	311	-0.20		-0.14		5	395	-0.09		-0.37	*	3
60	0.24		-0.45	**	3	144	-0.18		-0.40	*	3	228	-0.07		-0.52	**	3	312	-0.06		-0.29		5	396	-0.46	**	-0.27		4
61	0.18		-0.53	**	3	145	-0.19		-0.39	*	3	229	-0.13		-0.47	**	3	313	-0.01		-0.33	.	5	397	-0.34	.	-0.37	*	3
62	-0.24		-0.52	**	3	146	0.28		-0.58	***	3	230	-0.01		-0.54	**	3	314	0.05		-0.33	.	5	398	-0.47	**	-0.20		4
63	0.15		-0.35	.	5	147	0.06		-0.46	**	3	231	-0.24		-0.59	***	3	315	0.08		-0.29		5	399	-0.07		-0.25		5
64	0.08		-0.32	.	5	148	0.06		-0.46	**	3	232	-0.08		-0.56	***	3	316	0.17		-0.60	***	3	400	0.05		-0.17		5
65	0.13		-0.40	*	3	149	0.05		-0.41	*	3	233	0.09		-0.53	**	3	317	-0.12		-0.65	***	3	401	-0.21		-0.02		5
66	-0.01		-0.44	*	3	150	-0.06		-0.36	*	3	234	-0.18		-0.25		5	318	0.02		-0.66	***	3	402	-0.12		-0.09		5
67	-0.08		-0.38	*	3	151	-0.13		-0.38	*	3	235	0.00		-0.30	.	5	319	0.19		-0.69	***	3	403	-0.12		-0.20		5
68	-0.07		-0.33	.	5	152	0.36	*	-0.42	*	2	236	-0.17		-0.35	*	3	320	0.12		-0.61	***	3	404	0.08		-0.25		5
69	0.15		-0.44	*	3	153	-0.04		-0.46	**	3	237	-0.26		-0.50	**	3	321	0.47	**	-0.60	***	2	405	-0.20		-0.22		5
70	0.24		-0.23		5	154	-0.40	*	-0.25		4	238	0.13		-0.47	**	3	322	0.28		-0.54	**	3	406	0.10		-0.33	.	5
71	-0.12		-0.32	.	5	155	0.05		-0.64	***	3	239	-0.12		-0.41	*	3	323	-0.10		-0.50	**	3	407	-0.10		-0.34	.	5
72	-0.35	.	-0.41	*	3	156	0.15		-0.60	***	3	240	-0.08		-0.43	*	3	324	0.07		-0.34	.	5	408	0.00		-0.38	*	3
73	-0.19		-0.27		5	157	-0.02		-0.43	*	3	241	0.09		-0.35	.	5	325	0.20		-0.42	*	3	409	0.02		-0.34	.	5
74	0.02		-0.20		5	158	0.05		-0.46	**	3	242	-0.16		-0.39	*	3	326	0.18		-0.42	*	3	410	-0.16		-0.38	*	3
75	0.20		-0.34	.	5	159	-0.02		-0.34	.	5	243	-0.34	.	-0.37	*	3	327	0.12		-0.29		5	411	-0.22		-0.12		5
76	0.04		-0.35	*	3	160	-0.19		-0.43	*	3	244	0.11		-0.39	*	3	328	0.23		-0.26		5	412	-0.13		-0.21		5
77	0.31	.	-0.41	*	3	161	-0.04		-0.43	*	3	245	0.15		-0.42	*	3	329	0.26		-0.36	*	3	413	-0.01		-0.26		5
78	0.30		-0.53	**	3	162	0.09		-0.47	**	3	246	-0.07		-0.31	.	5	330	0.02		-0.18		5	414	-0.01		-0.32	.	5
79	0.18		-0.45	*	3	163	0.03		-0.40	*	3	247	-0.29		-0.30	.	5	331	-0.33	.	-0.15		5	415	-0.17		-0.35	*	3
80	-0.06		-0.38	*	3	164	-0.24		-0.52	**	3	248	-0.13		-0.19		5	332	-0.37	*	-0.13		4	416	-0.16		-0.36	*	3
81	-0.20		-0.46	**	3	165	-0.02		-0.52	**	3	249	0.01		-0.29		5	333	-0.17		-0.19		5	417	-0.05		-0.55	**	3
82	0.03		-0.42	*	3	166	-0.07		-0.31	.	5	250	0.07		-0.31	.	5	334	0.02		-0.12		5	418	-0.29		-0.56	***	3
83	0.02		-0.61	***	3	167	0.03		-0.54	**	3	251	-0.27		-0.36	*	3	335	-0.08		-0.12		5	419	-0.27		-0.42	*	3
84	0.24		-0.63	***	3	168	0.01		-0.60	***	3	252	-0.10		-0.45	**	3	336	0.22		-0.24		5	420	-0.16		-0.30	.	5

Table IV. Partial correlation coefficients of Total NO$_2$ and Total O$_3$ on Erythemal daily doses high values for March; asterisks mark statistically significant correlations.

Pixel	Total NO$_2$ $r_{partial}$	α	Total O$_3$ $r_{partial}$	α	Class
1	0.34	*	-0.35	*	2
2	0.00		-0.23		5
3	-0.30	.	-0.16		5
4	-0.14		-0.41	*	3
5	-0.28		-0.34	*	3
6	0.19		-0.47	**	3
7	-0.03		-0.41	*	3
8	0.16		-0.37	*	3
9	0.07		-0.34	.	5
10	0.06		-0.41	*	3
11	0.04		-0.35	*	3
12	0.05		-0.33	.	5
13	0.01		-0.35	*	3
14	-0.15		-0.38	*	3
15	-0.13		-0.36	*	3
16	0.02		-0.33	.	5
17	-0.04		-0.25		5
18	-0.08		-0.25		5
19	-0.22		-0.22		5
20	-0.31	.	-0.25		5
21	-0.18		-0.36	*	3
22	0.03		-0.29	.	5
23	-0.13		-0.15		5
24	-0.20		-0.17		5
25	-0.26		-0.06		5
26	-0.07		-0.18		5
27	-0.08		-0.24		5
28	-0.11		-0.24		5
29	-0.05		-0.28		5
30	-0.18		-0.21		5
31	0.00		-0.16		5
32	0.13		-0.22		5
33	0.05		-0.26		5
34	-0.27		-0.17		5
35	-0.09		-0.23		5
36	-0.15		-0.27		5
37	-0.02		-0.24		5
38	-0.17		-0.22		5
39	-0.09		-0.32	.	5
40	-0.05		-0.27		5
41	-0.15		-0.33	.	5
42	-0.06		-0.15		5
43	-0.14		-0.17		5
44	-0.20		-0.31	.	5
45	0.00		-0.34	*	5
46	-0.08		-0.45	**	3
47	0.33	.	-0.39	*	3
48	0.06		-0.43	*	3
49	0.14		-0.17		5
50	-0.05		-0.26		5
51	0.20		-0.19		5
52	0.04		-0.26		5
53	-0.09		-0.23		5
54	0.21		-0.35	*	3
55	-0.27		-0.29	.	5
56	0.02		-0.38	*	3
57	-0.11		-0.27		5
58	-0.37	*	-0.07		4
59	-0.01		-0.36	*	3
60	-0.09		-0.34	*	3
61	-0.25		-0.43	*	3
62	0.27		-0.44	*	3
63	0.17		-0.46	**	3
64	0.06		-0.31	.	5
65	-0.18		-0.11		5
66	-0.07		-0.10		5
67	0.12		-0.14		5
68	0.02		-0.18		5
69	0.13		-0.34	*	3
70	-0.07		-0.21		5
71	0.33	*	-0.36	*	2
72	0.09		-0.41	*	3
73	-0.01		-0.19		5
74	-0.18		-0.20		5
75	-0.32	.	-0.29	.	5
76	-0.25		-0.29	.	5
77	-0.26		-0.35	*	3
78	-0.11		-0.29		5
79	-0.17		-0.32	.	5
80	-0.15		-0.24		5
81	0.16		-0.22		5
82	-0.05		-0.27		5
83	-0.12		-0.20		5
84	-0.10		-0.13		5

Pixel	Total NO$_2$ $r_{partial}$	α	Total O$_3$ $r_{partial}$	α	Class
85	-0.07		-0.13		5
86	-0.10		-0.11		5
87	-0.07		-0.24		5
88	0.00		-0.30	.	5
89	0.09		-0.36	*	3
90	-0.15		-0.30	*	3
91	0.11		-0.40	*	3
92	-0.38	*	-0.28		4
93	-0.17		-0.14		5
94	-0.05		-0.29		5
95	-0.08		-0.38	*	3
96	-0.16		-0.32	.	5
97	-0.15		-0.37	*	3
98	-0.16		-0.25		5
99	-0.30		-0.39	*	3
100	-0.05		-0.23		5
101	-0.31	.	-0.25		5
102	-0.01		-0.22		5
103	-0.07		-0.29	.	5
104	0.02		-0.29		5
105	0.27		-0.33	.	5
106	0.15		-0.41	*	3
107	0.00		-0.37	*	3
108	0.00		-0.21		5
109	0.01		-0.18		5
110	0.12		-0.20		5
111	0.33		-0.21	.	5
112	0.00		-0.13		5
113	0.09		-0.19		5
114	-0.02		-0.21		5
115	-0.06		-0.10		5
116	-0.29		-0.12		5
117	-0.42	*	-0.22		4
118	-0.10		-0.11		5
119	-0.26		-0.17		5
120	0.05		-0.19		5
121	0.02		-0.24		5
122	-0.03		-0.25		5
123	0.21		-0.30	.	5
124	-0.14		-0.27		5
125	-0.15		-0.28		5
126	-0.19		-0.29	.	5
127	-0.02		-0.35	*	3
128	0.14		-0.35	*	3
129	0.33		-0.37	*	3
130	0.33		-0.32	.	5
131	0.06		-0.28		5
132	0.19		-0.22		5
133	0.22		0.05		5
134	0.12		-0.07		5
135	0.22		-0.14		5
136	-0.01		-0.24		5
137	-0.09		-0.33	.	5
138	0.01		-0.29		5
139	0.20		-0.14		5
140	-0.04		-0.25		5
141	-0.21		-0.21		5
142	-0.09		-0.14		5
143	-0.01		-0.21		5
144	0.16		-0.18		5
145	0.00		-0.20		5
146	0.05		-0.12		5
147	0.46	**	-0.14		4
148	-0.08		-0.24		5
149	-0.24		-0.30	.	5
150	-0.33	.	-0.36	*	3
151	-0.24		-0.28		5
152	-0.01		-0.36	*	3
153	-0.15		-0.33	.	5
154	-0.31		-0.34	*	3
155	-0.12		-0.29		5
156	-0.02		-0.28		5
157	0.20		-0.17		5
158	-0.47	**	-0.29	.	4
159	-0.22		-0.20		5
160	-0.15		-0.18		5
161	-0.26		-0.35	*	3
162	0.15		-0.33	.	5
163	0.14		-0.35	*	3
164	-0.33		-0.43	**	3
165	-0.16		-0.40	*	3
166	-0.20		-0.30	.	5
167	0.41	*	-0.23		4
168	0.33	.	-0.07		5

Pixel	Total NO$_2$ $r_{partial}$	α	Total O$_3$ $r_{partial}$	α	Class
169	-0.05		-0.25		5
170	-0.08		-0.29	.	5
171	-0.09		-0.28		5
172	0.23		-0.23		5
173	-0.10		-0.21		5
174	-0.14		-0.38	*	3
175	-0.03		-0.39	*	3
176	0.25		-0.18		5
177	-0.15		-0.25		5
178	-0.04		-0.27		5
179	-0.10		-0.17		5
180	-0.04		-0.39	*	3
181	0.06		-0.38	*	3
182	0.01		-0.38	*	3
183	0.05		-0.27		5
184	0.08		-0.23		5
185	-0.09		-0.27		5
186	-0.26		-0.18		5
187	-0.04		-0.24		5
188	-0.08		-0.37	*	3
189	-0.05		-0.39	*	3
190	0.29	.	-0.48	**	3
191	0.16		-0.46	**	3
192	-0.12		-0.36	*	3
193	-0.25		-0.37	*	3
194	-0.23		-0.31	.	5
195	-0.31	.	-0.41	*	3
196	0.01		-0.25		5
197	-0.05		-0.26		5
198	-0.22		-0.25		5
199	-0.04		-0.22		5
200	0.20		-0.22		5
201	0.05		-0.37	*	3
202	-0.11		-0.33	.	5
203	0.16		-0.26		5
204	0.22		-0.21		5
205	0.22		-0.24		5
206	0.00		-0.11		5
207	0.10		-0.09		5
208	-0.02		-0.19		5
209	-0.03		-0.44	**	3
210	0.05		-0.40	*	3
211	-0.01		-0.38	*	3
212	-0.05		-0.18		5
213	0.02		-0.27		5
214	0.08		-0.35	*	3
215	0.09		-0.41	*	3
216	-0.01		-0.34	.	5
217	0.37	*	-0.42	*	2
218	0.36	*	-0.47	**	1
219	0.01		-0.45	**	3
220	-0.10		-0.34	*	3
221	0.02		-0.23		5
222	-0.16		-0.38	*	3
223	-0.43	*	-0.47	**	1
224	-0.07		-0.29		5
225	-0.12		-0.26		5
226	-0.02		-0.23		5
227	0.04		-0.23		5
228	-0.27		-0.38	*	3
229	-0.09		-0.34	*	3
230	0.02		-0.30	.	5
231	0.04		-0.24		5
232	0.13		-0.17		5
233	0.12		-0.24		5
234	0.12		-0.11		5
235	-0.12		-0.16		5
236	0.13		-0.04		5
237	0.14		-0.42	*	3
238	-0.10		-0.34	*	3
239	-0.14		-0.25		5
240	-0.05		-0.33	.	5
241	-0.25		-0.33	*	3
242	-0.14		-0.36	*	3
243	-0.10		-0.40	*	3
244	-0.10		-0.36	*	3
245	0.39	*	-0.42	*	2
246	0.06		-0.35	*	3
247	-0.23		-0.38	*	3
248	0.23		-0.16		5
249	-0.33	.	-0.33	.	5
250	-0.27		-0.30	.	5
251	-0.02		-0.26		5
252	-0.11		-0.15		5

Pixel	Total NO$_2$ $r_{partial}$	α	Total O$_3$ $r_{partial}$	α	Class
253	-0.23		-0.21		5
254	0.16		-0.26		5
255	-0.20		-0.38	*	3
256	-0.23		-0.20		5
257	0.04		-0.26		5
258	0.16		-0.10		5
259	-0.06		-0.19		5
260	-0.09		-0.16		5
261	0.06		-0.13		5
262	0.08		-0.12		5
263	0.13		-0.04		5
264	-0.17		-0.04		5
265	-0.09		-0.34	*	3
266	-0.06		-0.30	.	5
267	-0.23		-0.33	.	5
268	-0.21		-0.33	.	5
269	-0.03		-0.26		5
270	0.09		-0.35	.	5
271	0.18		-0.34	*	3
272	0.18		-0.33	*	3
273	-0.10		-0.31	.	5
274	-0.18		-0.24		5
275	0.07		-0.27		5
276	0.00		-0.20		5
277	0.11		-0.36	*	3
278	0.02		-0.30	.	5
279	-0.09		-0.26		5
280	0.01		-0.24		5
281	0.07		-0.25		5
282	-0.01		-0.32	.	5
283	0.06		-0.34	*	3
284	0.10		-0.23		5
285	0.02		-0.15		5
286	0.11		-0.18		5
287	0.00		-0.16		5
288	0.07		-0.17		5
289	0.02		-0.09		5
290	0.03		0.04		5
291	-0.19		-0.32	.	5
292	-0.18		-0.23		5
293	0.14		-0.30	.	5
294	0.01		-0.33	.	5
295	0.31	.	-0.31	.	5
296	0.37	*	-0.31	.	4
297	-0.03		-0.28		5
298	0.09		-0.17		5
299	-0.07		-0.18		5
300	-0.29		-0.41	*	3
301	-0.11		-0.33	.	5
302	0.02		-0.31	.	5
303	-0.12		-0.28		5
304	-0.01		-0.32	.	5
305	0.15		-0.32	.	5
306	-0.01		-0.42	*	3
307	-0.39	*	-0.43	*	1
308	-0.26		-0.30	.	5
309	-0.06		-0.30	.	5
310	0.09		-0.26		5
311	0.02		-0.20		5
312	0.11		-0.25		5
313	0.16		-0.01		5
314	-0.04		0.08		5
315	-0.02		0.01		5
316	-0.05		-0.34	*	3
317	-0.10		-0.34	*	3
318	0.03		-0.27		5
319	0.17		-0.34	.	5
320	0.25		-0.40	*	3
321	0.21		-0.32	.	5
322	0.05		-0.20		5
323	-0.17		-0.24		5
324	-0.21		-0.36	*	3
325	-0.27		-0.31	.	5
326	-0.10		-0.30	.	5
327	-0.13		-0.24		5
328	-0.17		-0.26		5
329	-0.16		-0.36	*	3
330	-0.14		-0.35	*	3
331	-0.29	.	-0.32	.	5
332	-0.41	*	-0.38	*	1
333	-0.23		-0.28		5
334	-0.05		-0.23		5
335	0.18		-0.25		5
336	-0.06		-0.07		5

Pixel	Total NO$_2$ $r_{partial}$	α	Total O$_3$ $r_{partial}$	α	Class
337	-0.01		-0.03		5
338	-0.28		0.00		5
339	-0.21		0.05		5
340	0.11		0.12		5
341	-0.22		-0.37	*	3
342	-0.23		-0.33	.	5
343	-0.12		-0.29		5
344	-0.24		-0.36	*	3
345	-0.07		-0.33	*	3
346	0.13		-0.26		5
347	-0.10		-0.16		5
348	-0.36	*	-0.22		4
349	-0.18		-0.32	.	5
350	-0.06		-0.35	*	3
351	-0.14		-0.27		5
352	0.07		-0.27		5
353	-0.29	.	-0.26		5
354	-0.04		-0.42	*	3
355	-0.25		-0.49	**	3
356	-0.12		-0.39	*	3
357	-0.18		-0.24		5
358	-0.20		-0.28		5
359	0.05		-0.27		5
360	0.08		-0.13		5
361	-0.13		-0.13		5
362	-0.19		-0.38	*	3
363	-0.06		-0.34	*	3
364	0.05		-0.28		5
365	-0.18		-0.31	.	5
366	-0.02		-0.21		5
367	-0.02		-0.17		5
368	-0.09		-0.39	*	3
369	-0.23		-0.30	.	5
370	-0.36	*	-0.45	**	1
371	-0.33	.	-0.42	*	3
372	-0.30	.	-0.33	.	5
373	-0.22		-0.37	*	3
374	-0.01		-0.40	*	3
375	0.15		-0.19		5
376	-0.08		-0.25		5
377	-0.04		-0.25		5
378	0.05		-0.16		5
379	0.09		-0.08		5
380	-0.18		-0.19		5
381	-0.15		-0.30	.	5
382	0.04		-0.23		5
383	-0.10		-0.14		5
384	0.02		-0.20		5
385	0.02		-0.22		5
386	-0.09		-0.42	*	3
387	-0.35	*	-0.46	**	1
388	-0.44	**	-0.52	**	1
389	-0.35	*	-0.46	**	1
390	-0.47	**	-0.42	*	1
391	-0.37	*	-0.43	*	1
392	-0.14		-0.34	*	3
393	-0.03		-0.21		5
394	-0.18		-0.27		5
395	-0.27		-0.25		5
396	-0.06		-0.11		5
397	0.00		-0.07		5
398	0.20		-0.11		5
399	0.17		-0.25		5
400	-0.37	*	-0.16		4
401	-0.22		-0.32	.	5
402	-0.16		-0.30	.	5
403	-0.38	*	-0.47	**	1
404	-0.40	*	-0.46	**	1
405	-0.55	***	-0.48	**	1
406	-0.30	.	-0.37	*	3
407	-0.18		-0.32	.	5
408	-0.07		-0.23		5
409	-0.11		-0.20		5
410	-0.26		-0.31	.	5
411	-0.30	.	-0.25		5
412	-0.22		-0.31	.	5
413	-0.33	.	-0.27		5
414	-0.48	**	-0.32	.	4
415	-0.21		-0.31	.	5
416	-0.38	*	-0.43	*	1
417	-0.13		-0.32	.	5
418	-0.10		-0.37	*	3
419	-0.07		-0.27		5
420	-0.19		-0.26		5

Table V. Partial correlation coefficients of Total NO₂ and Total O₃ on Erythemal daily doses high values for April; asterisks mark statistically significant correlations.

Pixel	Total NO₂ $r_{partial}$	α	Total O₃ $r_{partial}$	α	Class
1	0.06		-0.59	***	3
2	0.14		-0.63	***	3
3	-0.07		-0.65	***	3
4	-0.21		-0.68	***	3
5	0.00		-0.58	***	3
6	-0.18		-0.52	**	3
7	-0.07		-0.55	***	3
8	-0.03		-0.50	**	3
9	0.12		-0.54	**	3
10	0.10		-0.56	***	3
11	0.02		-0.59	***	3
12	0.25		-0.48	**	3
13	-0.20		-0.61	***	3
14	-0.16		-0.61	***	3
15	-0.20		-0.56	***	3
16	-0.09		-0.49	**	3
17	0.24		-0.48	**	3
18	0.21		-0.48	**	3
19	-0.45	**	-0.54	***	1
20	-0.40	*	-0.61	***	1
21	-0.31	.	-0.60	***	3
22	-0.17		-0.52	**	3
23	-0.02		-0.46	**	3
24	0.11		-0.36	*	3
25	0.02		-0.43	**	3
26	-0.03		-0.59	***	3
27	0.10		-0.49	**	3
28	-0.28		-0.60	***	3
29	-0.40	*	-0.60	***	1
30	-0.12		-0.56	***	3
31	-0.09		-0.57	***	3
32	0.18		-0.50	**	3
33	-0.09		-0.34	.	5
34	-0.08		-0.40	*	3
35	-0.18		-0.29	.	5
36	0.21		-0.54	**	3
37	-0.10		-0.53	**	3
38	-0.11		-0.59	***	3
39	-0.09		-0.46	**	3
40	-0.32	.	-0.41	*	3
41	-0.37	*	-0.36	*	1
42	-0.43	*	-0.42	*	1
43	-0.18		-0.48	**	3
44	-0.37	*	-0.45	**	1
45	-0.04		-0.35	*	3
46	0.01		-0.24		5
47	-0.12		-0.28		5
48	-0.07		-0.34	.	5
49	0.27		-0.21		5
50	0.33	.	-0.34	.	5
51	0.06		-0.44	*	3
52	-0.11		-0.51	**	3
53	-0.13		-0.50	**	3
54	-0.13		-0.39	.	3
55	-0.04		-0.44	*	3
56	-0.22		-0.26		5
57	-0.30		-0.36	*	3
58	-0.08		-0.31	.	5
59	-0.13		-0.26		5
60	-0.06		-0.24		5
61	-0.13		-0.37	*	3
62	-0.29	.	-0.30	.	5
63	-0.17		-0.26		5
64	0.24		-0.30	.	5
65	0.36	*	-0.35	*	2
66	0.06		-0.35	*	3
67	0.13		-0.38	*	3
68	0.00		-0.39	*	3
69	-0.28		-0.35	*	3
70	-0.18		-0.44	**	3
71	-0.09		-0.29		5
72	-0.11		-0.36	*	3
73	0.19		-0.17		5
74	-0.30	.	-0.35	*	3
75	-0.18		-0.22		5
76	-0.24		-0.20		5
77	-0.18		-0.19		5
78	-0.11		-0.19		5
79	-0.46	**	-0.44	*	1
80	0.20		-0.35	*	3
81	0.49	**	-0.26		4
82	-0.26		-0.34	*	3
83	0.15		-0.17		5
84	0.11		-0.32	.	5
85	0.10		-0.31	.	5
86	-0.16		-0.32	.	5
87	-0.15		-0.20		5
88	0.04		-0.38	*	3
89	-0.02		-0.39	*	3
90	0.05		-0.35	*	3
91	-0.21		-0.23		5
92	-0.05		-0.21		5
93	0.09		-0.18		5
94	-0.12		-0.19		5
95	-0.07		-0.31	.	5
96	-0.19		-0.28		5
97	-0.02		-0.27		5
98	0.19		-0.21		5
99	-0.14		-0.19		5
100	-0.11		-0.28		5
101	0.12		-0.26		5
102	-0.16		-0.32	.	5
103	-0.26		-0.33	.	5
104	0.11		-0.31	.	5
105	-0.12		-0.35	*	3
106	-0.08		-0.23		5
107	0.09		-0.25		5
108	-0.17		-0.19		5
109	-0.13		-0.31	.	5
110	-0.18		-0.16		5
111	-0.27		-0.26		5
112	0.00		-0.30	.	5
113	0.09		-0.36	*	3
114	-0.05		-0.17		5
115	-0.25		-0.27		5
116	-0.26		-0.30	.	5
117	0.04		-0.22		5
118	-0.09		-0.22		5
119	-0.12		-0.14		5
120	-0.22		-0.21		5
121	0.01		-0.21		5
122	0.06		-0.25		5
123	0.01		-0.21		5
124	0.12		-0.22		5
125	-0.04		-0.21		5
126	-0.35	*	-0.30	.	4
127	0.08		-0.32	.	5
128	0.04		-0.36	*	3
129	0.14		-0.27		5
130	-0.14		-0.35	*	3
131	-0.08		-0.35	*	3
132	-0.01		-0.26		5
133	-0.09		-0.22		5
134	-0.10		-0.32	.	5
135	-0.19		-0.29	.	5
136	-0.29	.	-0.32	.	5
137	-0.08		-0.22		5
138	-0.27		-0.17		5
139	-0.41	*	-0.35	.	4
140	-0.47	**	-0.33	.	4
141	-0.22		-0.12		5
142	-0.06		-0.23		5
143	0.07		-0.13		5
144	-0.11		0.00		5
145	-0.07		-0.10		5
146	-0.07		-0.16		5
147	0.01		-0.23		5
148	0.05		-0.23		5
149	0.02		-0.23		5
150	-0.15		-0.18		5
151	-0.13		-0.26		5
152	-0.16		-0.19		5
153	0.02		-0.22		5
154	-0.27		-0.33	.	5
155	-0.20		-0.29		5
156	0.00		-0.29		5
157	0.08		-0.38	*	3
158	-0.03		-0.40	*	3
159	-0.02		-0.34	*	3
160	-0.15		-0.34	.	5
161	-0.02		-0.39	*	3
162	-0.05		-0.33	.	5
163	-0.13		-0.44	**	3
164	-0.12		-0.37	*	3
165	-0.19		-0.37	*	3
166	0.10		-0.39	*	3
167	0.26		-0.40	*	3
168	0.08		-0.33	.	5
169	-0.05		-0.29	.	5
170	0.20		-0.18		5
171	0.00		-0.15		5
172	0.32	.	0.07		5
173	0.10		0.02		5
174	0.17		0.03		5
175	0.13		-0.15		5
176	0.16		-0.17		5
177	0.30	.	-0.18		5
178	0.35	*	-0.13		4
179	0.19		-0.08		5
180	-0.15		-0.30	.	5
181	0.13		-0.23		5
182	-0.12		-0.26		5
183	-0.24		-0.26		5
184	-0.13		-0.33	.	5
185	0.19		-0.39	*	3
186	0.10		-0.33	.	5
187	0.00		-0.37	*	3
188	0.11		-0.29		5
189	0.21		-0.36	*	3
190	-0.15		-0.43	*	3
191	-0.27		-0.48	**	3
192	-0.26		-0.39	*	3
193	-0.27		-0.40	*	3
194	-0.13		-0.42	*	3
195	-0.23		-0.49	**	3
196	-0.20		-0.42	*	3
197	0.01		-0.32	.	5
198	-0.06		-0.14		5
199	0.02		-0.03		5
200	-0.20		-0.08		5
201	-0.09		0.04		5
202	0.10		0.05		5
203	0.20		-0.02		5
204	0.10		-0.03		5
205	0.07		0.00		5
206	0.30		-0.07		5
207	0.09		0.01		5
208	0.04		0.02		5
209	0.34	*	-0.26		4
210	0.21		-0.35	*	3
211	-0.18		-0.21		5
212	-0.19		-0.28		5
213	0.17		-0.38	*	3
214	-0.02		-0.33	.	5
215	-0.05		-0.24		5
216	-0.03		-0.40	*	3
217	-0.08		-0.48	**	3
218	-0.08		-0.46	**	3
219	-0.11		-0.42	*	3
220	-0.01		-0.43	*	3
221	-0.12		-0.44	**	3
222	0.08		-0.41	*	3
223	-0.23		-0.54	***	3
224	0.07		-0.46	**	3
225	0.29	.	-0.37	*	3
226	-0.12		-0.20		5
227	-0.33	.	-0.30	.	5
228	-0.48	**	-0.20		4
229	-0.22		-0.13		5
230	-0.10		-0.04		5
231	-0.02		0.01		5
232	0.03		0.06		5
233	0.21		0.23		5
234	0.06		0.20		5
235	-0.19		0.09		5
236	-0.30	.	0.21		5
237	-0.06		-0.29		5
238	-0.12		-0.31	.	5
239	-0.12		-0.19		5
240	-0.04		-0.23		5
241	-0.23		-0.27		5
242	-0.15		-0.26		5
243	-0.02		-0.32	.	5
244	-0.23		-0.44	**	3
245	-0.06		-0.37	*	3
246	0.06		-0.37	*	3
247	0.01		-0.33	.	5
248	0.07		-0.35	*	3
249	-0.08		-0.36	*	3
250	-0.03		-0.40	*	3
251	0.32	.	-0.34	*	3
252	0.25		-0.30	.	5
253	-0.04		-0.35	*	3
254	-0.12		-0.28		5
255	-0.20		-0.32	.	5
256	-0.27		-0.26		5
257	-0.15		-0.09		5
258	0.21		-0.06		5
259	0.01		0.04		5
260	0.24		0.24		5
261	-0.20		0.02		5
262	-0.32	.	0.07		5
263	-0.18		0.03		5
264	-0.01		0.14		5
265	-0.23		-0.38	*	3
266	-0.05		-0.15		5
267	-0.22		-0.09		5
268	-0.23		-0.05		5
269	-0.02		-0.22		5
270	0.05		-0.28		5
271	-0.10		-0.30	.	5
272	-0.07		-0.23		5
273	-0.12		-0.23		5
274	-0.11		-0.20		5
275	0.07		-0.26		5
276	0.19		-0.25		5
277	0.10		-0.28		5
278	0.40	*	-0.22		4
279	0.14		-0.25		5
280	-0.03		-0.29	.	5
281	-0.02		-0.31	.	5
282	0.01		-0.31	.	5
283	-0.02		-0.28		5
284	0.19		-0.21		5
285	0.09		-0.11		5
286	0.08		0.02		5
287	0.08		0.05		5
288	0.17		0.12		5
289	0.23		0.06		5
290	-0.03		0.07		5
291	-0.40	*	-0.08		4
292	-0.57	***	-0.09		4
293	-0.13		0.02		5
294	0.08		-0.20		5
295	-0.18		-0.13		5
296	-0.03		-0.16		5
297	-0.20		-0.11		5
298	-0.17		-0.13		5
299	-0.27		0.00		5
300	-0.10		-0.17		5
301	0.19		-0.14		5
302	0.09		-0.11		5
303	0.37	*	-0.18		4
304	0.13		-0.22		5
305	-0.12		-0.35	*	3
306	-0.08		-0.33	.	5
307	-0.05		-0.35	*	3
308	0.03		-0.10		5
309	0.04		-0.08		5
310	-0.21		-0.05		5
311	0.24		0.00		5
312	0.18		0.01		5
313	0.05		0.06		5
314	0.03		-0.02		5
315	-0.30	.	-0.02		5
316	-0.36	*	-0.12		4
317	0.10		-0.12		5
318	-0.14		-0.01		5
319	-0.24		-0.02		5
320	-0.03		-0.16		5
321	-0.36	*	-0.06		4
322	-0.22		-0.11		5
323	-0.27		-0.09		5
324	-0.35	.	-0.07		5
325	-0.17		0.03		5
326	-0.10		-0.14		5
327	0.00		-0.18		5
328	-0.34	.	-0.30	.	5
329	-0.32	.	-0.34	.	5
330	-0.22		-0.40	*	3
331	-0.25		-0.43	*	3
332	0.14		-0.39	*	3
333	-0.12		-0.11		5
334	-0.08		-0.09		5
335	0.14		0.03		5
336	-0.04		-0.03		5
337	-0.19		-0.05		5
338	-0.05		-0.07		5
339	0.02		-0.03		5
340	0.03		0.02		5
341	-0.16		-0.18		5
342	-0.13		-0.04		5
343	0.00		-0.06		5
344	-0.13		-0.08		5
345	0.11		-0.15		5
346	-0.21		-0.08		5
347	-0.29		-0.17		5
348	-0.15		-0.11		5
349	-0.16		-0.19		5
350	-0.34	*	0.04		4
351	-0.23		0.04		5
352	-0.33		-0.10		5
353	-0.17		-0.12		5
354	-0.26		-0.29		5
355	-0.10		-0.31	.	5
356	-0.25		-0.25		5
357	0.05		-0.26		5
358	-0.06		0.01		5
359	0.08		-0.02		5
360	-0.10		0.02		5
361	-0.16		0.00		5
362	-0.01		0.00		5
363	0.14		-0.17		5
364	-0.15		-0.12		5
365	-0.21		-0.10		5
366	0.10		0.07		5
367	-0.22		-0.13		5
368	-0.04		-0.13		5
369	-0.26		0.05		5
370	-0.12		0.05		5
371	-0.30	.	-0.15		5
372	-0.05		-0.25		5
373	-0.33	.	-0.38	*	3
374	-0.11		-0.34	.	5
375	-0.19		-0.27		5
376	-0.13		-0.11		5
377	0.02		-0.07		5
378	-0.09		0.00		5
379	-0.28		-0.07		5
380	-0.19		0.02		5
381	-0.05		-0.01		5
382	-0.17		-0.16		5
383	0.04		-0.11		5
384	0.16		0.02		5
385	-0.26		-0.06		5
386	0.10		0.08		5
387	-0.24		0.13		5
388	-0.09		0.11		5
389	-0.16		0.09		5
390	-0.12		-0.12		5
391	-0.47	**	-0.43	*	1
392	-0.13		-0.26		5
393	0.08		-0.08		5
394	-0.05		-0.07		5
395	0.06		0.00		5
396	-0.07		0.00		5
397	0.00		-0.03		5
398	0.11		-0.04		5
399	-0.16		0.05		5
400	-0.01		0.04		5
401	0.01		0.02		5
402	-0.36	*	0.02		4
403	-0.15		0.15		5
404	-0.29	.	0.08		5
405	-0.12		-0.17		5
406	-0.38	*	-0.25		4
407	-0.22		-0.27		5
408	0.06		-0.03		5
409	0.07		-0.03		5
410	0.03		-0.02		5
411	0.32	.	0.09		5
412	0.07		0.00		5
413	0.17		-0.01		5
414	0.08		-0.03		5
415	-0.08		0.05		5
416	-0.25		-0.14		5
417	-0.28		-0.12		5
418	-0.22		-0.07		5
419	-0.07		0.15		5
420	-0.02		0.01		5

Table VI. Partial correlation coefficients of Total NO2 and Total O3 on Erythemal daily doses high values for May; asterisks mark statistically significant correlations.

Pixel	Total NO₂ $r_{partial}$	α	Total O₃ $r_{partial}$	α	Class
1	0.08		-0.08		5
2	0.18		-0.19		5
3	0.22		-0.25		5
4	0.09		-0.16		5
5	0.15		-0.18		5
6	0.06		-0.23		5
7	-0.11		-0.20		5
8	0.05		-0.18		5
9	0.20		-0.06		5
10	0.01		-0.19		5
11	0.17		-0.17		5
12	0.20		-0.14		5
13	0.10		-0.20		5
14	0.23		-0.17		5
15	0.20		-0.17		5
16	0.37	*	-0.21		4
17	-0.14		-0.20		5
18	-0.01		-0.16		5
19	-0.02		-0.04		5
20	0.17		-0.07		5
21	0.21		-0.03		5
22	0.16		-0.13		5
23	-0.02		0.05		5
24	-0.17		0.02		5
25	0.01		-0.12		5
26	-0.03		0.01		5
27	0.07		-0.07		5
28	-0.07		-0.05		5
29	-0.07		-0.07		5
30	0.07		-0.02		5
31	0.02		0.07		5
32	-0.07		0.03		5
33	0.06		0.08		5
34	-0.03		0.00		5
35	-0.03		0.03		5
36	0.21		0.06		5
37	0.23		0.08		5
38	0.13		-0.01		5
39	-0.03		0.02		5
40	-0.06		-0.05		5
41	0.15		0.03		5
42	-0.18		0.05		5
43	0.03		-0.01		5
44	-0.18		-0.08		5
45	-0.18		-0.12		5
46	-0.13		0.01		5
47	-0.21		0.07		5
48	0.09		0.01		5
49	0.06		-0.06		5
50	-0.18		-0.14		5
51	-0.04		0.02		5
52	0.15		-0.03		5
53	-0.05		0.03		5
54	0.04		-0.07		5
55	-0.02		0.01		5
56	0.14		0.03		5
57	-0.11		-0.05		5
58	0.12		-0.06		5
59	-0.02		-0.09		5
60	-0.13		-0.14		5
61	-0.06		-0.03		5
62	-0.18		-0.03		5
63	0.01		0.04		5
64	-0.35	*	0.05		4
65	-0.24		-0.19		5
66	-0.06		-0.25		5
67	-0.11		-0.15		5
68	-0.10		-0.05		5
69	0.02		0.01		5
70	-0.09		-0.06		5
71	0.18		-0.06		5
72	0.10		-0.15		5
73	0.20		-0.05		5
74	-0.28		-0.09		5
75	-0.04		-0.08		5
76	-0.10		0.00		5
77	-0.16		0.03		5
78	0.00		0.05		5
79	0.09		0.03		5
80	0.08		-0.02		5
81	0.10		0.01		5
82	0.08		0.03		5
83	0.01		-0.02		5
84	-0.01		-0.12		5
85	-0.18		-0.20		5
86	-0.04		-0.08		5
87	-0.06		-0.06		5
88	0.10		-0.04		5
89	0.09		-0.01		5
90	-0.04		-0.05		5
91	0.33	.	-0.06		5
92	0.03		-0.15		5
93	0.19		-0.04		5
94	-0.13		-0.06		5
95	-0.18		0.00		5
96	-0.23		0.03		5
97	-0.21		0.03		5
98	0.30	.	0.03		5
99	-0.06		0.04		5
100	0.09		-0.02		5
101	0.25		0.01		5
102	0.27		-0.06		5
103	-0.28		-0.05		5
104	0.08		0.02		5
105	0.07		0.00		5
106	0.06		0.02		5
107	-0.07		-0.05		5
108	-0.02		-0.13		5
109	0.00		-0.03		5
110	0.12		0.07		5
111	0.13		0.04		5
112	-0.09		-0.02		5
113	0.19		0.01		5
114	0.00		-0.06		5
115	0.00		-0.10		5
116	-0.04		-0.13		5
117	0.17		-0.06		5
118	-0.28	.	-0.10		5
119	-0.32	.	-0.02		5
120	-0.30	.	-0.13		5
121	0.22		-0.07		5
122	-0.05		0.07		5
123	0.21		0.04		5
124	-0.11		0.07		5
125	-0.11		0.01		5
126	-0.17		0.00		5
127	0.10		0.03		5
128	0.07		0.04		5
129	0.23		0.05		5
130	-0.12		-0.02		5
131	-0.04		-0.04		5
132	0.04		0.03		5
133	-0.09		0.00		5
134	-0.03		0.03		5
135	0.13		0.06		5
136	0.00		0.01		5
137	-0.05		-0.02		5
138	-0.09		-0.07		5
139	-0.03		-0.12		5
140	-0.08		-0.10		5
141	0.09		-0.07		5
142	-0.32	.	0.10		5
143	-0.30	.	0.03		5
144	-0.35	*	-0.07		4
145	-0.03		0.00		5
146	0.03		-0.05		5
147	0.11		-0.06		5
148	-0.05		0.05		5
149	-0.12		0.12		5
150	-0.18		0.12		5
151	0.13		0.01		5
152	0.06		0.02		5
153	0.14		0.02		5
154	-0.17		0.00		5
155	0.11		0.11		5
156	-0.09		0.08		5
157	-0.33	.	-0.03		5
158	-0.08		0.07		5
159	0.21		0.12		5
160	0.20		0.21		5
161	0.22		0.17		5
162	0.05		0.14		5
163	0.35	*	0.29	.	4
164	0.27		0.26		5
165	0.12		0.26		5
166	0.15		0.10		5
167	0.24		0.05		5
168	-0.13		-0.13		5
169	-0.12		-0.11		5
170	-0.04		-0.08		5
171	-0.31	.	-0.07		5
172	-0.34	*	-0.05		4
173	-0.20		-0.14		5
174	-0.27		-0.09		5
175	-0.21		-0.04		5
176	0.03		-0.08		5
177	0.17		-0.10		5
178	0.18		0.03		5
179	0.11		-0.03		5
180	0.04		0.07		5
181	0.17		0.05		5
182	-0.08		0.06		5
183	0.21		0.14		5
184	-0.01		0.04		5
185	-0.22		0.02		5
186	-0.01		0.07		5
187	0.20		0.16		5
188	0.00		0.28		5
189	-0.06		0.16		5
190	0.04		0.20		5
191	0.02		0.19		5
192	0.03		0.10		5
193	-0.02		0.04		5
194	0.31	.	0.08		5
195	0.22		-0.02		5
196	-0.02		-0.06		5
197	0.05		-0.02		5
198	-0.08		-0.10		5
199	-0.21		-0.17		5
200	-0.31	.	-0.07		5
201	-0.36	*	-0.13		4
202	-0.16		-0.09		5
203	-0.14		-0.04		5
204	0.23		-0.04		5
205	0.11		-0.03		5
206	0.10		-0.02		5
207	-0.24		-0.10		5
208	0.09		-0.02		5
209	0.19		-0.02		5
210	0.02		-0.01		5
211	0.10		0.02		5
212	-0.17		0.03		5
213	-0.02		0.09		5
214	-0.04		0.10		5
215	-0.16		0.18		5
216	0.08		0.12		5
217	0.30	.	0.18		5
218	0.20		0.08		5
219	-0.14		0.05		5
220	-0.11		-0.08		5
221	0.21		-0.10		5
222	0.07		-0.08		5
223	0.29	.	-0.05		5
224	0.16		-0.12		5
225	-0.31	.	-0.17		5
226	-0.10		-0.14		5
227	-0.18		-0.09		5
228	-0.25		-0.09		5
229	-0.15		-0.20		5
230	-0.24		-0.20		5
231	-0.12		-0.20		5
232	0.11		-0.20		5
233	-0.01		-0.21		5
234	-0.06		-0.17		5
235	-0.06		-0.13		5
236	-0.01		-0.04		5
237	0.14		0.11		5
238	0.18		0.11		5
239	-0.01		0.07		5
240	-0.08		0.09		5
241	-0.25		0.04		5
242	-0.19		0.01		5
243	-0.04		0.04		5
244	0.25		0.05		5
245	0.25		-0.07		5
246	-0.01		-0.15		5
247	-0.28	.	-0.14		5
248	0.26		-0.14		5
249	0.20		-0.21		5
250	0.13		-0.22		5
251	-0.03		-0.14		5
252	-0.19		-0.28	.	5
253	-0.37	*	-0.15		4
254	-0.20		-0.13		5
255	-0.12		-0.13		5
256	-0.24		-0.21		5
257	-0.03		-0.22		5
258	-0.03		-0.19		5
259	-0.03		-0.16		5
260	-0.08		-0.17		5
261	-0.02		-0.13		5
262	-0.09		-0.11		5
263	-0.17		-0.04		5
264	-0.19		-0.15		5
265	-0.10		0.17		5
266	-0.04		0.11		5
267	-0.20		0.10		5
268	-0.26		0.11		5
269	-0.08		0.01		5
270	0.05		0.04		5
271	0.08		-0.06		5
272	0.10		-0.13		5
273	0.14		-0.15		5
274	0.09		-0.20		5
275	0.55	***	-0.20		4
276	0.20		-0.21		5
277	0.19		-0.09		5
278	0.19		-0.18		5
279	0.03		-0.18		5
280	-0.14		-0.24		5
281	0.10		-0.15		5
282	-0.08		-0.16		5
283	-0.14		-0.16		5
284	0.24		-0.24		5
285	0.20		-0.23		5
286	0.11		-0.16		5
287	-0.08		-0.11		5
288	-0.05		-0.10		5
289	-0.12		-0.08		5
290	0.14		-0.09		5
291	-0.10		0.04		5
292	-0.23		-0.01		5
293	-0.28		-0.16		5
294	-0.15		-0.08		5
295	0.22		0.01		5
296	0.06		-0.10		5
297	-0.02		-0.21		5
298	0.20		-0.19		5
299	0.24		-0.22		5
300	0.34	.	-0.21		5
301	0.22		-0.11		5
302	0.13		-0.05		5
303	0.21		-0.18		5
304	0.22		-0.23		5
305	-0.12		-0.26		5
306	0.11		-0.11		5
307	-0.08		-0.15		5
308	-0.18		-0.16		5
309	0.09		-0.20		5
310	0.33	.	-0.21		5
311	0.31	.	-0.06		5
312	0.15		-0.11		5
313	-0.12		-0.09		5
314	-0.18		-0.15		5
315	0.15		-0.03		5
316	-0.29	.	-0.08		5
317	-0.08		-0.10		5
318	-0.08		-0.19		5
319	0.28		-0.04		5
320	0.04		-0.08		5
321	-0.21		-0.10		5
322	0.03		-0.14		5
323	0.24		-0.17		5
324	0.21		-0.25		5
325	0.20		-0.14		5
326	0.17		-0.16		5
327	0.04		-0.16		5
328	0.00		-0.29	.	5
329	-0.06		-0.12		5
330	0.14		-0.09		5
331	-0.09		-0.25		5
332	-0.26		-0.25		5
333	0.15		-0.19		5
334	0.14		-0.22		5
335	0.30	.	-0.15		5
336	0.09		-0.12		5
337	-0.29	.	-0.13		5
338	0.09		-0.16		5
339	0.40	*	-0.09		4
340	0.00		-0.18		5
341	-0.43	*	-0.29	.	4
342	0.06		-0.08		5
343	0.06		-0.18		5
344	0.08		-0.05		5
345	0.11		-0.07		5
346	0.03		-0.09		5
347	0.03		-0.11		5
348	0.16		-0.11		5
349	0.37	*	-0.20		4
350	0.15		-0.02		5
351	0.18		-0.15		5
352	0.08		-0.15		5
353	-0.10		-0.16		5
354	0.08		-0.14		5
355	-0.03		-0.26		5
356	-0.31	.	-0.26		5
357	0.02		-0.23		5
358	0.17		-0.22		5
359	0.33	.	-0.16		5
360	0.11		-0.18		5
361	-0.06		-0.21		5
362	0.26		-0.11		5
363	0.18		-0.21		5
364	0.27		-0.07		5
365	0.19		-0.07		5
366	-0.17		-0.30	.	5
367	0.15		-0.20		5
368	0.25		-0.24		5
369	0.15		-0.09		5
370	0.37	*	-0.17		4
371	0.02		-0.13		5
372	-0.06		-0.09		5
373	0.18		-0.09		5
374	-0.12		-0.21		5
375	-0.24		-0.24		5
376	-0.01		-0.11		5
377	-0.02		-0.11		5
378	0.00		-0.09		5
379	0.11		-0.20		5
380	-0.27		-0.12		5
381	0.20		-0.15		5
382	0.18		-0.20		5
383	0.27		-0.29	.	5
384	0.05		-0.25		5
385	0.01		-0.36	*	3
386	0.07		-0.26		5
387	0.30	.	-0.11		5
388	0.27		-0.13		5
389	0.04		-0.17		5
390	-0.13		-0.20		5
391	0.24		-0.02		5
392	0.25		-0.16		5
393	0.01		-0.09		5
394	-0.10		-0.15		5
395	-0.15		-0.12		5
396	0.05		-0.07		5
397	-0.18		-0.16		5
398	0.32	.	-0.26		5
399	0.11		-0.32	.	5
400	0.01		-0.41	*	3
401	0.42	*	-0.04		4
402	0.31	.	0.01		5
403	0.21		-0.10		5
404	0.20		-0.10		5
405	0.12		-0.12		5
406	0.08		-0.18		5
407	0.21		-0.28		5
408	-0.20		-0.07		5
409	0.04		-0.17		5
410	0.06		-0.17		5
411	0.41	*	-0.25		4
412	0.39	*	-0.03		4
413	0.32	.	0.01		5
414	0.39	*	-0.12		4
415	0.26		-0.14		5
416	0.19		-0.12		5
417	0.27		-0.18		5
418	0.06		-0.09		5
419	0.06		-0.11		5
420	-0.21		-0.22		5

Table VII. Partial correlation coefficients of Total NO₂ and Total O₃ on Erythemal daily doses high values for June; asterisks mark statistically significant correlations.

Pixel	Total NO₂ r_partial	α	Total O₃ r_partial	α	Class	Pixel	Total NO₂ r_partial	α	Total O₃ r_partial	α	Class	Pixel	Total NO₂ r_partial	α	Total O₃ r_partial	α	Class	Pixel	Total NO₂ r_partial	α	Total O₃ r_partial	α	Class	Pixel	Total NO₂ r_partial	α	Total O₃ r_partial	α	Class
1	-0.14		-0.49	**	3	85	0.16		-0.68	***	3	169	0.15		-0.44	**	3	253	0.01		-0.42	*	3	337	-0.07		-0.63	***	3
2	0.03		-0.60	***	3	86	0.37	*	-0.60	***	2	170	0.10		-0.37	*	3	254	0.07		-0.38	*	3	338	-0.34	.	-0.65	***	3
3	-0.25		-0.50	**	3	87	-0.01		-0.55	**	3	171	-0.18		-0.38	*	3	255	0.43	*	-0.32	.	4	339	-0.21		-0.60	***	3
4	-0.09		-0.51	**	3	88	-0.09		-0.51	**	3	172	-0.06		-0.45	**	3	256	0.33		-0.41	*	3	340	-0.19		-0.57	***	3
5	-0.04		-0.38	*	3	89	0.15		-0.51	**	3	173	0.26		-0.45	*	3	257	0.18		-0.47	**	3	341	-0.04		-0.41	*	3
6	-0.06		-0.39	*	3	90	0.23		-0.54	**	3	174	0.32	.	-0.46	**	3	258	0.03		-0.52	**	3	342	-0.23		-0.37	*	3
7	-0.25		-0.53	**	3	91	-0.34	*	-0.49	**	1	175	0.12		-0.31	.	5	259	-0.28		-0.56	***	3	343	-0.48	**	-0.44	*	1
8	0.19		-0.49	**	3	92	-0.03		-0.47	**	3	176	-0.18		-0.26		5	260	-0.07		-0.55	**	3	344	-0.13		-0.38	*	3
9	0.02		-0.44	*	3	93	0.02		-0.47	**	3	177	-0.06		-0.40	*	3	261	-0.14		-0.56	**	3	345	0.07		-0.35	*	3
10	-0.26		-0.61	***	3	94	-0.09		-0.50	**	3	178	0.10		-0.39	*	3	262	0.06		-0.68	***	3	346	-0.23		-0.19		5
11	0.23		-0.41	*	3	95	0.06		-0.61	***	3	179	0.29		-0.49	**	3	263	0.24		-0.69	***	3	347	-0.16		-0.41	*	3
12	0.15		-0.49	**	3	96	0.36	*	-0.61	***	2	180	-0.02		-0.48	**	3	264	-0.02		-0.66	***	3	348	-0.21		-0.45	**	3
13	0.13		-0.61	***	3	97	0.16		-0.54	***	3	181	-0.12		-0.42	*	3	265	-0.14		-0.58	***	3	349	-0.11		-0.43	*	3
14	0.03		-0.61	***	3	98	0.09		-0.64	***	3	182	-0.09		-0.43	*	3	266	-0.31	.	-0.50	**	3	350	0.32	.	-0.46	**	3
15	0.00		-0.54	**	3	99	0.01		-0.62	***	3	183	0.03		-0.46	**	3	267	-0.23		-0.50	**	3	351	0.25		-0.47	**	3
16	0.12		-0.42	*	3	100	-0.07		-0.53	**	3	184	-0.09		-0.43	*	3	268	-0.09		-0.50	**	3	352	0.29		-0.46	**	3
17	0.27		-0.62	***	3	101	0.06		-0.47	**	3	185	-0.02		-0.56	***	3	269	-0.02		-0.50	**	3	353	0.15		-0.51	**	3
18	-0.29		-0.46	**	3	102	0.25		-0.47	**	3	186	0.09		-0.57	***	3	270	0.15		-0.45	*	3	354	-0.03		-0.40	*	3
19	0.20		-0.51	**	3	103	0.04		-0.49	**	3	187	0.11		-0.59	***	3	271	0.22		-0.60	***	3	355	-0.16		-0.41	*	3
20	-0.04		-0.68	***	3	104	-0.06		-0.57	***	3	188	-0.12		-0.59	***	3	272	0.01		-0.59	***	3	356	0.24		-0.46	**	3
21	-0.08		-0.69	***	3	105	-0.06		-0.63	***	3	189	0.02		-0.55	**	3	273	-0.05		-0.46	**	3	357	0.21		-0.51	**	3
22	-0.27		-0.48	**	3	106	0.04		-0.64	***	3	190	0.10		-0.49	**	3	274	0.03		-0.49	**	3	358	-0.05		-0.51	**	3
23	0.31	.	-0.59	***	3	107	-0.14		-0.67	***	3	191	0.01		-0.47	**	3	275	0.09		-0.52	**	3	359	-0.32	.	-0.52	**	3
24	-0.30	.	-0.60	***	3	108	0.00		-0.62	***	3	192	0.15		-0.44	**	3	276	-0.04		-0.51	**	3	360	-0.15		-0.38	*	3
25	-0.14		-0.50	**	3	109	0.10		-0.62	***	3	193	0.09		-0.42	*	3	277	0.19		-0.46	**	3	361	-0.01		-0.40	*	3
26	-0.19		-0.50	**	3	110	0.04		-0.49	**	3	194	0.03		-0.36	*	3	278	0.07		-0.58	***	3	362	-0.17		-0.39	*	3
27	-0.09		-0.57	***	3	111	0.06		-0.47	**	3	195	0.11		-0.40	*	3	279	-0.12		-0.55	***	3	363	0.10		-0.44	**	3
28	-0.04		-0.52	**	3	112	0.08		-0.51	**	3	196	0.22		-0.35	*	3	280	-0.07		-0.47	**	3	364	0.08		-0.43	*	3
29	-0.06		-0.64	***	3	113	0.07		-0.44	**	3	197	0.09		-0.34		5	281	0.06		-0.25		5	365	-0.16		-0.42	*	3
30	-0.10		-0.65	***	3	114	-0.48	**	-0.33	.	4	198	0.09		-0.44	**	3	282	-0.02		-0.41	*	3	366	-0.16		-0.45	**	3
31	-0.15		-0.54	**	3	115	0.11		-0.51	**	3	199	0.15		-0.50	**	3	283	0.04		-0.47	**	3	367	-0.04		-0.44	*	3
32	-0.07		-0.52	**	3	116	0.41	*	-0.57	***	2	200	0.35	.	-0.60	***	3	284	0.27		-0.49	**	3	368	0.16		-0.49	**	3
33	-0.38	*	-0.56	***	1	117	0.19		-0.49	**	3	201	0.48	**	-0.46	**	2	285	0.09		-0.48	**	3	369	0.29		-0.51	**	3
34	0.05		-0.59	***	3	118	0.17		-0.51	**	3	202	0.25		-0.38	*	3	286	-0.15		-0.57	***	3	370	0.40	*	-0.40	*	2
35	0.02		-0.57	***	3	119	0.21		-0.61	***	3	203	0.18		-0.37	*	3	287	-0.13		-0.57	***	3	371	0.22		-0.44	*	3
36	-0.24		-0.41	*	3	120	0.29		-0.66	***	3	204	-0.17		-0.39	*	3	288	0.06		-0.65	***	3	372	0.36	*	-0.41	*	2
37	-0.30		-0.55	**	3	121	0.02		-0.64	***	3	205	-0.02		-0.50	**	3	289	0.06		-0.65	***	3	373	0.21		-0.48	**	3
38	0.08		-0.60	***	3	122	0.13		-0.65	***	3	206	0.20		-0.53	**	3	290	0.11		-0.58	***	3	374	0.15		-0.47	**	3
39	-0.30	.	-0.61	***	3	123	0.02		-0.57	***	3	207	0.23		-0.60	***	3	291	-0.19		-0.45	**	3	375	0.36	*	-0.41	*	2
40	-0.24		-0.54	**	3	124	0.20		-0.50	**	3	208	0.10		-0.58	***	3	292	-0.07		-0.45	**	3	376	0.07		-0.62	***	3
41	0.21		-0.60	***	3	125	0.26		-0.47	**	3	209	-0.13		-0.52	**	3	293	-0.21		-0.44	**	3	377	-0.13		-0.63	***	3
42	0.34	.	-0.52	**	3	126	0.31	.	-0.56	***	3	210	-0.22		-0.50	**	3	294	0.04		-0.45	*	3	378	-0.28		-0.60	***	3
43	-0.12		-0.61	***	3	127	0.20		-0.74	***	3	211	-0.06		-0.47	**	3	295	0.13		-0.48	**	3	379	-0.18		-0.54	**	3
44	-0.13		-0.56	***	3	128	-0.03		-0.68	***	3	212	0.05		-0.56	***	3	296	0.18		-0.42	*	3	380	-0.17		-0.49	**	3
45	0.27		-0.56	***	3	129	-0.06		-0.66	***	3	213	-0.08		-0.61	***	3	297	0.15		-0.38	*	3	381	0.11		-0.45	**	3
46	-0.19		-0.54	**	3	130	-0.09		-0.65	***	3	214	0.13		-0.62	***	3	298	0.16		-0.36	*	3	382	0.11		-0.34	.	5
47	0.20		-0.46	**	3	131	-0.07		-0.66	***	3	215	0.25		-0.66	***	3	299	0.19		-0.35	*	3	383	-0.01		-0.40	*	3
48	0.08		-0.38	*	3	132	-0.14		-0.55	***	3	216	-0.18		-0.58	***	3	300	0.07		-0.53	**	3	384	-0.05		-0.46	**	3
49	-0.07		0.04		5	133	0.00		-0.52	**	3	217	-0.21		-0.57	***	3	301	0.16		-0.50	**	3	385	0.23		-0.33	.	5
50	-0.12		-0.24		5	134	-0.22		-0.51	**	3	218	-0.19		-0.50	**	3	302	0.49	**	-0.64	***	2	386	0.19		-0.40	*	3
51	-0.13		-0.46	**	3	135	-0.30	.	-0.53	**	3	219	-0.32	.	-0.56	***	3	303	0.11		-0.61	***	3	387	0.07		-0.50	**	3
52	-0.21		-0.53	**	3	136	-0.02		-0.55	***	3	220	-0.21		-0.46	**	3	304	-0.15		-0.43	*	3	388	0.11		-0.56	***	3
53	0.05		-0.51	**	3	137	0.08		-0.41	*	3	221	-0.08		-0.44	**	3	305	-0.04		-0.43	*	3	389	-0.09		-0.59	***	3
54	-0.32	.	-0.55	**	3	138	-0.26		-0.47	**	3	222	-0.14		-0.37	*	3	306	-0.04		-0.42	*	3	390	0.13		-0.54	**	3
55	-0.27		-0.52	**	3	139	0.26		-0.50	**	3	223	-0.14		-0.32	.	5	307	-0.17		-0.46	**	3	391	0.29		-0.59	***	3
56	0.08		-0.51	**	3	140	0.13		-0.52	**	3	224	-0.09		-0.38	*	3	308	-0.05		-0.50	**	3	392	0.16		-0.48	**	3
57	0.36	*	-0.49	**	2	141	0.16		-0.47	**	3	225	-0.16		-0.39	*	3	309	-0.01		-0.52	**	3	393	0.14		-0.51	**	3
58	-0.15		-0.55	***	3	142	0.29		-0.51	**	3	226	-0.03		-0.44	*	3	310	-0.10		-0.47	**	3	394	-0.17		-0.64	***	3
59	-0.06		-0.53	**	3	143	0.14		-0.48	**	3	227	0.06		-0.45	**	3	311	-0.29		-0.52	**	3	395	0.07		-0.61	***	3
60	0.15		-0.52	**	3	144	0.22		-0.65	***	3	228	-0.04		-0.26		5	312	-0.21		-0.54	**	3	396	0.13		-0.62	***	3
61	-0.35	*	-0.49	**	1	145	-0.22		-0.61	***	3	229	0.15		-0.34	.	5	313	0.21		-0.69	***	3	397	-0.14		-0.57	***	3
62	0.30		-0.37	*	3	146	-0.07		-0.64	***	3	230	-0.02		-0.41	*	3	314	0.00		-0.66	***	3	398	-0.03		-0.46	**	3
63	0.37	*	-0.38	*	2	147	-0.18		-0.47	**	3	231	-0.06		-0.45	**	3	315	-0.02		-0.64	***	3	399	-0.13		-0.40	*	3
64	0.12		-0.34	.	5	148	0.26		-0.61	***	3	232	-0.31	.	-0.51	**	3	316	-0.21		-0.51	**	3	400	0.04		-0.55	**	3
65	0.31	.	-0.64	***	3	149	0.20		-0.51	**	3	233	-0.08		-0.59	***	3	317	-0.37	*	-0.55	***	1	401	0.10		-0.52	**	3
66	0.28		-0.55	***	3	150	0.26		-0.38	*	3	234	-0.04		-0.59	***	3	318	0.01		-0.47	**	3	402	0.09		-0.62	***	3
67	0.00		-0.49	**	3	151	0.28		-0.36	.	5	235	-0.05		-0.64	***	3	319	-0.13		-0.50	**	3	403	-0.02		-0.59	***	3
68	-0.09		-0.51	**	3	152	-0.09		-0.31	.	5	236	0.12		-0.67	***	3	320	0.15		-0.29	.	5	404	0.04		-0.59	***	3
69	0.24		-0.54	***	3	153	-0.11		-0.39	*	3	237	-0.09		-0.57	***	3	321	0.02		-0.28		5	405	0.19		-0.57	***	3
70	0.10		-0.56	***	3	154	0.16		-0.57	***	3	238	-0.17		-0.62	***	3	322	0.08		-0.37	*	3	406	0.19		-0.57	***	3
71	0.05		-0.58	***	3	155	-0.09		-0.54	**	3	239	-0.03		-0.48	**	3	323	0.01		-0.26		5	407	-0.18		-0.40	*	3
72	0.01		-0.53	**	3	156	0.05		-0.57	***	3	240	-0.03		-0.61	***	3	324	0.09		-0.30		5	408	-0.16		-0.53	**	3
73	-0.03		-0.42	*	3	157	0.23		-0.49	**	3	241	0.12		-0.59	***	3	325	0.27		-0.35	*	3	409	0.02		-0.54	**	3
74	0.06		-0.61	***	3	158	0.28		-0.50	**	3	242	0.15		-0.64	***	3	326	0.34	*	-0.45	**	2	410	0.16		-0.55	***	3
75	-0.11		-0.57	***	3	159	0.21		-0.57	***	3	243	0.03		-0.56	***	3	327	0.43	*	-0.51	**	2	411	0.02		-0.55	**	3
76	0.17		-0.56	***	3	160	0.11		-0.57	***	3	244	0.17		-0.54	**	3	328	0.07		-0.47	**	3	412	0.20		-0.64	***	3
77	-0.10		-0.53	**	3	161	0.12		-0.47	**	3	245	0.04		-0.54	***	3	329	0.17		-0.59	***	3	413	0.05		-0.61	***	3
78	0.01		-0.57	***	3	162	0.21		-0.50	**	3	246	-0.25		-0.54	***	3	330	-0.20		-0.45	*	3	414	0.02		-0.62	***	3
79	0.15		-0.41	*	3	163	0.10		-0.47	**	3	247	-0.26		-0.53	**	3	331	-0.08		-0.49	**	3	415	-0.04		-0.56	***	3
80	0.38	*	-0.43	*	2	164	-0.01		-0.42	*	3	248	0.21		-0.39	*	3	332	-0.06		-0.52	**	3	416	0.22		-0.58	***	3
81	0.09		-0.36	*	3	165	0.11		-0.42	*	3	249	-0.04		-0.41	*	3	333	-0.10		-0.53	**	3	417	0.24		-0.61	***	3
82	0.20		-0.36	*	3	166	0.30		-0.40	*	3	250	-0.03		-0.43	*	3	334	-0.21		-0.48	**	3	418	-0.18		-0.56	***	3
83	-0.01		-0.60	***	3	167	0.28		-0.49	**	3	251	0.05		-0.41	*	3	335	-0.17		-0.56	***	3	419	-0.04		-0.45	**	3
84	-0.15		-0.73	***	3	168	0.12		-0.44	**	3	252	-0.21		-0.45	**	3	336	0.26		-0.60	***	3	420	-0.15		-0.63	***	3

Table VIII. Partial correlation coefficients of Total NO₂ and Total O₃ on Erythemal daily doses high values for July; asterisks mark statistically significant correlations.

Pixel	Total NO₂ $r_{partial}$	α	Total O₃ $r_{partial}$	α	Class
1	-0.07		-0.35	*	3
2	0.07		-0.52	**	3
3	0.21		-0.48	**	3
4	-0.08		-0.46	**	3
5	-0.01		-0.48	**	3
6	0.21		-0.05		5
7	0.38	*	-0.08		4
8	0.10		-0.07		5
9	-0.24		-0.18		5
10	0.20		-0.07		5
11	0.00		-0.11		5
12	-0.02		-0.15		5
13	0.09		-0.45	**	3
14	-0.34	*	-0.51	**	1
15	-0.29		-0.20		5
16	-0.09		-0.14		5
17	0.07		-0.16		5
18	-0.12		-0.30	.	5
19	0.14		-0.46	**	3
20	-0.19		-0.47	**	3
21	-0.21		-0.39	*	3
22	0.32	.	-0.38	*	3
23	0.03		-0.32		5
24	0.04		-0.29	.	5
25	0.19		-0.39	*	3
26	0.05		-0.55	**	3
27	0.13		-0.46	**	3
28	0.21		-0.43	*	3
29	0.03		-0.42	*	3
30	0.02		-0.39	*	3
31	0.32	.	-0.35	*	3
32	-0.01		-0.30	.	5
33	0.01		-0.31	.	5
34	0.21		-0.33	.	5
35	0.06		-0.33	.	5
36	-0.08		-0.56	***	3
37	0.03		-0.47	**	3
38	0.08		-0.50	**	3
39	-0.16		-0.45	**	3
40	-0.22		-0.46	**	3
41	0.04		-0.35	*	3
42	0.09		-0.38	*	3
43	-0.04		-0.27		5
44	-0.15		-0.33	.	5
45	0.17		-0.27		5
46	-0.06		-0.35	*	3
47	-0.22		-0.34	*	3
48	0.08		-0.35	*	3
49	-0.05		-0.50	**	3
50	-0.15		-0.52	**	3
51	-0.04		-0.53	**	3
52	0.07		-0.46	**	3
53	0.17		-0.46	**	3
54	-0.30	.	-0.42	*	3
55	-0.15		-0.55	***	3
56	0.12		-0.50	**	3
57	0.02		-0.46	**	3
58	0.02		-0.35	*	3
59	0.13		-0.26		5
60	0.12		-0.28	.	5
61	-0.15		-0.37	*	3
62	-0.06		-0.38	*	3
63	0.10		-0.28		5
64	0.03		-0.35	*	3
65	0.29	.	-0.44	**	3
66	-0.11		-0.46	**	3
67	-0.03		-0.49	**	3
68	0.12		-0.53	**	3
69	0.16		-0.51	**	3
70	0.15		-0.47	**	3
71	-0.12		-0.44	**	3
72	-0.08		-0.45	**	3
73	0.06		-0.52	**	3
74	-0.02		-0.45	**	3
75	-0.04		-0.42	*	3
76	0.03		-0.39	*	3
77	-0.03		-0.35	*	3
78	-0.11		-0.27		5
79	-0.02		-0.16		5
80	0.00		-0.17		5
81	-0.03		-0.28		5
82	0.15		-0.39	*	3
83	-0.11		-0.48	**	3
84	0.05		-0.44	**	3
85	0.00		-0.41	*	3
86	-0.07		-0.42	*	3
87	-0.09		-0.49	**	3
88	0.14		-0.51	**	3
89	-0.05		-0.56	***	3
90	-0.02		-0.46	**	3
91	-0.02		-0.50	**	3
92	0.05		-0.48	**	3
93	-0.01		-0.51	**	3
94	0.00		-0.55	***	3
95	-0.13		-0.48	**	3
96	-0.10		-0.41	*	3
97	0.09		-0.34	*	3
98	0.07		-0.28		5
99	-0.19		-0.31	.	5
100	-0.10		-0.24		5
101	0.06		-0.23		5
102	0.15		-0.30	.	5
103	0.13		-0.34	*	3
104	-0.14		-0.48	**	3
105	0.00		-0.42	*	3
106	-0.16		-0.45	**	3
107	-0.23		-0.48	**	3
108	-0.02		-0.42	*	3
109	0.09		-0.51	**	3
110	0.05		-0.52	**	3
111	0.03		-0.55	***	3
112	0.04		-0.41	*	3
113	-0.15		-0.51	**	3
114	-0.04		-0.52	**	3
115	-0.06		-0.42	*	3
116	0.05		-0.44	*	3
117	0.19		-0.49	**	3
118	0.15		-0.42	*	3
119	-0.01		-0.48	**	3
120	0.11		-0.50	**	3
121	0.23		-0.34	.	3
122	0.19		-0.28		5
123	0.03		-0.36	*	3
124	-0.01		-0.32	.	5
125	0.06		-0.24		5
126	0.00		-0.35	*	3
127	-0.14		-0.45	**	3
128	-0.16		-0.35	.	5
129	0.04		-0.40	*	3
130	-0.04		-0.44	**	3
131	0.08		-0.43	*	3
132	-0.10		-0.45	**	3
133	-0.08		-0.52	**	3
134	0.03		-0.52	**	3
135	-0.16		-0.52	**	3
136	-0.01		-0.43	*	3
137	-0.34	*	-0.47	**	1
138	0.02		-0.47	**	3
139	0.17		-0.41	*	3
140	0.25		-0.42	*	3
141	-0.07		-0.49	**	3
142	-0.05		-0.43	**	3
143	-0.14		-0.54	***	3
144	0.19		-0.46	**	3
145	-0.15		-0.52	**	3
146	0.11		-0.43	*	3
147	0.07		-0.36	*	3
148	-0.22		-0.52	**	3
149	-0.12		-0.45	**	3
150	0.01		-0.44	**	3
151	0.24		-0.43	*	3
152	-0.21		-0.37	*	3
153	-0.17		-0.36	*	3
154	-0.36	*	-0.48	**	1
155	-0.09		-0.49	**	3
156	0.08		-0.47	**	3
157	0.44	**	-0.42	*	2
158	0.23		-0.39	*	3
159	-0.11		-0.44	**	3
160	-0.14		-0.42	*	3
161	-0.35	.	-0.42	*	3
162	-0.13		-0.34	.	5
163	0.10		-0.36	*	3
164	0.09		-0.37	*	3
165	0.21		-0.39	*	3
166	-0.04		-0.43	*	3
167	0.11		-0.45	**	3
168	0.19		-0.48	**	3
169	0.18		-0.50	**	3
170	-0.25		-0.48	**	3
171	0.00		-0.47	**	3
172	0.11		-0.44	*	3
173	0.08		-0.47	**	3
174	-0.01		-0.48	**	3
175	0.03		-0.39	*	3
176	0.13		-0.35	*	3
177	-0.08		-0.41	*	3
178	-0.24		-0.37	*	3
179	-0.01		-0.36	*	3
180	-0.23		-0.38	*	3
181	-0.22		-0.48	**	3
182	-0.31	.	-0.50	**	3
183	0.06		-0.46	**	3
184	0.07		-0.51	**	3
185	0.13		-0.48	**	3
186	0.03		-0.50	**	3
187	-0.18		-0.56	***	3
188	-0.03		-0.43	*	3
189	-0.21		-0.39	*	3
190	-0.19		-0.40	*	3
191	-0.05		-0.41	*	3
192	-0.03		-0.38	*	3
193	0.05		-0.38	*	3
194	0.27		-0.41	*	3
195	0.30	.	-0.56	***	3
196	0.22		-0.50	**	3
197	0.17		-0.47	**	3
198	0.02		-0.44	**	3
199	0.11		-0.38	*	3
200	0.32		-0.42	*	3
201	-0.01		-0.41	*	3
202	0.13		-0.41	*	3
203	0.06		-0.38	*	3
204	-0.06		-0.39	*	3
205	0.01		-0.41	*	3
206	-0.07		-0.45	**	3
207	0.00		-0.44	*	3
208	-0.05		-0.45	**	3
209	-0.04		-0.44	**	3
210	0.08		-0.46	**	3
211	0.23		-0.44	**	3
212	0.22		-0.50	**	3
213	0.08		-0.51	**	3
214	0.07		-0.52	**	3
215	-0.17		-0.54	***	3
216	0.05		-0.48	**	3
217	-0.07		-0.36	*	3
218	0.15		-0.41	*	3
219	-0.02		-0.39	*	3
220	0.08		-0.36	*	3
221	-0.05		-0.42	*	3
222	0.30		-0.42	*	3
223	0.28	.	-0.53	**	3
224	0.17		-0.50	**	3
225	0.16		-0.48	**	3
226	0.10		-0.43	*	3
227	0.28		-0.39	*	3
228	0.32	.	-0.35	*	3
229	0.16		-0.40	*	3
230	0.08		-0.38	*	3
231	0.03		-0.39	*	3
232	-0.02		-0.38	*	3
233	-0.27		-0.42	*	3
234	-0.03		-0.45	**	3
235	0.02		-0.37	*	3
236	-0.19		-0.37	*	3
237	0.16		-0.50	**	3
238	-0.12		-0.53	**	3
239	-0.08		-0.54	***	3
240	-0.03		-0.47	**	3
241	-0.05		-0.50	**	3
242	-0.03		-0.42	*	3
243	-0.25		-0.45	**	3
244	-0.11		-0.41	*	3
245	0.21		-0.41	*	3
246	0.04		-0.37	*	3
247	-0.02		-0.39	*	3
248	0.01		-0.43	**	3
249	0.03		-0.45	**	3
250	0.14		-0.59	***	3
251	0.03		-0.46	**	3
252	0.12		-0.47	**	3
253	0.32	.	-0.44	**	3
254	0.42	*	-0.37	*	2
255	0.29		-0.38	*	3
256	0.28		-0.38	*	3
257	0.10		-0.37	*	3
258	-0.02		-0.36	*	3
259	0.05		-0.38	*	3
260	0.12		-0.33	.	5
261	-0.02		-0.38	*	3
262	0.05		-0.36	*	3
263	0.05		-0.44	**	3
264	-0.01		-0.40	*	3
265	-0.17		-0.56	***	3
266	0.23		-0.45	**	3
267	0.05		-0.46	**	3
268	0.06		-0.47	**	3
269	-0.06		-0.45	**	3
270	-0.15		-0.48	**	3
271	-0.07		-0.46	**	3
272	0.17		-0.52	**	3
273	0.06		-0.52	**	3
274	0.05		-0.45	**	3
275	-0.17		-0.54	***	3
276	0.13		-0.52	**	3
277	0.11		-0.51	**	3
278	0.00		-0.60	***	3
279	0.20		-0.57	***	3
280	0.35	*	-0.55	***	2
281	0.25		-0.52	**	3
282	0.15		-0.40	*	3
283	0.07		-0.44	**	3
284	0.03		-0.45	**	3
285	0.21		-0.32	.	5
286	0.21		-0.29	.	5
287	0.31		-0.36	*	3
288	0.08		-0.36	*	3
289	0.01		-0.38	*	3
290	0.24		-0.35	*	3
291	0.28		-0.42	*	3
292	0.07		-0.46	**	3
293	0.09		-0.47	**	3
294	0.01		-0.53	**	3
295	-0.23		-0.54	**	3
296	-0.36	*	-0.60	***	1
297	-0.17		-0.59	***	3
298	-0.03		-0.53	**	3
299	0.11		-0.52	**	3
300	0.18		-0.65	***	3
301	0.08		-0.59	***	3
302	0.08		-0.63	***	3
303	0.03		-0.62	***	3
304	0.01		-0.58	***	3
305	0.10		-0.53	**	3
306	-0.02		-0.53	**	3
307	0.24		-0.43	**	3
308	-0.16		-0.54	***	3
309	-0.06		-0.59	***	3
310	0.21		-0.47	**	3
311	0.03		-0.48	**	3
312	0.26		-0.34	.	5
313	0.00		-0.34	*	3
314	0.22		-0.39	*	3
315	0.00		-0.33	.	5
316	0.01		-0.44	**	3
317	0.36	*	-0.45	**	2
318	0.12		-0.48	**	3
319	-0.07		-0.47	**	3
320	-0.32	.	-0.57	***	3
321	-0.05		-0.55	***	3
322	0.03		-0.53	**	3
323	0.30		-0.53	**	3
324	0.18		-0.59	***	3
325	0.14		-0.60	***	3
326	0.17		-0.63	***	3
327	0.08		-0.65	***	3
328	-0.08		-0.53	***	3
329	-0.14		-0.52	**	3
330	-0.09		-0.52	**	3
331	-0.11		-0.57	***	3
332	-0.40	*	-0.63	***	1
333	-0.13		-0.56	***	3
334	0.03		-0.54	***	3
335	-0.34	.	-0.61	***	3
336	0.16		-0.37	*	3
337	-0.02		-0.24		5
338	0.50	**	-0.23		4
339	0.20		-0.25		5
340	0.02		-0.21		5
341	0.16		-0.44	**	3
342	0.21		-0.40	*	3
343	0.04		-0.41	*	3
344	0.03		-0.54	***	3
345	0.03		-0.53	***	3
346	0.11		-0.54	***	3
347	0.25		-0.51	**	3
348	0.48	**	-0.53	**	2
349	0.12		-0.51	**	3
350	0.02		-0.55	***	3
351	0.27		-0.59	***	3
352	0.01		-0.54	***	3
353	-0.09		-0.49	**	3
354	0.09		-0.47	**	3
355	-0.09		-0.58	***	3
356	-0.29	.	-0.57	***	3
357	-0.27		-0.57	***	3
358	-0.10		-0.48	**	3
359	-0.02		-0.45	**	3
360	0.01		-0.34	.	5
361	0.04		-0.35	*	3
362	-0.26		-0.52	**	3
363	-0.08		-0.56	***	3
364	0.15		-0.56	***	3
365	0.25		-0.58	***	3
366	0.18		-0.48	**	3
367	0.26		-0.52	**	3
368	0.30		-0.53	**	3
369	-0.07		-0.54	***	3
370	0.12		-0.59	***	3
371	-0.17		-0.57	***	3
372	0.04		-0.53	**	3
373	0.24		-0.51	**	3
374	0.09		-0.54	***	3
375	0.02		-0.55	***	3
376	-0.20		-0.57	***	3
377	-0.18		-0.52	**	3
378	-0.18		-0.49	**	3
379	0.10		-0.30	.	5
380	0.05		-0.35	*	3
381	-0.16		-0.59	***	3
382	-0.04		-0.53	**	3
383	0.36	*	-0.45	**	2
384	0.13		-0.50	**	3
385	0.07		-0.54	**	3
386	0.40	*	-0.52	**	2
387	0.20		-0.45	**	3
388	0.10		-0.51	**	3
389	-0.34	*	-0.57	***	1
390	0.01		-0.46	**	3
391	0.11		-0.49	**	3
392	0.19		-0.52	**	3
393	0.13		-0.55	***	3
394	-0.18		-0.57	***	3
395	-0.26		-0.53	**	3
396	-0.11		-0.45	**	3
397	-0.14		-0.35	.	5
398	0.27		-0.49	**	3
399	0.14		-0.39	*	3
400	0.05		-0.35	.	5
401	0.10		-0.41	*	3
402	0.45	**	-0.29	.	4
403	0.31	.	-0.27		5
404	-0.08		-0.44	**	3
405	0.08		-0.41	*	3
406	0.03		-0.40	*	3
407	-0.21		-0.46	**	3
408	0.06		-0.50	**	3
409	-0.05		-0.47	**	3
410	-0.13		-0.45	**	3
411	0.00		-0.48	**	3
412	-0.04		-0.47	**	3
413	0.30		-0.42	.	5
414	0.32		-0.39	*	3
415	0.35	*	-0.32	.	4
416	0.11		-0.36	*	3
417	0.11		-0.38	*	3
418	0.14		-0.47	**	3
419	-0.13		-0.50	**	3
420	0.37	*	-0.38	*	2

Table IX. Partial correlation coefficients of Total NO₂ and Total O₃ on Erythemal daily doses high values for August; asterisks mark statistically significant correlations.

Pixel	$r_{partial}$ (NO₂)	α	$r_{partial}$ (O₃)	α	Class	Pixel	$r_{partial}$ (NO₂)	α	$r_{partial}$ (O₃)	α	Class	Pixel	$r_{partial}$ (NO₂)	α	$r_{partial}$ (O₃)	α	Class	Pixel	$r_{partial}$ (NO₂)	α	$r_{partial}$ (O₃)	α	Class	Pixel	$r_{partial}$ (NO₂)	α	$r_{partial}$ (O₃)	α	Class
1	-0.02		-0.41	*	3	85	-0.06		-0.46	**	3	169	-0.15		-0.41	*	3	253	-0.26		-0.49	**	3	337	-0.18		-0.49	**	3
2	-0.10		-0.44	**	3	86	0.04		-0.47	**	3	170	-0.06		-0.45	**	3	254	-0.03		-0.49	**	3	338	0.16		-0.49	**	3
3	0.02		-0.42	*	3	87	0.12		-0.45	**	3	171	-0.03		-0.42	*	3	255	0.25		-0.53	**	3	339	-0.02		-0.47	**	3
4	-0.12		-0.48	**	3	88	0.12		-0.39	*	3	172	0.09		-0.50	**	3	256	0.14		-0.49	**	3	340	-0.14		-0.51	**	3
5	0.11		-0.40	*	3	89	-0.01		-0.33	.	5	173	-0.01		-0.55	***	3	257	0.06		-0.48	**	3	341	0.13		-0.45	**	3
6	-0.03		-0.46	**	3	90	-0.28	.	-0.36	*	3	174	0.06		-0.56	***	3	258	0.03		-0.54	***	3	342	0.22		-0.46	**	3
7	-0.09		-0.41	*	3	91	-0.14		-0.22		5	175	0.15		-0.50	**	3	259	0.11		-0.52	**	3	343	0.18		-0.47	**	3
8	-0.19		-0.39	*	3	92	-0.15		-0.29	.	5	176	-0.05		-0.53	**	3	260	0.16		-0.49	**	3	344	0.28		-0.50	**	3
9	0.13		-0.43	*	3	93	-0.22		-0.24		5	177	0.24		-0.49	**	3	261	0.08		-0.51	**	3	345	0.09		-0.48	**	3
10	-0.07		-0.39	*	3	94	-0.13		-0.27		5	178	-0.24		-0.52	**	3	262	-0.05		-0.60	***	3	346	0.11		-0.37	*	3
11	-0.09		-0.42	*	3	95	0.08		-0.39	*	3	179	-0.08		-0.49	**	3	263	-0.04		-0.60	***	3	347	0.07		-0.36	*	3
12	0.11		-0.38	*	3	96	-0.13		-0.46	**	3	180	0.06		-0.40	*	3	264	-0.12		-0.61	***	3	348	-0.11		-0.44	**	3
13	-0.17		-0.48	**	3	97	0.02		-0.48	**	3	181	-0.24		-0.40	*	3	265	-0.10		-0.47	**	3	349	-0.40	*	-0.38	*	1
14	-0.20		-0.45	**	3	98	0.05		-0.40	*	3	182	-0.15		-0.42	*	3	266	-0.11		-0.46	**	3	350	0.35	*	-0.49	**	2
15	0.02		-0.35	*	3	99	-0.06		-0.59	***	3	183	-0.07		-0.37	*	3	267	0.03		-0.44	**	3	351	-0.23		-0.48	**	3
16	0.20		-0.39	*	3	100	-0.10		-0.54	***	3	184	0.12		-0.45	**	3	268	-0.02		-0.40	*	3	352	-0.13		-0.50	**	3
17	0.12		-0.36	*	3	101	0.08		-0.55	***	3	185	0.28	.	-0.48	**	3	269	-0.10		-0.45	**	3	353	-0.16		-0.42	*	3
18	0.10		-0.30	.	5	102	-0.22		-0.49	**	3	186	-0.02		-0.48	**	3	270	0.04		-0.54	**	3	354	-0.25		-0.40	*	3
19	-0.25		-0.54	***	3	103	-0.30	.	-0.47	**	3	187	0.13		-0.44	**	3	271	-0.09		-0.41	*	3	355	-0.24		-0.33	.	5
20	-0.03		-0.44	**	3	104	-0.08		-0.55	***	3	188	0.18		-0.45	**	3	272	-0.30		-0.47	**	3	356	-0.40	*	-0.36	*	1
21	-0.02		-0.43	*	3	105	0.18		-0.52	**	3	189	0.25		-0.46	**	3	273	0.01		-0.36	*	3	357	-0.25		-0.42	*	3
22	0.19		-0.48	**	3	106	0.11		-0.54	***	3	190	-0.01		-0.45	**	3	274	0.07		-0.38	*	3	358	-0.33	.	-0.44	**	3
23	0.34	.	-0.28		5	107	0.07		-0.45	**	3	191	0.02		-0.37	*	3	275	0.25		-0.37	*	3	359	-0.08		-0.40	*	3
24	-0.26		-0.31	.	5	108	0.02		-0.51	**	3	192	-0.34	*	-0.40	*	1	276	0.29	.	-0.38	*	3	360	-0.16		-0.46	**	3
25	0.05		-0.34	*	3	109	-0.03		-0.44	**	3	193	-0.36	*	-0.36	*	1	277	0.23		-0.36	*	3	361	-0.05		-0.45	**	3
26	-0.30	.	-0.54	**	3	110	-0.12		-0.37	*	3	194	0.02		-0.40	*	3	278	0.38	*	-0.38	*	2	362	0.38	*	-0.53	**	2
27	0.10		-0.47	**	3	111	0.05		-0.42	*	3	195	-0.11		-0.44	**	3	279	0.15		-0.48	**	3	363	0.16		-0.45	**	3
28	-0.08		-0.50	**	3	112	0.24		-0.33	.	5	196	0.19		-0.45	**	3	280	-0.09		-0.51	**	3	364	-0.12		-0.45	**	3
29	0.00		-0.46	**	3	113	-0.20		-0.39	*	3	197	0.08		-0.47	**	3	281	-0.01		-0.55	***	3	365	0.30		-0.37	*	3
30	-0.28		-0.46	**	3	114	-0.17		-0.29	.	5	198	0.23		-0.39	*	3	282	-0.15		-0.47	**	3	366	0.17		-0.43	**	3
31	0.11		-0.38	*	3	115	-0.25		-0.29		5	199	0.25		-0.49	**	3	283	-0.24		-0.48	**	3	367	-0.11		-0.39	*	3
32	0.12		-0.38	*	3	116	-0.13		-0.37	*	3	200	0.12		-0.52	**	3	284	-0.01		-0.52	**	3	368	-0.18		-0.47	**	3
33	-0.17		-0.40	*	3	117	-0.13		-0.35	*	3	201	0.04		-0.56	***	3	285	-0.01		-0.55	***	3	369	0.32	.	-0.49	**	3
34	-0.01		-0.37	*	3	118	0.22		-0.40	*	3	202	-0.01		-0.52	**	3	286	-0.22		-0.56	***	3	370	-0.16		-0.42	*	3
35	0.29	.	-0.56	***	3	119	-0.01		-0.44	**	3	203	0.03		-0.53	**	3	287	-0.28		-0.57	***	3	371	0.00		-0.50	**	3
36	0.12		-0.49	**	3	120	-0.05		-0.41	*	3	204	-0.13		-0.53	**	3	288	0.01		-0.52	**	3	372	-0.23		-0.47	**	3
37	-0.09		-0.58	***	3	121	-0.05		-0.45	**	3	205	-0.26		-0.47	**	3	289	-0.03		-0.57	***	3	373	0.13		-0.40	*	3
38	-0.28		-0.50	**	3	122	-0.18		-0.58	***	3	206	0.03		-0.50	**	3	290	-0.21		-0.56	***	3	374	-0.11		-0.37	*	3
39	0.28		-0.48	**	3	123	-0.24		-0.47	**	3	207	-0.10		-0.52	**	3	291	0.41	*	-0.47	**	2	375	-0.24		-0.33	.	5
40	0.23		-0.47	**	3	124	0.12		-0.52	**	3	208	0.16		-0.59	***	3	292	0.12		-0.43	**	3	376	-0.25		-0.37	*	3
41	0.24		-0.55	***	3	125	-0.14		-0.51	**	3	209	-0.17		-0.44	**	3	293	-0.06		-0.42	*	3	377	-0.29	.	-0.46	**	3
42	0.24		-0.50	**	3	126	-0.30	.	-0.60	***	3	210	-0.21		-0.46	**	3	294	0.01		-0.45	*	3	378	0.16		-0.33	.	5
43	0.21		-0.43	*	3	127	-0.05		-0.43	*	3	211	0.09		-0.37	*	3	295	0.22		-0.54	**	3	379	-0.06		-0.46	**	3
44	-0.05		-0.41	*	3	128	-0.11		-0.43	*	3	212	0.40	*	-0.57	***	2	296	-0.19		-0.39	*	3	380	-0.16		-0.41	*	3
45	0.25		-0.47	**	3	129	-0.20		-0.39	*	3	213	0.22		-0.48	**	3	297	-0.22		-0.51	**	3	381	-0.06		-0.43	*	3
46	0.03		-0.39	*	3	130	-0.08		-0.40	*	3	214	0.14		-0.53	**	3	298	0.03		-0.40	*	3	382	-0.08		-0.32	.	5
47	0.13		-0.21		5	131	-0.12		-0.50	**	3	215	0.01		-0.55	***	3	299	0.06		-0.41	*	3	383	0.18		-0.38	*	3
48	-0.02		-0.33	.	5	132	-0.04		-0.44	**	3	216	-0.09		-0.50	**	3	300	0.06		-0.36	*	3	384	0.27		-0.34	*	3
49	-0.07		-0.50	**	3	133	-0.19		-0.27		5	217	0.21		-0.58	***	3	301	0.23		-0.44	**	3	385	0.00		-0.48	**	3
50	0.07		-0.44	*	3	134	0.00		-0.37	*	3	218	-0.11		-0.46	**	3	302	0.10		-0.46	**	3	386	0.03		-0.53	**	3
51	0.20		-0.54	**	3	135	-0.01		-0.37	*	3	219	-0.04		-0.36	*	3	303	0.05		-0.54	***	3	387	0.18		-0.51	**	3
52	0.01		-0.36	*	3	136	0.24		-0.37	*	3	220	-0.10		-0.35	*	3	304	-0.04		-0.52	**	3	388	0.04		-0.46	**	3
53	-0.03		-0.45	**	3	137	-0.02		-0.40	*	3	221	0.23		-0.40	*	3	305	-0.04		-0.53	**	3	389	0.10		-0.48	**	3
54	0.31	.	-0.53	**	3	138	-0.21		-0.33	.	5	222	-0.05		-0.42	*	3	306	-0.06		-0.50	**	3	390	0.08		-0.50	**	3
55	0.18		-0.50	**	3	139	-0.17		-0.33	.	5	223	-0.06		-0.52	**	3	307	-0.32	.	-0.39	*	3	391	0.21		-0.47	**	3
56	0.28		-0.58	***	3	140	-0.09		-0.38	*	3	224	0.06		-0.52	**	3	308	0.00		-0.50	**	3	392	-0.02		-0.37	*	3
57	0.30	.	-0.52	**	3	141	-0.15		-0.37	*	3	225	-0.08		-0.45	**	3	309	0.13		-0.44	**	3	393	0.17		-0.39	*	3
58	0.27		-0.47	**	3	142	-0.15		-0.42	*	3	226	-0.01		-0.45	**	3	310	-0.16		-0.47	**	3	394	-0.15		-0.41	*	3
59	-0.02		-0.13		5	143	-0.10		-0.43	**	3	227	0.21		-0.45	**	3	311	-0.01		-0.48	**	3	395	-0.11		-0.41	*	3
60	0.26		-0.22		5	144	-0.01		-0.48	**	3	228	0.25		-0.51	**	3	312	0.06		-0.50	**	3	396	-0.04		-0.31	.	5
61	0.11		-0.36	*	3	145	-0.19		-0.52	**	3	229	0.42	*	-0.54	***	2	313	-0.12		-0.54	***	3	397	-0.14		-0.46	**	3
62	0.02		-0.39	*	3	146	0.10		-0.60	***	3	230	0.09		-0.49	**	3	314	0.11		-0.59	***	3	398	0.23		-0.41	*	3
63	-0.13		-0.51	**	3	147	0.01		-0.53	***	3	231	-0.16		-0.55	***	3	315	0.01		-0.54	***	3	399	0.41	*	-0.46	**	2
64	0.05		-0.51	**	3	148	0.07		-0.56	***	3	232	-0.17		-0.56	***	3	316	0.31	.	-0.37	*	3	400	0.07		-0.54	**	3
65	-0.10		-0.55	***	3	149	-0.10		-0.48	**	3	233	0.18		-0.52	**	3	317	-0.04		-0.41	*	3	401	0.06		-0.54	**	3
66	-0.06		-0.49	**	3	150	-0.04		-0.51	**	3	234	0.23		-0.53	**	3	318	0.16		-0.47	**	3	402	-0.07		-0.47	**	3
67	0.14		-0.50	**	3	151	0.30	.	-0.58	***	3	235	0.00		-0.55	***	3	319	0.18		-0.49	**	3	403	0.06		-0.52	**	3
68	0.18		-0.46	**	3	152	0.17		-0.45	**	3	236	0.14		-0.60	***	3	320	0.02		-0.41	*	3	404	-0.05		-0.46	**	3
69	0.13		-0.29	.	5	153	0.00		-0.46	**	3	237	-0.18		-0.38	*	3	321	0.02		-0.39	*	3	405	0.13		-0.54	**	3
70	-0.05		-0.32	.	5	154	-0.17		-0.43	*	3	238	-0.12		-0.46	**	3	322	0.15		-0.45	**	3	406	0.28		-0.50	**	3
71	-0.02		-0.36	*	3	155	-0.35	*	-0.41	*	1	239	-0.03		-0.43	*	3	323	0.00		-0.38	*	3	407	0.52	**	-0.53	**	2
72	-0.11		-0.41	*	3	156	-0.26		-0.43	**	3	240	0.28	.	-0.40	*	3	324	-0.21		-0.48	**	3	408	0.18		-0.43	*	3
73	-0.26		-0.31	.	5	157	0.09		-0.42	*	3	241	0.07		-0.37	*	3	325	0.49	**	-0.54	***	2	409	-0.01		-0.46	**	3
74	-0.26		-0.29	.	5	158	0.11		-0.42	*	3	242	0.01		-0.42	*	3	326	0.05		-0.50	**	3	410	-0.11		-0.45	**	3
75	0.18		-0.28	.	5	159	-0.07		-0.38	*	3	243	0.08		-0.50	**	3	327	0.27		-0.53	**	3	411	0.00		-0.40	*	3
76	-0.12		-0.29	.	5	160	-0.18		-0.42	*	3	244	0.18		-0.46	**	3	328	-0.07		-0.46	**	3	412	0.19		-0.46	**	3
77	0.24		-0.34	*	3	161	0.17		-0.40	*	3	245	-0.19		-0.50	**	3	329	-0.34	.	-0.50	**	3	413	0.18		-0.46	**	3
78	0.19		-0.45	**	3	162	-0.04		-0.47	**	3	246	0.12		-0.34	*	3	330	-0.19		-0.49	**	3	414	-0.01		-0.42	*	3
79	0.03		-0.53	**	3	163	-0.15		-0.42	*	3	247	-0.03		-0.37	*	3	331	-0.28		-0.48	**	3	415	0.13		-0.44	**	3
80	0.09		-0.55	***	3	164	-0.16		-0.38	*	3	248	0.48	**	-0.33	*	2	332	-0.13		-0.43	**	3	416	0.36	*	-0.53	**	2
81	0.05		-0.57	***	3	165	-0.44	**	-0.43	**	1	249	0.28		-0.44	*	3	333	-0.23		-0.46	**	3	417	0.31	.	-0.47	**	3
82	-0.06		-0.60	***	3	166	0.24		-0.39	*	3	250	0.24		-0.41	*	3	334	-0.12		-0.40	*	3	418	0.23		-0.41	*	3
83	0.18		-0.54	**	3	167	-0.06		-0.43	*	3	251	-0.05		-0.46	**	3	335	0.16		-0.35	*	3	419	0.14		-0.37	*	3
84	0.09		-0.49	**	3	168	-0.02		-0.36	*	3	252	-0.10		-0.46	**	3	336	0.13		-0.41	*	3	420	-0.18		-0.43	*	3

Table X. Partial correlation coefficients of Total NO₂ and Total O₃ on Erythemal daily doses high values for September; asterisks mark statistically significant correlations.

Pixel	$r_{partial}$ (NO₂)	α	$r_{partial}$ (O₃)	α	Class	Pixel	$r_{partial}$ (NO₂)	α	$r_{partial}$ (O₃)	α	Class	Pixel	$r_{partial}$ (NO₂)	α	$r_{partial}$ (O₃)	α	Class	Pixel	$r_{partial}$ (NO₂)	α	$r_{partial}$ (O₃)	α	Class	Pixel	$r_{partial}$ (NO₂)	α	$r_{partial}$ (O₃)	α	Class
1	0.16		-0.33	.	5	85	-0.26		-0.48	**	3	169	0.06		-0.24		5	253	-0.05		-0.39	*	3	337	0.05		-0.36	*	3
2	0.35	*	-0.31	.	4	86	-0.22		-0.53	**	3	170	0.15		-0.33	.	5	254	0.06		-0.42	*	3	338	-0.01		-0.35	*	3
3	0.08		-0.30	.	5	87	0.10		-0.40	*	3	171	0.15		-0.33	.	5	255	-0.15		-0.37	*	3	339	-0.02		-0.39	*	3
4	0.02		-0.37	*	3	88	0.00		-0.38	*	3	172	0.05		-0.47	**	3	256	0.05		-0.36	*	3	340	0.03		-0.39	*	3
5	0.03		-0.32	.	5	89	0.30	.	-0.43	*	3	173	-0.09		-0.49	**	3	257	0.07		-0.51	**	3	341	0.28		-0.60	***	3
6	0.17		-0.27		5	90	0.10		-0.38	*	3	174	-0.17		-0.44	*	3	258	-0.03		-0.47	**	3	342	0.23		-0.56	***	3
7	-0.23		-0.30	.	5	91	0.24		-0.39	*	3	175	-0.06		-0.39	*	3	259	-0.20		-0.54	**	3	343	0.07		-0.65	***	3
8	-0.01		-0.18		5	92	0.17		-0.26		5	176	0.07		-0.34	.	5	260	-0.02		-0.51	**	3	344	-0.03		-0.67	***	3
9	0.06		-0.22		5	93	0.29		-0.26		5	177	-0.21		-0.36	*	3	261	-0.13		-0.44	*	3	345	0.13		-0.65	***	3
10	-0.02		-0.28		5	94	0.06		-0.14		5	178	-0.48	**	-0.53	**	1	262	-0.14		-0.52	**	3	346	0.13		-0.61	***	3
11	0.14		-0.21		5	95	-0.07		-0.19		5	179	-0.19		-0.46	**	3	263	-0.14		-0.59	***	3	347	-0.21		-0.67	***	3
12	0.21		-0.06		5	96	0.03		-0.17		5	180	-0.08		-0.50	**	3	264	0.00		-0.51	**	3	348	-0.03		-0.69	***	3
13	0.14		-0.37	*	3	97	0.29		-0.13		5	181	0.10		-0.55	***	3	265	0.24		-0.51	**	3	349	-0.05		-0.63	***	3
14	0.11		-0.40	*	3	98	0.47	**	-0.39	*	2	182	0.21		-0.60	***	3	266	0.10		-0.56	***	3	350	0.05		-0.72	***	3
15	0.11		-0.30	.	5	99	0.09		-0.34	.	5	183	0.30		-0.62	***	3	267	0.23		-0.55	***	3	351	0.21		-0.62	***	3
16	-0.06		-0.35	.	5	100	0.19		-0.38	*	3	184	0.05		-0.51	**	3	268	0.26		-0.56	***	3	352	0.16		-0.55	***	3
17	-0.12		-0.32	.	5	101	0.20		-0.40	*	3	185	0.17		-0.56	***	3	269	0.26		-0.63	***	3	353	0.21		-0.69	***	3
18	-0.07		-0.21		5	102	0.10		-0.14		5	186	0.16		-0.54	**	3	270	0.20		-0.60	***	3	354	-0.01		-0.63	***	3
19	-0.03		-0.45	**	3	103	0.18		-0.25		5	187	-0.18		-0.53	**	3	271	0.08		-0.62	***	3	355	-0.25		-0.67	***	3
20	-0.12		-0.53	**	3	104	-0.05		-0.62	***	3	188	-0.02		-0.54	**	3	272	0.17		-0.63	***	3	356	-0.24		-0.53	**	3
21	0.11		-0.32	.	5	105	0.11		-0.56	***	3	189	0.33	.	-0.49	**	3	273	0.08		-0.60	***	3	357	0.00		-0.39	*	3
22	-0.21		-0.41	*	3	106	0.14		-0.51	**	3	190	0.41	*	-0.50	**	2	274	0.06		-0.58	***	3	358	0.01		-0.31	.	5
23	-0.15		-0.30	.	5	107	0.20		-0.49	**	3	191	0.34		-0.57	***	3	275	-0.01		-0.55	***	3	359	0.03		-0.48	**	3
24	-0.05		-0.22		5	108	-0.30	.	-0.49	**	3	192	0.11		-0.53	**	3	276	-0.20		-0.56	***	3	360	0.10		-0.38	*	3
25	-0.11		-0.30	.	5	109	-0.10		-0.51	**	3	193	0.14		-0.51	**	3	277	-0.13		-0.51	**	3	361	0.37	*	-0.33	.	4
26	0.07		-0.40	*	3	110	0.28		-0.47	**	3	194	-0.24		-0.50	**	3	278	-0.08		-0.49	**	3	362	-0.05		-0.58	***	3
27	0.07		-0.50	**	3	111	0.05		-0.47	**	3	195	-0.15		-0.40	*	3	279	0.15		-0.47	**	3	363	-0.06		-0.66	***	3
28	-0.02		-0.43	*	3	112	0.10		-0.40	*	3	196	0.05		-0.38	*	3	280	0.20		-0.46	**	3	364	0.10		-0.51	**	3
29	-0.02		-0.47	**	3	113	-0.15		-0.30	.	5	197	0.05		-0.33	.	5	281	-0.09		-0.52	**	3	365	-0.23		-0.52	**	3
30	0.10		-0.32	.	5	114	0.07		-0.13		5	198	0.09		-0.32	.	5	282	-0.08		-0.38	*	3	366	-0.20		-0.64	***	3
31	-0.06		-0.38	*	3	115	0.12		-0.08		5	199	0.12		-0.35	*	3	283	-0.15		-0.36	*	3	367	0.01		-0.59	***	3
32	-0.10		-0.30	.	5	116	0.13		-0.11		5	200	0.01		-0.45	**	3	284	-0.24		-0.45	**	3	368	0.25		-0.62	***	3
33	-0.01		-0.23		5	117	0.13		-0.11		5	201	-0.04		-0.34	.	5	285	0.14		-0.35	.	5	369	-0.15		-0.62	***	3
34	-0.18		-0.28		5	118	0.01		-0.06		5	202	-0.13		-0.39	*	3	286	0.04		-0.35	*	3	370	-0.15		-0.56	***	3
35	0.04		-0.30	.	5	119	-0.02		-0.16		5	203	-0.16		-0.49	**	3	287	0.00		-0.48	**	3	371	0.09		-0.47	**	3
36	0.26		-0.51	**	3	120	0.17		-0.24		5	204	0.04		-0.50	**	3	288	-0.26		-0.47	**	3	372	0.08		-0.54	**	3
37	0.29		-0.43	*	3	121	0.13		-0.21		5	205	-0.16		-0.43	*	3	289	-0.17		-0.34	.	5	373	-0.21		-0.55	**	3
38	0.24		-0.43	*	3	122	0.10		-0.27		5	206	-0.11		-0.51	**	3	290	-0.10		-0.35	*	3	374	-0.33		-0.56	***	3
39	0.06		-0.38	*	3	123	0.07		-0.42	*	3	207	-0.02		-0.62	***	3	291	0.00		-0.55	***	3	375	-0.02		-0.53	**	3
40	-0.13		-0.38	*	3	124	0.08		-0.34	.	5	208	0.03		-0.62	***	3	292	-0.11		-0.59	***	3	376	0.27		-0.40	*	3
41	0.00		-0.34	.	5	125	-0.07		-0.26		5	209	0.02		-0.47	**	3	293	0.13		-0.63	***	3	377	0.16		-0.41	*	3
42	0.07		-0.16		5	126	0.09		-0.26		5	210	0.27		-0.54	**	3	294	0.12		-0.61	***	3	378	0.18		-0.45	**	3
43	0.00		-0.35	*	3	127	0.25		-0.65	***	3	211	0.26		-0.55	**	3	295	0.16		-0.63	***	3	379	0.15		-0.49	**	3
44	0.00		-0.31	.	5	128	0.04		-0.69	***	3	212	0.27		-0.56	***	3	296	0.20		-0.65	***	3	380	-0.07		-0.38	*	3
45	-0.08		-0.33	.	5	129	0.20		-0.62	***	3	213	0.32	.	-0.56	***	3	297	0.19		-0.64	***	3	381	-0.01		-0.60	***	3
46	0.08		-0.43	*	3	130	0.18		-0.47	**	3	214	0.32		-0.54	**	3	298	0.14		-0.59	***	3	382	-0.03		-0.52	**	3
47	0.05		-0.43	*	3	131	0.40	*	-0.56	***	2	215	0.16		-0.58	***	3	299	0.04		-0.55	***	3	383	-0.17		-0.63	***	3
48	0.31	.	-0.50	**	3	132	0.12		-0.50	**	3	216	0.13		-0.53	**	3	300	0.13		-0.52	**	3	384	-0.12		-0.61	***	3
49	0.15		-0.51	**	3	133	0.10		-0.53	**	3	217	0.23		-0.46	**	3	301	-0.10		-0.52	**	3	385	0.16		-0.54	**	3
50	-0.10		-0.53	**	3	134	0.23		-0.47	**	3	218	0.30	.	-0.57	***	3	302	0.03		-0.58	***	3	386	0.06		-0.52	**	3
51	-0.19		-0.48	**	3	135	0.42	*	-0.58	***	2	219	0.24		-0.57	***	3	303	0.06		-0.57	***	3	387	0.09		-0.60	***	3
52	0.27		-0.43	*	3	136	0.33	.	-0.53	**	3	220	0.23		-0.62	***	3	304	0.18		-0.59	***	3	388	0.01		-0.49	**	3
53	0.02		-0.36	*	3	137	0.16		-0.44	*	3	221	0.18		-0.63	***	3	305	0.06		-0.61	***	3	389	0.25		-0.45	**	3
54	-0.13		-0.40	*	3	138	0.14		-0.27		5	222	-0.31	.	-0.57	***	3	306	-0.32	.	-0.64	***	3	390	0.17		-0.50	**	3
55	-0.17		-0.33	.	5	139	0.09		-0.21		5	223	0.05		-0.50	**	3	307	-0.22		-0.44	**	3	391	-0.07		-0.62	***	3
56	0.15		-0.27		5	140	0.02		-0.10		5	224	0.06		-0.40	*	3	308	-0.15		-0.37	*	3	392	-0.27		-0.65	***	3
57	0.17		-0.14		5	141	-0.05		-0.08		5	225	-0.23		-0.31	.	5	309	-0.15		-0.40	*	3	393	-0.11		-0.57	***	3
58	0.23		-0.34	.	5	142	-0.07		-0.07		5	226	-0.01		-0.36	*	3	310	-0.02		-0.36	*	3	394	0.16		-0.46	**	3
59	0.17		-0.43	*	3	143	-0.08		-0.15		5	227	0.24		-0.34	.	5	311	-0.15		-0.33	.	5	395	0.16		-0.41	*	3
60	0.32	.	-0.46	**	3	144	0.07		-0.23		5	228	0.12		-0.32	.	5	312	-0.04		-0.37	*	3	396	0.23		-0.45	**	3
61	0.04		-0.41	*	3	145	0.06		-0.26		5	229	0.05		-0.38	*	3	313	0.12		-0.33	.	5	397	0.01		-0.51	**	3
62	0.05		-0.49	**	3	146	0.18		-0.35	.	5	230	-0.29		-0.39	*	3	314	-0.10		-0.33	.	5	398	-0.01		-0.57	***	3
63	-0.06		-0.45	*	3	147	0.04		-0.34	*	3	231	-0.05		-0.50	**	3	315	-0.11		-0.38	*	3	399	0.02		-0.56	***	3
64	0.10		-0.29		5	148	0.12		-0.39	*	3	232	-0.11		-0.42	*	3	316	-0.10		-0.55	**	3	400	0.03		-0.43	*	3
65	0.08		-0.48	**	3	149	0.02		-0.36	*	3	233	0.14		-0.42	*	3	317	0.08		-0.60	***	3	401	0.03		-0.46	**	3
66	-0.05		-0.52	**	3	150	-0.13		-0.44	*	3	234	-0.03		-0.53	**	3	318	-0.16		-0.61	***	3	402	0.04		-0.63	***	3
67	0.03		-0.49	**	3	151	0.09		-0.48	**	3	235	-0.03		-0.54	**	3	319	0.12		-0.68	***	3	403	-0.01		-0.62	***	3
68	0.10		-0.46	*	3	152	-0.04		-0.55	**	3	236	-0.09		-0.56	***	3	320	0.14		-0.67	***	3	404	0.26		-0.47	**	3
69	0.21		-0.42	*	3	153	-0.06		-0.54	**	3	237	-0.09		-0.49	**	3	321	0.21		-0.64	***	3	405	0.09		-0.45	**	3
70	0.26		-0.44	*	3	154	0.22		-0.60	***	3	238	0.15		-0.50	**	3	322	0.08		-0.63	***	3	406	-0.13		-0.59	***	3
71	-0.11		-0.33	.	5	155	0.46	**	-0.69	***	2	239	0.10		-0.52	**	3	323	0.03		-0.62	***	3	407	0.27		-0.61	***	3
72	-0.29		-0.22		5	156	0.31	.	-0.62	***	3	240	0.19		-0.54	***	3	324	0.13		-0.67	***	3	408	0.27		-0.60	***	3
73	0.16		-0.15		5	157	0.05		-0.54	**	3	241	0.23		-0.53	**	3	325	0.12		-0.64	***	3	409	0.18		-0.59	***	3
74	0.04		-0.12		5	158	0.11		-0.55	***	3	242	0.11		-0.56	***	3	326	-0.06		-0.61	***	3	410	0.44	**	-0.45	**	2
75	0.10		-0.24		5	159	0.14		-0.53	**	3	243	0.03		-0.52	**	3	327	0.04		-0.60	***	3	411	-0.25		-0.55	**	3
76	0.20		-0.23		5	160	0.01		-0.54	**	3	244	-0.24		-0.58	***	3	328	0.12		-0.60	***	3	412	-0.34	.	-0.69	***	3
77	0.37	*	-0.27		5	161	0.26		-0.52	**	3	245	0.10		-0.60	***	3	329	-0.01		-0.63	***	3	413	-0.30	.	-0.70	***	3
78	0.37	*	-0.44	*	2	162	0.19		-0.54	**	3	246	-0.09		-0.61	***	3	330	-0.11		-0.62	***	3	414	-0.20		-0.65	***	3
79	0.11		-0.47	**	3	163	0.18		-0.52	**	3	247	-0.04		-0.59	***	3	331	-0.24		-0.54	**	3	415	-0.05		-0.63	***	3
80	0.18		-0.39	*	3	164	-0.07		-0.46	**	3	248	-0.05		-0.57	***	3	332	-0.14		-0.44	*	3	416	-0.18		-0.49	**	3
81	0.25		-0.28		5	165	0.12		-0.47	**	3	249	-0.16		-0.53	**	3	333	0.01		-0.37	*	3	417	-0.07		-0.51	**	3
82	0.16		-0.25		5	166	-0.16		-0.36	*	3	250	-0.17		-0.49	**	3	334	-0.07		-0.37	*	3	418	0.29	.	-0.54	**	3
83	0.01		-0.59	***	3	167	-0.10		-0.36	.	5	251	-0.26		-0.49	**	3	335	0.09		-0.48	**	3	419	0.33	.	-0.51	**	3
84	-0.01		-0.55	***	3	168	-0.01		-0.34	.	5	252	-0.30	.	-0.44	*	3	336	0.46	*	-0.06		4	420	-0.02		-0.68	***	3

Table XI. Partial correlation coefficients of Total NO$_2$ and Total O$_3$ on Erythemal daily doses high values for October; asterisks mark statistically significant correlations.

Pixel	Total NO$_2$ $r_{partial}$	α	Total O$_3$ $r_{partial}$	α	Class
1	-0.09		-0.43	**	3
2	-0.12		-0.28		5
3	-0.09		-0.43	**	3
4	0.12		-0.44	**	3
5	0.13		-0.47	**	3
6	0.12		-0.41	*	3
7	0.11		-0.48	**	3
8	0.15		-0.31	.	5
9	0.27		-0.45	**	3
10	0.03		-0.50	**	3
11	-0.02		-0.49	**	3
12	0.23		-0.41	*	3
13	-0.07		-0.43	**	3
14	-0.21		-0.40	*	3
15	0.11		-0.48	**	3
16	0.36	*	-0.45	**	2
17	0.24		-0.30	.	5
18	0.02		-0.40	*	3
19	0.04		-0.35	*	3
20	-0.04		-0.35	*	3
21	0.30	.	-0.40	*	3
22	0.23		-0.46	**	3
23	-0.08		-0.46	**	3
24	0.12		-0.42	*	3
25	0.02		-0.42	*	3
26	0.32		-0.48	**	3
27	0.07		-0.46	**	3
28	-0.07		-0.48	**	3
29	-0.04		-0.44	**	3
30	0.28		-0.47	**	3
31	0.25		-0.59	***	3
32	0.17		-0.56	***	3
33	0.15		-0.54	***	3
34	0.12		-0.57	***	3
35	-0.01		-0.52	**	3
36	0.17		-0.45	**	3
37	0.23		-0.47	**	3
38	0.02		-0.42	*	3
39	-0.17		-0.47	**	3
40	-0.03		-0.48	**	3
41	0.08		-0.53	**	3
42	0.30	.	-0.57	***	3
43	0.14		-0.58	***	3
44	0.08		-0.54	***	3
45	0.00		-0.52	**	3
46	-0.26		-0.48	**	3
47	0.08		-0.56	***	3
48	0.27		-0.59	***	3
49	-0.05		-0.49	**	3
50	-0.05		-0.47	**	3
51	0.24		-0.53	**	3
52	0.02		-0.48	**	3
53	-0.14		-0.43	*	3
54	-0.10		-0.39	*	3
55	0.05		-0.54	***	3
56	-0.04		-0.63	***	3
57	0.09		-0.65	***	3
58	0.18		-0.62	***	3
59	0.11		-0.61	***	3
60	0.06		-0.59	***	3
61	0.01		-0.51	**	3
62	0.04		-0.45	**	3
63	0.23		-0.52	**	3
64	0.26		-0.63	***	3
65	-0.12		-0.56	***	3
66	0.00		-0.54	***	3
67	0.03		-0.49	**	3
68	0.17		-0.52	**	3
69	0.15		-0.49	**	3
70	0.09		-0.56	***	3
71	0.05		-0.57	***	3
72	0.14		-0.65	***	3
73	-0.05		-0.65	***	3
74	0.11		-0.64	***	3
75	0.29	.	-0.64	***	3
76	0.26		-0.62	***	3
77	0.28		-0.56	***	3
78	0.37	*	-0.61	***	2
79	0.34	.	-0.66	***	3
80	0.21		-0.61	***	3
81	0.11		-0.53	**	3
82	0.22		-0.48	**	3
83	-0.24		-0.48	**	3
84	-0.21		-0.45	**	3

Pixel	Total NO$_2$ $r_{partial}$	α	Total O$_3$ $r_{partial}$	α	Class
85	-0.06		-0.53	**	3
86	0.24		-0.61	***	3
87	0.21		-0.55	***	3
88	0.25		-0.51	**	3
89	0.05		-0.54	***	3
90	-0.20		-0.66	***	3
91	-0.06		-0.61	***	3
92	0.19		-0.67	***	3
93	-0.13		-0.62	***	3
94	0.24		-0.67	***	3
95	0.11		-0.65	***	3
96	0.09		-0.53	**	3
97	0.37	*	-0.60	***	2
98	0.18		-0.59	***	3
99	0.25		-0.67	***	3
100	0.13		-0.59	***	3
101	0.02		-0.56	***	3
102	0.02		-0.54	***	3
103	0.43	**	-0.58	***	2
104	-0.21		-0.52	**	3
105	-0.15		-0.57	***	3
106	0.00		-0.54	**	3
107	0.04		-0.50	**	3
108	-0.02		-0.43	*	3
109	0.01		-0.55	***	3
110	0.24		-0.58	***	3
111	0.26		-0.48	**	3
112	-0.11		-0.63	***	3
113	-0.12		-0.65	***	3
114	0.13		-0.65	***	3
115	0.40	*	-0.73	***	2
116	0.20		-0.68	***	3
117	0.20		-0.63	***	3
118	0.10		-0.56	***	3
119	-0.02		-0.56	***	3
120	0.12		-0.64	***	3
121	0.07		-0.60	***	3
122	0.15		-0.64	***	3
123	0.08		-0.58	***	3
124	0.13		-0.60	***	3
125	-0.03		-0.58	***	3
126	0.39	*	-0.56	***	2
127	0.05		-0.67	***	3
128	0.05		-0.52	**	3
129	0.05		-0.63	***	3
130	0.34	*	-0.64	***	2
131	0.20		-0.59	***	3
132	0.02		-0.48	**	3
133	-0.03		-0.56	***	3
134	0.16		-0.48	**	3
135	-0.06		-0.50	**	3
136	-0.25		-0.52	**	3
137	0.03		-0.54	***	3
138	0.11		-0.57	***	3
139	0.37	*	-0.56	**	2
140	0.34	*	-0.52	**	2
141	0.19		-0.54	***	3
142	-0.02		-0.56	***	3
143	-0.12		-0.64	***	3
144	0.01		-0.67	***	3
145	0.11		-0.65	***	3
146	0.29		-0.63	***	3
147	0.38	*	-0.59	***	2
148	0.22		-0.59	***	3
149	0.15		-0.38	*	3
150	0.13		-0.44	**	3
151	0.20		-0.53	**	3
152	0.14		-0.46	**	3
153	0.07		-0.42	*	3
154	0.36	*	-0.45	**	3
155	0.14		-0.20		5
156	-0.16		-0.40	*	3
157	-0.09		-0.55	***	3
158	0.15		-0.50	**	3
159	0.12		-0.61	***	3
160	0.27		-0.62	***	3
161	0.12		-0.55	**	3
162	0.20		-0.58	***	3
163	0.07		-0.58	***	3
164	-0.12		-0.48	**	3
165	-0.27		-0.43	**	3
166	0.23		-0.51	**	3
167	0.07		-0.57	***	3
168	-0.03		-0.58	***	3

Pixel	Total NO$_2$ $r_{partial}$	α	Total O$_3$ $r_{partial}$	α	Class
169	-0.27		-0.58	***	3
170	-0.10		-0.59	***	3
171	0.01		-0.64	***	3
172	0.17		-0.69	***	3
173	0.30	.	-0.72	***	3
174	0.04		-0.43	*	3
175	0.09		-0.52	**	3
176	-0.01		-0.53	**	3
177	0.26		-0.57	***	3
178	0.14		-0.48	**	3
179	0.11		-0.62	***	3
180	0.04		-0.45	**	3
181	0.12		-0.45	**	3
182	-0.12		-0.46	**	3
183	0.13		-0.28		5
184	-0.28		-0.48	**	3
185	-0.17		-0.48	**	3
186	-0.18		-0.44	**	3
187	-0.07		-0.48	**	3
188	0.07		-0.62	***	3
189	-0.04		-0.57	***	3
190	0.14		-0.56	***	3
191	-0.06		-0.53	**	3
192	-0.22		-0.46	**	3
193	-0.08		-0.50	**	3
194	0.49	**	-0.63	***	2
195	0.40	*	-0.48	**	2
196	0.06		-0.52	**	3
197	-0.04		-0.67	***	3
198	-0.12		-0.67	***	3
199	0.06		-0.64	***	3
200	0.34	.	-0.53	**	3
201	0.20		-0.51	**	3
202	0.20		-0.53	**	3
203	0.04		-0.51	**	3
204	0.17		-0.50	**	3
205	0.16		-0.54	***	3
206	-0.02		-0.61	***	3
207	-0.15		-0.56	***	3
208	-0.19		-0.58	***	3
209	-0.23		-0.47	**	3
210	-0.07		-0.28		5
211	0.13		-0.33	.	5
212	0.06		-0.47	**	3
213	-0.12		-0.44	**	3
214	-0.17		-0.42	*	3
215	0.10		-0.42	*	3
216	0.12		-0.55	**	3
217	-0.02		-0.53	**	3
218	0.01		-0.56	***	3
219	-0.22		-0.58	***	3
220	-0.04		-0.55	***	3
221	0.00		-0.61	***	3
222	0.48	**	-0.55	**	2
223	0.08		-0.49	**	3
224	0.06		-0.51	**	3
225	0.11		-0.56	***	3
226	0.42	*	-0.66	***	2
227	-0.09		-0.50	**	3
228	0.24		-0.54	**	3
229	0.16		-0.56	***	3
230	0.11		-0.59	***	3
231	-0.01		-0.61	***	3
232	0.29	.	-0.52	**	3
233	0.22		-0.59	***	3
234	0.03		-0.58	***	3
235	-0.03		-0.58	***	3
236	-0.31	.	-0.58	***	3
237	0.19		-0.40	*	3
238	0.32	.	-0.52	**	3
239	0.19		-0.51	**	3
240	0.09		-0.45	**	3
241	-0.17		-0.42	*	3
242	-0.11		-0.43	**	3
243	0.01		-0.59	***	3
244	0.02		-0.57	***	3
245	0.01		-0.58	***	3
246	-0.14		-0.69	***	3
247	0.15		-0.62	***	3
248	0.00		-0.64	***	3
249	0.44	*	-0.54	**	2
250	0.25		-0.45	**	3
251	0.33	.	-0.45	**	3
252	0.42	*	-0.59	***	2

Pixel	Total NO$_2$ $r_{partial}$	α	Total O$_3$ $r_{partial}$	α	Class
253	0.32	.	-0.42	*	3
254	0.16		-0.54	**	3
255	0.16		-0.53	**	3
256	0.31	.	-0.58	***	3
257	0.03		-0.62	***	3
258	0.19		-0.68	***	3
259	-0.08		-0.67	***	3
260	0.10		-0.55	**	3
261	0.20		-0.57	***	3
262	0.03		-0.43	*	3
263	-0.06		-0.43	*	3
264	-0.01		-0.48	**	3
265	0.31	.	-0.50	**	3
266	0.21		-0.45	**	3
267	0.43	*	-0.51	**	2
268	0.09		-0.45	**	3
269	0.07		-0.43	*	3
270	0.14		-0.56	***	3
271	0.17		-0.56	***	3
272	0.13		-0.67	***	3
273	0.06		-0.68	***	3
274	0.18		-0.65	***	3
275	0.35	*	-0.67	***	2
276	0.00		-0.53	**	3
277	0.26		-0.55	***	3
278	0.41	*	-0.49	**	2
279	0.34	*	-0.46	**	2
280	0.23		-0.50	**	3
281	0.35	*	-0.59	***	2
282	0.25		-0.58	***	3
283	0.17		-0.56	***	3
284	0.26		-0.57	***	3
285	0.23		-0.51	**	3
286	0.18		-0.47	**	3
287	0.13		-0.56	***	3
288	-0.14		-0.47	**	3
289	-0.08		-0.34	*	3
290	-0.06		-0.35	*	3
291	0.09		-0.38	*	3
292	0.38	*	-0.40	*	2
293	0.06		-0.35	*	3
294	0.15		-0.58	***	3
295	0.03		-0.53	**	3
296	0.30	.	-0.68	***	3
297	0.20		-0.65	***	3
298	0.06		-0.47	**	3
299	0.16		-0.46	**	3
300	0.43	*	-0.54	**	2
301	0.41	*	-0.46	**	2
302	0.47	**	-0.50	**	2
303	0.11		-0.51	**	3
304	0.32	.	-0.64	***	3
305	0.29	.	-0.61	***	3
306	0.19		-0.59	***	3
307	0.08		-0.50	**	3
308	0.19		-0.51	**	3
309	0.34	.	-0.51	**	3
310	0.11		-0.43	*	3
311	0.21		-0.48	**	3
312	-0.18		-0.43	*	3
313	-0.32	.	-0.28		5
314	0.04		-0.17		5
315	-0.06		-0.24		5
316	0.14		-0.57	***	3
317	0.16		-0.54	***	3
318	0.02		-0.37	*	3
319	0.09		-0.61	***	3
320	0.09		-0.61	***	3
321	0.09		-0.66	***	3
322	-0.04		-0.65	***	3
323	0.17		-0.61	***	3
324	0.49	**	-0.72	***	2
325	0.29	.	-0.61	***	3
326	0.12		-0.62	***	3
327	-0.15		-0.66	***	3
328	0.28		-0.57	***	3
329	0.15		-0.53	**	3
330	0.13		-0.46	**	3
331	0.20		-0.43	**	3
332	0.00		-0.40	*	3
333	-0.05		-0.34	*	3
334	0.18		-0.38	*	3
335	-0.02		-0.37	*	3
336	-0.07		-0.26		5

Pixel	Total NO$_2$ $r_{partial}$	α	Total O$_3$ $r_{partial}$	α	Class
337	-0.13		-0.26		5
338	-0.07		-0.20		5
339	-0.06		-0.10		5
340	-0.07		-0.12		5
341	0.16		-0.32	.	5
342	0.25		-0.37	*	3
343	0.11		-0.56	***	3
344	-0.23		-0.59	***	3
345	-0.04		-0.64	***	3
346	-0.02		-0.69	***	3
347	-0.18		-0.69	***	3
348	0.03		-0.65	***	3
349	0.29		-0.64	***	3
350	0.15		-0.64	***	3
351	-0.18		-0.51	**	3
352	-0.10		-0.54	**	3
353	-0.21		-0.54	***	3
354	-0.04		-0.42	*	3
355	0.07		-0.32	.	5
356	0.05		-0.33	.	5
357	0.04		-0.31	.	5
358	0.27		-0.43	*	3
359	0.20		-0.35	*	3
360	0.28		-0.48	**	3
361	-0.04		-0.38	*	3
362	0.17		-0.55	**	3
363	-0.29	.	-0.64	***	3
364	0.00		-0.53	**	3
365	-0.09		-0.63	***	3
366	-0.34	.	-0.71	***	3
367	-0.14		-0.66	***	3
368	0.07		-0.62	***	3
369	-0.28		-0.59	***	3
370	0.05		-0.45	**	3
371	-0.01		-0.47	**	3
372	-0.19		-0.53	**	3
373	0.04		-0.39	*	3
374	0.23		-0.22		5
375	0.15		-0.16		5
376	-0.05		-0.31	.	5
377	-0.04		-0.25		5
378	0.00		-0.19		5
379	0.09		-0.31	.	5
380	-0.03		-0.27		5
381	-0.26		-0.60	***	3
382	-0.18		-0.59	***	3
383	-0.12		-0.63	***	3
384	-0.13		-0.62	***	3
385	0.14		-0.54	**	3
386	0.09		-0.59	***	3
387	-0.23		-0.58	***	3
388	-0.08		-0.48	**	3
389	-0.17		-0.47	**	3
390	-0.16		-0.42	*	3
391	-0.07		-0.24		5
392	-0.06		-0.11		5
393	0.22		-0.06		5
394	0.14		-0.35	*	3
395	-0.05		-0.48	**	3
396	0.06		-0.38	*	3
397	0.20		-0.43	*	3
398	-0.14		-0.53	**	3
399	-0.05		-0.57	***	3
400	0.04		-0.53	**	3
401	-0.01		-0.63	***	3
402	0.15		-0.48	**	3
403	0.06		-0.40	*	3
404	-0.10		-0.41	*	3
405	0.02		-0.22		5
406	-0.08		-0.12		5
407	-0.26		-0.43	*	3
408	0.09		-0.43	*	3
409	0.24		-0.58	***	3
410	0.15		-0.50	**	3
411	-0.02		-0.49	**	3
412	0.04		-0.55	**	3
413	0.07		-0.55	***	3
414	0.01		-0.40	*	3
415	0.04		-0.36	*	3
416	0.15		-0.17		5
417	0.02		-0.33	.	5
418	-0.17		-0.35	*	3
419	0.25		-0.57	***	3
420	0.05		-0.41	*	3

Table XII. Partial correlation coefficients of Total NO_2 and Total O_3 on Erythemal daily doses high values for November; asterisks mark statistically significant correlations.

Pixel	Total NO₂ $r_{partial}$	α	Total O₃ $r_{partial}$	α	Class
1	-0.06		-0.55	***	3
2	0.01		-0.49	**	3
3	0.03		-0.58	***	3
4	0.07		-0.55	***	3
5	0.17		-0.54	**	3
6	0.13		-0.71	***	3
7	0.01		-0.61	***	3
8	0.06		-0.58	***	3
9	0.26		-0.68	***	3
10	0.10		-0.68	***	3
11	0.20		-0.64	***	3
12	-0.16		-0.65	***	3
13	-0.01		-0.72	***	3
14	-0.03		-0.70	***	3
15	-0.01		-0.65	***	3
16	0.12		-0.56	***	3
17	-0.12		-0.54	**	3
18	0.21		-0.63	***	3
19	-0.10		-0.71	***	3
20	0.02		-0.64	***	3
21	-0.01		-0.55	**	3
22	-0.17		-0.57	***	3
23	0.03		-0.54	**	3
24	0.23		-0.58	***	3
25	0.16		-0.61	***	3
26	-0.14		-0.67	***	3
27	0.31	.	-0.64	***	3
28	-0.01		-0.61	***	3
29	0.16		-0.54	**	3
30	0.09		-0.54	**	3
31	0.03		-0.55	**	3
32	0.14		-0.56	***	3
33	0.20		-0.54	**	3
34	0.22		-0.59	***	3
35	0.02		-0.56	***	3
36	-0.10		-0.61	***	3
37	-0.03		-0.53	**	3
38	0.17		-0.52	**	3
39	0.14		-0.44	*	3
40	0.23		-0.39	*	3
41	0.07		-0.53	**	3
42	-0.08		-0.51	**	3
43	0.08		-0.47	**	3
44	0.14		-0.45	**	3
45	0.17		-0.40	*	3
46	-0.18		-0.69	***	3
47	-0.22		-0.68	***	3
48	-0.08		-0.62	***	3
49	-0.08		-0.69	***	3
50	0.15		-0.63	***	3
51	0.27		-0.51	**	3
52	0.10		-0.57	***	3
53	-0.07		-0.45	**	3
54	0.02		-0.42	*	3
55	0.13		-0.41	*	3
56	0.04		-0.45	*	3
57	0.14		-0.43	*	3
58	0.17		-0.14		5
59	0.17		-0.30	.	5
60	0.15		-0.40	*	3
61	0.05		-0.43	*	3
62	-0.29		-0.55	**	3
63	-0.29		-0.54	**	3
64	-0.14		-0.41	*	3
65	0.11		-0.70	***	3
66	-0.01		-0.67	***	3
67	-0.07		-0.61	***	3
68	-0.06		-0.50	**	3
69	0.17		-0.44	**	3
70	0.10		-0.35	*	3
71	0.17		-0.43	*	3
72	0.08		-0.49	**	3
73	-0.01		-0.52	**	3
74	-0.05		-0.50	**	3
75	-0.09		-0.34	.	5
76	0.03		-0.40	*	3
77	-0.12		-0.45	*	3
78	0.02		-0.41	*	3
79	-0.32	.	-0.58	***	3
80	-0.18		-0.49	**	3
81	-0.01		-0.40	*	3
82	0.11		-0.53	**	3
83	0.16		-0.54	**	3
84	-0.02		-0.59	***	3

Pixel	Total NO₂ $r_{partial}$	α	Total O₃ $r_{partial}$	α	Class
85	0.02		-0.59	***	3
86	0.05		-0.56	***	3
87	-0.12		-0.59	***	3
88	-0.02		-0.49	**	3
89	0.04		-0.52	**	3
90	0.12		-0.45	**	3
91	-0.24		-0.49	**	3
92	-0.02		-0.53	**	3
93	-0.01		-0.55	**	3
94	-0.03		-0.52	**	3
95	-0.07		-0.26		5
96	-0.17		-0.34		5
97	-0.26		-0.36	*	3
98	0.12		-0.28		5
99	0.09		-0.37	*	3
100	-0.15		-0.30	.	5
101	-0.05		-0.36	*	3
102	-0.02		-0.47	**	3
103	0.05		-0.48	**	3
104	-0.02		-0.51	**	3
105	0.14		-0.46	**	3
106	0.03		-0.52	**	3
107	-0.08		-0.62	***	3
108	-0.02		-0.67	***	3
109	-0.02		-0.50	**	3
110	-0.19		-0.58	***	3
111	-0.29		-0.61	***	3
112	-0.21		-0.55	***	3
113	-0.08		-0.54	**	3
114	-0.14		-0.44	*	3
115	-0.14		-0.32	.	5
116	-0.11		-0.27		5
117	-0.21		-0.49	**	3
118	0.00		-0.44	*	3
119	-0.13		-0.44	*	3
120	-0.03		-0.41	*	3
121	-0.04		-0.26		5
122	0.05		-0.30	.	5
123	-0.13		-0.23		5
124	-0.08		-0.35	*	3
125	-0.15		-0.43	*	3
126	-0.13		-0.54	**	3
127	0.10		-0.54	**	3
128	0.10		-0.50	**	3
129	-0.11		-0.50	**	3
130	0.08		-0.49	**	3
131	-0.08		-0.55	**	3
132	-0.06		-0.57	***	3
133	-0.12		-0.61	***	3
134	0.06		-0.59	***	3
135	-0.32	.	-0.62	***	3
136	-0.09		-0.57	***	3
137	-0.33	.	-0.38	*	3
138	-0.27		-0.39	*	3
139	-0.12		-0.30		5
140	-0.20		-0.34	.	5
141	-0.26		-0.46	**	3
142	-0.07		-0.40	*	3
143	-0.02		-0.49	**	3
144	-0.13		-0.49	**	3
145	-0.13		-0.34	.	5
146	-0.09		-0.43	*	3
147	0.01		-0.43	*	3
148	-0.02		-0.46	**	3
149	-0.05		-0.41	*	3
150	-0.13		-0.53	**	3
151	-0.13		-0.51	**	3
152	0.20		-0.38	*	3
153	0.10		-0.46	**	3
154	-0.05		-0.39	*	3
155	0.05		-0.38	*	3
156	0.13		-0.43	*	3
157	0.15		-0.46	**	3
158	0.17		-0.49	**	3
159	0.02		-0.39	*	3
160	-0.04		-0.45	*	3
161	-0.03		-0.50	**	3
162	-0.11		-0.55	***	3
163	-0.07		-0.62	***	3
164	-0.28		-0.58	***	3
165	-0.28		-0.66	***	3
166	-0.22		-0.64	***	3
167	-0.18		-0.62	***	3
168	-0.08		-0.55	***	3

Pixel	Total NO₂ $r_{partial}$	α	Total O₃ $r_{partial}$	α	Class
169	-0.05		-0.56	***	3
170	0.05		-0.51	**	3
171	-0.19		-0.47	**	3
172	-0.01		-0.49	**	3
173	-0.12		-0.45	**	3
174	-0.04		-0.39	*	3
175	-0.01		-0.43	*	3
176	0.06		-0.38	*	3
177	0.02		-0.25		5
178	-0.22		-0.49	**	3
179	-0.06		-0.57	**	3
180	0.16		-0.49	**	3
181	0.10		-0.43	*	3
182	0.03		-0.43	*	3
183	-0.16		-0.44	*	3
184	-0.02		-0.50	**	3
185	0.06		-0.53	**	3
186	0.13		-0.51	**	3
187	0.08		-0.50	**	3
188	0.11		-0.51	**	3
189	-0.01		-0.50	**	3
190	-0.05		-0.63	***	3
191	-0.13		-0.65	***	3
192	-0.16		-0.68	***	3
193	0.15		-0.57	***	3
194	-0.26		-0.67	***	3
195	0.00		-0.59	***	3
196	0.16		-0.63	***	3
197	0.09		-0.58	***	3
198	0.12		-0.54	**	3
199	-0.09		-0.49	**	3
200	0.04		-0.49	**	3
201	-0.02		-0.50	**	3
202	0.01		-0.51	**	3
203	-0.06		-0.38	*	3
204	-0.13		-0.37	*	3
205	-0.11		-0.37	*	3
206	-0.16		-0.33	.	5
207	-0.21		-0.39	*	3
208	-0.17		-0.47	**	3
209	0.26		-0.44	**	3
210	0.14		-0.48	**	3
211	0.03		-0.53	**	3
212	0.15		-0.50	**	3
213	0.18		-0.59	***	3
214	0.19		-0.54	**	3
215	0.02		-0.64	***	3
216	0.10		-0.55	**	3
217	-0.09		-0.54	**	3
218	-0.22		-0.61	***	3
219	-0.21		-0.64	***	3
220	-0.17		-0.61	***	3
221	0.29	.	-0.63	***	3
222	0.10		-0.52	**	3
223	0.23		-0.51	**	3
224	-0.02		-0.58	***	3
225	-0.08		-0.54	**	3
226	-0.05		-0.56	***	3
227	-0.11		-0.62	***	3
228	0.00		-0.63	***	3
229	-0.10		-0.60	***	3
230	-0.22		-0.57	***	3
231	-0.07		-0.46	**	3
232	-0.26		-0.50	**	3
233	-0.01		-0.25		5
234	-0.23		-0.24		5
235	-0.31	.	-0.45	**	3
236	-0.22		-0.47	**	3
237	0.03		-0.51	**	3
238	0.17		-0.43	*	3
239	0.08		-0.47	**	3
240	0.07		-0.58	***	3
241	0.12		-0.57	***	3
242	0.06		-0.62	***	3
243	-0.02		-0.57	***	3
244	-0.01		-0.61	***	3
245	-0.28		-0.67	***	3
246	-0.12		-0.67	***	3
247	-0.02		-0.65	***	3
248	0.20		-0.56	***	3
249	0.04		-0.49	**	3
250	0.06		-0.58	***	3
251	0.04		-0.53	**	3
252	-0.03		-0.46	**	3

Pixel	Total NO₂ $r_{partial}$	α	Total O₃ $r_{partial}$	α	Class
253	0.00		-0.50	**	3
254	-0.11		-0.54	**	3
255	-0.12		-0.54	**	3
256	-0.12		-0.59	***	3
257	-0.49	**	-0.66	***	1
258	-0.41	*	-0.56	***	1
259	-0.36	*	-0.46	**	1
260	0.10		-0.31	.	5
261	-0.34	.	-0.38	*	3
262	-0.17		-0.35	*	3
263	-0.14		-0.32	.	5
264	-0.13		-0.27		5
265	-0.07		-0.63	***	3
266	-0.17		-0.64	***	3
267	-0.11		-0.71	***	3
268	-0.07		-0.71	***	3
269	-0.26		-0.61	***	3
270	-0.04		-0.54	**	3
271	0.21		-0.64	***	3
272	0.02		-0.68	***	3
273	0.09		-0.70	***	3
274	0.23		-0.68	***	3
275	0.08		-0.62	***	3
276	-0.09		-0.60	***	3
277	-0.15		-0.52	**	3
278	0.19		-0.48	**	3
279	0.01		-0.60	***	3
280	0.10		-0.57	***	3
281	0.03		-0.57	***	3
282	0.19		-0.57	***	3
283	-0.05		-0.57	***	3
284	-0.29		-0.58	***	3
285	-0.50	**	-0.61	***	1
286	-0.31	.	-0.53	**	3
287	-0.06		-0.42	*	3
288	-0.02		-0.26		5
289	-0.23		-0.43	*	3
290	-0.06		-0.51	**	3
291	0.13		-0.67	***	3
292	0.14		-0.60	***	3
293	-0.09		-0.57	***	3
294	-0.14		-0.57	***	3
295	-0.09		-0.51	**	3
296	0.28		-0.48	**	3
297	-0.15		-0.65	***	3
298	-0.08		-0.66	***	3
299	0.33	.	-0.66	***	3
300	0.04		-0.72	***	3
301	-0.16		-0.65	***	3
302	-0.21		-0.58	***	3
303	-0.02		-0.54	**	3
304	0.07		-0.56	***	3
305	-0.13		-0.70	***	3
306	0.03		-0.63	***	3
307	-0.09		-0.57	***	3
308	-0.24		-0.58	***	3
309	-0.04		-0.58	***	3
310	-0.12		-0.51	**	3
311	-0.08		-0.51	**	3
312	-0.09		-0.43	*	3
313	0.07		-0.39	*	3
314	-0.12		-0.43	*	3
315	0.06		-0.51	**	3
316	0.16		-0.54	**	3
317	0.02		-0.57	***	3
318	-0.07		-0.64	***	3
319	0.08		-0.65	***	3
320	0.16		-0.63	***	3
321	-0.12		-0.63	***	3
322	-0.07		-0.62	***	3
323	0.26		-0.59	***	3
324	0.09		-0.69	***	3
325	-0.12		-0.66	***	3
326	-0.32	.	-0.63	***	3
327	-0.05		-0.69	***	3
328	0.05		-0.68	***	3
329	0.02		-0.61	***	3
330	0.06		-0.49	**	3
331	-0.22		-0.48	**	3
332	-0.14		-0.50	**	3
333	0.07		-0.44	*	3
334	-0.19		-0.54	**	3
335	0.02		-0.39	*	3
336	-0.07		-0.59	***	3

Pixel	Total NO₂ $r_{partial}$	α	Total O₃ $r_{partial}$	α	Class
337	-0.12		-0.45	**	3
338	-0.15		-0.47	**	3
339	-0.15		-0.46	**	3
340	-0.03		-0.44	*	3
341	0.29	.	-0.62	***	3
342	0.31	.	-0.67	***	3
343	0.01		-0.64	***	3
344	0.11		-0.72	***	3
345	0.16		-0.61	***	3
346	0.06		-0.65	***	3
347	0.03		-0.61	***	3
348	0.05		-0.65	***	3
349	-0.06		-0.71	***	3
350	0.16		-0.71	***	3
351	-0.34	.	-0.71	***	3
352	-0.13		-0.61	***	3
353	-0.08		-0.66	***	3
354	-0.10		-0.60	***	3
355	0.07		-0.56	***	3
356	0.06		-0.49	**	3
357	0.22		-0.41	*	3
358	0.16		-0.42	*	3
359	-0.05		-0.43	*	3
360	-0.01		-0.41	*	3
361	-0.07		-0.70	***	3
362	0.04		-0.58	***	3
363	-0.05		-0.59	***	3
364	0.24		-0.48	**	3
365	-0.01		-0.56	***	3
366	-0.06		-0.63	***	3
367	-0.17		-0.64	***	3
368	0.06		-0.72	***	3
369	0.16		-0.69	***	3
370	-0.20		-0.64	***	3
371	-0.29	.	-0.69	***	3
372	-0.29	.	-0.67	***	3
373	-0.16		-0.63	***	3
374	-0.24		-0.56	***	3
375	0.00		-0.49	**	3
376	0.15		-0.56	***	3
377	0.24		-0.46	**	3
378	-0.10		-0.44	*	3
379	-0.07		-0.45	*	3
380	-0.01		-0.54	**	3
381	-0.06		-0.52	**	3
382	0.22		-0.56	***	3
383	0.06		-0.46	**	3
384	0.12		-0.50	**	3
385	-0.12		-0.72	***	3
386	-0.02		-0.71	***	3
387	-0.16		-0.67	***	3
388	-0.15		-0.66	***	3
389	-0.19		-0.74	***	3
390	-0.03		-0.65	***	3
391	0.01		-0.57	***	3
392	-0.21		-0.54	**	3
393	-0.07		-0.64	***	3
394	0.13		-0.53	**	3
395	0.04		-0.49	**	3
396	-0.17		-0.53	**	3
397	-0.49	**	-0.58	***	1
398	-0.19		-0.59	***	3
399	0.08		-0.59	***	3
400	0.00		-0.66	***	3
401	-0.10		-0.63	***	3
402	-0.14		-0.67	***	3
403	-0.36	*	-0.67	***	1
404	-0.17		-0.72	***	3
405	-0.02		-0.58	***	3
406	-0.01		-0.55	***	3
407	-0.12		-0.61	***	3
408	-0.30	.	-0.61	***	3
409	0.11		-0.49	**	3
410	0.06		-0.43	*	3
411	-0.07		-0.58	***	3
412	0.01		-0.55	***	3
413	-0.15		-0.59	***	3
414	-0.25		-0.68	***	3
415	0.15		-0.56	***	3
416	-0.10		-0.53	**	3
417	-0.07		-0.63	***	3
418	0.13		-0.46	*	3
419	-0.02		-0.41	*	3
420	0.10		-0.46	**	3

Table XIII. Partial correlation coefficients of Total NO$_2$ and Total O$_3$ on Erythemal daily doses high values for December; asterisks mark statistically significant correlations.

Pixel	Total NO$_2$ $r_{partial}$	α	Total O$_3$ $r_{partial}$	α	Class
1	-0.04		-0.57	***	3
2	0.16		-0.65	***	3
3	-0.03		-0.69	***	3
4	-0.03		-0.61	***	3
5	0.06		-0.62	***	3
6	0.13		-0.62	***	3
7	-0.12		-0.61	***	3
8	0.35	*	-0.58	***	2
9	0.28		-0.55	**	3
10	-0.24		-0.74	***	3
11	0.04		-0.53	**	3
12	0.30		-0.49	**	3
13	-0.05		-0.75	***	3
14	0.07		-0.70	***	3
15	0.04		-0.62	***	3
16	0.08		-0.62	***	3
17	0.42	*	-0.51	**	2
18	0.04		-0.64	***	3
19	-0.07		-0.56	***	3
20	0.36	*	-0.59	***	2
21	0.21		-0.63	***	3
22	0.27		-0.55	***	3
23	0.33	.	-0.54	**	3
24	-0.01		-0.54	**	3
25	0.11		-0.52	**	3
26	-0.10		-0.57	***	3
27	-0.22		-0.47	**	3
28	-0.19		-0.49	**	3
29	0.16		-0.57	***	3
30	0.21		-0.54	**	3
31	0.01		-0.45	*	3
32	0.08		-0.53	**	3
33	-0.02		-0.55	**	3
34	-0.04		-0.59	***	3
35	0.14		-0.61	***	3
36	0.04		-0.69	***	3
37	-0.07		-0.47	**	3
38	-0.13		-0.54	***	3
39	-0.05		-0.56	***	3
40	0.21		-0.60	***	3
41	0.10		-0.48	**	3
42	-0.01		-0.52	**	3
43	-0.15		-0.61	***	3
44	0.13		-0.63	***	3
45	0.20		-0.47	**	3
46	0.14		-0.62	***	3
47	0.19		-0.60	***	3
48	0.17		-0.42	*	3
49	-0.22		-0.72	***	3
50	0.04		-0.66	***	3
51	0.15		-0.64	***	3
52	-0.03		-0.52	**	3
53	-0.02		-0.48	**	3
54	0.04		-0.57	***	3
55	-0.03		-0.64	***	3
56	-0.25		-0.76	***	3
57	-0.20		-0.75	***	3
58	-0.40	*	-0.79	***	1
59	0.04		-0.67	***	3
60	0.13		-0.58	***	3
61	-0.07		-0.56	***	3
62	0.06		-0.46	**	3
63	-0.03		-0.33	.	5
64	-0.01		-0.22		5
65	0.22		-0.68	***	3
66	-0.13		-0.73	***	3
67	0.00		-0.62	***	3
68	0.14		-0.59	***	3
69	0.27		-0.44	**	3
70	0.01		-0.62	***	3
71	-0.15		-0.62	***	3
72	-0.22		-0.73	***	3
73	-0.12		-0.71	***	3
74	-0.22		-0.78	***	3
75	-0.23		-0.72	***	3
76	-0.06		-0.55	***	3
77	0.03		-0.49	**	3
78	-0.01		-0.49	**	3
79	0.02		-0.39	*	3
80	-0.19		-0.32	.	5
81	0.13		-0.24		5
82	0.06		-0.24		5
83	-0.14		-0.72	***	3
84	0.30	.	-0.58	***	3
85	0.28		-0.70	***	3
86	0.01		-0.68	***	3
87	-0.06		-0.61	***	3
88	-0.06		-0.56	**	3
89	0.29	.	-0.41	*	3
90	0.16		-0.48	**	3
91	-0.32	.	-0.57	***	3
92	-0.07		-0.44	**	3
93	0.04		-0.49	**	3
94	-0.04		-0.56	***	3
95	0.12		-0.46	**	3
96	0.02		-0.43	*	3
97	0.07		-0.40	*	3
98	0.09		-0.45	**	3
99	0.28		-0.37	*	3
100	-0.06		-0.54	**	3
101	-0.06		-0.43	*	3
102	-0.13		-0.41	*	3
103	0.08		-0.38	*	3
104	0.07		-0.79	***	3
105	0.03		-0.62	***	3
106	0.05		-0.45	**	3
107	0.32		-0.50	**	3
108	0.33	.	-0.49	**	3
109	0.04		-0.61	***	3
110	-0.02		-0.58	***	3
111	0.27		-0.62	***	3
112	0.26		-0.54	***	3
113	0.26		-0.56	***	3
114	-0.03		-0.60	***	3
115	0.16		-0.52	**	3
116	0.05		-0.62	***	3
117	0.04		-0.58	***	3
118	0.11		-0.52	**	3
119	0.19		-0.49	**	3
120	0.18		-0.46	**	3
121	0.33	.	-0.48	**	3
122	0.10		-0.60	***	3
123	-0.15		-0.62	***	3
124	-0.22		-0.69	***	3
125	-0.37	*	-0.69	***	1
126	0.09		-0.47	**	3
127	0.22		-0.66	***	3
128	-0.09		-0.68	***	3
129	-0.19		-0.59	***	3
130	-0.24		-0.53	**	3
131	0.11		-0.45	**	3
132	0.06		-0.57	***	3
133	0.11		-0.57	***	3
134	0.15		-0.65	***	3
135	0.21		-0.61	***	3
136	0.14		-0.57	***	3
137	0.24		-0.58	***	3
138	0.15		-0.49	**	3
139	0.14		-0.46	**	3
140	-0.02		-0.53	**	3
141	-0.09		-0.61	***	3
142	0.01		-0.47	**	3
143	-0.09		-0.43	*	3
144	0.04		-0.47	**	3
145	-0.10		-0.66	***	3
146	-0.20		-0.69	***	3
147	-0.02		-0.68	***	3
148	-0.18		-0.61	***	3
149	0.00		-0.63	***	3
150	-0.15		-0.50	**	3
151	-0.30	.	-0.43	*	3
152	0.02		-0.45	**	3
153	-0.12		-0.63	***	3
154	-0.27		-0.61	***	3
155	0.14		-0.55	**	3
156	-0.14		-0.67	***	3
157	-0.05		-0.61	***	3
158	-0.05		-0.66	***	3
159	-0.11		-0.63	***	3
160	0.01		-0.56	***	3
161	0.15		-0.56	**	3
162	0.24		-0.43	*	3
163	0.00		-0.34	*	3
164	0.10		-0.52	**	3
165	-0.17		-0.44	**	3
166	-0.02		-0.46	**	3
167	0.09		-0.46	**	3
168	-0.11		-0.45	**	3
169	-0.06		-0.56	***	3
170	-0.09		-0.70	***	3
171	0.37	*	-0.79	***	2
172	0.02		-0.73	***	3
173	0.03		-0.70	***	3
174	0.29	.	-0.79	***	3
175	0.24		-0.76	***	3
176	0.14		-0.65	***	3
177	-0.12		-0.61	***	3
178	0.10		-0.61	***	3
179	-0.08		-0.71	***	3
180	0.06		-0.54	***	3
181	0.08		-0.55	***	3
182	-0.13		-0.54	**	3
183	-0.02		-0.51	**	3
184	0.08		-0.44	**	3
185	-0.12		-0.60	***	3
186	-0.11		-0.58	***	3
187	0.02		-0.58	***	3
188	0.01		-0.46	**	3
189	0.03		-0.47	**	3
190	0.02		-0.45	**	3
191	-0.01		-0.42	*	3
192	-0.06		-0.51	**	3
193	-0.06		-0.59	***	3
194	-0.06		-0.53	**	3
195	0.00		-0.55	***	3
196	-0.21		-0.59	***	3
197	0.11		-0.44	**	3
198	-0.04		-0.68	***	3
199	0.04		-0.68	***	3
200	-0.14		-0.77	***	3
201	-0.10		-0.77	***	3
202	0.20		-0.70	***	3
203	0.17		-0.74	***	3
204	0.48	**	-0.77	***	2
205	0.15		-0.62	***	3
206	0.33	.	-0.59	***	3
207	-0.08		-0.72	***	3
208	0.00		-0.72	***	3
209	0.03		-0.53	**	3
210	-0.40	*	-0.56	***	1
211	-0.32	.	-0.48	**	3
212	-0.08		-0.52	**	3
213	0.05		-0.46	**	3
214	0.03		-0.45	**	3
215	0.13		-0.39	*	3
216	-0.09		-0.54	**	3
217	0.04		-0.52	**	3
218	-0.07		-0.48	**	3
219	-0.15		-0.50	**	3
220	-0.13		-0.53	**	3
221	0.29		-0.37	*	3
222	-0.06		-0.56	***	3
223	0.04		-0.57	***	3
224	-0.03		-0.57	***	3
225	0.43	*	-0.53	**	2
226	0.17		-0.64	***	3
227	0.05		-0.69	***	3
228	-0.10		-0.76	***	3
229	-0.20		-0.77	***	3
230	-0.10		-0.69	***	3
231	0.22		-0.61	***	3
232	0.40	*	-0.65	***	2
233	0.25		-0.69	***	3
234	-0.02		-0.61	***	3
235	-0.14		-0.77	***	3
236	-0.09		-0.80	***	3
237	-0.31	.	-0.60	***	3
238	-0.26		-0.62	***	3
239	-0.21		-0.54	***	3
240	-0.08		-0.47	**	3
241	-0.01		-0.43	*	3
242	-0.05		-0.40	*	3
243	-0.45	*	-0.48	**	1
244	-0.21		-0.47	**	3
245	-0.24		-0.50	**	3
246	-0.27		-0.51	**	3
247	-0.07		-0.54	***	3
248	0.00		-0.57	***	3
249	-0.03		-0.61	***	3
250	-0.16		-0.66	***	3
251	-0.15		-0.70	***	3
252	0.40	*	-0.51	**	2
253	0.16		-0.57	***	3
254	-0.02		-0.66	***	3
255	-0.46	**	-0.73	***	1
256	-0.36	*	-0.75	***	1
257	-0.27		-0.71	***	3
258	0.06		-0.48	**	3
259	0.05		-0.51	**	3
260	-0.09		-0.67	***	3
261	-0.33	.	-0.73	***	3
262	-0.16		-0.59	***	3
263	-0.04		-0.51	**	3
264	0.05		-0.52	**	3
265	-0.34	*	-0.49	**	1
266	-0.08		-0.37	*	3
267	-0.01		-0.25		5
268	0.20		-0.20		5
269	-0.08		-0.45	**	3
270	-0.22		-0.50	**	3
271	-0.20		-0.54	***	3
272	-0.30	.	-0.56	***	3
273	-0.57	***	-0.65	***	1
274	-0.37	*	-0.59	***	1
275	-0.31	.	-0.54	***	3
276	-0.14		-0.59	***	3
277	-0.43	*	-0.69	***	1
278	-0.46	**	-0.67	***	1
279	-0.08		-0.63	***	3
280	-0.19		-0.64	***	3
281	-0.26		-0.68	***	3
282	-0.16		-0.56	***	3
283	-0.46	**	-0.71	***	1
284	-0.05		-0.61	***	3
285	-0.39	*	-0.71	***	1
286	-0.06		-0.52	**	3
287	0.05		-0.63	***	3
288	-0.26		-0.69	***	3
289	-0.29		-0.64	***	3
290	-0.12		-0.58	***	3
291	-0.10		-0.33	.	5
292	-0.13		-0.48	**	3
293	0.09		-0.24		5
294	0.03		-0.33	.	5
295	-0.14		-0.33	.	5
296	-0.27		-0.43	*	3
297	-0.15		-0.47	**	3
298	-0.43	*	-0.58	***	1
299	-0.36	*	-0.53	***	1
300	-0.31	.	-0.53	**	3
301	-0.22		-0.48	**	3
302	-0.33	.	-0.51	**	3
303	-0.10		-0.45	**	3
304	0.16		-0.44	**	3
305	-0.01		-0.51	**	3
306	-0.13		-0.58	***	3
307	-0.07		-0.56	***	3
308	-0.33	.	-0.56	***	3
309	-0.19		-0.43	*	3
310	-0.22		-0.54	***	3
311	-0.25		-0.56	***	3
312	-0.05		-0.59	***	3
313	-0.04		-0.62	***	3
314	-0.16		-0.63	***	3
315	0.09		-0.53	**	3
316	-0.29		-0.49	**	3
317	0.00		-0.37	*	3
318	-0.03		-0.46	**	3
319	-0.21		-0.46	**	3
320	-0.27		-0.54	**	3
321	-0.27		-0.60	***	3
322	-0.31	.	-0.44	**	3
323	-0.21		-0.50	**	3
324	-0.14		-0.41	*	3
325	-0.15		-0.45	**	3
326	-0.20		-0.42	*	3
327	-0.05		-0.45	**	3
328	0.10		-0.37	*	3
329	-0.05		-0.38	*	3
330	0.03		-0.47	**	3
331	-0.28		-0.54	***	3
332	-0.38	*	-0.56	***	1
333	-0.39	*	-0.66	***	1
334	0.04		-0.55	***	3
335	-0.07		-0.44	*	3
336	0.19		-0.47	**	3
337	-0.05		-0.45	**	3
338	-0.03		-0.47	**	3
339	-0.08		-0.34	*	3
340	0.11		-0.29	.	5
341	-0.21		-0.58	***	3
342	0.15		-0.48	**	3
343	0.14		-0.42	*	3
344	0.13		-0.44	**	3
345	-0.21		-0.42	*	3
346	0.04		-0.28	.	5
347	-0.09		-0.32	.	5
348	-0.18		-0.33	.	5
349	-0.35	.	-0.46	**	3
350	-0.39	*	-0.54	**	1
351	-0.30	.	-0.44	**	3
352	-0.28		-0.47	**	3
353	-0.17		-0.40	*	3
354	0.12		-0.36	*	3
355	0.03		-0.50	**	3
356	-0.39	*	-0.50	**	1
357	-0.46	**	-0.64	***	1
358	-0.17		-0.56	***	3
359	-0.07		-0.45	**	3
360	0.08		-0.54	**	3
361	-0.11		-0.44	*	3
362	0.15		-0.43	*	3
363	-0.04		-0.44	**	3
364	0.05		-0.27		5
365	-0.23		-0.33	.	5
366	-0.20		-0.17		5
367	-0.42	*	-0.35	*	1
368	-0.34	.	-0.47	**	3
369	-0.26		-0.45	**	3
370	-0.22		-0.46	**	3
371	-0.16		-0.44	**	3
372	-0.06		-0.45	**	3
373	0.16		-0.33	.	5
374	0.09		-0.49	**	3
375	0.01		-0.49	**	3
376	-0.05		-0.54	***	3
377	-0.09		-0.52	**	3
378	-0.09		-0.62	***	3
379	-0.13		-0.65	***	3
380	-0.34	.	-0.49	**	3
381	-0.16		-0.48	**	3
382	-0.10		-0.27		5
383	-0.18		-0.25		5
384	-0.11		-0.29	.	5
385	-0.24		-0.45	*	3
386	-0.22		-0.37	*	3
387	-0.18		-0.34	*	3
388	-0.28		-0.33	.	5
389	0.12		-0.49	**	3
390	0.14		-0.30	.	5
391	0.14		-0.30	.	5
392	0.12		-0.36	*	3
393	0.23		-0.45	**	3
394	0.10		-0.55	***	3
395	0.24		-0.65	***	3
396	-0.05		-0.70	***	3
397	0.28		-0.65	***	3
398	-0.20		-0.30	.	5
399	0.00		-0.29	.	5
400	0.11		-0.26		5
401	-0.07		-0.39	*	3
402	-0.26		-0.38	*	3
403	0.30	.	-0.37	*	3
404	0.30	.	-0.31	.	5
405	0.10		-0.40	*	3
406	0.21		-0.34	*	3
407	0.05		-0.38	*	3
408	0.09		-0.32	.	5
409	0.16		-0.45	**	3
410	0.25		-0.63	***	3
411	-0.22		-0.40	*	3
412	-0.08		-0.43	*	3
413	-0.12		-0.42	*	3
414	0.26		-0.51	**	3
415	-0.01		-0.19		5
416	0.02		-0.37	*	3
417	0.23		-0.39	*	3
418	0.07		-0.44	**	3
419	-0.03		-0.45	**	3
420	0.34	*	-0.36	*	2

4 CONCLUSÕES

Nas últimas cinco décadas, o aprimoramento tanto nos instrumentos terrestres quanto orbitais, e o desenvolvimento de novas tecnologias nos permitiram estimar e quantificar a radiação ultravioleta, assim como determinar sua variabilidade, a qual, por sua vez, depende de mudanças nas condições locais. A partir dsta premissa, o objetivo geral desta tese foi gerar conhecimento básico sobre o comportamento da radiação ultravioleta no Rio Grande do Sul, no intuito de contribuir na tomada de decisões para mitigar os efeitos causados pela exposição. As principais contribuições desta tese foram:

➢ Em um cenário de redução de atividades antrópicas, as emissões de dióxido de nitrogênio diminuíram, e os níveis de ozônio total e ultravioleta aumentaram. O aumento simultâneo de ozônio e ultravioleta sugerem que o ozônio não é o único fator que influencia a radiação ultravioleta na superfície. Estes resultados somam mais evidências sobre a correlação de NO_2 ao O_3 total e à radiação ultravioleta.

➢ Tendo em vista que as estações de monitoramento ambiental existentes no Rio Grande do Sul são esparsas e distribuídas de forma desigual, tal problema foi abordado através do uso de novas tecnologias como o método Random Forest, em combinação com uma extensa coleta de dados de múltiplos parâmetros de satélite e de fontes terrestres, sendo mostrado que o método é uma ferramenta válida para prever variáveis ao nível do solo, bem como para reconstruções espaço-temporais a longo prazo.

➢ Partindo da percepção que através de dados de sensoriamento remoto pode-se analisar as características espaço-temporais, determinamos que no Rio Grande do Sul locais em latitudes mais baixas e altitudes mais elevadas apresentam maiores incidências de radiação ultravioleta; há um padrão temporal bem definido, com maior valor no verão e menor valor no inverno; e que ocasiões de incidência da radiação mais intensa é correlacionada de forma negativa com ozônio total, e em alguns casos de forma variável com dióxido de nitrogênio total, havendo, no entanto, outros casos em que estas intensidades não podem ser explicadas pelas variáveis citadas.

Esta tese utilizou como área de estudo de caso o Rio Grande do Sul, e, mesmo que parte de nossos resultados dêem origem a perguntas que demandam investigações adicionais, a informação gerada pode ser de relevante utilidade para a formulação de políticas e conscientização pública e ocupacional regional para prevenção de neoplasias de pele, pois a região está entre as mais altas do Brasil com relação a estes problemas de saúde.

Limitações no presente estudo poderão ser abordadas em trabalhos futuros, como a parametrização dos efeitos de nuvens e outros poluentes presentes (por exemplo, aerossóis) na baixa atmosfera que possam atenuar esta radiação, e a quantificação em escalas menores, como áreas urbanas altamente poluídas.

FINANCIAMENTO

REFERÊNCIAS

ANDRÉ, I.R.N.; FERREIRA, N.J.; CONFORTE, J.C. Análise do comportamento do ozônio estratosférico na América do Sul e vizinhanças utilizando-se imagens do satélite NIMBUS7/TOMS. *In*: **Anais do XI Simpósio Brasileiro de Sensoriamento Remoto**, Belo Horizonte – MG, p. 1117−1124, 2003. SBSR. INPE.

ANDRADE, R. **Estimativa da irradiância solar ultravioleta horária no semi-árido pernambucano – Recife**. 2007. Dissertação (Mestrado) – Programa de Pós-Graduação em Tecnologias Energéticas e Nucleares, Universidade Federal de Pernambuco, Recife, 2007.

ANDRADE, R.C.; TIBA, C. Extreme global solar irradiance due to cloud enhancement in northeastern Brazil. **Renewable Energy,** v. 86, p. 1433–1441, 2016. Disponível em: https://doi.org/10.1016/j.renene.2015.09.012

BAIS, A.F. *et al.* Ozone depletion and climate change: impacts on UV radiation. **Photochemical & Photobiological Sciences**, v. 14, n. 1, p. 19–52, 2015. Disponível em: https://doi.org/10.1039/C4PP90032D

BAIS, A.F *et al*. **Surface ultraviolet radiation: past, present, and future. In: Scientific assessment of ozone depletion: 2006.** World Meteorological Organization, 21, Geneva, 2007.

BATES, D.R. Rayleigh scattering by air. **Planetary and Space Science**, v. 32, n. 6, p. 785–790, 1984. Disponível em: https://doi.org/10.1016/0032-0633(84)90102-8

BODHAINE, B.A. *et al*. Spectral UV measurements at Mauna Loa: July 1995–July 1996. **Journal of Geophysical Research: Atmospheres**, v. 102, n. d15, p. 19265–19273, 1997. Disponível em: https://doi.org/10.1029/97JD01391

BREIMAN, L. Random forests. **Machine Learning**, v. 45, n. 1, p. 5–32, 2001. Disponível em: https://doi.org/10.1023/A:1010933404324

BREWER, A.W.; MCELROY, C.T.; KERR, J.B. Nitrogen dioxide concentrations in the atmosphere. **Nature**, v. 246, n. 5429, p. 129–133, 1973. Disponível em: https://doi.org/10.1038/246129a0

CALDWELL, M.M. *et al*. Terrestrial ecosystems, increased solar ultraviolet radiation and interactions with other climatic change factors. **Photochemical & Photobiological Sciences**, v. 2, p. 29–38, 2003. Disponível em: https://doi.org/10.1039/B211159B

CARDOSO, V.M. **Efeitos da radiação ultravioleta-A e ultravioleta-B sobre os embriões do camarão de água-doce Macrobrachium olfersii (Crustacea, Decapoda) e o papel da radiação ultravioleta-A na fotorreativação**. 2011. Dissertação (Mestrado) – Programa de Pós-graduação em Biologia Celular e do Desenvolvimento, Universidade Federal de Santa Catarina, Santa Catarina, 2011.

CEDE, A. *et al*. Measurements of nitrogen dioxide total column amounts using a Brewer double spectrophotometer in direct sun mode. **Journal of Geophysical**

Research: Atmospheres, v. 111, n. D05304, p. 1–12, 2006. Disponível em: https://doi.org/10.1029/2005JD006585

CEDE, A.; HERMAN, J. Measurements of O_3, SO_2, NO_2 and HCHO column amounts using a Brewer spectrometer. Ultraviolet Ground-and Space-Based Measurements, Models, And Effects V. **International Society for Optics and Photonics,** v. 5886, p. 1–9, 2005. Disponível em: https://doi.org/10.1117/12.620167

CHEYMOL, A.; DE BACKER, H. Retrieval of the aerosol optical depth in the UV-B at Uccle from Brewer ozone measurements over a long time period 1984–2002. **Journal of Geophysical Research: Atmospheres**, v. 108, n. D24, p. 1–10, 2003. Disponível em: https://doi.org/10.1029/2003JD003758

CHIPPERFIELD, M. P. *et al*. Global ozone: Past and future. In: **Scientific Assessment of Ozone Depletion***: 2002*, World Meteorological Organization, 2003.

CHUVIECO, E. **Fundamentos de Teledetección Espacial**. Ediciones Rialp, p. 568, 1996.

CHUBAROVA, N.E. Influence of aerosol and atmospheric gases on ultraviolet radiation in different optical conditions including smoky mist of 2002. **Doklady earth sciences**, v. 394, n. 1, p. 62–67, 2004.

COARITI, J.R. **Análise dos efeitos da radiação solar ultravioleta (r-uv) em populações habitantes a diferentes altitudes**. 2011. Dissertação (Mestre em Meio Ambiente e Recursos Hídricos) – Instituto de Recursos Naturais, Universidade Federal de Itajubá, Minas Gerais, 2011.

COARITI J.R. **Características da Radiação Ultravioleta Solar e seus efeitos na saúde humana nas cidades de La Paz – Bolívia e Natal – Brasil.** 2017. Tese (Doutorado em Ciências Climáticas) – Centro de Ciências Exatas e da Terra, Universidade Federal do Rio Grande do Norte, Natal, 2017.

CORRÊA, M. **Índice Ultravioleta: Avaliações e Aplicações**. 2003. Tese (Doutorado em Ciências) – Instituto de Astronomia, Geofísica e Ciências Atmosféricas, Universidade de São Paulo, São Paulo, 2003.

CORRÊA, M. Solar ultraviolet radiation: properties, characteristics and amounts observed in Brazil and South America. *In:* **Anais Brasileiros de Dermatologia**, v. 90, n.3, p. 297–313, 2015. Disponível em: http://dx.doi.org/10.1590/abd1806-4841.20154089

CORRÊA, M.; PIRES, L. Doses of erythemal ultraviolet radiation observed in Brazil. **International Journal of Dermatology,** n. 52, p. 966−973, 2013. Disponível em: https://doi.org/10.1111/j.1365-4632.2012.05834.x

DAVIS, A.; SIMS, D. **Weathering of polymers**. Springer Science & Business Media, 1983.

DIAZ, S. *et al*. Ozone and UV Radiation over Southern South America: Climatology and Anomalies. **Photochemistry and Photobiology,** v. 82, n. 4, p. 834−843, 2006. Disponível em: https://doi.org/10.1562/2005-09-26-RA-697

DIAZ, S. *et al.* Solar irradiances over Ushuaia (54.49°S, 68.19°W) and San Diego (32.45°N, 117.11°W) geographical and seasonal variation. **Journal of Atmospheric and Solar-Terrestrial Physics**, v. 63, n. 4, p. 309−320, 2001. Disponível em: https://doi.org/10.1016/S1364-6826(00)00178-4

DI SARRA, A. *et al.* Effects of desert dust and ozone on the ultraviolet irradiance at the Mediterranean island of Lampedusa during PAUR II. **Journal of Geophysical Research: Atmospheres**, v. 107, n. D18, p. PAU 2-1-PAU 2-14, 2002. Disponível em: https://doi.org/10.1029/2000JD000139

DUNCAN, B. N. et al. Satellite data of atmospheric pollution for US air quality applications: Examples of applications, summary of data end-user resources, answers to FAQs, and common mistakes to avoid. **Atmospheric Environment**, v. 94, p. 647– 662, 2014. Disponível em: https://doi.org/10.1016/j.atmosenv.2014.05.061

FAHEY, D.W.; HEGGLIN, M.I. Twenty questions and answers about the ozone layer: 2010 update. *In:* **Assessment of Ozone Depletion***: 2002*, World Meteorological Organization, 2011.

FARMAN, J.C.; GARDINER, B.G.; SHANKLIN, J.D. Large losses of total ozone in Antarctica reveal seasonal ClO x/NO x interaction. **Nature**, v. 315, p. 207−210, 1985. Disponível em: https://doi.org/10.1038/315207a0

FEPAM (Fundação Estadual de Proteção Ambiental). **Rede estadual de monitoramento automático da qualidade do ar**. Disponível em: http://www.fepam.rs.gov.br/qualidade/relatorios.asp. Acesso em: 19 jan. 2022.

FIOLETOV, V.E.; KERR, J.B.; WARDLE, D.I. The relationship between total ozone and spectral UV irradiance and its use for deriving total ozone from UV measurements. **Geophysical Research Letters**, v. 24, n. 23, p. 2997–3000, 1997. Disponível em: https://doi.org/10.1029/97GL53153

FIOLETOV, V.E. *et al.* Long term variations of UV-B irradiance over Canada estimated from Brewer observations and derived from ozone and pyranometer measurements. **Journal of Geophysical Research: Atmospheres**, v. 106, n. D19, p. 23009−23027, 2001. Disponível em: https://doi.org/10.1029/2001JD000367

GELARO, R. *et al.* The Modern-Era Retrospective Analysis for Research and Applications,Version 2 (MERRA-2). **Journal of Climate**, v. 30, n.14, p. 5419−5454, 2017. Disponível em: https://doi.org/10.1175/JCLI-D-16-0758.1

GONZÁLEZ-RODRÍGUEZ, L. *et al.* Ultraviolet erythemal radiation in Central Chile: direct and indirect implication for public health. **Air Quality, Atmosphere & Health**, v. 14, n. 10, p. 1533-1548, 2021. Disponível em: https://doi.org/10.1007/s11869-021-01037-3

GLANDORF, M. *et al.* Possibilities to detect trends in spectral UV irradiance. **Theoretical and Applied Climatology***,* v. 81, n. 1, p. 33–34, 2005. Disponível em: https://doi.org/10.1007/s00704-004-0109-9

HERMAN, J. 2010. Changes in ultraviolet and visible solar irradiance 1979 to 2008. Changes in Ultraviolet and Visible Solar Irradiance 1979 to 2008. **UV Radiation in Global Climate Change**, Springer, Berlin, p. 106-159, 2010. Disponível em: https://doi.org/10.1007/978-3-642-03313-1_5

ITACA. **The Sun as a source of energy: Solar energy reaching the Earth's surface.** Disponível em: https://www.itacanet.org/the-sun-as-a-source-of-energy/part-2-solar-energy-reaching-the-earths-surface/. Acesso em: 24 jan. 2022.

IALONGO, I.; CASALE, G.R.; SIANI, A.M. Comparison of total ozone and erythemal UV data from OMI with ground-based measurements at Rome station. **Atmospheric Chemistry and Physics**, v. 8, n. 12, p. 3283−3289, 2008. Disponível em: https://doi.org/10.5194/acp-8-3283-2008

INCA (Instituto Nacional de Cancer José Alencar Gomes**). Incidência de Câncer no Brasil**. Disponível em: https://www.inca.gov.br/sites/ufu.sti.inca.local/files//media/document//estimativa-2020-incidencia-de-cancer-no-brasil.pdf. Acesso em: 10 ago. 2021.

INIRC (International Non-Ioning Radiation Committee). Review of concepts, quantities, units and terminology for non-ionizing radiation protection. **Health Phys**, v.49, p.1329–1362, 1985.

ISAKSEN, I.S.A. et al. Tropospheric ozone changes at unpolluted and semipolluted regions induced by stratospheric ozone changes. **Journal of Geophysical Research: Atmospheres**, v. 110, n. D2, p. 1–15, 2005. Disponível em: https://doi.org/10.1029/2004JD004618

JENSEN, J. **Sensoriamento Remoto do Ambiente: uma Perspectiva em Recursos Terrestres**. Parêntese. São José dos Campos−SP, 2009.

KENDALL, M. G. **Rank correlation methods**. Book series, Charles Griffin. 1975.

KERR, J.B. Trends in total ozone at Toronto between 1960 and 1991. **Journal of Geophysical Research: Atmospheres**, v. 96, n. D11, p. 20703−20709, 1991. Disponível em: https://doi.org/10.1029/91JD02282

KERR, J.B. Diurnal variation of column ozone at Toronto and Edmonton. Atmospheric Ozone. *In* **Proceedings of the XVIII Quadrennial Ozone Symposium**. Italy, p. 53–56, 1998.

KERR, J.B. New methodology for deriving total ozone and other atmospheric variables from Brewer spectrophotometer direct sun spectra. **Journal of Geophysical Research: Atmospheres**, v. 107, n. D23, p. ACH 22-1-ACH 22-17, 2002. Disponível em: https://doi.org/10.1029/2001JD001227

KERR, J.B. Understanding the factors that affect surface ultraviolet radiation. **Optical Engineering**, v. 44, n. 4, p. 041002, 2005. Disponível em: https://doi.org/10.1117/1.1886817

KERR, J.B.; DAVIS, J.M. New methodology applied to deriving total ozone and other atmospheric variables from global irradiance spectra. **Journal of Geophysical**

Research: Atmospheres, v. 112, n. D21, p. 021301, 2007. Disponível em: https://doi.org/10.1029/2007JD008708.

KERR, J.B.; MCELROY, C.T. Evidence for large upward trends of ultraviolet- B radiation linked to ozone depletion. **Science**, v. 262, p. 1032–1034, 1993. Disponível em: https://doi.org/10.1126/science.262.5136.1032

KERR, J.B. *et al*. Surface Ultraviolet Radiation: Past and Future. *In:* **Scientific Assessment of Ozone Depletion**: 2002. World Meteorological Organization, 2003.

KERR, J.B. *et al*. The Canadian Ozone Watch and UV-B advisory programs. *In*: Ozone in the Trophosphere and Stratosphere. Springer-Verlag, Berlin, p. 794–797, 1994.

KERR, J.B.; FIOLETOV, V.E. Surface ultraviolet radiation. **Atmosphere-Ocean**, v. 46, n. 1, p. 159–184, 2008. Disponível em: https://doi.org/10.3137/ao.460108

KIRCHHOFF, V.W.J.H. *et al*. A variação sazonal da radiação ultravioleta solar biologicamente ativa. **Revista Brasileira de Geofísica**, v.18, p. 63–74, 2000. Disponível em: https://doi.org/10.1590/S0102-261X2000000100006

KOLLER, L.R. **Ultraviolet Radiation**. John Wiley and Sons. New York, 1965.

KORONAKIS, P.S. *et al*. Interrelations of UV-global/global/diffuse solar irradiance components and UV-global attenuation on air pollution episode days in Athens, Greece. **Atmospheric Environment**, v. 36, n. 19, p. 3173–3181, 2002. Disponível em: https://doi.org/10.1016/S1352-2310(02)00233-9

KRUEGER, A.J. *et al*. Volcanic sulfur dioxide measurements from the total ozone mapping spectrometer instruments. **Journal of Geophysical Research: Atmospheres**, v. 100, n. D7, p. 14057–14076, 1995. Disponível em: https://doi.org/10.1029/95JD01222

KROTKOV, N.A. *et al*. Satellite estimation of spectral UV irradiance. Effects of homogeneous clouds and snow. **Journal of Geophysical Research**, v. 106, n. D11, p. 11743–11759, 2001. Disponível em: https://doi.org/10.1029/2000JD900721

KUMAR, S. *et al*. Changes in land use enhance the sensitivity of tropical ecosystems to fire-climate extremes. **Scientific Reports**, v. 12, n. 1, p. 1-11, 2022. Disponível em: https://doi.org/10.1038/s41598-022-05130-0

LAHOZ, W. A. et al. Monitoring air quality from space - The Case for the Gesostationary Plataform. **Bulletin of the American Meteorological Society**, v. 93, n. 2, p. 221–233, 2012. Disponível em: https://doi.org/10.1175/BAMS-D-11-00045.1

LOPO, A. B. *et al*. Radiação ultravioleta, ozônio total e aerossóis na cidade de Natal-RN. **Holos**, v. *6*, p. 3−21, 2013.

LIVI, F.P. O clima em Porto Alegre no século XX: uma análise de séries temporais. 2012. Dissertação (Mestrado em Geografia) – Instituto de Geociências, Programa de Pós-graduação em Geografia, Universidade Federal do Rio Grande do Sul, Porto Alegre, 2012.

LEE-TAYLOR, J. *et al*. A climatology of UV radiation, 1979–2000, 65S–65N. *In:* **UV radiation in global climate change**. Springer, Berlin, 2010.

MANN, H. B. Nonparametric tests against trend. **Econometrica: Journal of the econometric society**, v. 13, p. 245–259, 1945. Disponível em: https://doi.org/10.2307/1907187

MORAES, G. **Projeções de fluxos de R-UV para a América do Sul com base nas estimativas de conteúdo de ozônio para o século XXI.** 2015. Dissertação (Mestrado em Meio Ambiente e Recursos Hídricos) – Programa de Pós-Graduação Meio Ambiente e Recursos Hídricos. Universidade Federal de Itajubá. Itajubá, 2015.

MCKENZIE, R. L. *et al*. Changes in biologically-active ultraviolet radiation reaching the Earth's surface. **Photochemical & Photobiological Sciences**, v. 6, n. 3, p. 218-231, 2007. Disponível em: https://doi.org/10.1039/B700017K

MCKENZIE, R.L.; CONNOR, B.; BODEKER, G. Increased summertime UV radiation in New Zealand in response to ozone loss. **Science**, v. 285, n. 5434, p. 1709–1711, 1999. Disponível em: https://doi.org/10.1126/science.285.5434.1709

NISPERUZA, T. D. *et al*. **Teledetección: una herramienta para estudios de calidad del aire en la zona urbana del Valle de Aburrá.** Disponível em: https://dspace.tdea.edu.co/handle/tdea/1133. Acesso em: 10 jan. 2022.

OMI (Ozone Monitoring Instrument). **Data User's guide**. 2012. Disponível em: https://docserver.gesdisc.eosdis.nasa.gov/repository/Mission/OMI/3.3_ScienceDataP roductDocumentation/3.3.2_ProductRequirements_Designs/README.OMI_DUG.pdf . Acesso em: 10 jan. 2022

ORPHAL, J. A critical review of the absorption cross-sections of O_3 and NO_2 in the ultraviolet and visible. **Journal of Photochemistry and Photobiology A: Chemistry**, v. 157, n. 2−3, p. 185−209, 2003. Disponível em: https://doi.org/10.1016/S1010-6030(03)00061-3

PARISI, A.V. *et al*. Measured and modeled contributions to UV exposures by the albedo of surfaces in an urban environment. **Theoretical and applied climatology**, v. 76, n. 3, p. 181–188, 2003. Disponível em: https://doi.org/10.1007/s00704-003-0012-9

PAN, Y.; ZHAO, C.; LIU, Z. Estimating the daily NO_2 concentration with high spatial resolution in the Beijing–Tianjin–Hebei Region Using an Ensemble Learning Model. **Remote Sensing**, v. 13, n. 4, p, 758, 2021. Disponível em: https://doi.org/10.3390/rs13040758

RAMANATHAN, V.; FENG, Y. Air pollution, greenhouse gases and climate change: Global and regional perspectives. **Atmospheric environment**, v. 43, n. 1, p. 37−50, 2009. Disponível em: https://doi.org/10.1016/j.atmosenv.2008.09.063

ROBINSON, N. **Solar Radiation**. Elsevier. Amsterdam, 1996.

SEINFELD, J.; PANDIS, S. **Atmospheric Chemistry and Physics: from air pollution to climate change**. Wiley Interscience, New York, 1998.

SERAFINI, L. **Análise da série temporal dos dados de radiação ultravioleta incidente no observatório espacial do sul.** Relatório final de projeto de iniciação científica PIBIC/INPE-CNPq/MCT.

SICILIANO, B. *et al.* Increased ozone levels during the COVID-19 lockdown: Analysis for the city of Rio de Janeiro, Brazil. **Science of the Total Environment**, v. 737, p. 139765, 2020. Disponível em: https://doi.org/10.1016/j.scitotenv.2020.139765

SILVA, F.; OLIVEIRA, H.S.M.; MARINHO, G.S. Variação do índice de radiação solar ultravioleta em Natal-RN entre 2001 e 2007. In: **II Congresso Brasileiro de Energia Solar e III Conferência Regional Latino-Americana da ISES**. Florianópolis, 2008.

SILVA PORFIRIO, A. *et al.* An assessment of the global UV solar radiation under various sky conditions in Maceió-Northeastern Brazil. **Energy**, v. 44, n. 1, p.584–592, 2012. Disponível em: https://doi.org/10.1016/j.energy.2012.05.042

SLINEY, D.H. Radiometric quantities and units used in photobiology and photochemistry: recommendations of the commission internationale de L'eclairage. **Photochemistry and Photobiology**, v.83, n.2, p.425−432, 2007. Disponível em: https://doi.org/10.1562/2006-11-14-RA-1081

TERAMOTO, E.; ESCOBEDO, C.; MARTINS, D. Modelos estatísticos para estimativa da irradiação solar uv horária em Botucatu/SP/Brasil. **Revista Brasileira de Energia Solar**, v.5, n.1, p.44–51, 2014.

TERAMOTO, E. *et al.* Comparação de Métodos de Estimativa da Radiação Solar Ultravioleta Horária: Modelos Empíricos, Redes Neurais Artificiais e Máquina de Vetores de Suporte. **Revista Brasileira de Meteorologia**, v. 35, 35-43, 2020. Disponível em: https://doi.org/10.1590/0102-7786351010

TIEGTE J.E. *et al.* Ambient solar UV radiation causes mortality in larvae of three species of Rana under controlled exposure conditions. **Photochemistry and Photobiology**, v.74, n.2, p.261–268, 2001. Disponível em: https://doi.org/10.1562/0031-8655(2001)0740261ASURCM2.0.CO2

USGS (U.S. Geological Survey). **USGS EROS Archive−Digital Elevation - Shuttle Radar Topography Mission.** Disponível em: https://www.usgs.gov/centers/eros/science/usgs-eros-archive-digital-elevation-shuttle-radar-topography-mission-srtm-1. Acesso em: 10 jan. 2022

WARDLE, D.I. *et al.* **Ozone science: A Canadian perspective on the changing ozone layer**. Environment Canada, 1997.

WAKAMATSU, S. *et al.* Observational study of stratospheric ozone intrusions into the lower troposphere. **Atmospheric Environment**, v. 23, n. 8, p. 1815–1826, 1989. Disponível em: https://doi.org/10.1016/0004-6981(89)90065-6

WANG, B. *et al.* Future climate impacts on forest growth and implications for carbon sequestration through reforestation in southeast Australia. **Journal of Environmental Management**, v. 302, p. 113964, 2022. **Disponível em: https://doi.org/10.1016/j.jenvman.2021.113964**

WANG, P. *et al*. Airborne multi-axis DOAS measurements of tropospheric SO_2 plumes in the Po-valley, Italy. **Atmospheric Chemistry and Physics Discussions**, v. 5, n.2, p. 2017–2045, 2005a.

WANG, P. *et al*. Measurements of tropospheric NO_2 with an airborne multi-axis DOAS instrument. **Atmospheric Chemistry and Physics**, v. 5, n.2, p.337–343, 2005b. Disponível em: https://doi.org/10.5194/acp-5-337-2005

WASTI, A. *et al*. Climate change and the hydropower sector: A global review. **Wiley Interdisciplinary Reviews: Climate Change**, p. e757, 2022. Disponível em: https://doi.org/10.1002/wcc.757

WMO (World Meteorological Organization). **Scientific assessment of ozone depletion, 1998**. Global Ozone Research and Monitoring Project, World Meteorological Organization, Switzerland, 1999.

ZARATTI, F. *et al*. Proposal for a modification of the UVI risk scale. **Photochemical & Photobiological Sciences**, v. 13, p. 980−985, 2014. Disponível em: https://doi.org/10.1039/C4PP00006D

ZEREFOS, C.S. *et al*. On changes of spectral UV-B in the 90's in Europe, **Advances in Space Research**, v. 26, n. 12, p. 1971–1978, 2000. Disponível em: https://doi.org/10.1016/S0273-1177(00)00167-8

ZEREFOS, C.S. Long-term ozone and UV variations at Thessaloniki, Greece, **Physics and Chemistry of the Earth**, v. 27, n. 6−8, p. 455–460, 2002. Disponível em: https://doi.org/10.1016/S1474-7065(02)00026-8

APÊNDICE A. TRABALHO APRESENTADO EM CONGRESSO

ANÁLISE ANUAL DAS COMPONENTES DIRETA, DIFUSA E GLOBAL DA RADIAÇÃO SOLAR EM PORTO ALEGRE, RS

Adriana Becerra-Rondon – abecerrarondon@gmail.com
Jorge Ducati – jorge.ducati@ufrgs.br
Universidade Federal do Rio Grande do Sul, Programa de Pós-Graduação em Sensoriamento Remoto
Rafael Haag – rafael-haag@uergs.edu.br
Universidade Estadual do Rio Grande do Sul, Programa de Pós-Graduação em Ambiente e Sustentabilidade

Resumo. A radiação solar incide na superfície da Terra sob condições atmosféricas diferentes, o que afeta a quantidade da radiação obtida na superfície terrestre durante o dia. A partir da razão entre irradiância global solar medida na superfície e a irradiância no topo da atmosfera (índice de claridade), pode-se estimar a quantidade de radiação solar global incidente em várias condições do céu. Desde março de 2018 a estação solarimétrica da UERGS, localizada na cidade de Porto Alegre - RS (-30.080022, -51.12856) vem registrando dados de radiação solar e outros parâmetros meteorológicos. Neste trabalho analisamos os dados obtidos para as componentes direta, difusa e global da radiação solar e o comportamento da radiação solar em três cenários de nebulosidade (céu claro, cobertura intermédia e nublado) por meio do índice de claridade "Kt", a partir dos dados diários registrados pela estação durante um ano (março 2018 a fevereiro 2019). Como resultado obteve se, 72 dias com céu claro, 184 dias com cobertura intermédia e 109 dias nublado; com radiação média de 285 W/m2 em dias de céu claro, 187 W/m2 em cobertura intermédia, 76 W/m2 em dias nublados; sendo os meses de novembro e dezembro os que apresentaram a maior quantidade de dias com céu claro. Nos três cenários a irradiância global apresentou um comportamento exponencial conforme aumentou o índice Kt; entanto que, o comportamento da difusa e direta variou conforme o cenário, sendo a relação destas a determinante de cada categoria.

Palavras-chave: Índice de claridade, atmosfera, radiação solar

1.   INTRODUÇÃO

A radiação solar incide sobre a superfície da Terra sob condições atmosféricas variáveis, o que influi na quantidade de radiação que atinge o solo ao longo do dia. Ao atravessar a atmosfera e interagir com seus componentes a radiação passa por processos de reflexão, difusão e absorção, chegando à superfície como radiação direta (que provém diretamente do Sol), radiação difusa (energia dispersada) e radiação global (soma das componentes anteriores) (Iqbal, 1983). A transmissão desta energia é um processo físico complexo, devido ao grande número de parâmetros físicos que descrevem a atmosfera e a influenciam. A energia radiativa é o responsável direto no aporte de energia primária para a maioria dos processos terrestres, desde os biológicos, como a fotossíntese, até os meteorológicos, como o desenvolvimento de tempestades (Souza et al., 2005).

As nuvens são um dos constituintes atmosféricos com maior variação no tempo e maior impacto sobre a energia radiante (Souza Echer et al., 2006) ao nível do solo. A nebulosidade, ou a taxa de nuvens presentes na atmosfera, especificada para um determinado local, influi fortemente na quantidade de radiação que chega ao solo, sendo possível definir um "índice de claridade" Kt (Liu e Jordan 1960; Rensheng et al., 2004). Na definição deste índice, consideramos Ho como sendo a irradiância fora da atmosfera, ou seja, a irradiância extraterrestre que tem como origem o Sol; Ho tem como valor de referência a Constante Solar, igual a 1367 W/m2, sendo este valor a média ao longo do ano, considerando a variação da distância Sol-Terra devido à excentricidade da órbita da Terra em torno do Sol. Ainda, H é a irradiância global horizontal, que é a quantidade total de radiação recebida ao nível do solo por uma superfície horizontal, após os processos de espalhamento, reflexão e absorção na atmosfera que agiram sobre Ho. O índice Kt é a razão H/Ho, grandeza usada para expressar a transparência da atmosfera à radiação solar, sendo um coeficiente de transmitância da atmosfera.

O conhecimento sobre a quantidade de energia que chega ao solo e sua variabilidade temporal é importante na avaliação do desempenho de projetos envolvendo energia solar, e o registro deste dado é considerado como sendo uma ferramenta importante em pesquisas interdisciplinares como previsão do rendimento das culturas ou como uma ferramenta de avaliação do impacto das alterações climáticas (Abdullahi e Nasir, 2014).

Neste contexto, este trabalho analisa o comportamento das componentes solares global, direta e difusa em três cenários de nebulosidade ou transmissividade atmosférica. Os dados são oriundos da estação solarimétrica automática da Universidade Estadual do Rio Grande do Sul, UERGS, localizada na cidade de Porto Alegre, Rio Grande do Sul.

2.   MATERIAL E MÉTODOS

2.1   Área de estudo

A área de estudo está localizada no Bairro Agronomia, município de Porto Alegre, RS (Figura 1). Nesta região o terreno é pouco acidentado, com altitudes que variam entre 4 e 300 metros; nas áreas onde há vegetação esta corresponde às classes herbácea e de matas/florestas, sendo esta última dominante (Vieira, 1984; Müller et al., 2011). Segundo a classificação de Koppen, a área possui clima subtropical úmido (Cfa) devido às suas temperaturas médias mensais (19,5 °C) e à distribuição anual de chuvas (1397 mm) (Livi, 1998). As temperaturas mais baixas se concentram nos meses de junho e julho, as maiores temperaturas de dezembro a março, e as maiores chuvas ocorrem nos meses de junho a setembro (Livi, 2002). Na área de estudo (-30.080022, -51.12856). está instalada a Estação Solarimétrica da Universidade Estadual do Rio Grande do Sul (UERGS).
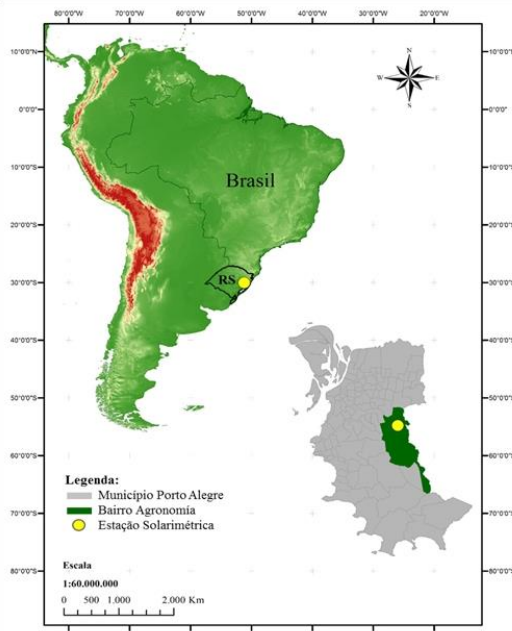
Figura 1 - Mapa de localização da área de estudo no município de Porto Alegre, RS – Brasil.

2.2 Estação solarimétrica

A estação solarimétrica iniciou sua operação em fevereiro de 2018 e está alojada num contêiner climatizado. Os equipamentos de medição estão instalados na base superior do contêiner. A estação possui três piranômetros termoelétricos, modelo MS-410 da fabricante japonesa EKO, destinados às medidas das componentes global horizontal, global inclinada (inclinação de 30 graus) e difusa, por meio de esfera de sombreamento acoplada a um sistema de rastreamento automático. A componente direta normal da radiação solar é obtida através de um pireliômetro modelo MS-56 (fabricante EKO), montado sobre um rastreador solar de dois eixos, modelo STR-22G (fabricante EKO) com GPS integrado. A Fig. 2 mostra a estação solarimétrica e seus principais instrumentos de medidas.

Figura 2 – Estação solarimétrica da UERGS. São vistos os principais instrumentos de medidas das componentes da radiação solar e instrumentos meteorológicos.

A estação solarimétrica conta com um *datalogger* Ammonit, modelo Meteo-40, equipamento que faz a coleta e armazenamento dos dados medidos pelos instrumentos de medição que compõem a estação. As medidas são coletadas a cada 1 segundo e os dados são integrados a cada 10 minutos. Estas informações são disponibilizadas em uma plataforma *on-line* via Internet. Além dos sensores para medidas da radiação solar, a estação solarimétrica possui outros instrumentos para coleta de dados meteorológicos, como anemoscópio, anemômetro, barômetro, termômetros, Pluviômetro e termo-higrômetro.

2.3 Cenários de nebulosidade

Estes cenários foram definidos através do índice de claridade (*Kt*), número adimensional que varia de acordo com a quantidade de nuvens e aerossóis na atmosfera, levando a um aumento ou uma redução das componentes direta ou difusa da radiação solar que atinge a superfície, possibilitando a classificação do céu quanto à sua nebulosidade (Tavares, 2005).

Para estimativa de *Ho* foi utilizada a expressão proposta por Duffie and Beckman (2013), calculada em função da constante solar (*Gsc*=1367 W/m²), latitude ("*φ*)" , posição angular do Sol (*δ*) ao meio-dia solar com relação ao plano do Equador, ângulo do pôr do Sol (*ωss*), e dia Juliano (*N*):

$$H_o = \frac{24}{\pi} \cdot G_{sc} \cdot \left[1 + 0,033 \cdot \cos\left(\frac{360N}{365}\right)\right] \cdot \left(\cos\varphi \cdot \cos\delta \cdot \mathrm{sen}\ \omega_s + \frac{\pi\ \omega_s}{180} \cdot \mathrm{sen}\varphi \cdot \mathrm{sen}\delta\right) \tag{1}$$

A partir do resultado da equação 1 e dos valores medidos de *H*, a classificação de cobertura de céu adotada foi uma modificação da proposta de Escobedo et al. (2009) onde os cenários de céu parcialmente nublado (0,35 ≥ *Kt* ≤ 0,55) e céu parcialmente claro (0,55 ≥ *Kt* ≤ 0,65) foram combinados em uma categoria. Os cenários estabelecidos neste trabalho foram: céu nublado (*Kt* < 0,35), céu com cobertura intermédia (0,35 ≥ *Kt* ≤ 0,65) e céu claro (*Kt* > 0,65).

3. RESULTADOS E DISCUSSÕES

3.1 Componentes solares

Os valores médios mensais de irradiância global horizontal medidos entre março de 2018 e fevereiro de 2019 pela estação solarimétrica da UERGS são apresentados na Tab. 1. A variação da média mensal indicou que em dezembro ocorreram os maiores valores, com médias de 272,79 W/m² e no mês de julho as menores intensidades com 80,37 W/m² (Tabela 1).

Tabela 1 - Irradiância global horizontal (W/m²) média mensal registrada entre março de 2018 e fevereiro de 2019.

Mês	Média	Mínima	Máxima
Janeiro	229,51	74,71	345,41
Fevereiro	214,10	28,11	314,74
Março	189,37	30,07	293,14
Abril	156,22	39,53	217,74
Maio	106,65	14,70	157,12
Junho	86,96	12,99	136,07
Julho	80,37	3,54	153,13
Agosto	131,02	19,61	223,94
Setembro	149,05	21,11	255,60
Outubro	205,45	49,86	306,96
Novembro	255,43	68,70	355,09
Dezembro	272,79	102.97	363,08

Na Fig 3 pode-se visualizar o comportamento da irradiância no topo da atmosfera e na superfície durante um ano inteiro. Observa-se que a intensidade de radiação solar que atinge a superfície é variável, devido à atenuação sofrida ao atravessar a atmosfera. Para os dados registrados da estação solarimétrica, entre o período juliano 150 - 195 (inverno) 195 (inverno) ocorre a maior absorção de energia solar, que coincide com os meses de maior umidade e variação astronômica.
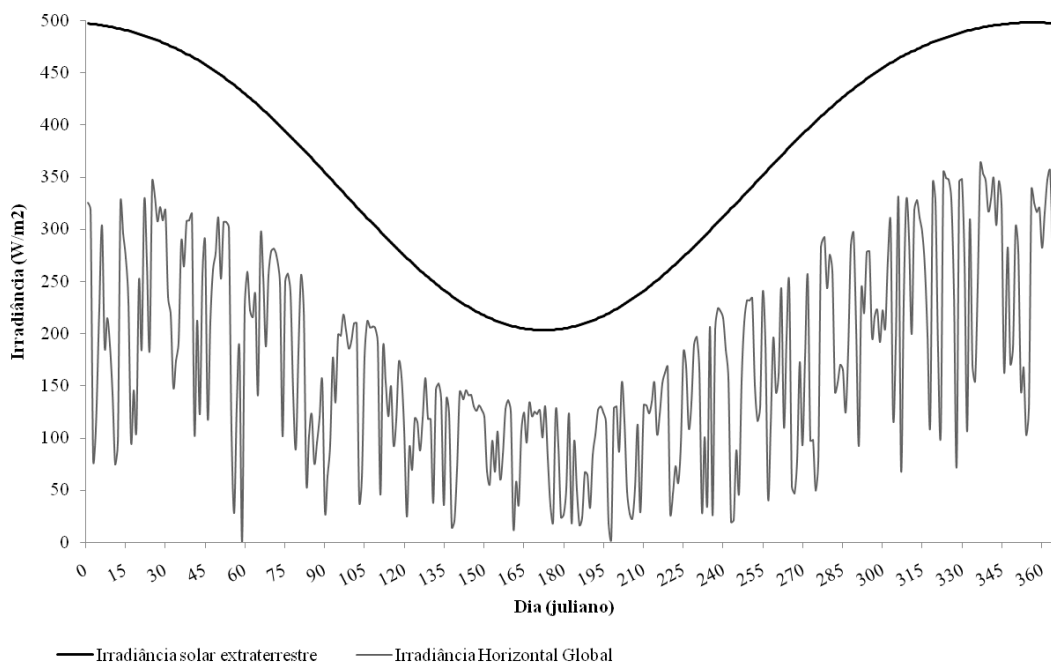
Figura 3 - Intensidade da radiação no topo da atmosfera e na superfície durante um ano.

A Tab. 2 mostra os valores da componente difusa da radiação solar. A maior dispersão de radiação difusa aconteceu em junho com média mensal de 37,55 W/m² (Tabela 2) e a menor dispersão em janeiro com 97,21 W/m².

Tabela 2 - Irradiância Difusa (W/m2) média mensal registrada entre março de 2018 e fevereiro de 2019.

Mês	Média	Mínima	Máxima
Janeiro	97,21	34,61	148,67
Fevereiro	79,68	27,65	150,95
Março	71,96	29,80	120,68
Abril	56,00	23,23	91,22
Maio	44,44	14,6	84,49
Junho	37,55	13,10	66,87
Julho	40,31	3,55	75,58
Agosto	41,87	19,50	85,63
Setembro	65,87	21,05	111,84
Outubro	91,59	34,40	157,25
Novembro	79,88	27,44	154,58
Dezembro	89,34	31,36	147,69

Para a irradiação direta, a variação da média mensal indicou que em dezembro acontece a maior intensidade solar direta com 238,87 W/m² e em julho a menor intensidade com 36,89 W/m2 (Tabela 3).

Tabela 3 - Irradiância Direta (W/m²) média mensal registrada entre março de 2018 e fevereiro de 2019.

Mês	Média	Mínima	Máxima
Janeiro	211,60	71,79	314,26
Fevereiro	209,03	28,43	316,03
Março	112,12	0,00	252,65
Abril	92,90	0,00	177,91
Maio	59,46	0,00	124,60
Junho	47,94	0,00	117,25

Julho	36,89	0,00	118,06
Agosto	76,46	0,00	176,78
Setembro	70,04	0,00	190,70
Outubro	97,00	0,00	235,97
Novembro	234,7	66,46	319,13
Dezembro	238,87	89,99	310,96

3.2 Índice de claridade

Para o período de estudo, foi calculado um *Kt* mínimo de 0,01 e máximo de 0,73. Na Fig. 4 está representada a distribuição das irradiâncias na horizontal em função do índice de claridade (*Kt*). No intervalo de *Kt* <0,35 a global e difusa são praticamente iguais e a irradiação direta é próxima de zero, o que classifica a cobertura do céu como nublado; para $0,35 \geq Kt \leq 0,65$ existe alternância entre a difusa e direta, o que classifica o céu como cobertura intermédia; para $Kt > 0,65$, a direta tende a se aproximar da global, enquanto a irradiação difusa tende a um mínimo, o que classifica o céu como claro.
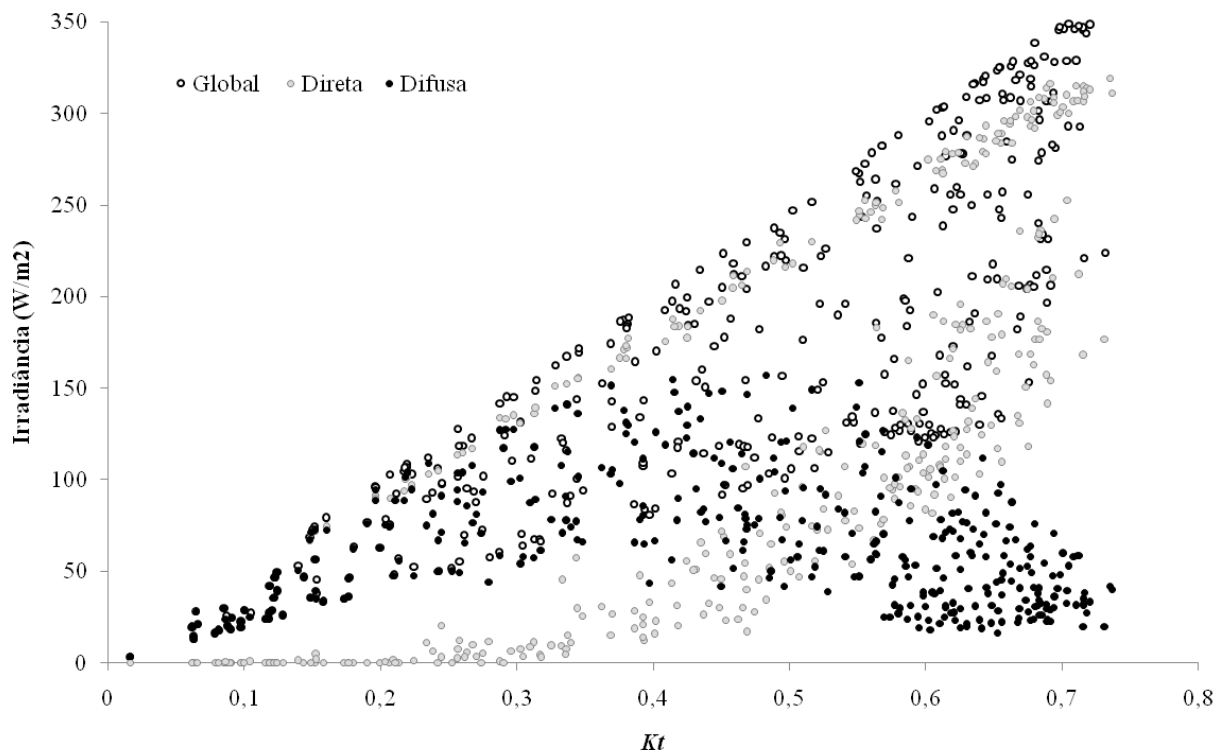
Figura 4 - Distribuição da irradiância global, difusa e direta, em função do índice de claridade (*Kt*).

A Fig. 5 mostra as frequencias de *Kt* para cada mês, sendo novembro e dezembro os meses com o maior número de dias com céu claro 13 e 11 respectivamente. O mês com mais dias nublados foi julho com 14 dias.
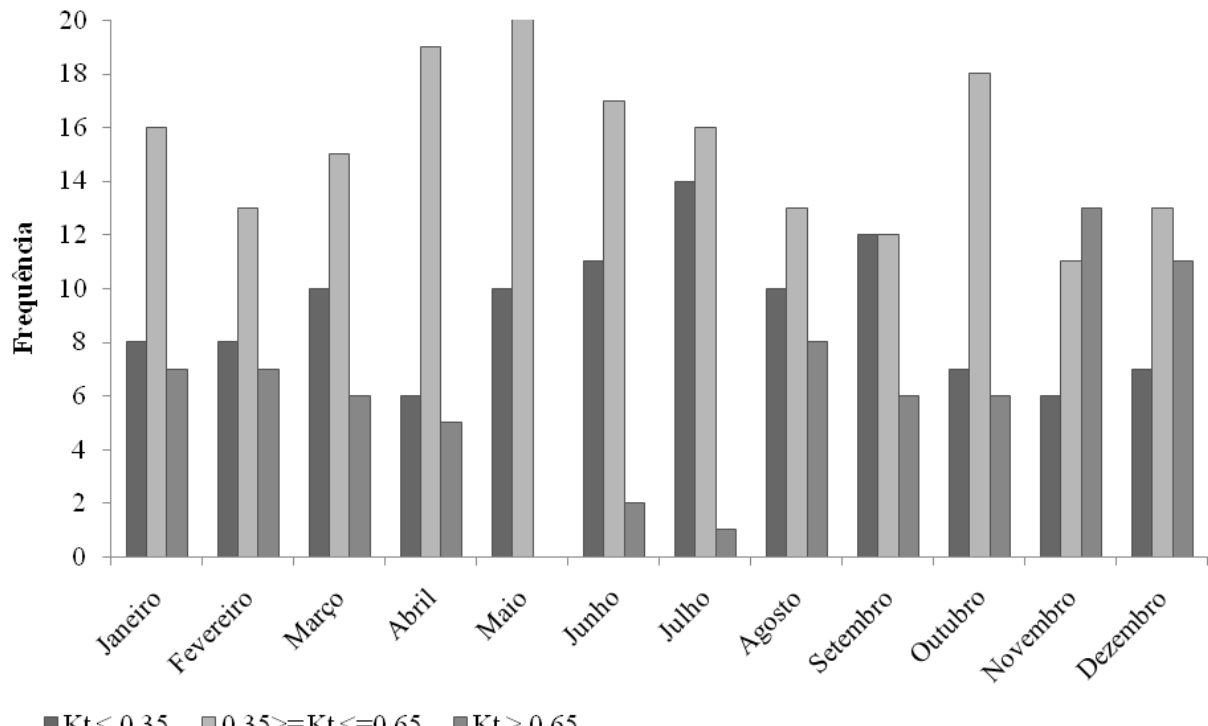
Figura 5 - Distribuição de frequências do índice de claridade (*Kt*) para cada mês durante o periodo de março 2018 até fevereiro 2019.

Em geral obteve-se um total de 72 dias com céu claro, 184 dias com céu com cobertura intermédia e 109 dias com céu nublado; com radiação média de 285 W/m^2 em dias com céu claro, 187 W/m^2 em dias de céu cobertura intermédia, 76 W/m^2 em dias de céu nublado (Tabela 4).

Tabela 4 - Intensidade média anual (W/m^2) das componentes solares em cada cenário atmosferico.

Kt	Global	Difusa	Direta
Kt <0,35	74,95	64,86	31,46
0,35 ≥ *Kt* ≤ 0,65	187,13	76,20	130,02
Kt > 0,65	284,61	43,02	245,45

A variação mensal na intensidade de radiação recebida através de cada componte em cada cenário é apresentada na Tab. 5. Em cenários nublados a época de verão aprentou uma irradiância média global máxima de 147 W/m^2 (dezembro), difusa de 113 W/m^2(dezembro) e direta de 133 W/m^2 (dezembro), e a época de inverno uma irradiância global média mínima de 33 W/m^2 (julho), difusa de 32 W/m^2(julho) e direta de 0,72 W/m^2 (julho). Para cenários de cobertura intermedia a época de verão aprentou uma irradiância média global máxima de 280 W/m^2 (dezembro), difusa de 119 W/m^2(novembro) e direta de 245 W/m^2 (dezembro), e a época de inverno uma irradiância global média mínima de 111 W/m^2 (junho), difusa de 39 W/m^2(junho) e direta de 63 W/m^2 (julho). Entretanto, o cenário de céu claro na época de verão aprentara uma irradiância média global máxima de 343 W/m^2 (dezembro), difusa de 61 W/m^2(janeiro) e direta de 306 W/m^2 (novembro e março), e a época de inverno uma irradiância global média mínima de 134 W/m^2 (junho), difusa de 19 W/m^2(junho) e direta de 113 W/m^2 (junho).

Tabela 5 - Intensidade média (W/m^2) da componente global, difusa e direta na superfície para cada mês nos três cenários de nebulosidade.

	Irradiância Global			Irradiância Difusa			Irradiância Direta		
	Nublado	Intermédio	Claro	Nublado	Intermédio	Claro	Nublado	Intermédio	Claro
Janeiro	106,16	248,25	327,66	98,77	112,05	61,51	100,00	228,86	299,70
Fevereiro	94,90	236,82	308,12	77,25	97,69	49,00	91,13	229,86	306,50
Março	93,47	219,72	273,31	80,22	78,77	41,14	9,47	133,87	228,85
Abril	66,27	171,04	207,85	59,64	61,88	29,30	4,03	101,38	167,30

Maio	52,04	132,65	0,00	45,85	43,77	0,00	4,17	85,79	0,00
Junho	40,67	111,27	134,93	37,99	39,43	19,06	2,61	69,59	113,29
Julho	33,88	116,50	153,13	32,58	47,86	27,88	0,72	63,46	118,06
Agosto	50,97	147,20	204,78	43,87	50,60	25,18	5,63	84,69	151,63
Setembro	75,50	178,14	237,96	67,71	82,59	28,76	2,89	80,87	182,66
Outubro	100,64	218,11	289,76	83,24	108,50	50,62	12,30	89,66	217,83
Novembro	105,81	242,69	335,27	89,78	119,40	41,87	98,29	224,86	306,14
Dezembro	147,45	280,62	343,30	113,84	102,30	58,42	133,49	245,50	298,08

Analisando a Tab. 5, observa-se que a média anual da radiação solar global foi de 172,86 W/m², sendo que, em condições de céu nublado, cobertura intermédia e céu claro, a média foi 74,95 W/m², 187,13 W/m² e 284,61 W/m², indicando que houve variações na energia recebida pela superfície terrestre com relação ao tipo de cobertura do céu. Esta variação é devido à atenuação sofrida ao atravessar a atmosfera; onde o índice de claridade mostrará um quociente atenuado em função da presença de nuvens, poeira, poluição e outros. Em um dia nublado, naturalmente, a intensidade da radiação solar será menor e, conseguintemente o índice também será menor. Ocorre o contrário em um dia claro ou com céu sem nuvens (Marques et al., 2000). Os intervalos do índice de claridade reportados neste estudo coincidem com os intervalos de Kt encontrados nas cidades de Cascavel ‒ PR e Botucatu ‒ SP, mesmo se tratando de latitudes e condições climáticas diferentes (De Oliveira, 2005; Escobedo et al., 2009).

4. CONCLUSÕES

Este trabalho apresentou os resultados do primeiro ano de medidas das componentes da radiação solar obtidas através da estação solarimétrica da UERGS em Porto Alegre. A variação anual das componentes solares sobre a área estudo é influenciada principalmente pela cobertura de núvens e outros parâmetros atmosféricos (vapor d'agua, aerossóis, azônio, etc). A distribuição da frequência do índice de claridade indica que está área dominram dias parcialmente nublados, seguido por dias nublados e em menor frequência dias de céu claro. No verão foram registradas as máximas intensidades de radiação solar direta com aumento na dispersão de radiação difusa; entanto que, para o inverno o comportamento foi inverso.

Agradecimentos

REFERÊNCIAS

Abdullahi, M. e Nasir, M., 2014. Evaluation of monthly total global and diffuse solar radiation in Ibi, Taraba state, Nigeria. Pelagia Research Library. Advances in Applied Science Research, vol. 5, n. 2, pp 144‒148.

Escobedo, J., Gomes, E., Oliveira, A. e Soares, J., 2009. Modeling hourly and daily fractions of UV, PAR and NIR to global solar radiation under various sky conditions at Botucatu, Brazil. Applied Energy, vol. 86, pp. 299–309.

Duffie, J., Beckman, W., 2013. Solar engineering of thermal processes. Fourth Edition. Wiley.

De Oliveira, P., 2005. Comportamento e correção da radiação solar difusa obtida com o anel de sombreamento ‒ Paraná. Dissertação de Mestrado. PGEAGRI. UNIOESTE, Paraná.

De Souza, J., Mendonça, R. e Lima, M., 2005. Global solar radiation measurements in Maceió ‒ Brazil. Renewable Energy, vol. 30, pp. 1203–1220.

De Souza, Echer., Martins, F., Pereira, E., 2006. A importância dos dados de cobertura de nuvens e de sua variabilidade: Metodologias para aquisição de dados. Revista Brasileira de Ensino de Física, vol. 28, n. 3, pp. 341‒352.

Iqbal, M., 1983. An Introduction to Solar Radiation. Academic Press. Toronto, Canada.

Liu, B., Jordan, R., 1960. The interrelationship and characteristic distribution of direct, diffuse and total solar radiation. Solar Energy, Washington, vol. 4, n. 3, pp. 1–19.

Livi, F.P., 1998. Elementos do clima: o contraste de tempos frios e quentes. Pp.73–78. Em: Menegat, R. (Ed.), Atlas Ambiental de Porto Alegre. Editora da Universidade. UFRGS, Porto Alegre.

Livi, F.P., 2002. O Clima em Porto Alegre no Século XX: Uma análise de séries Temporais. Dissertação de Mestrado. PPGEO, UFRGS, Porto Alegre.

Haag, R., Schirmer, R., Andrade G., Brazil, C., Perin, F. e Blauth da Silva, A., 2018. Atlas Solar do Rio do Grande do Sul. UERGS. Porto Alegre.

Marques, K., Pereira, T. e Assis, S., 2000. Análise do comportamento mensal do Índice de Limpidez. Anais Congressos Brasileiros de Meteorologia, edição XI – Rio de Janeiro.

Müller, S.C., Overbeck, G. e Setubal, R.B., 2011. A coexistência entre campos e florestas: qual a vegetação natural de Porto Alegre. Em: Setubal, R.B.; Boldrini, I.I.; Ferreira, P.M.A. (Eds.). Campos dos Morros de Porto Alegre. Primeira edição. Igré Associação Sócio-Ambientalista. Porto Alegre.

Rensheng, C., Ersi, K., Jianping, Y., Shihua, L., Wenzhi, Z. e Yongjian, D., 2004. Estimation of horizontal diffuse solar radiation with measured daily data in China. Renewable Energy, vol. 29, pp.717–726.

Tavares, P. 2005. Observação e análise da radiação solar global e fotossinteticamente ativa na região de Maceió. Trabalho Final de Graduação. UFA. Maceió.

Vieira, E., 1984. Rio Grande do Sul: Geografia Física e Vegetação. Porto Alegre.

ANNUAL ANALYSIS OF THE DIRECT, DIFFUSE AND GLOBAL COMPONENTS OF SOLAR RADIATION IN PORTO ALEGRE, RS

Abstract. *Solar radiation incident in the surface of the Earth in different atmospheric conditions, which affects the amount of radiation obtained in the surface during the day. The amount of global solar radiation can be estimated in several conditions of the sky from the relation between the global solar radiation measured in the surface and the radiation in the upper part of the atmosphere (index of clarity). Since March 2018 the UERGS solarimetric station, located in Porto Alegre - RS (-30.080022, -51.12856) has been recording solar radiation data and other meteorological parameters. In this work, we analyze the data obtained for the direct, diffuse and global components of solar radiation and the behavior of solar radiation in three cloud scenarios (clear sky, intermediate cover and cloudy) through the clarity index "Kt" and with daily data for one year (March 2018 to February 2019). As a result it was obtained, 72 days with clear sky, 184 days with sky with intermediate coverage and 109 days with cloudy sky; with average radiation of 285 W/m2 in clear sky, 187 W/m2 in days of intermediate coverage of the sky, 76 W/m2 in cloudy days; being the months of November and December those that presented greater amount of days to clear sky. In the three scenarios the global irradiance showed an exponential behavior as the "Kt" index increased; however, the behavior of diffuse and direct varied according to the scenario, being the relation of these the determinant of each category.*

Key words: clarity index, atmosphere, solar radiation.